

Numerical and Experimental Investigations on Corrosion and Self-Protection Processes in Reinforced Concrete

Dissertation

**zur Erlangung des akademischen Grades
Doktor der Ingenieurwissenschaften
(Dr.-Ing.)
der Technischen Fakultät
der Christian-Albrechts-Universität zu Kiel**

Zahid Mohammad Mir

**aus
Srinagar, Indien**

Kiel, 2020

Gutachtern der Dissertation:

1. Gutachter: Prof. Dr. Mikhail L. Zheludkevich
2. Gutachter: Prof. Dr.-Ing. Stephan Wulfinghoff
3. Gutachter: Prof. Dr.-Ing. habil. Wolfgang Weber

Vorsitzender des Promotionsausschusses:

Prof. Dr.-Ing. Jeffrey McCord

Tag der mündlichen Prüfung:

27. 10. 2020

Erklärung:

Hiermit erkläre ich, dass die beigefügte Dissertation, abgesehen von der Beratung durch die Betreuer, nach Inhalt und Form meine eigene Arbeit ist.

Die Arbeit, ganz oder zum Teil, wurde nie schon einer anderen Stelle im Rahmen eines Prüfungsverfahrens vorgelegt und ist abgesehen, von den im Anhang angegebenen Veröffentlichungen, nicht anderweitig zur Veröffentlichung vorgelegt worden.

Außerdem ist die Arbeit unter Einhaltung der Regeln guter wissenschaftlicher Praxis der Deutschen Forschungsgemeinschaft entstanden.

Geesthacht, den 23. 06. 2020

Zahid Mohammad Mir

Abstract

The chloride induced corrosion of steel in concrete is one of the biggest durability issues affecting structures worldwide. Concrete structures that are installed in marine environment and those exposed frequently to de-icing salts in the winter season, such as bridges and parking structures, are particularly susceptible to corrosion induced damage. In worst cases, the structure is unable to fulfil its entire service life and needs extensive repairs or is decommissioned quite early. Such situations can have a strong impact on society which is dependent on infrastructures for mobility and transportation of essential materials. Moreover, the economic losses are predicted in billions in the coming future and can impact the global economy.

In an attempt to increase the service life of concrete structures with respect to chloride durability, Layered Double Hydroxides (LDH) are introduced as chloride ion entrapping additive in concrete. LDH encapsulates chloride ions from the environment which can extend the service life of concrete structures. It can also be tailored to deliver corrosion inhibiting ions which can mitigate the chloride induced damage in concrete. A new concrete mix with LDH was developed in this work for building long lasting infrastructure exposed to chloride ingress in submerged marine zones.

Predictive modelling approaches are used to study the corrosion processes and chloride durability of concrete. Multi-ion transport model is used to predict the efficiency of LDH in concrete concerning chloride ingress. Computational results are presented which compare chloride ingress in concrete with and without LDH. Formation factor has been used in this study to determine the microstructure related properties of concrete with and without LDH. Additionally, experimental investigations are presented which report on the stability and chloride binding capacity of LDH in synthetic alkaline solutions, concrete pore solutions, mortars and also in concrete. The compatibility of LDH with cement is also presented. The work highlights that LDH is able to improve the chloride durability of concrete. Furthermore, In-situ investigations are carried out to understand the stability of LDH inside concrete.

Kurzfassung

Weltweit stellt die chloridinduzierte Korrosion von Stahl in Beton eine der größten Herausforderung für die Gewährleistung der Strukturintegrität von Bauwerken dar. Insbesondere Betonkonstruktionen, die in Meeresumgebung installiert werden oder in der Wintersaison häufig Streusalz ausgesetzt sind, wie z.B. Brücken und Parkhäuser, sind besonders anfällig für korrosionsbedingte Schäden. Im schlimmsten Fall kann das Bauwerk nicht seine geplante Lebensdauer erreichen und benötigt umfangreiche Reparaturen oder muss sogar stillgelegt werden. Die damit einhergehenden Beeinträchtigungen der Mobilität sowie des Transports wichtiger Güter kann folglich ausgeprägte gesellschaftliche Auswirkungen haben, da diese Sektoren auf funktionierende Infrastrukturen angewiesen sind. Bereits jetzt werden für die Zukunft enorme wirtschaftliche Verluste aufgrund maroder Infrastrukturen vorhergesagt, die sich auf die Weltwirtschaft auswirken werden.

Eine Strategie, die Lebensdauer von Betonstrukturen im Hinblick auf die Chloridbeständigkeit zu erhöhen, stellt die Beimischung von Layered Double Hydroxides (LDH) dar. LDH kapselt Chloridionen aus der Umgebung ein, was die Lebensdauer der Struktur verlängern sollte. Gleichzeitig können durch den zugrundeliegenden Einlagerungsmechanismus korrosionshemmende Ionen in den Beton eingebracht und so bereits verursachte Schäden im Beton abgemildert werden. Um diesen Lösungsansatz auf Infrastrukturen in maritimer Umgebung zu übertragen und so ihre Lebenszeit zu verlängern, wurde in dieser Arbeit eine neue LDH-haltige Betonmischung für die Konstruktion entwickelt und auf ihre Eigenschaften hin untersucht.

Darüber hinaus wurden prädiktive Modellierungskonzepte entwickelt und dazu verwendet, um die Korrosionsprozesse und die Chloridbeständigkeit von Beton zu untersuchen. Zu diesem Zweck wurde ein computerbasiertes Multi-Ionen-Transportmodell verwendet, um die Effizienz von LDH-haltigem Beton in Bezug auf die Einlagerung von schädlichen Chloridionen vorherzusagen. Es werden Berechnungsergebnisse vorgestellt, die das Chlorid-Tiefenprofil in Beton mit und ohne LDH vergleichen. Dafür wurde in dieser Studie ein Formfaktor verwendet, der es ermöglicht, mikrostrukturabhängige Eigenschaften von Beton mit und ohne LDH einzubeziehen. Darüber hinaus werden experimentelle Untersuchungen präsentiert, die über die Stabilität und das Chloridbindevermögen von LDH in synthetischen Alkalilösungen, Betonporenlösungen, Mörteln und auch im Beton selbst berichten. Die Kompatibilität von LDH mit Zement wird ebenfalls betrachtet. Es konnte gezeigt werden, dass die Chloridbindungskapazität von LDH-haltigem Beton zu einer Verbesserung der Materialbeständigkeit führt. Darüber hinaus konnte durch die durchgeführten in-situ-Untersuchungen ein besseres Verständnis des Verhaltens und der Stabilität von LDHs in Beton erlangt werden.

Acknowledgments

The work presented in this dissertation was carried out during my employment at Helmholtz-Zentrum Geesthacht as a Doctoral candidate. To be able to work at this great research campus has been an incredible experience and I will always cherish the time spent here. In the last 3.5 years, I embarked on a journey which transformed me not only as a professional but as a person in whole. It has been a time of immense learning, patience and self improvement. Now that this journey is coming to end, it can only be complete by sincerely thanking those who've been a part of it.

To begin with, I would like to express my sincere gratitude to Prof. Mikhail L. Zheludkevich for mentoring me all these years. His support, guidance, encouragement and intriguing discussions helped me in shaping my work and gave me confidence along the way. Apart from work, his inviting and calm personality made it possible to share any concern or personal problems that I had over the years. I am truly thankful to him for all that. I would also like to thank my daily supervisor Dr. Daniel Höche who helped and pushed me to achieve my thesis objectives. His humour filled way of working made even the difficult task look easy and achievable. I truly appreciate him for all things that he taught me and the opportunities that he gave me all these years. I would also like to thank all former and current staff members of WZK who have been very helpful and kind to me all these years.

It has been a rewarding experience to work with Dr. Alexandre Bastos and Dr. Philippe Maincon. It is hard to put in words all the things that I have learned from them till date and I truly thank them for all that. It has been nice to have them as colleagues and friends.

I am very thankful to all the LORCENIS project colleagues who contributed to this work in one way or the other. Special thanks to Dr. Urs Müller, Dr. M. C. Alonso, Dr. Miguel P. Rabade, Kristina Villar, Celestino Gomes and Rui Sampaio for their support towards completion of a vast experimental program in a relatively short time. I am also thankful to Dr. Frederico Maia, Dr. Emmanuel Gallucci, Dr. Dirk Qvaeschning, Dr. Sara Irico and Prof. M.G.S. Ferreira for their technical advice and guidance. The help and support of Dr. Jesper Friis, Dr. Inga G. Ringladden, Dr. Ingeborg-Helene Svenum, Dr. Berit Zeller-Plumhoff, Dr. Monika Pilz and Dr. Christian Simon is much appreciated. I would also like to thank my friends and colleagues at University of Aveiro who made me feel like home on my extended visits to Aveiro.

It has been a pleasure to share office space with Dr. Christian Feiler, Dr. Natalia A. Konchakova and Xuejiao Li. Their company created a wonderful atmosphere in the office. I would like to specially thank M. Umer bilal, Anissa Bouali and Dr. Maria Rosario Silva Campos for their

friendship and support all these years. Their warm company and their humour will always be missed.

The kind help of Sabine Schrader with all the administrative issues is greatly acknowledged. Her caring personality and her two lovely dogs will be missed. I would like to thank Anke Roering from the HZG library for her help in obtaining every article that I needed. I also appreciate the continuous support of Sybille Ziemann regarding articles publishing formalities.

It has been a pleasure to run countless miles alongside Dr. Anna-Lisa Chaudhary and Robin Luckey. Their like minded attitude towards sports kept me fit all these years.

Although miles apart, I have never felt short of support from Rodion Kalistuk, Daesik Kwak and Marta Besalú Canals. From the very first days in Stuttgart and all these years till now, they have been a rock solid support to me all these years.

I consider myself blessed to have a younger brother like Abid M. Mir who has always supported me in thick and thin and keeps inspiring and motivating me every single day. I would also like to thank my mother and father who have always been very patient with me and stood by me in all decisions of life. Staying apart from them all these years has not been easy and I hope I can make them proud enough.

Last but not the least, I would like to thank the Almighty God with all my heart and soul for blessing and decorating my life with so many wonderful things. It is my relentless faith in him that I always see the glass half full. It is his presence that I always feel around me, which gives me hope and orients me towards the greater goals in life.

Funding

This research was funded by the European Union's HORIZON 2020 collaborative project "LORCENIS" (Long Lasting Reinforced Concrete for Energy Infrastructure under Severe Operating Conditions) under grant agreement no. 685445 and partly by the European Union's COST Action "SARCOS" (Self-healing as Preventive Repair of Concrete Structures) under grant agreement no. CA15202.

Thesis

This thesis consists of a summary of the following papers¹

Articles in peer-reviewed journals

- Paper 1** Z. Mir, A. Bastos, D. Höche and M. L. Zheludkevich, "Recent Advances on the Application of Layered Double Hydroxides in Concrete - A Review" in: *Materials* 2020, 13(6), 1426
- Paper 2** Z. Mir, D. Höche, C. Gomes, R. Sampaio, A.C. Bastos, P. Mainçon, M.G.S. Ferreira and M. L. Zheludkevich, "Enhanced Predictive Modelling of Steel Corrosion in Concrete in Submerged Zone Based on a Dynamic Activation Approach" in: *International Journal of Concrete Structures and Materials* 2019, 13,11
- Paper 3** Z. Mir, C. Gomes, A.C. Bastos, R. Sampaio, F. Maia, C. Rocha, J. Tedim, D. Höche, M.G.S. Ferreira and M. L. Zheludkevich, "The Stability and Chloride Entrapping Capacity of Zn-Al-NO₂ LDH in High Alkaline/Cementitious Environment" in: *Corrosion and Materials Degradation* 2021, 2, 78-99
- Paper 4** Z. Mir, A. Bastos, C. Gomes, U. Mueller, M.C. Alonso, K. Villar, M. P. Rabade, F. Maia, C. Rocha, P. Mainçon, D. Höche, M.G.S. Ferreira and M. L. Zheludkevich, "Numerical and Experimental Analysis of Self-Protection Processes in Reinforced Concrete due to Application of Mg-Al-NO₂ Layered Double Hydroxides" in: *Advanced Engineering Materials* 2020, Early view version
- Paper 5** Z. Mir, J. Friis, T.F. Hagelien, I-H. Svenum, I.G. Ringdalen, N. Konchakova, M.L. Zheludkevich, D. Höche, "Interoperability Architecture for Bridging Computational Tools: Application to Steel Corrosion in Concrete" in: *Modelling and Simulation in Materials Science and Engineering* 2020, 28(2)

Other publications during candidature

- Paper 6** J.C. Gomes, Z. Mir, R. Sampaio, A. Bastos, J. Tedim, F. Maia, C. Rocha and M.G.S Ferreira, "Use of ZnAl-Layered Double Hydroxide (LDH) to Extend the Service Life of Reinforced Concrete" in: *Materials* 2020, 13(7), 1769

¹The papers included in this work are open access articles under the terms of the Creative Commons Attribution License, which permits use, distribution and reproduction in any medium, provided the original work is properly cited.

-
- Paper 7** P. Maincon, J. Psihogios, **Z. Mir**, D. Dragatogiannis, D. Höche, "Towards an engineering tool for concrete coverage design in the presence of chloride-capturing additives" in: *to be submitted to an international journal*
- Paper 8** E.Sola, J. Ožbolt, G. Balabanić, **Z. Mir**, "Experimental and numerical study of accelerated corrosion of steel reinforcement in concrete: Transport of corrosion products" in: *Cement and Concrete Research*, 2019, 120, p.119-131
- Paper 9** D. Snihirova, D. Höche, S. Lamaka, **Z. Mir**, T. Hack and M.L. Zheludkevich, "Galvanic corrosion of Ti6Al4V-AA2024 joints in aircraft environment: Modelling and experimental validation" in: *Corrosion Science*, 2019, 157, p.70-78

Articles in conference proceedings

- Paper 10** **Z. Mir**, J.C. Gomes, R. Sampaio, A. Bastos, M.G.S. Ferreira, D.Höche and M.L. Zheludkevich, "An Overview on the Numerical Modelling of "Self-Protection" Processes in Concrete: Application to Layered Double Hydroxides" in: *Durable Concrete for Infrastructure under Severe Conditions – Smart Admixtures, Self-responsiveness and Nanoadditions, Ghent, Belgium, September 10-11, 2019*
- Paper 11** P. Maincon, J. Psihogios, **Z. Mir**, D. Höche and D.A. Dragatogiannis, "Providing structural Engineers with a tool for the design of concrete coverage" in: *Durable Concrete for Infrastructure under Severe Conditions – Smart Admixtures, Self-responsiveness and Nanoadditions, Ghent, Belgium, September 10-11, 2019*
- Paper 12** J.C. Gomes, **Z. Mir**, A. Bastos, F. Maia., C. Rocha, J. Tedim, M.L. Zheludkevich and M.G.S. Ferreira, "Effect of Layered Double Hydroxides on the Performance and Service Life of Reinforced Concrete" in: *Durable Concrete for Infrastructure under Severe Conditions – Smart Admixtures, Self-responsiveness and Nanoadditions, Ghent, Belgium, September 10-11, 2019*

Contents

List of Figures	xii
List of Symbols	xiii
1. Introduction	1
1.1. Motivation and objectives of the work	1
1.2. Structure of the study	6
2. Literature review	7
2.1. Article 1 - Recent advances on the application of layered double hydroxides in concrete - A review	7
2.1.1. A brief summary of Article 1	7
2.1.2. Author contribution	7
3. Materials and methods	31
3.1. Materials	31
3.1.1. Cement binder	31
3.1.2. Concrete mix	32
3.1.3. Layered Double Hydroxides	32
3.2. Numerical techniques	33
3.2.1. Uni-directional diffusion problem	33
3.2.2. Space discretization	35
3.2.3. Time discretization	37
3.3. Experimental techniques and methods	38
3.3.1. X-ray diffraction analysis and particle size analysis	38
3.3.2. Stability and ion exchange analysis	38
3.3.3. Chloride sequestration analysis in aqueous solutions	39
3.3.4. Chloride binding isotherms	40
3.3.5. Determination of Formation Factor	41
3.3.6. Accelerated natural diffusion test	44
3.3.7. Other tests:	44

4. Results on the basis of published work	45
4.1. Article 2 - Enhanced Predictive Modelling of Steel Corrosion in Concrete in Submerged Zone Based on a Dynamic Activation Approach	45
4.1.1. A brief summary of Article 2	45
4.1.2. Author contribution	45
4.2. Article 3 - The Stability and Chloride Entrapping Capacity of Zn-Al-NO ₂ LDH in High Alkaline/Cementitious Environment	64
4.2.1. A brief summary of Article 3	64
4.2.2. Author contribution	64
4.3. Article 4 - Numerical and Experimental Analysis of Self-Protection Processes in Reinforced Concrete due to Application of Mg-Al-NO ₂ Layered Double Hydroxides	87
4.3.1. A brief summary of Article 4	87
4.3.2. Author contribution	87
5. Discussion of published results	101
5.1. Chloride sequestration efficiency of LDH in alkaline environment	101
5.2. Stability analysis of LDH in alkaline environment	104
5.3. Effect of LDH dissolution on hydration kinetics	105
5.4. Stability analysis of Mg-Al-NO ₂ in cementitious environment	106
5.5. A predictive modelling approach towards evaluation of chloride sequestration capacity of LDH in concrete	107
5.6. Numerical modelling of corrosion initiation processes at the steel-concrete interface	110
6. Conclusions and Future Work	112
7. Outlook on multiscale modelling	114
7.1. Article 5 - Interoperability architecture for bridging computational tools: application to steel corrosion in concrete	114
7.1.1. A brief summary of Article 5	114
7.1.2. Author contribution	115
A. Appendix	135
A.1. Chloride diffusion in concrete - a test example	135
Bibliography	142

List of Figures

1.1.	Schematic representation of corrosion initiation and propagation stage of a structure based on chloride ion concentration at the steel concrete interface . . .	2
1.2.	Schematic representation of processes occurring at the steel concrete interface and inside the bulk concrete	5
3.1.	Test matrix for Cl^- sequestration analysis	39
3.2.	Experimental sequence for Cl^- capture tests under stirring conditions	40
3.3.	Schematic representation of Formation Factor measurement	42
3.4.	Setup for pore pressing method test	43
3.5.	Setup for electrical resistivity measurement	43
5.1.	Chloride sequestration by LDH in an aqueous salt solution at a starting pH of 11.95 under continuous stirring	102
5.2.	Variation of chloride binding capacity of LDH at various pH levels	103
5.3.	Stability of Zn-Al- NO_2 across the entire pH spectrum	105
5.4.	Effect of the LDH particle size and dosage on cement hydration	106
5.5.	(a) One-dimensional modelling domain. (b) Evolution of pore solution concentration for Na^+ and Cl^- ion at 10 mm, 20 mm and 30 mm from the exposed end. (c) Total chloride profiles for the REF mix plotted against penetration direction	109
5.6.	Ratio of experimentally obtained and numerically predicted chloride profiles .	110
5.7.	Current density in passive and active states for a total exposure time of 41 years	111
A.1.	1D domain in test example discretized with linear elements in space	136
A.2.	A comparison of implicit numerical solution with analytical solution	136
A.3.	A comparison of explicit numerical solution with analytical solution	137

List of Symbols

The following list describes the symbols that have been used in this dissertation. Symbols in the appended papers take precedence.

α, β	parameters for Freundlich isotherm
$\delta \mathbf{C}_e^c$	discrete test function for an element
δC^c	test function
Γ	boundary of the domain
Γ_D	part of boundary with Dirichlet conditions
Γ_N	part of boundary with Neumann conditions
γ_{Cl^-}	chemical activity coefficient
$\overline{\mathbf{K}}$	global transport operator
$\overline{\mathbf{M}}$	global capacity matrix
$\overline{\mathbf{M}}_{i,i}$	diagonalized capacity matrix
$\overline{\mathbf{F}}$	global force vector
\mathbf{C}^c	array with global concentrations
\mathbf{C}_e^c	array with local discrete concentrations
\mathbf{N}	array of shape functions
Ω	domain of the model
ψ_e	electric potential
σ_c^b	bulk conductivity of concrete
σ_c^p	conductivity of pore solution
θ_p	porosity of concrete

List of Symbols

A^o	constant cross section of 1D domain in Appendix A.1
$C_{Cl^-}^f$	free chloride concentration
$C_{Cl^-}^b$	bound chloride concentration
C^c	chloride concentration in concrete
$C_{Cl^-}^{Eq.}$	equilibrium chloride concentration of the solution
$C_{Cl^-}^i$	initial chloride concentration of the solution
C_s	surface concentration in analytical solution for Fick's second law
D^α	apparent diffusion coefficient of chloride ions
$D_{Cl^-}^\infty$	diffusion coefficient of Cl^- ion at infinite dilution
$D_{Cl^-}^{eff}$	effective/micro-structural diffusion coefficient
f_e	local force vector
FF_c	formation factor
J^c	chloride flux through a plane perpendicular to direction of diffusion
K_e	element transport operator
M_e	element capacity matrix
M_{ds}	mass of sample powder
S^c	chloride source term
$V_{sol.}$	volume of solution
z_{Cl^-}	charge number of Cl^- ion
$\mathbf{N}_{,x}$	array with gradient of shape functions
F	Faraday's constant
PS	pore solution
R	ideal gas constant
T	temperature in kelvin

1. Introduction

This work presents numerical and experimental investigations focusing on chloride induced corrosion processes in concrete and the role of chloride entrapping nano-containers such as layered double hydroxides (LDH) in concrete. The processes involving the role of LDH in mitigating the chloride ingress in concrete have been termed as the "self-protection" processes in concrete. Prior to discussing the contents of this work in detail, this chapter presents an introduction into the topic at hand, the goals of this work as well as the underlying motivation. This chapter also discusses the organization and the structure of this work.

1.1. Motivation and objectives of the work

Concrete is the most used material on earth after water [1]. The ability of concrete to take up any desired shape upon hardening has made this material indispensable for human consumption. With a rapid rise of population in recent decades [2], the demand for housing and infrastructure has also increased proportionally. As a consequence, cement production has increased considerably in recent years. In 2014, cement production was estimated to be about 4.3 billion tonnes [3]. On one hand, the water consumption due to the extensive use of concrete is foreseen to have a big impact on the available water resources in the near future [4]. On the other hand, the cement production industry is a major contributor towards global warming. The carbon footprint of cement production is estimated at around 5% of the global carbon emissions [5]. It is foreseen that in the coming times, carbon emissions from cement production could increase due to high demand in developing as well as in developed countries. Therefore, it is desirable to have concrete structures with longer service life in order to reduce cement production by avoiding frequent repairs and rebuilding of infrastructure.

However, the service life of structures is usually shorter than the design life due to various degradation phenomena associated with concrete. Corrosion, ice abrasion, acid attack, freeze-thaw, creep, shrinkage, fracture etc. are some of the degradation mechanisms associated with concrete [6]. One of the major degradation phenomenon affecting structures worldwide is the chloride induced corrosion associated with reinforced concrete structures [7]. It affects infrastructure that is exposed to marine environments [8] usually in coastal and offshore areas

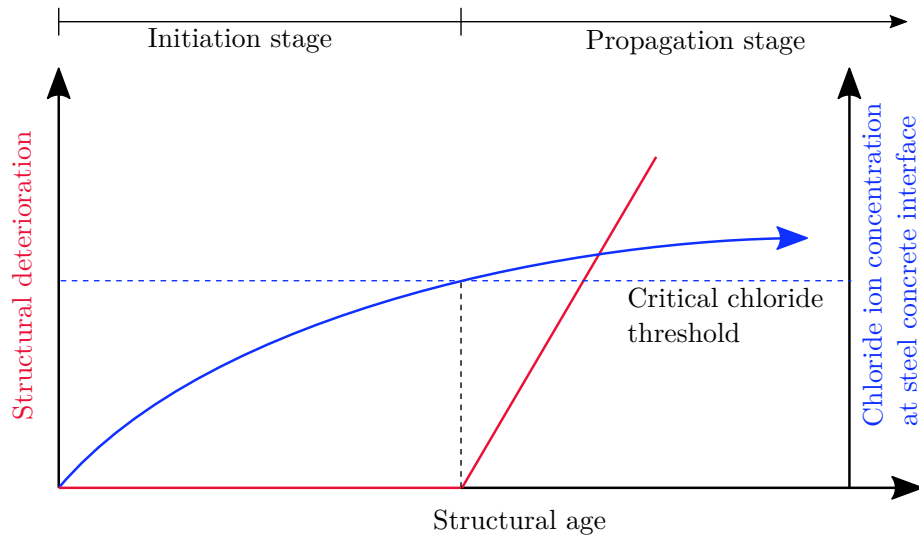


Figure 1.1.: Schematic representation of corrosion initiation and propagation stage of a structure based on chloride ion concentration at the steel concrete interface (based on Tuutti's model [11, 12]).

or onshore structures like parking houses and bridge decks which are frequently exposed to de-icing salts in the winter season [9]. The problem is very severe as frequent repairs and maintenance is required. In worst cases, the entire structural integrity may be lost. As such, the economic and social aspects of chloride induced corrosion are very big [10] and can lead to huge investments in costs related to repairs or closing of infrastructures such as bridges, tunnels etc. This can in turn affect transportation of water, food, energy as well as public mobility.

Concrete itself is not susceptible to corrosion, in fact it is the embedded steel that is prone to such degradation processes. Reinforcing steel in the form of bars or stirrups is added to concrete so that it is able to withstand tensile stresses and to provided confinement to structural members. Concrete acts as an alkaline medium around the steel, due to which a protective passive layer is formed on the steel surface [13, 14, 15]. Concrete is a porous material and when it is exposed to an environment containing aggressive salts, such as sea water in case of bridge piers, the aggressive ions from the environment can pass through the pore network. Under prolonged exposure, the chloride ions can penetrate through the concrete cover and reach the steel concrete interface [16]. As the chloride concentration increases beyond a certain threshold [11], the passive layer on the rebar surface can be damaged [17]. This instant is termed as the end of the corrosion initiation stage as shown in Figure 1.1. This leads to the start of electrochemical processes on the rebar surface and this stage is termed as the corrosion propagation stage (Figure 1.1). Corrosion reactions

are initiated on the rebar interface which lead to the formation of corrosion products [18]. These products keep on accumulating at the steel concrete interface. These hydroxides and oxides have a higher volume as compared to the parent steel and an outward pressure is generated at the interface due to limitations of space at the steel concrete interface [19]. As a consequence, micro-cracks are generated around the interface which in due course of time coalesce to form macro-cracks originating outward from rebar surface [20]. Formation of big cracks can even cause spalling of concrete around the rebars which is very dangerous for the structural integrity [21]. Depending on the severity of damage, the structure might need repair work or become non-operational.

Apart from protecting the embedded steel by its alkalinity, concrete is able to slow down chloride ingress as it is able to bind chlorides chemically as well as physically [22]. As concrete is exposed to a salt containing environment, the aggressive ions such as chloride ions, penetrate the concrete microstructure through the pore network. The pore network itself is surrounded by cement hydration phases with chloride binding abilities such as calcium aluminate hydrates (AFm, AFt), calcium silicate hydrate phases (C-S-H) etc. [23]. The incoming chloride ions interact and bind with the surrounding cementitious microstructure around the cement pore system [24, 25]. As such, chloride ions that are bound to cement hydration products are termed as bound chlorides and the remaining chlorides that keep moving freely in the pore network are thereby termed as free chlorides. The binding of chlorides slows down the ingress of free chlorides along the pore network.

A longer corrosion initiation stage can be achieved if the chloride binding capacity of concrete is increased. Supplementary cementitious materials such as fly ash, blast furnace slag etc. have been reported to increase the chloride binding capacity of concrete [26, 27, 28]. A new class of additives that can potentially increase the chloride binding capacity of concrete is the layered double hydroxide [29]. In the LORCENIS project [30], two novel chloride entrapping LDH were developed with a specific target of increasing the chloride binding capacity of concrete. LDH are clay like materials, usually available in a powdered state or in a slurry form. LDH can be easily mixed in concrete during the casting stage. In this work, two types of LDH (Zn-Al-NO_2 and Mg-Al-NO_2) were used with the aim of increasing the chloride binding capacity of concrete.

LDH can be prepared by co-precipitation of divalent and trivalent cations in the form of hydroxides from their respective salts in an alkaline medium [31]. The resulting material has a layered structure, where the layers are positively charged. During the synthesis process, the interlayer spacing is filled with exchangeable anions for charge compensation [32]. LDH possess a unique property by which the anions present in the external environment can be captured by exchanging them with the anions present in their interlayer spaces [33]. This

property is termed as the ion-exchange property of LDH [34]. This property can be exploited in concrete with LDH acting as a chloride entrapping additive. This can be beneficial in increasing the chloride entrapping capacity of concrete and also elongate the duration of the corrosion initiation stage (see Figure 1.1). Additionally, LDH can also be synthesized with corrosion inhibiting molecules in their interlayer e.g. with NO_2^- ion and the resulting LDH can be used for a dual benefit i.e. capture Cl^- ion from the environment and deliver a NO_2^- ion in its place. This application can not only increase the duration of corrosion initiation stage but can also reduce the severity of corrosion in the propagation stage.

In the context of addition of LDH to concrete, other aspects such as the influence of LDH on the mechanical and microstructure properties have to be taken into account. A higher dosage of LDH can make the concrete very porous and lead to aggregation of LDH particles inside concrete [35]. This can be disadvantageous towards chloride durability of concrete. In this regard, recommendations on threshold dosage of LDH are required so that the key properties of concrete such as compressive strength, flexural strength, porosity, etc. are not severely affected [36]. Therefore, the present work also includes investigations on the basic understanding of LDH as a concrete additive. This objective is fulfilled by understanding the compatibility and stability of LDH in concrete as well as in artificial cementitious environments such as synthetic alkaline solutions and cement pore solutions.

In this work, numerical models are created based on finite element method (FEM) with an intended application of understanding the transport of ions in concrete and predicting the corrosion currents. The finite element method is a powerful mathematical tool in which the physical domain is discretized into very small finite elements and the solution is computed over them. The biggest advantage of using this method is that it enables the user to compute solutions over any physical geometry, loading conditions, boundary conditions etc. where otherwise analytical solutions are very difficult to obtain. The finite element method has been in use for engineering applications since early 1960's with one of the earliest distributed code originating from Berkeley and intended for structural applications [37]. Since then the method has evolved and can be easily applied to any physical process that can be described by a differential equation or a set of differential equations. In recent times, the use of finite element method has increased considerably and is widely applied in diverse fields of science and engineering such as crash analysis, aerospace engineering, acoustics, fluid mechanics, marine engineering, heat transport, electromagnetism and many more.

The models developed in this work belong to a broader set of models created within the LORCENIS project. LORCENIS is an acronym for "Long Lasting Reinforced Concrete for Energy Infrastructure under Severe Operating Conditions" [30]. One of the objectives of the LORCENIS project is to develop novel additives and numerical models which can provide an

understanding of chloride ingress and role of additives in concrete. In this work, only a few of these models are presented, which are author's own work and independent of other models developed in LORCENIS. During the course of this work, Julia programming language [38] and COMSOL Multiphysics® software were extensively used.

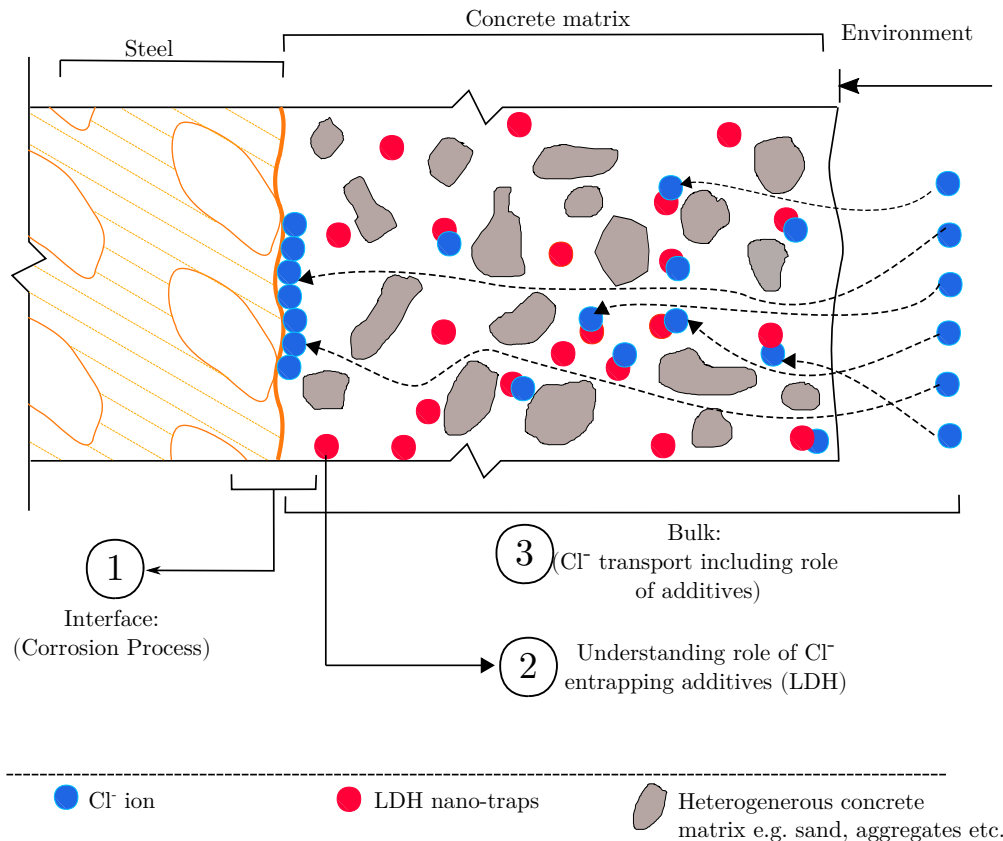


Figure 1.2.: Schematic representation of processes occurring at the steel concrete interface and inside the bulk concrete.

As mentioned in the title of this work, the corrosion processes in concrete due to chloride ingress and the role of LDH in carrying additional chloride binding in concrete was studied both numerically and experimentally. The work carried out can be divided into three major aspects as shown in Figure 1.2 and includes the following:

1. The first part of the work presents a numerical understanding of corrosion processes occurring at the steel concrete interface. The underlying processes include ingress of chloride ions into concrete, depassivation events at rebar surface and prediction of corrosion currents after depassivation events. An accurate prediction of corrosion currents is the main objective of this part.
2. Prior to using LDH as a concrete additive and before conducting experimental investi-

gation with LDH in concrete; it is important to understand the basic behavior of LDH as an engineering material. Therefore, the second part is experimental in nature and answers vital questions such as chloride capturing capacity of LDH in salt solutions, synthetic alkaline solutions and in various types of concrete pore solutions. Additionally, the stability of LDH in alkaline environment, especially in high pH range is discussed in depth. Lastly, attention is paid to the compatibility of LDH with cement.

3. This last part showcases a numerical model for chloride ingress in concrete which includes the influence of chloride binding additives. Formation factor is used to determine information about the microstructure parameters affecting chloride transport. The model compares chloride ingress in concrete mixes with and without LDH. This part is complemented by stability analysis and highlights the effectiveness of LDH in capturing chlorides inside concrete. Part 2 and part 3 form the major part of this work.

1.2. Structure of the study

The present work is structured as follows: In Chapter 2, a review on the state-of-the-art of applications of LDH in concrete is presented. This chapter includes an article and presents an insight into the chloride transport, electrochemical processes in concrete, working mechanism of LDH as well as compatibility of LDH with cement. The chapter mainly focuses on the ion exchange property of LDH in concrete but other important aspects such as relevant LDH dosage, effect on mechanical properties and hydration kinetics etc. are also discussed. In Chapter 3, a brief introduction of the materials and methods used in this work is presented. This includes description of cement/concrete mixes, experimental techniques and numerical tools used in this work. Chapter 4 has three parts and includes three published articles. The first article discusses the corrosion model developed in this work. The second article focuses on the experimental investigation of LDH (Zn-Al-NO₂). The investigations are restricted to aqueous solutions, cement pastes and mortars. The third article includes applications of LDH (Mg-Al-NO₂) in concrete and presents a transport model which evaluates the chloride binding capacity of LDH in concrete. A comparison is drawn between concrete with and without Mg-Al-NO₂ and the model is validated with supporting experiments. In Chapter 5, a discussion on the results stated in chapter 4 is presented. Chapter 6 presents a summary of the entire work and also highlights future research perspectives. Chapter 7 presents an outlook on data linking aspects between computational solvers. This chapter is accompanied with an article. An appendix with supplementary information is provided at the end.

2. Literature review

2.1. Article 1 - Recent advances on the application of layered double hydroxides in concrete - A review

Note: See attached article in the next pages. Reprinted without modification from [39] under CC BY 4.0 license. Published by MDPI, Basel, Switzerland.

2.1.1. A brief summary of Article 1

An enhancement of chloride binding capacity of concrete by additives such as Layered Double Hydroxides (LDH) can potentially increase the service life of concrete structures. LDH can entrap corrosive ions from the environment and this property makes them very attractive as potential anti-corrosive additives for concrete. The primary objective of LDH is to enhance the chloride binding capacity of concrete. Other potential applications include delivery of corrosion inhibiting ions and improvement of carbonation resistance of concrete. However, addition of LDH to concrete can also affect hydration processes, mechanical strength as well as porosity of concrete. One of the major objectives of this study is to investigate the feasibility of the application of LDH in concrete. Prior to discussing the experimental and numerical studies conducted on LDH in this work, an extensive review is presented which reports on the state-of-the-art of applications of LDH in concrete.

2.1.2. Author contribution

In the following, the author of this dissertation is denoted by his initials ZMM. The names and initials of co-authors can be found in the appended manuscript. ZMM and MLZ proposed the concept behind the study. ZMM and AB did the literature study and co-wrote the script. AB, MLZ and DH revised the script, provided critical comments and supervised the work.

Review

Recent Advances on the Application of Layered Double Hydroxides in Concrete—A Review

Zahid M. Mir ^{1,*}, Alexandre Bastos ², Daniel Höche ¹ and Mikhail L. Zheludkevich ¹

¹ Institute of Materials Research, Helmholtz-Zentrum Geesthacht Centre for Materials and Coastal Research, Max-Planck Str. 1, 21502 Geesthacht, Schleswig Holstein, Germany; daniel.hoeche@hzg.de (D.H.); mikhail.zheludkevich@hzg.de (M.L.Z.)

² DEMaC—Department of Materials and Ceramic Engineering, and CICECO—Aveiro Institute of Materials, Universidade de Aveiro, 3810-193 Aveiro, Portugal; acbastos@ua.pt

* Correspondence: zahid.mir@hzg.de

Received: 6 February 2020; Accepted: 16 March 2020; Published: 20 March 2020



Abstract: The issue of chloride induced corrosion of reinforced concrete is a serious problem affecting infrastructure globally and causing huge economic losses. As such this issue has gained a considerable attention in the scientific community in the recent past. Layered Double Hydroxides (LDHs) have recently emerged as a new class of concrete-additives with a potential to increase the chloride resistance of concrete and mitigate corrosion. LDHs are clay like structures consisting of positively charged layers of cations with associated hydroxides and exchangeable anions in between the layers. Due to this charge balanced structure, LDHs possess the property of encapsulating an anion from the environment and replacing it with an exchangeable anion present in its layers. Potential applications include chloride entrapment in concrete and delivery of corrosion inhibiting anions. However, many versatile compositions of LDHs can be easily synthesized and their application as cement additives reach far beyond corrosion mitigation in concrete. This review presents a summary of recent advances on the applications of LDH in concrete. An extensive set of recently published literature has been critically reviewed and trends have been identified.

Keywords: layered double hydroxides; reinforcement; ion exchange; corrosion; concrete

1. Introduction

Our planet has experienced an unprecedented population growth in the last century [1]. The rise of population has been accompanied by an increase in building infrastructure [2], mostly concrete and steel. As a consequence, the cement production industry has significantly added to global warming with a contribution of almost 5% to the global CO₂ emissions [3]. The carbon footprint of concrete industry is getting bigger as emerging economies in Asian and South-Asian regions are focusing on a rapid expansion of infrastructure. Furthermore, obsolete or outdated production facilities/methods have also contributed to an increased environmental impact of cement production [4–6]. To reduce the environmental impact of cement production, it is desirable to have concrete infrastructure with longer service life. However, due to the various degradation phenomena associated with reinforced concrete structures such as steel corrosion [7–14], freeze thaw cycles [15,16], ice abrasion [17–19], acid attack [20,21] etc., the service life of infrastructure is considerably reduced.

Out of the above mentioned degradation mechanisms, reinforced concrete structures are particularly susceptible to chloride induced corrosion [7,22]. Chloride induced corrosion occurs in bridge decks, parking decks and pavements exposed to de-icing salts as well as in infrastructure exposed to marine and coastal environments such as offshore bridge piers etc. The rapid deterioration of such vital infrastructure can have severe economic, environmental and social implications

worldwide [23]. The need of the hour is to steer concrete research towards applications of innovative low-cost materials that can increase the chloride resistance of concrete structures.

In recent times, layered double hydroxides (LDHs) have emerged as a new class of engineering materials [24,25] which can aid in the corrosion control of concrete structures and potentially prolong their service life. LDHs are clay-like powdered materials which are often referred to as nano-containers or nano-reservoirs and have the ability of entrapping ions from the environment e.g., Cl^- ions. Potential applications include chloride ion and carbonate ion entrapment in concrete. This work provides an overview on the state-of-the-art on the applications of LDHs in concrete technology, based on a critical review of recently published reports and articles. One of the first reviews on application of LDHs in concrete was provided by Raki et al. [26] in 2004 and Yang et al. [27,28] in 2013. Since then many research groups and companies around the globe have started to work extensively with LDHs. Therefore a lot of applications of LDH can be found across various branches of concrete technology. The authors have attempted to review cited literature up to the end of year 2019. The paper presents an understanding of corrosion processes in concrete, chloride binding aspects as well as recent advances made in the applications of LDHs in concrete. The chloride binding aspects of LDH in concrete are critically reviewed but other related effects such as influence of LDH addition on mechanical properties, dosage, effect on microstructure etc. are also discussed.

2. Chloride Induced Steel Corrosion in Concrete

Concrete is the most widely used engineering material [29,30] which is prepared by mixing together cement binder, fine and coarse aggregates and water. After the mixing phase the concrete is able to take any desired shape upon hardening. The resulting concrete is very good to resist compressive stresses but does not display similar capabilities under tensile loading. To improve this, steel reinforcement is embedded in the concrete which is able to take tensile stresses and also provide confinement to concrete. Concrete itself being non-metallic in nature is not susceptible to corrosion, however it is the embedded metallic steel that is susceptible to corrosion and can lead to structural failure under prolonged exposure in corrosive environments.

Concrete is an alkaline environment [31–33] and the alkalinity has a protective effect towards embedded steel bars as it helps in developing a thin protective layer on the steel surface, usually referred to as the passive layer [34,35]. This passive layer is very thin, usually a few nanometers in thickness [36] and protects the steel rebar from corrosion. At this stage, the rebar is said to be passivated and the structure is said to be in the initiation stage [7]. The porous nature of the concrete [37] allows chloride ions to pass through. In due time, chloride ions reach the steel concrete interface [38]. An accumulation of chloride ions on the rebar surface beyond a critical threshold can destroy the passive layer. At this stage the rebar is said to be depassivated [39] and the structure is said to be in its propagation stage, as shown in Figure 1. The amount of chloride ions which can cause depassivation of steel is termed critical chloride threshold [40]. A faster ingress of chloride can shorten the initiation stage of the structure and accelerate depassivation stage leading to shorter service life of structure. On the other hand, a slower or reduced ingress of chlorides can increase the service life of structure. Innovative cement additives that can slow down the chloride ingress can lead to an extension of the initiation stage. Similarly, corrosion inhibitors can reduce the severity of corrosion and mitigate structural deterioration, see Figure 1.

Once the critical threshold is reached at the steel-concrete interface, the onset of corrosion is said to take place. This leads to the formation of active anodic regions, and in the presence of moisture and oxygen lead to the formation of a corrosion cell between anodic and cathodic parts of the rebar. As corrosion progresses, rust products are generated as a result of corrosion reactions. Rust products are more expansive than parent steel [41] and their accumulation at the steel-concrete interface generates considerable internal pressure leading to micro-cracking of concrete [42,43]. As time progresses, microcracks coalesce to form visible macro-cracks which eventually can lead to the deterioration of structural elements [44].

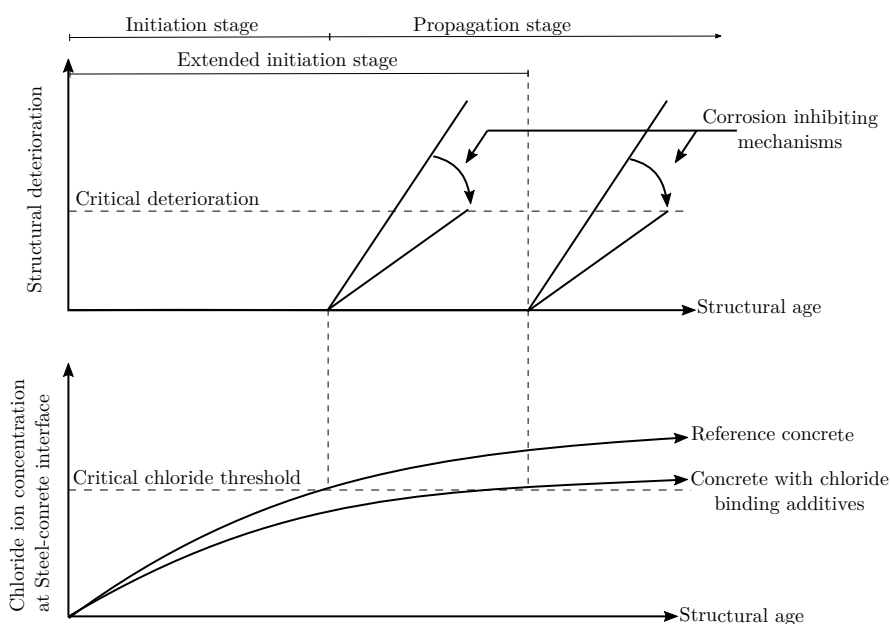


Figure 1. Schematic representation of service life stages of concrete structures under chloride induced corrosion and associated chloride profiles based on modified Tuutti's diagram [7,40].

3. Chloride Binding in Concrete

The transport of chloride ions in concrete matrix occurs through the pore network [45,46]. It is widely accepted that a considerable fraction of chloride ions are physically and chemically bound to the surrounding cementitious matrix [47]. These chlorides are usually named in the literature as bound chlorides. The rest of the chlorides are termed free chlorides and move freely inside the concrete pore system. It is the accumulation of free chloride on the steel concrete interface that is responsible for corrosion initiation [48]. On the other hand, the capability of concrete to bind chloride ions as well as ratio of bound chlorides to free chlorides are vital parameters regarding performance and service life estimation. Increasing the amount of bound chlorides in concrete can help in extending the time to reach the critical chloride concentration [40] on the steel concrete interface (Figure 1).

A significant contribution of bound chlorides is attributed to tricalcium aluminate (C_3A) and tetracalcium aluminoferrite (C_4AF) content in binders [49,50] as they lead to the formation of aluminat monosulphate (AFm) phases upon hydration. AFm is able to chemically bind chlorides in concrete [51,52] forming Friedel's salt which can be chemically expressed as $3CaO \cdot Al_2O_3 \cdot CaCl_2 \cdot 10H_2O$ or its iron analogue $3CaO \cdot Fe_2O_3 \cdot CaCl_2 \cdot 10H_2O$. Depending on the concentration of chloride ion, other salts may be formed such as Kuzel's salt $3CaO \cdot Al_2O_3 \cdot 0.5CaCl_2 \cdot 0.5CaSO_4 \cdot 11H_2O$ [53]. Florea et al. [51] quantified the chloride binding of different AFm phases such as monosulphate-AFm ($3CaO \cdot Al_2O_3 \cdot CaSO_4 \cdot 14H_2O$) and hydroxy-AFm ($3CaO \cdot Al_2O_3 \cdot CaOH_2 \cdot 12H_2O$) and observed different binding capacities depending upon external Cl^- level.

On the other hand, the physical binding of Cl^- in terms of surface adsorption occurs on the calcium silicate hydrate (CSH) interlayers by replacement of loosely bound OH^- ion by Cl^- thereby maintaining electroneutrality in the system. This physical adsorption mostly proceeds on the external layers of CSH layers [54]. Tang et al. [55] reported that the amount of CSH gel is mainly responsible for the amount of chloride binding [49] whereas Florea et al. [51] considered that CSH binds fewer chlorides than AFm phases. Furthermore, it is to be noted that the chloride binding capacity varies depending on the type of the cation present in the salt [56].

Additionally, supplementary cementitious materials (SCM) are added to concrete mixes to replace cement binder, usually as a replacement. One of the motivations behind replacement of cement binder by SCM is to reduce the carbon footprint of concrete industry and also to impart additional functionality to concrete [57]. As such, fly ash (FA), ground-granulated blast furnace slag (GGBFS), silica Fume(SF), metakaolin (MTK) etc. are used as SCM in concrete. Likewise, the addition of SCM also significantly effects the chloride binding properties of concrete. It is now widely accepted that chloride binding increases with the addition of FA, GGBFS [58,59], MTK [57] whereas the addition of SF reduces the amount of bound chlorides [49]. It is believed that ion exchange mechanism is responsible for the chloride binding.

In the last two decades, Layered Double Hydroxides have emerged a new class of nanoscale engineered concrete additives which can impart additional functionality to concrete. Although the role of LDHs in concrete technology is widespread in different areas, the most outstanding application of LDH is its ability to trap anions (possibly aggressive ions such as Cl^-) from the environment and release a tailored anion in its place (like a corrosion inhibiting anion such as NO_2^-) via a controlled release mechanism. This property has been termed as “*Self-Protection*” of concrete and can result in an extended corrosion initiation stage as well as a reduced corrosion degradation in the propagation stage as shown schematically in Figure 1. This review highlights the most notable applications of LDH in concrete technology with a detailed insight into the chloride binding capacity of concrete with LDH.

4. Layered Double Hydroxides

Layered double hydroxides are nano-materials with a layered structure as shown in Figure 2. The layers themselves are formed of bivalent and trivalent cations coinciding with the layered structure of Brucite $\text{Mg}(\text{OH})_2$. The layers in LDHs are positively charged in nature as they are formed due to replacement of some divalent cations by trivalent cations during their formation. This leads to a charge imbalance and in order to compensate this positive charge excess, the interlayers can hold negatively charged anions, as well as some loosely bound $\text{OH}^- / \text{H}_2\text{O}$ in between the layers. LDHs can be represented by the general formula $\text{M}_{1-\alpha}^{\text{II}}\text{M}_{\alpha}^{\text{III}}(\text{OH})_2(\text{X}^{n-})_{\alpha/n} \cdot m\text{H}_2\text{O}$ with α ranging from 0.2–0.33, m equal to $1 - 3\alpha/2$, M^{II} is the divalent cation (e.g., Mg^{2+} , Ni^{2+} , Zn^{2+} , Ca^{2+}), M^{III} is the trivalent cation (e.g., Co^{3+} , Al^{3+} , Fe^{3+} , Ga^{3+}) etc. and X^{n-} is the exchangeable anion with valency n present in interlayer galleries and can be CO_3^{2-} , SO_4^{2-} , Cl^- , OH^- , NO_3^- , NO_2^- etc. The molar ratio of M^{II} to M^{III} is in the range between 2 to 4 [27,60]. The interlayer anion in LDH galleries can be easily exchanged with an anion present in the external environment. Due to this ion exchange property, LDHs are also called anionic clays [61]. This unique property makes LDH a very versatile material as they can help in sequestration of anions from the environment with a possibility of releasing a tailored anion in its places. LDH can therefore be used as a potential additive for the capture of corrosion causing species and release of corrosion inhibiting anions in cementitious environments. LDH can be synthesized in powdered form and added as a percentage of the binder content or in the slurry form wherein corrections to the total w/c ratio should be made considering the amount of water originally present in the slurry.

The ion exchange property of LDH has been used for a wide range of applications across different disciplines such as drug delivery systems [62], treatment of stomach ulcers [63], genetic science [64], removal of toxic anions from water [65–68], protective coatings against corrosion on metal surfaces [69], cleansing of sea water to obtain usable cultivation water [70], removal of pollutants [71], asphalt mixes with deicing property [72] etc. are a few noteworthy applications. In concrete technology, studies on LDH as a cement additive began towards the end of 20th century, and in recent years, LDHs have gained a considerable popularity as concrete additives.

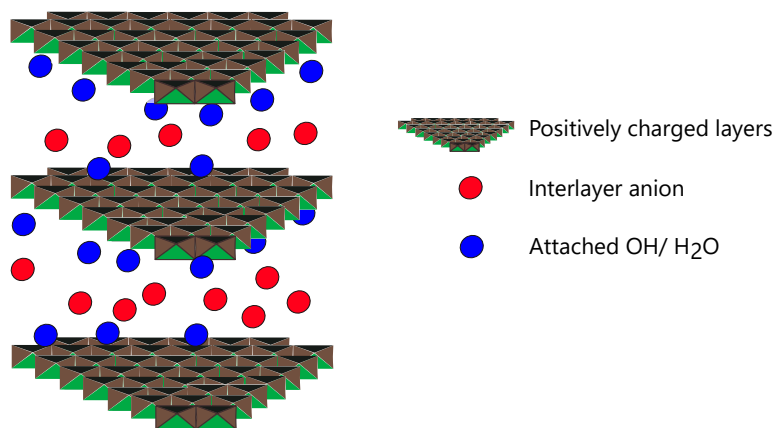


Figure 2. Schematic representation of Layered Double Hydroxide (LDH) structure.

4.1. Preparation Methods

LDHs can be prepared by various techniques. The easiest and commonly used is the co-precipitation method. In this method aqueous solution of desired divalent and trivalent metallic salts are slowly added into a mixer containing water and allowed to simultaneously co-precipitate in an alkaline environment. The pH is held constant by adding an alkaline solution of desired pH [73]. Usually co-precipitation is done in the pH range of 8–10 [74]. Another simple method is the ion-exchange method in which a pre-synthesised LDH precursor is modified by allowing it to conduct ion exchange of its interlayer anions with desired guest anion present in the external solution. It is important to note that the ion-exchange method is strictly influenced by the affinity of LDH towards the guest anion [75,76], the type of the exchange medium [77], temperature [78], pH value of the medium [79] as well as the chemical composition of the LDH itself [80]. Both the co-precipitation method and the ion-exchange method can be used to synthesize LDH with corrosion inhibiting ions, e.g., NO_2^- . Using oxide of divalent cation and salt of trivalent cation, Zuo et al. [81] was able to directly synthesize LDH- NO_2 in an alkaline environment containing NaNO_2 . Another method of obtaining the same LDH would be to first synthesize LDH- NO_3 and then allow the LDH to conduct ion exchange with an environment containing NO_2^- ions. Both the synthesis paths provide different quantities of intercalated NO_2^- in LDH [81].

Another method that is commonly followed is the calcination [82,83] method where LDH is heated to high temperatures in order to remove interlayer water/ OH^- and interlayer anions, thereby losing its layered structures and forming amorphous metallic oxides. Upon rehydration the LDH is able to reconstruct its structure using its “memory effect” property [84] upon exposure to water and also intercalate new anions which were not present in the parent LDH [80]. Apart from these preparation procedures, other methods of synthesis do exist [85,86] and the interested reader is directed to the work of He et al. [80]. LDHs also occur freely in nature. Hydrotalcite is a naturally occurring mineral and belongs to the family of LDH, being known since the 19th century. Chemically, it can be represented as $\text{Mg}_6\text{Al}_2(\text{OH})_{16}[\text{CO}_3]\cdot 4\text{H}_2\text{O}$. It was first discovered in Norway and reported by German-Austrian chemist Carl C. F. Hochstetter in 1842 [87].

LDHs are not strange to concrete chemistry either. The hydration of cement binder is accompanied by the formation of a family of hydrated calcium aluminate phases (AFm) which belong to the broader class of the LDH family. According to Matschei et al. [88], in some blended cements AFm phases content can be up to 20%. AFm phases just like synthetic LDH can be represented by the formula $[\text{Ca}_2(\text{Al}/\text{Fe})\text{OH}_6]\cdot A\cdot x\text{H}_2\text{O}$ with A as the exchangeable anion [89]. AFm phases resembling LDH compounds consist of brucite like sheets with some divalent cations replaced with trivalent cations such as Fe^{3+} or Al^{3+} . Similar to LDH, these AFm show anion exchange capabilities with more affinity

to divalent anions such as CO_3^{2-} , SO_4^{2-} etc. than mono-valent anions Cl^- , OH^- etc. Additions of ground granulated blast furnace slag (GGBFS) as SCM also leads to the production of hydrotalcite like phases [90,91] which has chloride binding properties [92]. Studies of Kayali et al. [93] revealed hydrotalcite formation exists in cement blends with GGBFS. Formation of hydrotalcite lead to reduced chloride ingress due to ion exchange capabilities of these LDH.

4.2. Ion Exchange Property Of LDH

As mentioned previously, the ion exchange property is the most vital property concerning the application of LDH in concrete. Figure 3 (left) depicts the ability of LDH to capture ions from the environment. In this test 1g of LDH was exposed to 50 mM of Cl^- containing solution at time ($t = 0$ s) under stirring conditions. Chloride ion concentration was constantly monitored for 300 s after LDH immersion. It is evident that LDH was able to reduce the Cl^- concentration from the surrounding solution. Figure 3 (right) depicts the ion release property of LDH. In this work from Tedim et al. [94] release of NO_3^- ion from Zn-Al-NO_3 due to step wise exposure to Cl^- ions is presented. This confirms the ion release property of LDH. An in-depth explanation on the ion-exchange property is presented later. Apart from the ion exchange property, LDHs posses numerous other interesting properties which are of vital importance in other branches of science and technology. The interested reader is referred to the extended literature on LDH by Evans et al. [74], Forano et al. [95] and Kuang et al. [96].

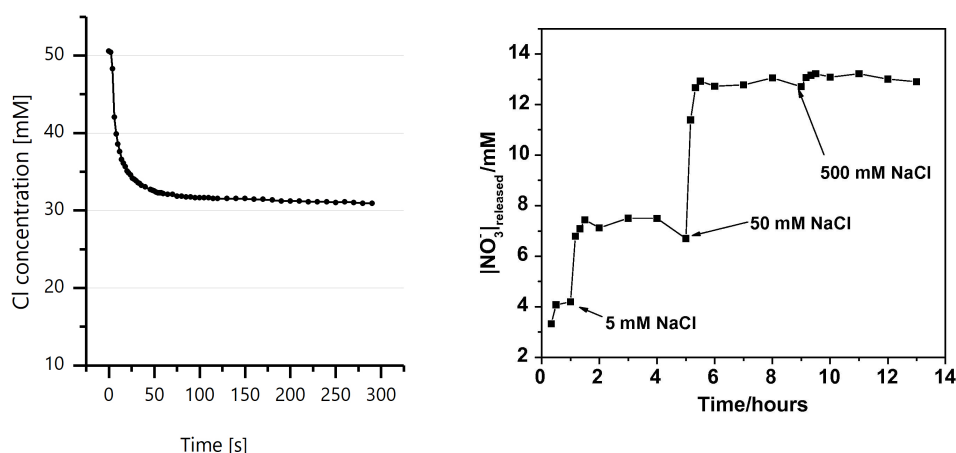


Figure 3. (Left) Decrease in chloride ion concentration due to addition of Zn-Al-NO_2 to the solution containing 50mM of initial chloride concentration. (Right) Release of NO_3^- ion from Zn-Al-NO_3 after exposure to Cl^- ion (reprinted from [94] with permission from Elsevier).

5. Compatibility of Ldh with Cementitious Environments

LDHs have been mostly used in concrete in order to improve its chloride resistance by harnessing the ion exchange property of LDH. However, prior to discussing the ion exchange property and chloride encapsulation of Cl^- by LDH in cement/concrete, it is important to understand the compatibility of LDH with cement. In this section, compatibility with cement, influence on mechanical properties and the effect of dosage on the microstructure are discussed. The discussion is based on a critical analysis of recently published literature in this field.

5.1. Effect on Mechanical Properties

LDH are nanoparticles which are reported to refine the microstructure of concrete without causing a substantial increase in porosity. As LDH is usually added in its powdered form to concrete mixes,

these nanoparticles are uniformly distributed in the matrix and in the course of cement hydration process, LDH can provide additional nucleation sites for cement hydration. This in turn can promote growth of CSH gel into the voids, thereby refining the microstructure. Additionally, the particles themselves act as micro-fillers or micro-aggregates inside the cementitious matrix. Depending on the type of LDH in use, it can have a positive effect on the mechanical properties of concrete especially its compressive strength, see Table 1. LDHs have hexagonal platelet like structures and if they are able to retain their structure in mature concrete, the resulting concrete can also show enhanced flexural strength as these thin LDH platelets can act as micro-beam elements [97] between cementitious materials and therefore help in an efficient transfer of bending stresses. Table 1 presents a compilation of compressive and flexural strength enhancement of concrete together with type of LDH and dosages used by different authors.

Table 1. Effect of addition of LDH on the mechanical properties of concrete. CS: Compressive strength; FS: Flexural strength.

LDH Type	Cement Type	Dosage *	Concrete Properties		Age	Year	Ref.
			CS	FS			
CaAl LDH	CEM 42.5	1–5%	+6% (2%LDH)	-	28d	2009	Xu et al. [98]
MgAl CO ₃	[99]	1–2%	inconclusive	-	28, 48d	2013	Duan et al. [99]
MgAl LDH	[82]	8.5%	~ -2%	-	28d	2014	Yoon et al. [82]
MgAl pAB	CEM I 42.5N	5–10%	-17.2% (10%LDH)	-21.38% (10%LDH)	28d	2015	Yang et al. [100]
MgAl NO ₂	CEM I 42.5N	5–10%	-14.2% (10%LDH)	-19.1% (10%LDH)	28d	2015	Yang et al. [100]
MgAl LDH	[101]	1%	-25% (28d)	-	28–178d	2015	Xiong et al. [101]
LiAl LDH	[102]	1–3%	+25%	-	7d	2017	Haiyan et al. [102]
CaAl NO ₃	CEM I 52.5R	0.5–2 Vol.	+17% (1% LDH)	+55% (1%LDH)	28d	2018	Qu et al. [97]
MgAl CO ₃	CEM I 52.5	1–3%	~+3.5% (3% LDH)	-	28d	2018	Wu et al. [103]
MgAl LDH	[104]	1–2%	+8.2% (1% LDH)	-	56d	2018	Chen et al. [104]
LiAl LDH	[105]	0.5–1.5%	+46.2% (1%LDH)	-	28d	2019	Zou et al. [105]

* In mentioning the dosage, no distinction has been made for LDH added as % of binder content or % of binder replacement or % of total cementitious materials.

From Table 1, it can be observed that Ca based LDH has a profound positive effect on mechanical properties whereas multiple entries report a Mg based LDH to have a negative or inconclusive effect on mechanical properties. Qu et al. [97] used Ca based LDH and observed a strong increase in the compressive strength and flexural strength in samples with LDHs as compared with reference samples. A 17.2% increase in compressive strength was observed in samples with 1% dosage of LDH (mean particle size 3.2 μm) but only 1.7% strength increase for 2% LDH, see Figure 4. It can be inferred that a dosage of up to 2% could be safe for application in concrete and will not drastically affect the compressive strength. Higher dosages can lead to agglomeration of the particles and may not play any significant role in enhancing the strength of concrete. The particle size is also important as smaller particles can have a filler effect and refine microstructure leading to higher compressive strengths despite only a slight change in porosity. In the same study, the flexural strength increased with addition of LDH. The particle size was also a dominating factor as finer the particle, higher was the strength increase. However, as dosage of LDH (mean particle size 3.2 μm) increased from 1% (+55% increase) to 1.5% (+44.3% increase) and 2% (+40.5% increase), the flexural strength started decreasing although still considerable higher \sim >40% than reference sample, see Figure 4. The authors concluded that overall dosages up to 2% can have a positive influence on mechanical properties of concrete. Higher dosages than 2% can be the threshold for particle agglomeration [97].

Contrary to the studies of Qu and colleagues [97], Yang et al. [100] used Mg based LDH (see Table 1) and reported a trend of decreasing compressive strength as dosage of LDH increased, for all specimens at all ages. The strength decrease was still in the acceptable range in samples with up to 5% LDH. The negative effect on compressive strength due to addition of Mg LDH was also reported in the studies of Duan et al. [99]. However the results were found to be inconclusive as with 1% LDH, the compressive strength slightly increased but remained almost the same with 2% LDH. In another

study, Xiong et al. [101] used calcined Mg-Al-LDH and reported a reduced compressive strength for mortars with LDH. A 28d strength test revealed a decrease of about 25% in the compressive strength. Studies by Yoon et al. also reported a slight decrease in compressive strength [82].

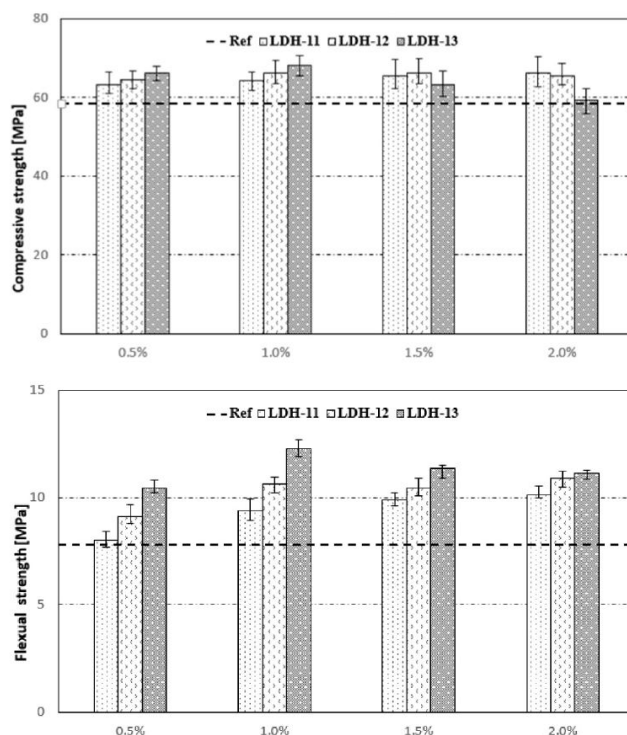


Figure 4. LDH dosage and effect on compressive and flexural strength. LDH-11, LDH-12, LDH-13 refer to mean particle size of 9.5 μm , 6.3 μm and 3.2 μm respectively. Reprinted from [97] with permission from Elsevier.

5.2. Effect of LDH Dosage on Microstructure

Different authors who have worked with LDH have resorted to different dosages of LDHs for applications in concrete. Usually a range of values is evaluated and higher dosages are used with the aim of improving a desired property of concrete or to check the ultimate threshold of the dosage in relation to the desired property. However, while one property might improve, addition of LDH can affect other important properties of mortars and concrete. One of the predominant effects is on porosity as found by Yang et al. [100] where porosity increased with the increasing dosage of LDH. This can have detrimental effect on other associated concrete properties such as chloride penetration. Increase of porosity can lead to faster ingress of chloride ions upon exposure and shorten the corrosion initiation stage. As the porosity increases the chloride ingress can increase despite high chloride binding. It is important to emphasize that more parameter studies must be conducted while selecting a suitable LDH dosage for applications in concrete, as dosage can have a big impact on the properties on concrete mixes.

Previous studies by Qu et al. [97] have revealed that low dosages of LDH do not have a strong influence on porosity increase. They observed that dosages up to 2 vol.%, are a good choice for incorporation of LDHs in concrete. Moreover, additions of nanoparticles like LDH up to a certain dosage can refine the microstructure without changing the total porosity which is advantageous towards chloride durability. This has also been reported by other authors working with nano-additives

for concrete [106,107]. The use of LDH for pore refinement was carried out by Duan et al. [99]. They used Mg-Al-LDH in raw and calcined form in cement pastes and concretes (The dosage is presented in Table 1) and observed pore refinement due to addition of Mg based LDH.

5.3. Effect ON Hydration

LDHs have also been used to modify the hydration kinetics of concrete. It is generally believed that the addition of nano-particles can lower the energy barrier for precipitation reactions taking place in liquid state and also provide additional nucleation sites for cement hydration due to their very small size and very high surface area [98,108,109]. In a recent study, Xu et al. [98] observed by using XRD that adding nano-particles of Ca based LDH accelerated the formation of hydration products, notably CSH. This in turn resulted in a increase of early age strength development. The authors used Ca-Al-Cl LDH in their study and it is well known that both Ca^{2+} and Cl^- are the most accelerating cation and anion respectively [110]. One can therefore attribute the accelerating effect of LDH addition to the role of Ca^{2+} and Cl^- ions. The underlying mechanisms regarding effect of various ion on the hydration kinetics are not fully understood and the reader is directed to the works of Myrdal [110] for further reading.

Additionally, Xu et al. conducted in situ XRD analysis of cement mortars with and without Ca^{2+} based LDH and observed that higher amounts of CSH gel are formed at early ages confirming the strength increase effect and hydration acceleration property of Ca-Al-Cl LDH. XRD analysis revealed higher intensity of CSH peaks occurring at early ages and this effect was amplified as concrete aged, see Figure 5. Li based LDH can also potentially be used to accelerate hydration [105,111] and impart early strength to concrete although the mechanism is unclear. Haiyan et al. [102] observed that setting time was reduced to almost half by using 3% addition of Li based LDH but they did not comment on the working mechanism. Moreover the authors also reported a sharp increase in the early strength development for samples with Li based LDH, see Table 1. Mg-based LDH have also been reported to have a slight accelerating effect on cement hydration. In the studies of Wu et al. [103], the authors observed that a 3% Mg LDH addition had an accelerating effect on cement hydration. They attributed this effect to the reaction of sulphate ions from gypsum with LDH that could potentially accelerate cement hydration.

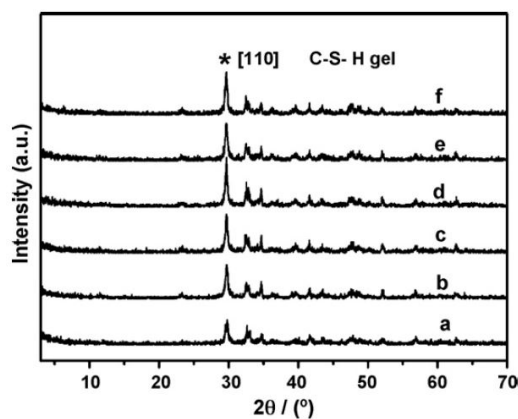


Figure 5. In situ XRD patterns of cement mortar (a) without and (b–f) with LDHs additives after different aging times: (b) 6 min; (c) 1 d; (d) 3 d; (e) 7 d; (f) 28 d. Symbol of * shows the characteristic [1 1 0] reflection peak of C–S–H gel. Reprinted from [98] with permission from Elsevier.

On the other hand, LDH can also decelerate or retard cement hydration. Recent studies by Gomes et al. [25] revealed that addition of ZnAl LDH had a decelerating effect on hydration processes

and early strength development. They used a dosage of 2–5% LDH to cement with an average particle size of 25 μm in cement pastes. The samples depicted an unusually long hardening time. The authors attributed this effect to the partial dissolution of ZnAl LDH in high alkaline pH which releases Zn^{2+} ions in to the pore solution. Zn^{2+} ions are known to have a strong retarding effect on cement hydration [112,113]. The presence of Zn^{2+} ions in the early stages of cement hydration can lead to formation of Zn-Ca complexes such as $\text{Ca}(\text{Zn}(\text{OH})_3)_2 \cdot 2\text{H}_2\text{O}$ which in turn reduce the concentration of Ca^{2+} and OH^- in the pore solution thereby retarding the hydration reactions [114]. Gomes et al. [25] also observed that particle size matters because bigger agglomerates $\sim 125 \mu\text{m}$ did not affect the hydration. This can be understood considering the reduced surface area of bigger agglomerates which do not suffer so significant dissolution as compared to finer particles.

6. Ion Exchange Property and Self Protection of Concrete

LDHs by their nature and unique chemical structure are able to exchange anions present in the external environment by an anion from their inter layers. This process is governed by the difference of chemical potential in the direction of decrease of Gibbs free energy. In order to maintain electro-neutrality, a charge balance is maintained before and after the ion exchange [26,27,81,94,115–124]. This property has been termed as the ion exchange property of LDH [122]. As such LDHs can act as anion adsorbents or anion scavengers, in different environments [125]. Furthermore, as LDHs can be synthesised with different cations and exchangeable anions, this makes them a very versatile class of materials which can be tailored to deliver a desired anion and capture selective ions from the environment. Figure 6 shows a schematic representation of the structure of LDH with interlayer anions. Upon exposure to external anions, the LDH is able to capture these anions and the process is accompanied with the release of interlayer anions. This property has been exploited in corrosion mitigation of concrete structures where functional LDH is used to conduct chloride ion capture and simultaneously deliver a corrosion inhibiting anion. Not only does this prolong/extend the corrosion inhibition stage but also protects the steel from initiating corrosion processes. This dual benefit has been termed as *self-protection* process in concrete.

The ion exchange property of LDH is also used to produce LDH with a desired anion by exposing LDH to a solution of this anion. The desired anion is captured by LDH by replacing the anion originally present in its galleries. The LDH is then usually centrifuged and separated from the filtrate, washed and dried. It must be noted that anion uptake is governed by many factors such as temperature [78], particle size [97], anion type [126,127], anion charge and size [128,129] etc.

Calcined LDH has also been used to conduct ion capture in concrete [103]. Calcination of LDH results in the collapse of the layered structure of LDH. In this process the interlayer anions and the attached $\text{OH}^-/\text{H}_2\text{O}$ molecules are lost. Upon exposure to moisture and external anions, the LDH is able to regenerate its layered structure with new guest anions and water molecules as shown schematically in Figure 6. The use of calcined LDH in concrete is best demonstrated by the work of Duan et al. [130] where authors used calcined Mg LDH to increase the carbonation resistance of concrete and reported very promising results.

During the ion exchange process, the ion uptake is governed by thermodynamics as it represents a heterogeneous equilibrium between chloride ions present in solid species (LDH) and the Cl^- ions present in the pore solution at equilibrium. Studies report that higher the external Cl^- ion concentration, higher is the Cl^- binding due to LDH. As such, the binding behavior can be represented by Freundlich or Langmuir type isotherms (Figure 7 right). In both these isotherms, uptake increases as free chloride ion concentration increases. Furthermore, for each type of LDH, its ion exchange property is governed by many factors. The most important factor ruling ion exchange is the selectivity series for that LDH. LDH is able to conduct preferential ion exchange based on the order of ions in the selectivity series. Chen et al. [131] concluded that for $\text{CaAl}(\text{NO}_3)_3$ LDH in alkaline environment, the selectivity series is $\text{Cl}^- > \text{OH}^- > \text{NO}_3^-$ whereas Costa et al. [127] computationally derived the selectivity series for ZnAl LDH to be $\text{CO}_3^{2-} > \text{OH}^- > \text{F}^- > \text{Cl}^- > \text{Br}^- > \text{NO}_3^-$. Although, in general the

selectivity series governs the ion exchange, the series order might change if the concentration of one of the non-preferential anions is too high in the external environment as compared to the preferred anion in the series. According to the selectivity series, CO_3^{2-} ions are very stable inside LDH and difficult to replace by ion exchange. However, studies by Iyi et al. [60] concluded that LDH containing carbonate ions can even be de-carbonated by a non-preferential anion such as Cl^- , if Cl^- is present in a very high concentration. In this case, the anion present in high concentration can potentially force its uptake. The size of the anion also governs ion uptake as Iyi et al. [60] was not able to replace carbonate ion using a high concentration of iodide ions. The ion exchange property of LDH prefers smaller sized anions over larger anions. However, as the ion exchange is based on charge conservation, LDHs are particularly affine to divalent anions as compared to monovalent anions with carbonate anions being the most preferred anion for most of the LDHs. As such, LDHs have been used to increase the carbonation resistance of concrete [132] as they can efficiently capture carbonate ions.

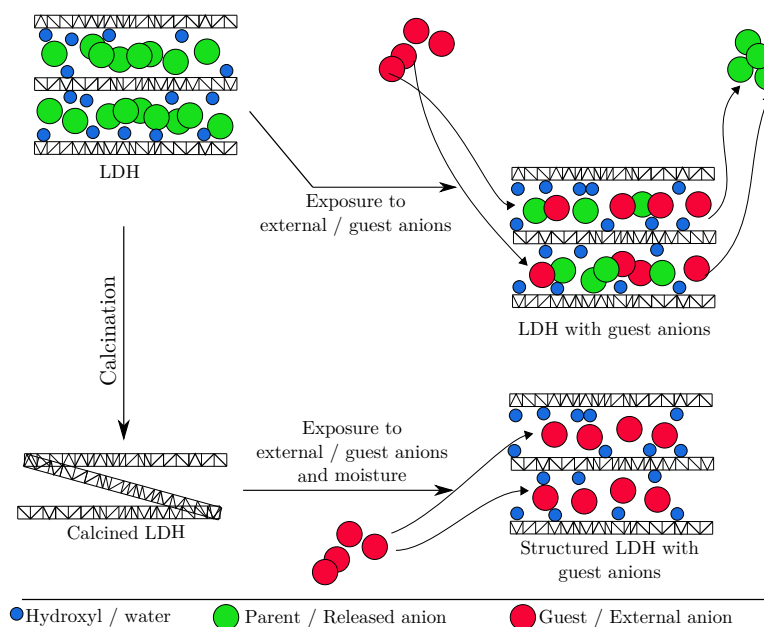


Figure 6. Schematic representation of the LDH structure and ion exchange/capture mechanism.

6.1. Chloride Entrapment and Corrosion Performance

The ion exchange property of LDH has been used extensively in the corrosion protection of concrete. Many authors have used LDH to conduct additional chloride binding in concrete as well as controlled delivery of corrosion inhibiting anions. Numerous applications also report on the use of LDH for mitigation of carbonation induced steel corrosion in concrete. Table 2 presents a list of recent works where LDH has been used as an anion exchanger focusing either on capture of chloride or carbonate ion, as well as delivery of corrosion inhibitor. Based on a detailed literature study summarized in Table 2, only a few of the reported studies are conducted in concrete and literature reports a majority of studies in salt solutions and concrete pore solutions. Table 2 also presents the preparation methods, target application exploiting ion exchange property as well as LDH dosages used. This table can aid researchers and engineers to decide on starting materials and dosages of LDH. Moreover, it is interesting to note the disparity in dosages that different authors have used in various investigations. The reported dosage varies from 0.2 wt.% [133] to 10% [100]. Attention must be paid to avoid high LDH dosage as it can strongly affect the properties of mortars and concrete, as mentioned earlier. Higher dosages can indeed increase the chloride binding capacity as more LDH will be present

to capture Cl^- but on the other hand, higher dosages can certainly increase the porosity of concrete which facilitates Cl^- ingress.

LDH is able to capture Cl^- ions from the pore solutions lessening its concentration. Zhonghe et al. [134] studied Mg-Al- NO_3 and Mg-Al- CO_3 LDH and observed a higher chloride binding capacity when LDH was present. The binding capacity was lower with the carbonate based LDH because this ion is difficult to replace. Yoon et al. [82] used commercially available Mg-Al LDH and calcined it at 450 °C. The resulting LDH was applied as a chloride entrapping additive with a 8.5 wt.% dosage in cement pastes and the authors reported enhanced chloride uptake capabilities. Based on their results, the authors confirmed the positive benefits of LDH in increasing the service life of concrete structures.

Although chloride capture due to LDHs has been mostly due to the ion exchange property, other binding mechanisms do exist. Chen et al. [131] suggested that apart from ion exchange, LDHs are able to bind Cl^- ion following a mechanism of dissolution and recrystallisation, similar in behavior to AFm phases in concrete. The authors concluded that the ion exchange mechanism is the major contributor but it is hard to distinguish between these mechanisms in cementitious environment. The selectivity series were demonstrated to be $\text{Cl}^- > \text{OH}^- > \text{NO}_3^-$. Surface adsorption of ions on LDH surface has also been reported as an uptake mechanism for LDHs. Ke et al. [83] concluded that for hydrotalcite phases in concrete, which also belong to the LDH family, surface adsorption of anions could contribute to 90% uptake capacity and the rest was attributed to ion exchange.

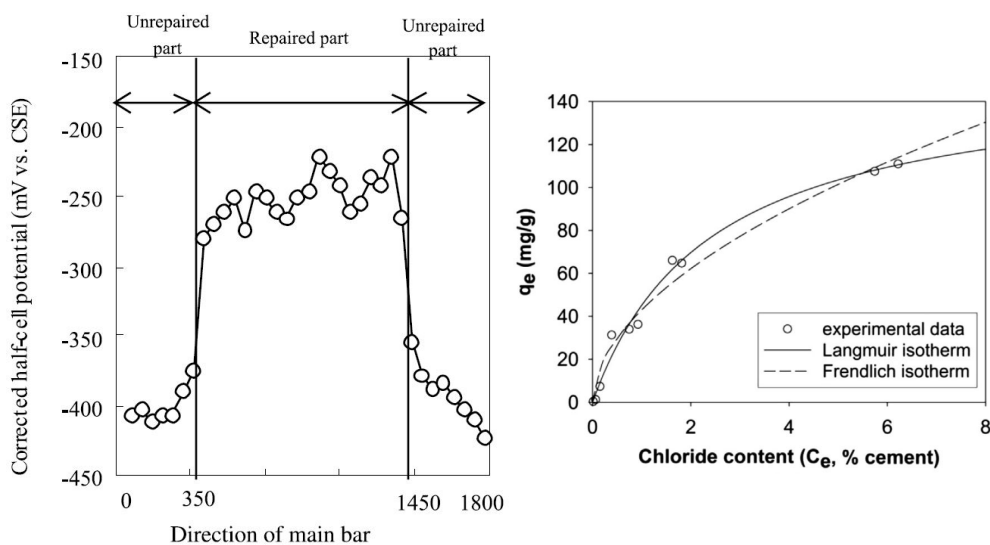


Figure 7. (Left) Figure shows steel with protective potential in the repaired part containing LDH with corrosion inhibitor (reprinted from [133] with permission from Elsevier). (Right) Experimental and fitted isotherms, both Langmuir and Freundlich for chloride uptake by LDH in cement paste (reprinted from [82] with permission from Elsevier).

One of the best real life tests on the use of LDHs in concrete structural members was carried out by Tatematsu et al. [133]. In their study, a concrete slab was used as a test specimen. A central portion of the slab was retrofitted with a reinforcement cover made of mortar with Ca-Al- NO_2 as additive. They applied LDH as a 1 mm coat on rebars and then added LDH with mortar to form a 15 mm cover on top. Other parts of the specimen did not contain additive. The specimen was left in an exposure site for seven years. After seven years, the regions with Ca-Al- NO_2 showed no signs of corrosion and more positive potentials whereas the surrounding regions were corroding as shown in Figure 7

(left). Secondary reinforcement was also affected in the non-protected areas. The authors observed a macro-cell on the interface of protected and non-protected areas.

As mentioned previously, AFm phases in concrete also belong to LDH family and are responsible for the majority of the chloride binding [49,51,135,136]. The exchange mechanism is mostly believed to be ion exchange [135,137]. AFm phases just like synthetic LDHs lead to the formation of Friedel's salt and Kuzel's salt upon exposure to chloride [53,138]. The conversion of Hydroxy-AFm to Friedel's salt upon exposure to NaCl was stated to be a dominating chloride uptake mechanism by Jones et al. [139]. The Cl^- uptake was observed to be followed by a delivery of OH^- ion from AFm phases [140]. Hirao et al. [141] experiments on chloride uptake revealed a Freundlich type isotherm for chloride uptake, signifying that uptake capacity would improve as the external concentration increases. It can therefore be concluded that AFm phases in general contribute considerably to the inherent chloride binding capacity of concrete via ion exchange mechanism [142].

The dual benefit of self-protection of reinforced concrete can be achieved by the capture of Cl^- ion and simultaneous release of a corrosion inhibiting ion. LDHs can be easily loaded with corrosion inhibiting ions. The use of NO_2^- as a corrosion inhibitor has been well documented [143,144] and also NO_2^- can be easily incorporated into LDH. However, it is important to note that the inhibitive action takes place only at the steel-concrete interface. The nitrite ions released in the bulk will have to transport themselves to the steel-concrete interface. On the other hand, LDH loaded with inhibiting ions can also be applied as a cement slurry coating on the rebar surface prior to embedment. Yang et al. [145], applied a coating of 20 wt.% LDH on the reinforcing steel and reported an extended time regarding depassivation of steel. The combined role of chloride capture from the pore solution and inhibitor delivery can be represented as



Use of NO_2^- ion in corrosion inhibition was previously tested by Dry [146] who used $\text{Ca}(\text{NO}_2)_2$ in concrete and reported a delay in corrosion as compared to control samples. Gomes et al. [25] used LDH loaded with NO_2^- ion with the aim of capturing Cl^- ion and releasing NO_2^- ion and reported positive results.

Many authors [25,100] have conducted natural diffusion test on concrete with added LDH in order to ascertain the enhanced chloride capture in such mixes. Yang et al. [100] conducted a rapid chloride migration tests on concrete with and without LDH. Two levels of LDH were used, namely 5% and 10% for two LDH types as shown in Figure 8. Samples with 5% Mg-Al-PAB(p-aminobenzoate) demonstrated improved chloride resistance as compared to other dosages of LDH. The authors concluded that higher dosages could possibly bind more chloride but at the same time also increase the porosity which has a counter effect on chloride transport in concrete.

Chloride diffusion test were also conducted by Qu et al. [97] with 0.5%, 1% and 2% by volume LDH dosage. They observed excellent chloride resistance of concrete for an optimum 1% LDH dosage. A 25% reduction of D_{RCM} (rapid chloride migration coefficient) was found for this dosage as compared to reference. The study also included natural diffusion test and demonstrated a 53% reduction in apparent diffusion coefficient. The authors explained their observations by the physical barrier properties of LDH particles acting as a filler material. This effect was complemented by chemical inhibition i.e., anion exchange property of LDH. The low dosages of up to 2% did not seem to cause any unnecessary porosity increase which is detrimental towards chloride resistance. Moreover, it was considered that smaller particles of LDH can improve the tortuosity of the cementitious matrix without actually influencing the porosity so much.

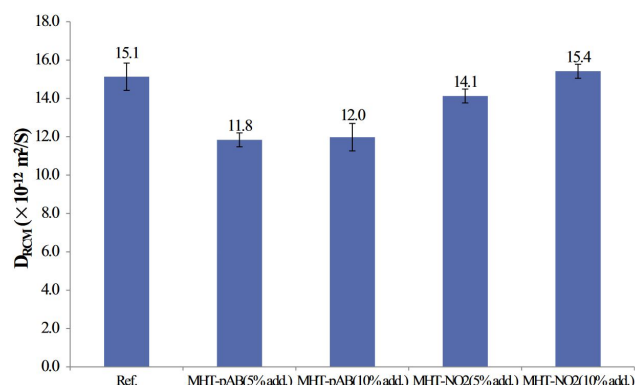


Figure 8. Chloride diffusion coefficients of mortar with 5% and 10% dosage of LDH. (Reprinted from [100], with permission from Elsevier).

6.2. Role of Ldh in Carbonation Control

It is well understood that the CO_3^{2-} form of LDH is the most stable because LDH has a preference to multivalent ions than monovalent ions [83]. Due to this very fact, LDH has also been used to improve the carbonation resistance of concrete [147,148]. In a recent work by Ma et al. [61], cement pastes with 2% Mg based LDH showed reduced carbonation depth as compared with reference samples. They observed a 30% reduction in carbonation depth at 42 day age. Similar findings were also reported by Shui et al. [132]. This highlights the positive benefits of employing LDH in carbonation control of structures.

The high affinity of LDH towards carbonate ions can have a negative impact on chloride binding capacity of LDH. It is important to note that, if the LDH was previously exposed to Cl^- ions and has bound Cl^- ions, it might release these bound chlorides upon exposure to carbonates, since uptake of carbonate ions is preferred over chlorides [83]. Ke et al. [83] studied the chloride uptake by Mg-Al based and Strätlingite in carbonated and non-carbonated salt solutions. They reported that chloride uptake decreases as concentration of carbonate increased. Kayali et al. [58] concluded that carbonation is a risk because Cl^- can be replaced with CO_3^{2-} , thereby inducing risk of accelerated steel corrosion. However under certain circumstances, LDH can be decarbonated and exchanged with other anions. Iyi et al. [60] was able to exchange Cl^- with CO_3^{2-} calling it the “decarbonation” of LDH under high concentrations of externally present Cl^- . The study was extended to other anions as well but it was observed that only small ions such as Cl^- and Br^- are able to exchange themselves with CO_3^{2-} . Much less or insignificant exchange was observed for larger anions such as NO_3^- and ClO_4^- . The anion size effect was also demonstrated by Miyata [126].

Table 2. Reported LDH types and their application in the literature together with preparation and experimental details. Abbreviations are mentioned in the end of the text. SS: Salt solution; PS: Pore solution; CP: Cement Paste; M: Mortar; C: Concrete

LDH	Experiments Conducted in				Preparation Method	Dosage +		Application	Year / Ref.
	SS	PS	CP	M		C	SS / PS		
CaAlNO ₂	-	-	✓	✓	-	-	0.2 wt. %	Cl ⁻ uptake & Corr. inhibition	2003 / [133]
MgAlNO ₃	✓	-	✓	-	-	1 g/10 mL	1 wt. %	Cl ⁻ uptake	2012 / [134]
MgAlCO ₃	✓	-	✓	-	-	1 g/10 mL	1 wt. %	Cl ⁻ uptake	2012 / [134]
hydrocalcite	✓	-	-	-	calcination	8–16 g/80 mL	-	Cl ⁻ uptake	2012 / [93]
MgAlNO ₃	-	-	-	✓	-	-	0.5–3 wt. %	Cl ⁻ uptake	2012 / [149]
MgAlLDH	✓	-	✓	-	calcination	-	8.5 wt. %	Cl ⁻ uptake	2014 / [82]
MgAlCO ₃	-	-	✓	✓	-	-	1–2 wt. %	Cl ⁻ / CO ₃ ²⁻ uptake & Pore ref.	2013 / [99]
CaAl-pAB	-	✓	-	-	Ion-exchange	0.5 g/10 mL	-	Cl ⁻ uptake	2014 / [150]
CaAlNO ₃	-	✓	-	-	co-precipitation	0.5 g/10 mL	-	Cl ⁻ uptake	2014 / [150]
CaAlNO ₃	✓	✓	✓	-	co-precipitation	1 g/100 mL	8.5 wt. %	Cl ⁻ uptake	2015 / [131]
MgAl-pAB	-	-	-	✓	calcination-rehydration [151]	-	5–10 wt. %	Cl ⁻ uptake	2015 / [100]
MgAl-NO ₂	-	-	-	✓	calcination-rehydration [151]	-	5–10 wt. %	Cl ⁻ uptake	2015 / [100]
MgAlLDH	-	-	-	✓	calcination	-	1 wt. %	Cl ⁻ uptake & bond stress	2015 / [101]
Strätlingite	-	✓	-	-	[152]	0.4 g/40 g	-	Cl ⁻ / CO ₃ ²⁻ uptake	2017 / [83]
MgAlLDH	-	✓	-	-	calcination	0.4 g/40 g	-	Cl ⁻ / CO ₃ ²⁻ uptake	2017 / [83]
MgAlNO ₃	-	✓	✓	-	calcination-rehydration	0.5 g/20 mL	0–10%(M), 20 wt.%(CP)	Cl ⁻ uptake & Corr. inhibition	2017 / [145]
MgAl-pAB	-	✓	✓	-	calcination-rehydration	0.5 g/20 mL	0–10%(M), 20 wt.%(CP)	Cl ⁻ uptake & Corr. inhibition	2017 / [145]
CaAlNO ₃	-	-	-	✓	co-precipitation	-	0.5–2 vol. %	Cl ⁻ uptake	2018 / [97]
MgAlCO ₃	-	-	-	✓	calcination, other [130]	-	2 wt. %	CO ₃ ²⁻ uptake	2018 / [130]
MgAlLDH	-	-	-	✓	calcination, other [132]	-	2–4 wt. %	CO ₃ ²⁻ uptake	2018 / [132]
MgAlNO ₂	-	✓	-	-	Ion-exchange	1 g/10 mL, 1–2 wt. %	-	Cl-uptake & Corr. inhibition	2018 / [153]
MgAlNO ₃	-	✓	-	-	co-precipitation	1 g/10 mL, 1–2 wt. %	-	Cl ⁻ uptake	2018 / [153]
MgAlLDH	-	-	✓	-	calcination	-	1–2 wt. %	Cl ⁻ uptake	2018 / [104]
CaAlLDH	✓	-	-	✓	co-precipitation	50 g/L	10 wt. %	Cl ⁻ uptake	2019 / [154]
ZnAlNO ₂ /NO ₃	✓	-	✓	-	co-precipitation	1 g/50 mL	2–5 wt. %	Cl ⁻ uptake & Corr. inhibition	2019 / [24,25]
MgAlCO ₃	-	-	-	✓	calcination	-	2 wt. %	CO ₃ ²⁻ uptake	2019 / [61]

+ In mentioning the dosage in cement paste, mortars and concrete, no distinction has been made for LDH added as % of binder content or % of binder replacement or % of total cementitious materials.

7. Conclusions

In this study a review on the applications of LDH in concrete is presented. The main advantage of using LDH in concrete is to improve the chloride and carbonation resistance of concrete. This can consequently extend the service life of concrete structures exposed to corrosive environments. In this aspect, this review presents many recent studies reporting on the application of LDH not only in pore solutions but also in concretes, mortars and pastes. The review also showcases that even though LDH addition is primarily aimed to improve chloride/carbonation resistance, its addition can also affect hydration, strength, microstructure and other properties of concrete. Additionally, recommendations on LDH dosage are presented. In general, this review should aid scientists and engineers to develop a basic understanding on the use of LDH as an engineering material and help in the design of experiments and be able to foresee main results. Depending of the type of LDH as starting material, quantitative and qualitative effects on desired property as well as associated properties of concrete are presented, trends are identified and selected results are discussed. A compilation of focused results are presented in text as well as in tables, highlighting the benefits of LDH as well as details of the experiments and main results.

The ion exchange property of LDH has been widely exploited in concrete technology with a majority of applications aimed towards increasing the chloride and carbonation resistance of concrete. Although the underlying mechanics for these applications are well researched and thoroughly discussed in this text, many other mechanisms are still not fully clear and vary with the type of LDH, such as, the effect of increase of compressive strength and flexural strength upon addition of LDH, as well as acceleration of hydration kinetics. Moreover, there is no general consensus on the optimum dosage of LDH in concrete, although a 2% dosage has been identified as the threshold of LDH addition from the presented literature. A higher dosage can cause agglomeration of particles and have a profound effect on key properties such as chloride durability and compressive strength.

Despite the recent advances in the application of LDH in concrete technology, many issues stay unresolved and need further understanding. Firstly, the stability of LDH particles inside concrete is not well understood and needs more research in the future. Higher pH of fresh concrete can potentially cause partial dissolution of LDH particles which can in turn reduce their functionality. Apart from that, particle size is a very important parameter as finer particles exhibit more surface area than coarse particles. It has been reported that particle size effects LDH functionality as well as some vital concrete properties. Very few studies have reported on these issues and more research is required in this area. Additionally, one important factor is the economic aspect of using LDH as a concrete additive and not much information is available on the cost of LDH and its carbon footprint. These two factors are very important for acceptance of LDH in the concrete infrastructure market. Dismantling buildings made with nano-particles can be dangerous as there is the chance that these nano particles might be released in the environment. Therefore, proper guidelines should be made available to building engineers and these buildings should be classified for easy recognition in the distant future. More research must be conducted on the interaction of humans against long term exposure to LDH. All these points need more efforts and extensive research.

However, the authors strongly believe that LDH due to its unique chemistry, versatile combinations, facile preparation and ease of incorporation into concrete, will be used more in the future to produce smart concrete structures. To make LDH a promising concrete additive, more research should be focused towards their application in concrete. One of the biggest foreseeable benefit of using LDH in concrete is the enhanced chloride/carbonate binding effect, although other notable benefits have been presented. This class of additive can result in smart structures which can potentially show extended service life and can directly result in a substantial economic benefit in the global infrastructure market.

Author Contributions: Z.M.M. and M.L.Z. proposed the concept behind the study. Z.M.M. and A.B. did the literature study and co-wrote the script. A.B., M.L.Z. and D.H. revised the script, provided critical comments and supervised the work. All authors have read and agreed to the published version of the manuscript.

Funding: This research has received funding from the European Union’s Horizon 2020 research and innovation program under grant agreement No: 685445 (LORCENIS—Long Lasting Reinforced Concrete for Energy infrastructure under Severe Operating Conditions).

Acknowledgments: Ralf T. Schmitt, Museum für Naturkunde Berlin.

Conflicts of Interest: The authors declare no conflicts of interest.

Abbreviations

The following abbreviations are used in this manuscript:

LDH	Layered Double Hydroxide
CSE	Copper sulphate electrode
pAB	P-aminobenzoate
C ₃ A	tricalcium aluminate
C ₄ AF	tetracalcium aluminoferrite
AFm	aluminoferrite monosulphate
CSH	calcium silicate hydrate

References

1. DESA; UN. *World Population Prospects 2019: Highlights*; United Nations Department for Economic and Social Affairs: New York, NY, USA, 2019.
2. Mehta, P.K. Greening of the concrete industry for sustainable development. *Concr. Int.* **2002**, *24*, 23–28.
3. Huntzinger, D.N.; Eatmon, T.D. A life-cycle assessment of Portland cement manufacturing: Comparing the traditional process with alternative technologies. *J. Clean. Prod.* **2009**, *17*, 668–675. [[CrossRef](#)]
4. Uwasu, M.; Hara, K.; Yabar, H. World cement production and environmental implications. *Environ. Dev.* **2014**, *10*, 36–47. [[CrossRef](#)]
5. Kim, Y.; Worrell, E. CO₂ emission trends in the cement industry: An international comparison. *Mitig. Adapt. Strateg. Glob. Chang.* **2002**, *7*, 115–133. [[CrossRef](#)]
6. Chen, C.; Habert, G.; Bouzidi, Y.; Jullien, A. Environmental impact of cement production: Detail of the different processes and cement plant variability evaluation. *J. Clean. Prod.* **2010**, *18*, 478–485. [[CrossRef](#)]
7. Tuutti, K. *Corrosion of Steel in Concrete - (Technical Report)*; Cement-och Betonginst CBI Sweden: Stockholm, Sweden, 1982.
8. Bertolini, L.; Elsener, B.; Pedferri, P.; Redaelli, E.; Polder, R. *Corrosion of Steel in Concrete*; Wiley-Vch.: Weinheim, Germany, 2013; Volume 392.
9. Broomfield, J.P. *Corrosion of Steel in Concrete: Understanding, Investigation and Repair*; CRC Press: Boca Raton, FL, USA, 2003.
10. Poursaeed, A. Corrosion of steel in concrete structures. In *Corrosion of Steel in Concrete Structures*; Elsevier: Amsterdam, The Netherlands, 2016; pp. 19–33.
11. Raupach, M.; Elsener, B.; Polder, R.; Mietz, J. *Corrosion of Reinforcement in Concrete: Monitoring, Prevention and Rehabilitation Techniques*; Woodhead Publishing: Sawston, UK, 2014; Volume 38.
12. Lewis, D.; Copenhagen, W. Corrosion of reinforcing steel in concrete in marine atmospheres. *Corrosion* **1959**, *15*, 60–66. [[CrossRef](#)]
13. Hausmann, D. Steel corrosion in concrete—How does it occur? *Mater. Prot.* **1967**, *6*, 19–23.
14. Page, C. Mechanism of corrosion protection in reinforced concrete marine structures. *Nature* **1975**, *258*, 514. [[CrossRef](#)]
15. Cai, H.; Liu, X. Freeze-thaw durability of concrete: Ice formation process in pores. *Cem. Concr. Res.* **1998**, *28*, 1281–1287. [[CrossRef](#)]
16. Berto, L.; Saetta, A.; Talledo, D. Constitutive model of concrete damaged by freeze-thaw action for evaluation of structural performance of RC elements. *Constr. Build. Mater.* **2015**, *98*, 559–569. [[CrossRef](#)]
17. Huovinen, S. *Abrasion of Concrete by Ice in Arctic Sea Structures*; Technical Research Centre of Finland: Espoo, Finland, 1990.
18. Jacobsen, S.; Scherer, G.W.; Schulson, E.M. Concrete–ice abrasion mechanics. *Cem. Concr. Res.* **2015**, *73*, 79–95. [[CrossRef](#)]

19. Ryan, A. Ice Wear and Abrasion of Marine Concrete: Design of Experimental Apparatus and Procedures. Ph.D. Thesis, Memorial University of Newfoundland, St. John's, NL, Canada, 2018.
20. Marchand, J.; Odler, I.; Skalny, J.P. *Sulfate Attack on Concrete*; CRC Press: Boca Raton, FL, USA, 2001.
21. Attiogbe, E.K.; Rizkalla, S.H. Response of concrete to sulfuric acid attack. *ACI Mater. J.* **1988**, *85*, 481–488.
22. Glass, G.; Buenfeld, N. Chloride-induced corrosion of steel in concrete. *Prog. Struct. Eng. Mater.* **2000**, *2*, 448–458. [[CrossRef](#)]
23. Angst, U.M. Challenges and opportunities in corrosion of steel in concrete. *Mater. Struct.* **2018**, *51*, 4. [[CrossRef](#)]
24. Gomes, C.; Mir, Z.; Sampaio, R.S.; Bastos, A.; Maia, F.; Rocha, C.; Tedim, J.; Ferreira, M. Effect of Layered Double Hydroxides on the Performance and Service Life of Reinforced Concrete. In *Durable Concrete for Infrastructure under Severe Conditions Smart Admixtures, Self-Responsiveness and Nano-Additions Proceedings 10–11 September 2019*; Ghent: Ghent University, Ghent, Belgium, 2019; pp. 51–54.
25. Gomes, C.; Mir, Z.; Sampaio, R.S.; Bastos, A.; Tedim, J.; Maia, F.; Rocha, C.; Ferreira, M. On the use of ZnAl layered double hydroxide (LDH) to extend the service life of reinforced concrete. *Front. Mater.* (in review).
26. Raki, L.; Beaudoin, J.; Mitchell, L. Layered double hydroxide-like materials: Nanocomposites for use in concrete. *Cem. Concr. Res.* **2004**, *34*, 1717–1724. [[CrossRef](#)]
27. Yang, Z.; Fischer, H.; Polder, R. Modified hydrotalcites as a new emerging class of smart additive of reinforced concrete for anticorrosion applications: A literature review. *Mater. Corros.* **2013**, *64*, 1066–1074. [[CrossRef](#)]
28. Yang, Z.; Fischer, H.; Polder, R. Possibilities for improving corrosion protection of reinforced concrete by modified hydrotalcites—a literature review. In *Advances in Modeling Concrete Service Life*; RILEM Bookseries, vol 3. Springer: Dordrecht, The Netherlands, 2012; pp. 95–105.
29. USGS. *Cement: 2007 Minerals Yearbook - US. Geological Survey*; USGS: Reston, VA, USA, 2010.
30. Gagg, C.R. Cement and concrete as an engineering material: An historic appraisal and case study analysis. *Eng. Fail. Anal.* **2014**, *40*, 114–140. [[CrossRef](#)]
31. Poursaee, A.; Hansson, C. Reinforcing steel passivation in mortar and pore solution. *Cem. Concr. Res.* **2007**, *37*, 1127–1133. [[CrossRef](#)]
32. Ghods, P.; Isgor, O.; McRae, G.; Li, J.; Gu, G. Microscopic investigation of mill scale and its proposed effect on the variability of chloride-induced depassivation of carbon steel rebar. *Corros. Sci.* **2011**, *53*, 946–954. [[CrossRef](#)]
33. Andrade, C.; Merino, P.; Novoa, X.; Perez, M.; Soler, L. Passivation of reinforcing steel in concrete. In *Materials Science Forum*; Trans Tech Publications Ltd: Stafa-Zurich, Switzerland, 1995; Volume 192, pp. 891–898.
34. Saremi, M.; Mahallati, E. A study on chloride-induced depassivation of mild steel in simulated concrete pore solution. *Cem. Concr. Res.* **2002**, *32*, 1915–1921. [[CrossRef](#)]
35. Ghods, P.; Isgor, O.; McRae, G.; Miller, T. The effect of concrete pore solution composition on the quality of passive oxide films on black steel reinforcement. *Cem. Concr. Compos.* **2009**, *31*, 2–11. [[CrossRef](#)]
36. Ghods, P.; Isgor, O.; Carpenter, G.; Li, J.; McRae, G.; Gu, G. Nano-scale study of passive films and chloride-induced depassivation of carbon steel rebar in simulated concrete pore solutions using FIB/TEM. *Cem. Concr. Res.* **2013**, *47*, 55–68. [[CrossRef](#)]
37. Lian, C.; Zhuge, Y.; Beecham, S. The relationship between porosity and strength for porous concrete. *Constr. Build. Mater.* **2011**, *25*, 4294–4298. [[CrossRef](#)]
38. Angst, U.M.; Geiker, M.R.; Michel, A.; Gehlen, C.; Wong, H.; Isgor, O.B.; Elsener, B.; Hansson, C.M.; François, R.; Hornbostel, K.; et al. The steel–concrete interface. *Mater. Struct.* **2017**, *50*, 143. [[CrossRef](#)]
39. Alonso, C.; Andrade, C.; Castellote, M.; Castro, P. Chloride threshold values to depassivate reinforcing bars embedded in a standardized OPC mortar. *Cem. Concr. Res.* **2000**, *30*, 1047–1055. [[CrossRef](#)]
40. Angst, U.; Elsener, B.; Larsen, C.K.; Vennesland, Ø. Critical chloride content in reinforced concrete—A review. *Cem. Concr. Res.* **2009**, *39*, 1122–1138. [[CrossRef](#)]
41. Suda, K.; Misra, S.; Motohashi, K. Corrosion products of reinforcing bars embedded in concrete. *Corros. Sci.* **1993**, *35*, 1543–1549. [[CrossRef](#)]
42. Molina, F.; Alonso, C.; Andrade, C. Cover cracking as a function of rebar corrosion: Part 2—Numerical model. *Mater. Struct.* **1993**, *26*, 532–548. [[CrossRef](#)]
43. Sola, E.; Ožbolt, J.; Balabanić, G.; Mir, Z. Experimental and numerical study of accelerated corrosion of steel reinforcement in concrete: Transport of corrosion products. *Cem. Concr. Res.* **2019**, *120*, 119–131. [[CrossRef](#)]

44. Sola, E. Experimental and Numerical Study of Chloride Induced Corrosion in Reinforced Concrete. Ph.D. Thesis, University of Stuttgart, Stuttgart, Germany, 2017.
45. Ožbolt, J.; Oršanić, F.; Balabanić, G. Modeling influence of hysteretic moisture behavior on distribution of chlorides in concrete. *Cem. Concr. Compos.* **2016**, *67*, 73–84. [[CrossRef](#)]
46. Yuan, Q.; Shi, C.; De Schutter, G.; Audenaert, K.; Deng, D. Chloride binding of cement-based materials subjected to external chloride environment—a review. *Constr. Build. Mater.* **2009**, *23*, 1–13. [[CrossRef](#)]
47. Arya, C.; Buenfeld, N.; Newman, J. Factors influencing chloride-binding in concrete. *Cem. Concr. Res.* **1990**, *20*, 291–300. [[CrossRef](#)]
48. Page, C.L. Initiation of chloride-induced corrosion of steel in concrete: Role of the interfacial zone. *Mater. Corros.* **2009**, *60*, 586–592. [[CrossRef](#)]
49. Justnes, H. A review of chloride binding in cementitious systems. *Nord. Concr. Res. Publ.* **1998**, *21*, 48–63.
50. Neville, A. Chloride attack of reinforced concrete: An overview. *Mater. Struct.* **1995**, *28*, 63. [[CrossRef](#)]
51. Florea, M.; Brouwers, H. Chloride binding related to hydration products: Part I: Ordinary Portland Cement. *Cem. Concr. Res.* **2012**, *42*, 282–290. [[CrossRef](#)]
52. Suryavanshi, A.; Scantlebury, J.; Lyon, S. Mechanism of Friedel’s salt formation in cements rich in tri-calcium aluminate. *Cem. Concr. Res.* **1996**, *26*, 717–727. [[CrossRef](#)]
53. Zibara, H. Binding of External Chlorides by Cement Pastes. Ph.D. Thesis, National Library of Canada=Bibliothèque nationale du Canada, Ottawa, ON, Canada, 2001.
54. Traetteberg, A. The mechanism of chloride penetration in concrete. *SINTEF Rep. STF65 A* **1977**, 77070, 1977.
55. Luping, T.; Nilsson, L.O. Chloride binding capacity and binding isotherms of OPC pastes and mortars. *Cem. Concr. Res.* **1993**, *23*, 247–253. [[CrossRef](#)]
56. Al-Hussaini, M.; Sangha, C.; Plunkett, B.; Walden, P. The effect of chloride ion source on the free chloride ion percentages in OPC mortars. *Cem. Concr. Res.* **1990**, *20*, 739–745. [[CrossRef](#)]
57. Juenger, M.C.; Siddique, R. Recent advances in understanding the role of supplementary cementitious materials in concrete. *Cem. Concr. Res.* **2015**, *78*, 71–80. [[CrossRef](#)]
58. Kayali, O.; Ahmed, M.; Khan, M. Friedel’s salt and hydrotalcite-layered double hydroxides and the protection against chloride induced corrosion. *Civ. Envir. Res* **2013**, *5*, 111–117.
59. Dhir, R.; El-Mohr, M.; Dyer, T. Chloride binding in GGBS concrete. *Cem. Concr. Res.* **1996**, *26*, 1767–1773. [[CrossRef](#)]
60. Iyi, N.; Okamoto, K.; Kaneko, Y.; Matsumoto, T. Effects of anion species on deintercalation of carbonate ions from hydrotalcite-like compounds. *Chem. Lett.* **2005**, *34*, 932–933. [[CrossRef](#)]
61. Ma, J.; Duan, P.; Ren, D.; Zhou, W. Effects of layered double hydroxides incorporation on carbonation resistance of cementitious materials. *J. Mater. Res. Technol.* **2019**, *8*, 292–298. [[CrossRef](#)]
62. Alcantara, A.; Aranda, P.; Darder, M.; Ruiz-Hitzky, E. Bionanocomposites based on alginate–zein/layered double hydroxide materials as drug delivery systems. *J. Mater. Chem.* **2010**, *20*, 9495–9504. [[CrossRef](#)]
63. Bejoy, N. Hydrotalcite. *Resonance* **2001**, *6*, 57–61. [[CrossRef](#)]
64. Kwak, S.Y.; Jeong, Y.J.; Park, J.S.; Choy, J.H. Bio-LDH nanohybrid for gene therapy. *Solid State Ionics* **2002**, *151*, 229–234. [[CrossRef](#)]
65. Cai, P.; Zheng, H.; Wang, C.; Ma, H.; Hu, J.; Pu, Y.; Liang, P. Competitive adsorption characteristics of fluoride and phosphate on calcined Mg–Al–CO₃ layered double hydroxides. *J. Hazard. Mater.* **2012**, *213*, 100–108. [[CrossRef](#)]
66. Kameda, T.; Takeuchi, H.; Yoshioka, T. Uptake of heavy metal ions from aqueous solution using Mg–Al layered double hydroxides intercalated with citrate, malate, and tartrate. *Sep. Purif. Technol.* **2008**, *62*, 330–336. [[CrossRef](#)]
67. Lv, L.; He, J.; Wei, M.; Evans, D.; Duan, X. Uptake of chloride ion from aqueous solution by calcined layered double hydroxides: Equilibrium and kinetic studies. *Water Res.* **2006**, *40*, 735–743. [[CrossRef](#)] [[PubMed](#)]
68. Douglas, G.; Wendling, L.; Pleysier, R.; Trefry, M. Hydrotalcite formation for contaminant removal from Ranger mine process water. *Mine Water Environ.* **2010**, *29*, 108–115. [[CrossRef](#)]
69. Alvarez, D.; Collazo, A.; Hernández, M.; Nóvoa, X.R.; Pérez, C. Corrosion protective properties of hydrotalcites doped hybrid sol-gel coatings on aluminium substrates. In *Materials Science Forum*; Trans Tech Publications Ltd: Stafa-Zurich, Switzerland, 2010; Volume 636, pp. 996–1003.
70. Wajima, T.; Shimizu, T.; Ikegami, Y. New simple process of making agricultural cultivation solution from seawater. *Bull. Soc. Sea Water Sci. Jpn.* **2006**, *60*, 201–202.

71. Mohapatra, L.; Parida, K. Zn–Cr layered double hydroxide: Visible light responsive photocatalyst for photocatalytic degradation of organic pollutants. *Sep. Purif. Technol.* **2012**, *91*, 73–80. [[CrossRef](#)]
72. Peng, C.; Yu, J.; Zhao, Z.; Dai, J.; Fu, J.; Zhao, M.; Wang, W. Synthesis and properties of a clean and sustainable deicing additive for asphalt mixture. *PLoS ONE* **2015**, *10*, e0115721. [[CrossRef](#)] [[PubMed](#)]
73. Rives, V. *Layered Double Hydroxides: Present and Future*; Nova Publishers: Hauppauge, NY, USA, 2001.
74. Duan, X.; Evans, D.G. *Layered Double Hydroxides*; Springer Science & Business Media: Berlin/Heidelberg, Germany, 2006; Volume 119.
75. Bontchev, R.P.; Liu, S.; Krumhansl, J.L.; Voigt, J.; Nenoff, T.M. Synthesis, characterization, and ion exchange properties of hydrotalcite $Mg_6Al_2(OH)_{16}(A)_x(A')_{2-x} \cdot 4H_2O$ ($A, A' = Cl^-, Br^-, I^-, \text{and } NO_3^-$, $2 \geq x \geq 0$) derivatives. *Chem. Mater.* **2003**, *15*, 3669–3675. [[CrossRef](#)]
76. Newman, S.P.; Jones, W. Comparative study of some layered hydroxide salts containing exchangeable interlayer anions. *J. Solid State Chem.* **1999**, *148*, 26–40. [[CrossRef](#)]
77. Newman, S.P.; Jones, W. Synthesis, characterization and applications of layered double hydroxides containing organic guests. *New J. Chem.* **1998**, *22*, 105–115. [[CrossRef](#)]
78. Lv, L.; Sun, P.; Gu, Z.; Du, H.; Pang, X.; Tao, X.; Xu, R.; Xu, L. Removal of chloride ion from aqueous solution by ZnAl-NO₃ layered double hydroxides as anion-exchanger. *J. Hazard. Mater.* **2009**, *161*, 1444–1449. [[CrossRef](#)]
79. de Sá, F.P.; Cunha, B.N.; Nunes, L.M. Effect of pH on the adsorption of Sunset Yellow FCF food dye into a layered double hydroxide (CaAl-LDH-NO₃). *Chem. Eng. J.* **2013**, *215*, 122–127. [[CrossRef](#)]
80. He, J.; Wei, M.; Li, B.; Kang, Y.; Evans, D.G.; Duan, X. Preparation of layered double hydroxides. In *Layered Double Hydroxides*; Springer-Verlag: Berlin, Heidelberg, Germany, 2006; pp. 89–119.
81. Zuo, J.; Wu, B.; Luo, C.; Dong, B.; Xing, F. Preparation of MgAl layered double hydroxides intercalated with nitrite ions and corrosion protection of steel bars in simulated carbonated concrete pore solution. *Corros. Sci.* **2019**, *152*, 120–129. [[CrossRef](#)]
82. Yoon, S.; Moon, J.; Bae, S.; Duan, X.; Giannelis, E.P.; Monteiro, P.M. Chloride adsorption by calcined layered double hydroxides in hardened Portland cement paste. *Mater. Chem. Phys.* **2014**, *145*, 376–386. [[CrossRef](#)]
83. Ke, X.; Bernal, S.A.; Provis, J.L. Uptake of chloride and carbonate by Mg-Al and Ca-Al layered double hydroxides in simulated pore solutions of alkali-activated slag cement. *Cem. Concr. Res.* **2017**, *100*, 1–13. [[CrossRef](#)]
84. Wong, F.; Buchheit, R. Utilizing the structural memory effect of layered double hydroxides for sensing water uptake in organic coatings. *Prog. Org. Coatings* **2004**, *51*, 91–102. [[CrossRef](#)]
85. Wei, J.; Gao, Z.; Song, Y.; Yang, W.; Wang, J.; Li, Z.; Mann, T.; Zhang, M.; Liu, L. Solvothermal synthesis of Li–Al layered double hydroxides and their electrochemical performance. *Mater. Chem. Phys.* **2013**, *139*, 395–402. [[CrossRef](#)]
86. Bergaya, F.; Lagaly, G. *Handbook of Clay Science*; Elsevier: Amsterdam, The Netherlands, 2013.
87. Hochstetter, C. Untersuchung über die Zusammensetzung einiger Mineralien. *J. Für Prakt. Chem.* **1842**, *27*, 375–378. [[CrossRef](#)]
88. Matschei, T.; Lothenbach, B.; Glasser, F. The AFm phase in Portland cement. *Cem. Concr. Res.* **2007**, *37*, 118–130. [[CrossRef](#)]
89. Renaudin, G.; Francois, M.; Evrard, O. Order and disorder in the lamellar hydrated tetracalcium monocarboaluminate compound. *Cem. Concr. Res.* **1999**, *29*, 63–69. [[CrossRef](#)]
90. Provis, J.L.; Bernal, S.A. Geopolymers and related alkali-activated materials. *Annu. Rev. Mater. Res.* **2014**, *44*, 299–327. [[CrossRef](#)]
91. Wang, S.D.; Scrivener, K.L. Hydration products of alkali activated slag cement. *Cem. Concr. Res.* **1995**, *25*, 561–571. [[CrossRef](#)]
92. Ke, X.; Bernal, S.A.; Provis, J.L. Chloride binding capacity of hydrotalcite in near-neutral and alkaline environments. In Proceedings of the 34th Cement and Concrete Science Conference, University of Sheffield, Sheffield, UK, 14–17 September 2014.
93. Kayali, O.; Khan, M.; Ahmed, M.S. The role of hydrotalcite in chloride binding and corrosion protection in concretes with ground granulated blast furnace slag. *Cem. Concr. Compos.* **2012**, *34*, 936–945. [[CrossRef](#)]
94. Tedim, J.; Kuznetsova, A.; Salak, A.; Montemor, F.; Snihirova, D.; Pilz, M.; Zheludkevich, M.; Ferreira, M. Zn–Al layered double hydroxides as chloride nanotraps in active protective coatings. *Corros. Sci.* **2012**, *55*, 1–4. [[CrossRef](#)]

95. Forano, C.; Hibino, T.; Leroux, F.; Taviot-Guého, C. Chapter 13.1 layered double hydroxides in Handbook of Clay science. *Dev. Clay Sci.* **2006**, *1*, 1021–1095.
96. Kuang, Y.; Zhao, L.; Zhang, S.; Zhang, F.; Dong, M.; Xu, S. Morphologies, preparations and applications of layered double hydroxide micro-/nanostructures. *Materials* **2010**, *3*, 5220–5235. [[CrossRef](#)]
97. Qu, Z.; Yu, Q.; Brouwers, H. Relationship between the particle size and dosage of LDHs and concrete resistance against chloride ingress. *Cem. Concr. Res.* **2018**, *105*, 81–90. [[CrossRef](#)]
98. Xu, S.; Chen, Z.; Zhang, B.; Yu, J.; Zhang, F.; Evans, D.G. Facile preparation of pure CaAl-layered double hydroxides and their application as a hardening accelerator in concrete. *Chem. Eng. J.* **2009**, *155*, 881–885. [[CrossRef](#)]
99. Duan, P.; Chen, W.; Ma, J.; Shui, Z. Influence of layered double hydroxides on microstructure and carbonation resistance of sulphoaluminate cement concrete. *Constr. Build. Mater.* **2013**, *48*, 601–609. [[CrossRef](#)]
100. Yang, Z.; Fischer, H.; Polder, R. Laboratory investigation of the influence of two types of modified hydrotalcites on chloride ingress into cement mortar. *Cem. Concr. Compos.* **2015**, *58*, 105–113. [[CrossRef](#)]
101. Xiong, L.X.; Liu, C.J.; Yuan, X.W. Effects of calcined Mg-Al-CO₃ layered double hydroxides on resistance of cement mortar to chloride erosion. *Ind. J. Eng. and Mater. Sci.* **2015**, *22*, 225–230.
102. Li, H.; Guan, X.; Yang, L.; Liu, S.; Zhang, J.; Guo, Y. Effects of LiAl-layered double hydroxides on early hydration of calcium sulphoaluminate cement paste. *J. Wuhan Univ. Technol.-Mater. Sci. Ed.* **2017**, *32*, 1101–1107. [[CrossRef](#)]
103. Wu, Y.; Duan, P.; Yan, C. Role of layered double hydroxides in setting, hydration degree, microstructure and compressive strength of cement paste. *Appl. Clay Sci.* **2018**, *158*, 123–131. [[CrossRef](#)]
104. Chen, Y.; Yu, R.; Wang, X.; Chen, J.; Shui, Z. Evaluation and optimization of Ultra-High Performance Concrete (UHPC) subjected to harsh ocean environment: Towards an application of Layered Double Hydroxides (LDHs). *Constr. Build. Mater.* **2018**, *177*, 51–62. [[CrossRef](#)]
105. Zou, D.; Wang, K.; Li, H.; Guan, X. Effect of LiAl-layered double hydroxides on hydration of calcium sulfoaluminate cement at low temperature. *Constr. Build. Mater.* **2019**, *223*, 910–917. [[CrossRef](#)]
106. Du, H.; Gao, H.J.; Dai Pang, S. Improvement in concrete resistance against water and chloride ingress by adding graphene nanoplatelet. *Cem. Concr. Res.* **2016**, *83*, 114–123. [[CrossRef](#)]
107. Du, H.; Dai Pang, S. Enhancement of barrier properties of cement mortar with graphene nanoplatelet. *Cem. Concr. Res.* **2015**, *76*, 10–19. [[CrossRef](#)]
108. Land, G.; Stephan, D. Controlling cement hydration with nanoparticles. *Cem. Concr. Compos.* **2015**, *57*, 64–67. [[CrossRef](#)]
109. Bräu, M.; Ma-Hock, L.; Hesse, C.; Nicoleau, L.; Strauss, V.; Treumann, S.; Wiench, K.; Landsiedel, R.; Wohlleben, W. Nanostructured calcium silicate hydrate seeds accelerate concrete hardening: A combined assessment of benefits and risks. *Arch. Toxicol.* **2012**, *86*, 1077–1087. [[CrossRef](#)]
110. Myrdal, R. *Accelerating Admixtures for Concrete. State of the Art - (Technical Report SINTEF)*; SINTEF: Trondheim, Norway 2007.
111. Guan, X.; Li, H.; Luo, S.; Liu, X.; Zhang, J. Influence of LiAl-layered double hydroxides with 3D micro-nano structures on the properties of calcium sulphoaluminate cement clinker. *Cem. Concr. Compos.* **2016**, *70*, 15–23. [[CrossRef](#)]
112. Šiler, P.; Kolářová, I.; Másilko, J.; Novotný, R.; Opravil, T. The Effect of Zinc on the Portland Cement Hydration. In *Key Engineering Materials*; Trans Tech Publications Ltd: Stafa-Zurich, Switzerland, 2018; Volume 761, pp. 131–134.
113. Asavapisit, S.; Fowler, G.; Cheeseman, C. Solution chemistry during cement hydration in the presence of metal hydroxide wastes. *Cem. Concr. Res.* **1997**, *27*, 1249–1260. [[CrossRef](#)]
114. Trezza, M.A. Hydration study of ordinary portland cement in the presence of zinc ions. *Mater. Res.* **2007**, *10*, 331–334. [[CrossRef](#)]
115. Li, F.; Duan, X. Applications of layered double hydroxides. In *Layered Double Hydroxides*; Springer-Verlag: Berlin, Heidelberg, Germany, 2006; pp. 193–223.
116. Martin, K.J.; Pinnavaia, T. Layered double hydroxides as supported anionic reagents. Halide-ion reactivity in zinc chromium hexahydroxide halide hydrates [Zn₂Cr(OH)₆X.nH₂O](X= Cl, I). *J. Am. Chem. Soc.* **1986**, *108*, 541–542. [[CrossRef](#)] [[PubMed](#)]
117. Tian, Y.; Dong, C.; Wang, G.; Cheng, X.; Li, X. Zn–Al–NO₂ layered double hydroxide as a controlled-release corrosion inhibitor for steel reinforcements. *Mater. Lett.* **2019**, *236*, 517–520. [[CrossRef](#)]

118. Poznyak, S.; Tedim, J.; Rodrigues, L.; Salak, A.; Zheludkevich, M.; Dick, L.; Ferreira, M. Novel inorganic host layered double hydroxides intercalated with guest organic inhibitors for anticorrosion applications. *ACS Appl. Mater. Interfaces* **2009**, *1*, 2353–2362. [[CrossRef](#)]
119. Cao, Y.; Dong, S.; Zheng, D.; Wang, J.; Zhang, X.; Du, R.; Song, G.; Lin, C. Multifunctional inhibition based on layered double hydroxides to comprehensively control corrosion of carbon steel in concrete. *Corros. Sci.* **2017**, *126*, 166–179. [[CrossRef](#)]
120. Carlino, S. The intercalation of carboxylic acids into layered double hydroxides: a critical evaluation and review of the different methods. *Solid State Ionics* **1997**, *98*, 73–84. [[CrossRef](#)]
121. DAvo, L. Anion-exchange in takovite: Applications to other hydroxide minerals. *Bull. Miner.* **1980**, *103*, 170–175.
122. Meyn, M.; Beneke, K.; Lagaly, G. Anion-exchange reactions of layered double hydroxides. *Inorg. Chem.* **1990**, *29*, 5201–5207. [[CrossRef](#)]
123. Costa, F.R.; Abdel-Goad, M.; Wagenknecht, U.; Heinrich, G. Nanocomposites based on polyethylene and Mg–Al layered double hydroxide. I. Synthesis and characterization. *Polymer* **2005**, *46*, 4447–4453. [[CrossRef](#)]
124. Pöllmann, H.; Göske, J. Fixation of Chromate in Layered Double Hydroxides of the TCAH Type and Some Complex Application Mixtures. In *Minerals as Advanced Materials II*; Springer: Berlin, Heidelberg, 2011; pp. 103–114.
125. Hibino, T. Anion Selectivity of Layered Double Hydroxides: Effects of Crystallinity and Charge Density. *Eur. J. Inorg. Chem.* **2018**, *2018*, 722–730. [[CrossRef](#)]
126. Miyata, S. Anion-exchange properties of hydrotalcite-like compounds. *Clays Clay Miner.* **1983**, *31*, 305–311. [[CrossRef](#)]
127. Costa, D.G.; Rocha, A.B.; Souza, W.F.; Chiaro, S.S.X.; Leitão, A.A. Comparative Structural, thermodynamic and electronic analyses of Zn–Al–A^{n−} hydrotalcite-like compounds (A^{n−} = Cl[−], F[−], Br[−], OH[−], CO₃^{2−} or NO₃[−]): An ab initio study. *Appl. Clay Sci.* **2012**, *56*, 16–22. [[CrossRef](#)]
128. Miyata, S. The Syntheses of Hydrotalcite-Like Compounds and Their Structures and Physico-Chemical Properties—I: The Systems Mg²⁺–Al³⁺–NO₃[−], Mg²⁺–Al³⁺–Cl[−], Mg²⁺–Al³⁺–ClO₄[−], Ni²⁺–Al³⁺–Cl[−] and Zn²⁺–Al³⁺–Cl[−]. *Clays Clay Miner.* **1975**, *23*, 369–375. [[CrossRef](#)]
129. Miyata, S.; Okada, A. Synthesis of hydrotalcite-like compounds and their physico-chemical properties—The systems Mg²⁺–Al³⁺–SO₄^{2−} and Mg²⁺–Al³⁺–CrO₄^{2−}. *Clays Clay Miner.* **1977**, *25*, 14–18. [[CrossRef](#)]
130. Duan, P.; Yan, C.; Zhou, W. Effects of calcined layered double hydroxides on carbonation of concrete containing fly ash. *Constr. Build. Mater.* **2018**, *160*, 725–732. [[CrossRef](#)]
131. Chen, Y.; Shui, Z.; Chen, W.; Chen, G. Chloride binding of synthetic Ca–Al–NO₃ LDHs in hardened cement paste. *Constr. Build. Mater.* **2015**, *93*, 1051–1058. [[CrossRef](#)]
132. Shui, Z.; Yu, R.; Chen, Y.; Duan, P.; Ma, J.; Wang, X. Improvement of concrete carbonation resistance based on a structure modified Layered Double Hydroxides (LDHs): Experiments and mechanism analysis. *Constr. Build. Mater.* **2018**, *176*, 228–240. [[CrossRef](#)]
133. Tatsumatsu, H.; Sasaki, T. Repair materials system for chloride-induced corrosion of reinforcing bars. *Cem. Concr. Compos.* **2003**, *25*, 123–129. [[CrossRef](#)]
134. Zhonghe, S.; Juntao, M.; Wei, C.; Xiaoxing, C. Chloride binding capacity of cement paste containing layered double hydroxide (LDH). *J. Test. Eval.* **2012**, *40*, 796–800. [[CrossRef](#)]
135. Glasser, F.; Kindness, A.; Stronach, S. Stability and solubility relationships in AFm phases—Its solid solutions and their role in chloride binding. *Cem. Concr. Res.* **1999**, *29*, 861–866. [[CrossRef](#)]
136. Larsen, C. Chloride Binding in Concrete, Effect of Surrounding Environment and Concrete Composition. Ph.D. Thesis, The Norwegian University of Science and Technology, Trondheim, Norway, 1998; Volume 95, p. 337.
137. Hobbs, M.Y. Solubilities and Ion Exchange Properties of Solid Solutions between the Hydroxyl, Chlorine and Carbon Trioxide end Members of the Monocalcium Aluminate Hydrates. Ph.D. Thesis, University of Waterloo, Waterloo, ON, USA, 2001.
138. Suryavanshi, A.; Swamy, R.N. Stability of Friedel’s salt in carbonated concrete structural elements. *Cem. Concr. Res.* **1996**, *26*, 729–741. [[CrossRef](#)]
139. Jones, M.; Macphree, D.E.; Chudek, J.; Hunter, G.; Lannegrand, R.; Talero, R.; Scrimgeour, S. Studies using ²⁷Al MAS NMR of AFm and AFt phases and the formation of Friedel’s salt. *Cem. Concr. Res.* **2003**, *33*, 177–182. [[CrossRef](#)]

140. Struble, L. Synthesis and characterization of ettringite and related phases. In Proceedings of the 8th International Congress on the Chemistry of Cement, Rio de Janeiro, Brazil, 22–27 September 1986; Volume 1, pp. 449–482.
141. Hirao, H.; Yamada, K.; Takahashi, H.; Zibara, H. Chloride binding of cement estimated by binding isotherms of hydrates. *J. Adv. Concr. Technol.* **2005**, *3*, 77–84. [[CrossRef](#)]
142. Birnin-Yauri, U.; Glasser, F. Friedel's salt, $\text{Ca}_2\text{Al}(\text{OH})_6(\text{Cl},\text{OH})\cdot 2\text{H}_2\text{O}$: Its solid solutions and their role in chloride binding. *Cem. Concr. Res.* **1998**, *28*, 1713–1723. [[CrossRef](#)]
143. Berke, N.S.; Rosenberg, A. Technical review of calcium nitrite corrosion inhibitor in concrete. *Transp. Res. Rec.* **1989**, *1211*, 18–27.
144. Ann, K.Y.; Jung, H.; Kim, H.; Kim, S.; Moon, H.Y. Effect of calcium nitrite-based corrosion inhibitor in preventing corrosion of embedded steel in concrete. *Cem. Concr. Res.* **2006**, *36*, 530–535. [[CrossRef](#)]
145. Yang, Z.; Polder, R.; Mol, J. Modified hydrotalcites as chloride scavengers and inhibitor release agents for improved corrosion protection of reinforced concrete. *Heron* **2017**, *62*, 61.
146. Dry, C.; Corsaw, M. A time-release technique for corrosion prevention. *Cem. Concr. Res.* **1998**, *28*, 1133–1140. [[CrossRef](#)]
147. Chen, L.J.; Chen, X.X.; Chen, W. Research on the Carbonation of Cement Paste Modified with Layered Double Hydroxides. In *Applied Mechanics and Materials*; Trans Tech Publications Ltd: Stafa-Zurich, Switzerland, 2012; Volume 174, pp. 706–710.
148. Cao, Y.; Zheng, D.; Dong, S.; Zhang, F.; Lin, J.; Wang, C.; Lin, C. A Composite corrosion inhibitor of MgAl layered double hydroxides co-intercalated with hydroxide and organic anions for carbon steel in simulated carbonated concrete pore solutions. *J. Electrochem. Soc.* **2019**, *166*, C3106–C3113. [[CrossRef](#)]
149. Shui, Z.H.; Ma, J.T.; Chen, W.; Gao, X. The effect of layered double hydroxides on the concrete resistance of chloride-ion penetration. In *Key Engineering Materials*; Trans Tech Publications Ltd: Stafa-Zurich, Switzerland, 2012; Volume 509, pp. 99–105.
150. Yang, Z.; Fischer, H.; Polder, R. Synthesis and characterization of modified hydrotalcites and their ion exchange characteristics in chloride-rich simulated concrete pore solution. *Cem. Concr. Compos.* **2014**, *47*, 87–93. [[CrossRef](#)]
151. Yang, Z.; Fischer, H.; Cerezo, J.; Mol, J.; Polder, R. Aminobenzoate modified MgAl hydrotalcites as a novel smart additive of reinforced concrete for anticorrosion applications. *Constr. Build. Mater.* **2013**, *47*, 1436–1443. [[CrossRef](#)]
152. Matschei, T.; Lothenbach, B.; Glasser, F.P. Thermodynamic properties of Portland cement hydrates in the system $\text{CaO}-\text{Al}_2\text{O}_3-\text{SiO}_2-\text{CaSO}_4-\text{CaCO}_3-\text{H}_2\text{O}$. *Cem. Concr. Res.* **2007**, *37*, 1379–1410. [[CrossRef](#)]
153. Xu, J.; Song, Y.; Zhao, Y.; Jiang, L.; Mei, Y.; Chen, P. Chloride removal and corrosion inhibitions of nitrate, nitrite-intercalated MgAl layered double hydroxides on steel in saturated calcium hydroxide solution. *Appl. Clay Sci.* **2018**, *163*, 129–136. [[CrossRef](#)]
154. Chung, C.W.; Jung, H.Y.; Kwon, J.H.; Jang, B.K.; Kim, J.H. Use of calcium aluminum-layered double hydroxide to control chloride ion penetration of cement-based materials. *J. Struct. Integr. Maint.* **2019**, *4*, 37–42. [[CrossRef](#)]



© 2020 by the authors. Licensee MDPI, Basel, Switzerland. This article is an open access article distributed under the terms and conditions of the Creative Commons Attribution (CC BY) license (<http://creativecommons.org/licenses/by/4.0/>).

3. Materials and methods

This chapter provides a description of the materials, numerical methods and experimental procedures/techniques used in this work. At first, a detailed information about the binder composition, concrete mix and additives used in this study is provided. This is followed by a description of the numerical methods used in this study. A test case on chloride diffusion in concrete is discussed to introduce the finite element method. Finally, an introduction is provided regarding the experimental techniques and procedures followed in this study. Wherever available, testing guidelines according to European or national standards have been followed and are also described briefly in this chapter.

3.1. Materials

3.1.1. Cement binder

The cement binder used in this study is of type CEM I 52.5 R provided by Dyckerhoff AG (Germany). The chemical and mineralogical composition is shown in Table 3.1. This cement has been used in all the experiments conducted in this work except for compatibility tests described in chapter 4, wherein the type of cement has been specified.

Chemical composition	[%] ^A	[%] ^B	Mineralogical composition	[%] ^A	[%] ^B
SiO ₂	21.39	21.57	C ₃ S	70.3	72.3
Al ₂ O ₃	3.69	4.15	C ₂ S	6.5	7.7
Fe ₂ O ₃	1.29	1.41	C ₃ A	8.9	8.6
CaO	64.66	65.39	C ₄ AF	2.4	4.3
MgO	0.72	0.66	Calcite	4.7	
SO ₃	3.43	2.78	Gypsum	3.7	
K ₂ O	0.57	0.57	Others	3.6	
Na ₂ O	0.21	0.21			
Cl ⁻		0.06			

^A according to manufacturer (Dyckerhoff AG, Germany), ^B as measured at Instituto Eduardo Torroja - CSIC (Spain)

Table 3.1.: Chemical and mineralogical composition of CEM I 52.5 R binder.

3. Materials and methods

Property	[Unit]	Value
Binder (CEM I / 52.5 R)	[Kg/m ³]	350
Mg-Al-NO ₂	[mass % binder]	0 - 2
Aggregate 0-4 mm	[Kg/m ³]	1151
Aggregate 4-8 mm	[Kg/m ³]	265
Aggregate 8-16 mm	[Kg/m ³]	355
Viscocrete 3082	[mass % binder]	0.8
Water content	[w/c]	0.6

Table 3.2.: Concrete mix used in this study. A 2% dosage of Mg-Al-NO₂ is used in concrete mix with LDH.

3.1.2. Concrete mix

The concrete mix used in this study was developed by Swedish Cement and Concrete Research Institute (RISE) using cement binder provided by Dyckerhoff AG (Germany). A relatively higher water to cement (w/c) ratio of 0.6 was chosen in order to have a less dense and slightly porous concrete as compared to concrete resulting from conventional w/c ratios closer to 0.4. This property was desired in order to speed up chloride penetration in chloride durability tests, so that the performance of the concrete mix could be assessed within a reasonable time frame under accelerated natural diffusion conditions (section 3.3.6). The details of the concrete mix are presented in Table 3.2. This concrete has been used in all the experiments in this work unless explicitly stated.

3.1.3. Layered Double Hydroxides

The Layered Double Hydroxides (LDH) used in this study were provided by Smallmatek, Lda (Portugal) and used in "as-received" state without any further processing or modifications. Briefly, (Mg/Zn)-Al-NO₂ LDHs were prepared by co-precipitation of divalent and trivalent metallic salts in an alkaline environment containing an excess of sodium nitrite. The synthesis procedure as detailed out in Poznyak et al. [31] was followed.

3.2. Numerical techniques

Finite element method (FEM) is a numerical discretization method which is used to solve arbitrary differential equations over complex physical domains. The method finds its application in problems where analytical solutions are difficult to obtain. Such situations arise when the domain has a complex geometry or complex boundary/loading conditions, etc. The methodology of FEM is to reduce differential equations to an algebraic system of equations without losing the essence of the problem at hand. The resulting set of algebraic equations can be programmed and solved by a computer. From a mathematical point of view, the method consists of finding an approximate solution for a system of differential equations. Despite that, the method is also exact enough to be used for engineering applications, in the sense that it can converge reasonably well to the analytical solutions when a sufficient amount of mesh elements are used. A high number of elements i.e. a fine mesh, in turn increases the computing effort.

This section presents a brief overview of the finite element method. As an example, the solution of a second order parabolic problem is presented. A one-dimensional transient diffusion equation is solved using the FEM method and its comparison with analytical solution is presented. The motivation behind presenting a diffusion problem is that in this work many natural diffusion tests are conducted to ascertain the chloride durability of concrete. In a standard natural diffusion test, a concrete sample is subjected to a uni-directional chloride influx [40]. The governing equation for this process is the one-dimensional transient diffusion equation. This section presents the numerical treatment of this equation using the finite element method. A complete description of the FEM is beyond the scope of this work and the interested reader is directed to comprehensive text books on FEM by Belytscho et al. [37], Hughes [41], Zienkiewicz et al. [42] and Cook et al. [43].

3.2.1. Uni-directional diffusion problem

In the following text, subscripts "t" and "x" refer to time and space derivative respectively. Occasionally, a time derivative may also be represented by a dot ($\dot{\cdot}$) over a quantity. A time variant one dimensional diffusion for chloride ions in a homogenized concrete matrix can be represented by

$$C^c(x, t)_{,t} - (D^a C^c(x, t)_{,x})_{,x} = S^c(x, t) , \quad (3.1)$$

where:

C^c = chloride concentration [mol/m³ of concrete]
 D^α = apparent diffusion coefficient of chloride ions [m²/s]
 S^c = chloride source term [mol/(m³s)]

In this problem, the chloride source term is removed as there is no chloride source/sink. As such, eq.(3.1) reduces to the well known Fick's second law [25] and is expressed as

$$C^c(x, t)_{,t} + J_x^c = 0, \quad (3.2)$$

with the chloride flux J^c defined as

$$J^c = -D^\alpha C^c(x, t)_{,x}. \quad (3.3)$$

Eq.(3.1) and eq.(3.2) are referred to as the *strong form*, in the sense that they must be verified at every point in the domain Ω . The boundary Γ around the domain Ω is partitioned into Dirichlet boundary Γ_D and Neumann boundary Γ_N . The FEM involves choosing of a trial function C^c with following restrictions

$$\begin{aligned} C^c &= \bar{C}^c && \text{on } \Gamma_D, \\ -D^\alpha C^c(x, t)_{,x} \cdot \vec{n} &= J^c && \text{on } \Gamma_N, \end{aligned} \quad (3.4)$$

where, \bar{C}^c is the value of the trial function on Γ_D and J_c is the normal flux on Γ_N . We now introduce a test function δC^c which exactly satisfies the following

$$\delta C^c = 0 \quad \text{on } \Gamma_D. \quad (3.5)$$

We now introduce the trial function C^c in the residual of eq.(3.1) and further multiply by the test function δC^c . The resulting equation is integrated over the entire volume to obtain the corresponding Galerkin formulation which is expressed as

$$\int_{\Omega} \delta C^c (C^c_{,t} - (D^\alpha C^c_{,x})_{,x} - S^c) dv = 0, \quad (3.6)$$

$$\int_{\Omega} \delta C^c (C_{,t}^c) dv - \int_{\Omega} \delta C^c (D^\alpha C_{,x}^c)_{,x} dv - \int_{\Omega} \delta C^c S^c dv = 0 .$$

Splitting the second term using integration by parts (Green's theorem in one dimension) and for a constant cross section A^o , the resulting 1D formulation can be expressed as

$$\int_{\ell} \delta C^c (C_{,t}^c) A^o dx + \int_{\ell} \delta C^c_{,x} (D^\alpha C_{,x}^c) A^o dx - \int_{\ell} (\delta C^c D^\alpha C_{,x}^c)_{,x} A^o dx - \int_{\ell} \delta C^c S^c A^o dx = 0 .$$

Applying Gauss's theorem on the third term, we obtain

$$\int_{\ell} \delta C^c (C_{,t}^c) dx + \int_{\ell} \delta C^c_{,x} (D^\alpha C_{,x}^c) dx - \int_{\ell} \delta C^c S^c dx + (\delta C^c J^c) \Big|_{\Gamma_N} = 0 . \quad (3.7)$$

The eq.(3.7) is called the *weak form* of eq.(3.1). Instead of having to be verified everywhere on Γ , it is verified once for each test function. The weak form in this case has only a first order space derivative as compared to the second order in the strong form in eq.(3.1).

3.2.2. Space discretization

The 1D domain is now discretized into many small finite elements. The subscript "e" denotes local concentration values at nodes. In the following, the weak form is discretized using Bubnov-Galerkin method. In this method, both the trial and test functions are approximated as

$$\begin{aligned} C^c(x, t) &= \mathbf{N}(x) \mathbf{C}_e^c(t) , \\ \delta C^c(x, t) &= \mathbf{N}(x) \delta \mathbf{C}_e^c(t) . \end{aligned} \quad (3.8)$$

where, \mathbf{N} contains ansatz for concentration and \mathbf{C}_e^c represents concentration at each node. Introducing eq.(3.8) into the weak form eq.(3.7), we obtain

$$\delta \mathbf{C}_e^c{}^T \left\{ \int_{\ell_e} \mathbf{N}^T \mathbf{N} dx \dot{\mathbf{C}}_e^c + \int_{\ell_e} \mathbf{N}_{,x}{}^T D^\alpha \mathbf{N}_{,x} dx \mathbf{C}_e^c - \int_{\ell_e} \mathbf{N}^T S^c dx + (\mathbf{N}^T J^c) \Big|_{\Gamma_N} \right\} = 0 . \quad (3.9)$$

The eq.(3.9) is a system of equations for all nodes in an element domain "e" with a local boundary. As the above equation is true for all $\delta \mathbf{C}_e^c$, therefore

$$M_e \dot{\mathbf{C}}_e^c + K_e \mathbf{C}_e^c - f_{s,e} + f_{j^c,e} = 0 . \quad (3.10)$$

The above equation can be further expressed as

$$M_e \dot{\mathbf{C}}_e^c + K_e \mathbf{C}_e^c = f_e , \quad (3.11)$$

where, M_e is the local consistent capacity matrix, K_e is the local transport operator and f_e contains the source term and flux terms. They are expressed as

$$\begin{aligned} M_e &= \int_{\ell_e} \mathbf{N}^T \mathbf{N} dx , \\ K_e &= \int_{\ell_e} \mathbf{N}_{,x}^T D^\alpha \mathbf{N}_{,x} dx , \\ f_e &= \int_{\ell_e} \mathbf{N}^T S^c dx - \left(\mathbf{N}^T J^c \right) \Big|_{\Gamma_N} . \end{aligned} \quad (3.12)$$

The global expressions for the entire domain Ω can be obtained from the expressions for element domain "e" in eq.(3.12) using an operation called "assembly" [37]. The global expressions are similar to the element expressions, and can be expressed by dropping the subscript "e" in eq.(3.12) and extending the limits of the integration to the entire domain Ω . Correspondingly, the global force vector is also obtained in a similar fashion where the Neumann boundary in the element force vector now corresponds to the Neumann boundary of the entire domain. Therefore, by dropping the subscript for the element domain "e", we can write global matrices as

$$\overline{\mathbf{M}} \dot{\mathbf{C}}^c + \overline{\mathbf{K}} \mathbf{C}^c = \overline{\mathbf{F}} , \quad (3.13)$$

with $\overline{\mathbf{M}}$ as the global capacity matrix, $\overline{\mathbf{K}}$ as the global transport operator and $\overline{\mathbf{F}}$ as the force vector.

3.2.3. Time discretization

To solve the semi-discrete system of equations in eq.(3.13), various finite difference time discretization schemes are available [37, 44]. There are generally two systems of time integration schemes i.e. explicit type and implicit type. These methods differ mainly in speed, stability and accuracy. Explicit methods usually have a limitation on time step but are faster than implicit methods. Implicit methods are less stringent on time step but need more floating point operations at each time step and also more processing power. Here we present an implicit scheme approximation of eq.(3.13). The time derivative is approximated by using an implicit scheme, where at time " t " the values of the solution are known and at time " $t + \Delta t$ " the solution is unknown. The system of equations of expressed as

$$\overline{\mathbf{M}} \left(\frac{\mathbf{C}_{t+\Delta t}^c - \mathbf{C}_t^c}{\Delta t} \right) + \overline{\mathbf{K}} \mathbf{C}_{t+\Delta t}^c = \overline{\mathbf{F}}_{t+\Delta t}, \quad (3.14)$$

$$\left(\Delta t^{-1} \overline{\mathbf{M}} + \overline{\mathbf{K}} \right) \mathbf{C}_{t+\Delta t}^c = \overline{\mathbf{F}}_{t+\Delta t} + \Delta t^{-1} \overline{\mathbf{M}} \mathbf{C}_t^c. \quad (3.15)$$

The eq.(3.15) now contains a linear set of equations. The method is unconditionally stable; for linear problems convergence is guaranteed independent of time step size. However, precision will decrease with increasing time step size. For non-linear problems, the convergence is not always guaranteed [37]. In the context of this work, we now use eq.(3.15) to compute one-directional diffusion of chloride ions in a homogenized concrete matrix. In this example, a test problem is defined with realistic values in Appendix A.1. The problem is solved with FEM using a program written in the Julia programming language [38]. The test code along with some selected results is also provided in Appendix A.1.

3.3. Experimental techniques and methods

3.3.1. X-ray diffraction analysis and particle size analysis

The chemical stability and phase composition of LDH powders and cement pastes with and without LDH was determined by obtaining X-ray diffraction (XRD) diffractograms using a PANalytical X'Pert MPD PRO (Almedo, Holland) diffractometer with Bragg-Brentano geometry, Ni-filtered $\text{CuK}\alpha$ radiation, PIXcel^{1D} detector, and step 0.026° . The measurements were conducted for an angular range between 3° and 65° with an exposition of 2 s per step. In-situ X-ray diffractograms (XRD) of hydrating cement pastes were obtained by Rigaku Miniflex 600 with a Cu X-ray tube. Particle size analysis for LDH particles was carried out with a Coulter LS230 Particle Size Analyzer. Additional details are mentioned in section 4.2.

3.3.2. Stability and ion exchange analysis

LDH have a potential of capturing anions from the environment by interchanging them with anions present inherently in their galleries [45, 33, 46, 47, 48, 31, 49, 50]. In cementitious environment, this ion-exchange property can be exploited to perform additional capture of chloride ions, thereby retarding their ingress, together with the release of anions, which could be NO_3^- , NO_2^- (corrosion inhibitor) or any other anion depending on the type of LDH. In order to verify the anion capture/release nature of "as-received" Zn-Al- NO_2 , ion exchange analysis was carried out in the pH range of 11 to 13.5. Alkaline solutions were prepared by adding KOH salt in distilled water. As such, seven different alkaline solutions were prepared with pH 11, 11.5, 12, 12.2, 12.5, 13 and 13.5. This encompasses the pH range of fresh concrete as well as mature concrete. 1 g of powdered Zn-Al- NO_2 was added to 50 ml of alkaline solution and stored in an air tight container for 30 days. The capture of OH^- ion by Zn-Al- NO_2 was investigated by measuring the pH drop after 30 days by potentiometric method using commercially available S47 SevenMulti meter fitted with a pH/conductivity module and an Inlab Expert Pro pH combined electrode from Mettler Toledo. Additionally, the release of corrosion inhibitor NO_2^- from the LDH galleries was also measured with a UV-3100 UV-Vis-NIR spectrophotometer Shimadzu (Japan) with the peak of interest occurring at 354 nm. Furthermore, the stability of Zn-Al- NO_2 was investigated by removing the powders from closed containers after 30 days. The powders were washed, oven dried at 40°C and analysed with XRD in order to study the chemical stability at various pH values after a long period of exposure (30 days).

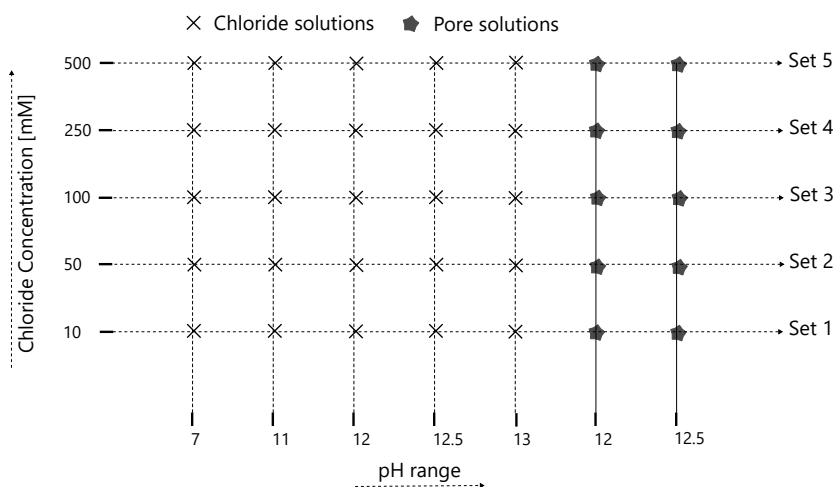


Figure 3.1.: Test matrix for Cl^- sequestration analysis. Reprinted without modifications from [51] under CC BY 4.0 license.

3.3.3. Chloride sequestration analysis in aqueous solutions

In this study, a pivotal point of interest was to study the chloride sequestration capacity of LDH in cementitious environment. This was carried out by exposing Zn-Al- NO_2 to NaCl solutions ranging in concentration from 0.01 M to 0.5 M at neutral pH and also at pH ranging between 11 to 13. The entire test matrix is shown in Figure 3.1. Additionally, these selectivity tests were extended to concrete pore solution environment in order to replicate a multi-ion competition scenario. In this case, pore solutions PS1 and PS2 were prepared with a pH of 12 and 12.5 respectively.

For each test, 50 ml of the solution was added to a beaker fitted with a pH sensor and a DX235- Cl^- ion selective electrode sensor from Mettler Toledo. A schematic representation of the experimental setup is shown in Figure 3.2. The solution was vigorously stirred with a magnetic stirrer. After receiving a stable signal from the sensor, 1 g of Zn-Al- NO_2 was added at time $t = 0$ seconds to the solution under continuous stirring conditions. Cl^- measurements were carried out continuously from $t = 0$ seconds to $t = 300$ seconds (5 minutes) after adding Zn-Al- NO_2 . Additionally, pH measurements were carried out at discrete points i.e. $t = 0$ and $t = 300$ seconds i.e. just before adding LDH and after 5 minutes. For some tests, the LDH solid was recovered after 5 minutes of exposure and characterized by XRD. In order to study the effect of time on chloride capture, Cl^- and pH measurements were taken again after 15 days.

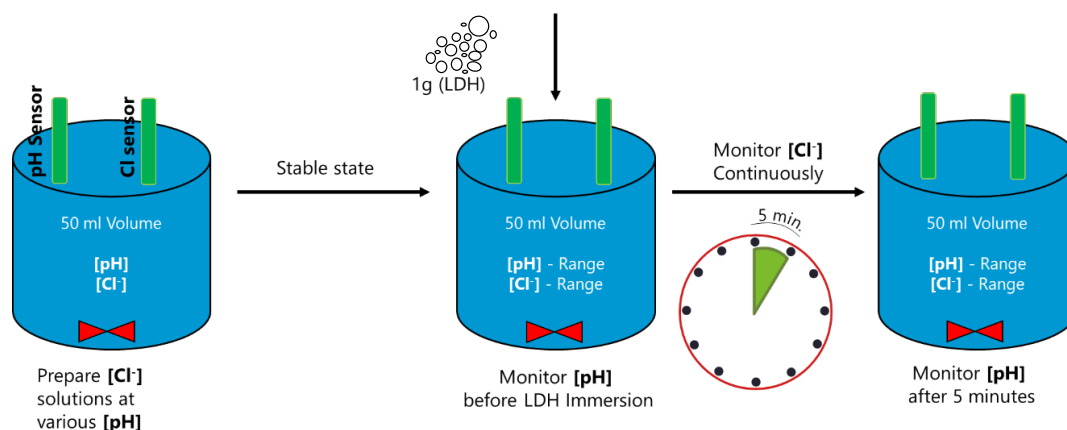


Figure 3.2.: Experimental sequence for Cl⁻ capture tests under stirring conditions. Reprinted without modifications from [51] under CC BY 4.0 license.

3.3.4. Chloride binding isotherms

The chloride sequestration analysis were carried out to understand the behavior of Zn-Al-NO₂ in terms of Cl⁻ loading capacity and selectivity of ion exchange in aqueous solutions. As a next step, the Cl⁻ sequestration capacity of Mg-Al-NO₂ was studied in cement pastes. In this regard, two series of cement pastes were compared, one without LDH and another one with 2% LDH. The cement pastes were prepared with distilled de-ionised water and cured for 28 days. A direct comparison between the two recipes was carried out by determining the chloride binding isotherms for each recipe. A chloride binding isotherm provides a quantitative relationship between the bound chlorides and the free chlorides, by encompassing a wide range of chloride concentrations usually 0.1 M to 3 M. The test procedure to determine the chloride binding isotherm was followed based on works of Perez et al. [25], Tang et al. [52] and Delagrave et al. [53]. The measurement procedure consists of following steps:

1. The cured cement paste samples were crushed to result in a particle size ranging between 0.25 mm to 2 mm. The crushed samples were then vacuum dried in a desiccator with silica gel and sodalime for 7 days in order to completely remove free water and avoid carbonation.
2. After drying, 10 g of crushed powder from each sample was exposed to 50 ml of NaCl solution at seven different concentrations: 0.1 M, 0.3 M, 0.5 M, 0.7 M, 1.0 M, 2.0 M and 3.0 M for 7 days. The samples were kept under isothermal conditions at 20 ± 2 °C.
3. The samples were stirred each day for 1 hour followed by 23 hours of resting. This procedure was carried out for 7 days in a row. The samples were completely sealed to prevent carbonation.

4. After 7 days, it is accepted that an equilibrium is achieved between bound and free chlorides. Several aliquots of solution were taken with a syringe, filtered with 0.45 μm nylon filter membranes and checked for chloride concentration and pH of the solution.
5. The amount of bound chlorides was determined from the decrease of chloride concentration in the solution. The bound chlorides can then be calculated as

$$C_{Cl^-}^b = \frac{(C_{Cl^-}^i - C_{Cl^-}^{Eq.}) \cdot V_{sol.}}{M_{ds}}, \quad (3.16)$$

where:

- $C_{Cl^-}^b$ = amount of bound chloride in [mol/kg of sample]
- $C_{Cl^-}^i$ = initial chloride concentration of the solution [mol/m³]
- $C_{Cl^-}^{Eq.}$ = equilibrium chloride concentration of the solution [mol/m³]
- $V_{sol.}$ = volume of solution [ml]
- M_{ds} = mass of sample powder [g]

6. A plot between $C_{Cl^-}^b$ and $C_{Cl^-}^{Eq.}$ results in a binding isotherm.

3.3.5. Determination of Formation Factor

Formation Factor FF_c is a material property which is used to characterize a porous microstructure [54]. This property can be used to determine the effective diffusion coefficient of concrete accurately, which otherwise is a parameter difficult to obtain experimentally from conventional diffusion tests, due to ionic interactions such as chloride binding causing deviations. The accurate determination of effective diffusion coefficient is very important for chloride transport models, see section 4.3. A detailed description about FF_c can be found in [55, 56, 57]. FF_c is defined as the ratio of conductivity of pore solution to the conductivity of saturated microstructure and can be expressed by eq.(3.17). Mathematically, FF_c is also equal to the ratio of diffusion coefficient of Cl^- ion at infinite dilution to the effective/micro-structural diffusion coefficient [58] and can be expressed as

$$FF_c = \frac{\sigma_c^p}{\sigma_c^b} = \frac{D_{Cl^-}^\infty}{D_{Cl^-}^{eff}}, \quad (3.17)$$

where:

- σ_c^p = conductivity of pore solution [S/m]
 σ_c^b = bulk conductivity of concrete [S/m]
 D_{Cl}^∞ = diffusion coefficient of Cl^- ion at infinite dilution [m^2/s]
 D_{Cl}^{eff} = effective/micro-structural diffusion coefficient [m^2/s]

In order to experimentally measure FF_c , the pore solution resistivity test and concrete bulk resistivity tests were conducted. The procedure is described below and shown schematically in Figure 3.3. The cement used in this study was provided by Dyckerhoff AG (Germany) and the tests were conducted at Instituto Eduardo Torroja - CSIC (Spain). A brief description of these tests is provided below.

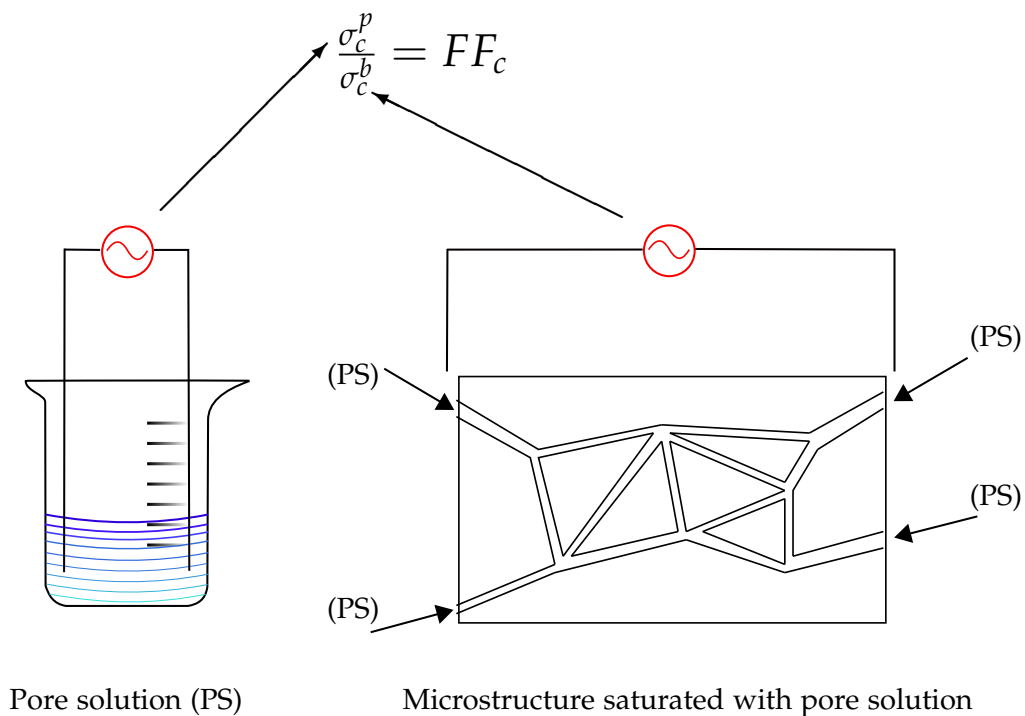


Figure 3.3.: Schematic representation of Formation Factor measurement.

Pore solution resistivity test

The electrical resistivity of pore solution was measured by extracting pore solution from cement paste samples after 7 days of curing time. The pore solution was extracted according to procedure stated by Alonso et al. [59], following which approximately 125 g of the sample was weighed and placed into the cavity of the pore pressing apparatus. Pressure was applied from the piston gradually from 400-500 MPa up to a maximum pressure of 650 MPa with a gradual rate increase of 50 MPa/min. The setup is shown in Figure 3.4. The pore fluid is

collected in a syringe, which was connected to the hole of the bottom plate via a short flexible plastic tube. After collection, the pore fluid was immediately filtered through a $0.45\ \mu\text{m}$ filter and stored in a sealed plastic container to avoid exposure from CO_2 in the atmosphere until further analysis. Pore pressing tests were performed for each cement paste type i.e. with and without LDH. Two samples were weighed at the same time right before the beginning of the test. One sample was used to determine the moisture content of the cement paste after 7 days of curing and the other one to measure the electrical conductivity, the pH of the pore solution and the ion content (cations and anions). For the determination of the moisture content in the cement paste, the samples were dried in a lab oven at $105\ ^\circ\text{C}$ for 24 hours. These tests were conducted for three different w/c ratio i.e. 0.5, 0.55 and 0.6 and for both types of pastes i.e. with and without 2% LDH. For each set, a minimum of two specimens were used.



Figure 3.4.: Setup for pore pressing method test (CSIC, Spain).



Figure 3.5.: Setup for electrical resistivity measurement (CSIC, Spain).

Concrete bulk resistivity test

Electrical resistivity of the concrete was measured in a vacuum saturated state based on UNE 83988-I direct method [60]. The test was conducted at 28 days of age. The electrical resistivity was measured by impedance with an AC current with a frequency of 1000 Hz and a voltage amplitude of 0.032 V. The saturated samples were placed in contact with steel mesh electrodes connected to the resistivity measurement equipment. Moist sponges were used to improve the contact. The setup is shown in Figure 3.5. This procedure was followed for samples of each type of concrete (with and without 2% LDH). The electrical resistivity was measured under saturated conditions at first with deionised water and later with lime water.

3.3.6. Accelerated natural diffusion test

In order to determine the chloride durability of concrete mixes used in this work, 28 day aged specimens were subjected to a uni-directional natural chloride diffusion as per SS-EN 12390-11 [61]. For each mix, a minimum of 3 samples were tested. Briefly, cubical specimens at a curing age of ≤ 28 days were vacuum saturated with deionised water. The specimen sides were then coated with epoxy except for one face which was left free for chloride ingress. The specimen was then immersed in a bath with salt solution. For this reason, this category of tests are also known as ponding tests. In order to accelerate the test, the salt concentration in the bath was maintained at 165 g/l as per Nord Test (NT Build 443) [62]. The sample was then analysed for chloride ingress depth after 46 days of exposure. This was done by grinding off 8-10 layers of concrete from the exposed surface of the specimen. For each layer, the acid soluble chloride content and the distance of the layer from the exposed face was determined as per SS-EN 12390-11 [61].

3.3.7. Other tests:

The compatibility of cement paste with LDH was investigated by casting cement paste with 2% LDH and 0.5 w/c in cubical molds with 2.5 cm side length. The samples were left to cure in a humidity chamber and analysed every 24 hours by scratching the surface with a metal spatula. The curing time was measured relative to control specimens without LDH. These tests were performed at University of Aveiro, Portugal.

Furthermore, the extracted pore solutions from cement pastes were analysed for their ionic content and pH. The cation content (Al^{3+} , Ca^{2+} , Mg^{2+} , K^{+} and Na^{+}) was measured by inductively coupled plasma - optical emission spectrometry (ICP-OES). The anion content (NO_3^- , NO_2^- , SO_4^{2-} and Cl^-) was determined by ionic chromatography (IC).

Additionally, the density of concrete and water accessible porosity in saturated conditions was measured at 28 day of age, 98% RH and 20 °C according to UNE 83890 [63]. These tests were performed at CSIC Institute, Spain.

4. Results on the basis of published work

4.1. Article 2 - Enhanced Predictive Modelling of Steel Corrosion in Concrete in Submerged Zone Based on a Dynamic Activation Approach

Note: See attached article in the next pages. Reprinted without modification from [64] under CC BY 4.0 license. Published by SpringerOpen.

4.1.1. A brief summary of Article 2

This article showcases a 2D numerical model which focuses on chloride induced corrosion of steel in reinforced concrete. In this study, a concrete structure is subjected to a chloride ingress occurring in the submerged marine zone. As time progresses, the continuation of chloride ingress leads to the initiation of corrosion processes on the rebar surface. In this model the theory of dilute species is adopted. The transport processes in the bulk concrete are coupled with electrochemical processes at the rebar surface. The model is able to predict corrosion currents in submerged zone. The model is validated with supporting studies from the literature.

4.1.2. Author contribution

In the following, the author of this dissertation is denoted by his initials ZMM. The names and initials of co-authors can be found in the appended manuscript. ZMM, DH, CG, RS, ACB and PM devised the main conceptual idea, discussed the numerical strategy, evaluated the results and contributed in drafting the script. MGSF and MLZ supervised the work and gave critical comments to this manuscript. All authors discussed and contributed to the final manuscript. All authors read and approved the final manuscript.

RESEARCH

Open Access



Enhanced Predictive Modelling of Steel Corrosion in Concrete in Submerged Zone Based on a Dynamic Activation Approach

Zahid Mohammad Mir^{1*}, Daniel Höche^{1,2}, Celestino Gomes³, Rui Sampaio³, Alexandre C. Bastos³, Philippe Maincon⁴, M. G. S. Ferreira³ and Mikhail L. Zheludkevich^{1,5}

Abstract

A numerical model for enhanced service life prediction of concrete infrastructure is presented which includes transient analysis of processes during corrosion initiation as well as propagation stage. The temporal and spatial transition of Steel–Concrete Interface during depassivation events is described by a randomly varying chloride threshold function. As such random activation events can be accounted for, rather than having to pre-describe the anode size and location as in many existing models. The aim of the study is to investigate random spatial activation events in concrete structures in submerged zones based on dynamically changing boundary conditions on the rebar surface to control transition from passive to active state. Investigations are carried out to realize the sustainability of corrosion processes in limiting oxygen concentrations in dissolved seawater. The model showcases the numerical architecture, the associated concept of randomly varying chloride threshold and predicts that among other factors, the rate of oxygen strongly influences corrosion rate in submerged locations.

Keywords: rebar corrosion, chloride-induced depassivation, finite element method, submerged zone

1 Introduction

The corrosion-induced degradation of reinforced concrete (RC) structures is a well-known issue in the infrastructure community and is still one of the biggest challenging problems affecting structures worldwide (Page 1975; Tuutti 1982; British Cement Association 1997; Bertolini et al. 2013) amounting to losses in billions (Koch et al. 2001). The current societal, economic and technological challenges due to corrosion of steel in concrete outweigh the ongoing efforts and, as such, more scientific investment is necessary in this direction (Angst 2018). Furthermore, the situation is foreseen to get even worse due to the gradual aging of the infrastructure especially in developed countries and, to

some extent, in developing countries as well (Angst and Elsener 2017). Although, the corrosion-induced degradation can be caused by a variety of factors such as carbonation, chloride, acid exposure etc., the present work focusses entirely on chloride-induced corrosion of steel in concrete. The porous nature of the concrete allows the chloride ions to pass through it, ultimately reaching the rebar surface via a shortest path, i.e. concrete cover. The attainment of sufficiently high chloride concrete at the rebar surface marks the beginning of the corrosion process. This duration of time is called the initiation phase and can last several years or even decades, depending on the quality of concrete and exposure conditions. The corresponding chloride concentration is called critical chloride threshold (Cl_{th}) level.

In principle, the numerical calculation of corrosion parameters inside concrete depends on the accurate modelling of transport processes inside concrete for water content, temperature, chloride and oxygen, coupled with electrochemical processes at the Steel–Concrete Interface (SCI). Furthermore, one has to account

*Correspondence: zahid.mir@hzg.de

¹ Institute of Materials Research, Helmholtz-Zentrum Geesthacht Centre for Materials and Coastal Research, Max-Planck Str. 1, 21502 Geesthacht, Schleswig-Holstein, Germany

Full list of author information is available at the end of the article

Journal information: ISSN 1976-0485/eISSN 2234-1315

the mechanical effects of the generated rust products, such as creep around the rebar and eventually account for the induced damage in concrete (Ozbolt et al. 2012). Currently, there is a large number of numerical models (Bazant 1979; Page et al. 1981; Balabanic et al. 1996; Zhang and Gjorv 1996; Andrade et al. 1997; Thomas and Bamforth 1999; Glass and Buenfeld 2000; Ishida et al. 2009; Marsavina et al. 2009; Ozbolt et al. 2010, 2011, 2014) which are able to accurately model the above mentioned processes, i.e. before and after depassivation. However, very few of these focus on the accurate description of activation events and spatial location of active zones. In most of these models, either the anode size is pre-described or the initiation stage is decoupled from the propagation stage. This is contrary to what is observed in real life structures, where there is a random generation of activation events i.e. at SCI. The activation events demonstrate a stochastic temporal and spatial generation due to the heterogeneity at the SCI. This heterogeneous nature of the SCI has been confirmed in many studies (Angst and Elsener 2015; Angst et al. 2017). Given this random nature of SCI, an approach is proposed based on a varying chloride threshold ($f_{CL,T}^p$) to account for the random and probabilistic nature of SCI with regard to varying Cl_{th} levels. Therefore, in this study, a varying chloride function $f_{CL,T}^p$ accounts for factors which arise due to inhomogeneity at SCI. Examples of local factors are Pre-cracks (Borosnyói and Balázs 2005), air voids (Angst et al. 2017), interfacial transition zone (ITZ) and associated chemistry (Page 1975; Gjorv 1995; Horne et al. 2007; Jakobsen et al. 2016; Vollpracht et al. 2016), presence of mill scale (Ghods et al. 2011; Karadakis et al. 2016), pre-existing rust (Angst and Elsener 2015; Stefanoni et al. 2015), passive film (Hansson et al. 2006; Poursaeed and Hansson 2007; Ghods et al. 2009; Zhang and Poursaeed 2015; Poursaeed 2016), bleed zones (Mohammed et al. 2002; Castel et al. 2003; Soylev and Francois 2003; Castel et al. 2006; Horne et al. 2007), nature of steel (Ray et al. 1997; Nikolaou and Papadimitriou 2004; Scully and Hurley 2007; Cadoni et al. 2013), structural loads (Feng et al. 2011a, b) as shown in Fig. 1 and as well as the bar-orientation (Angst and Elsener 2015) etc. The combination of these varying parameters leads to varying temporal and spatially Cl_{th} levels and consequently varying time for corrosion initiation.

Varying chloride threshold levels were experimentally measured by Silva et al. (2013) and the results indicated that along the SCI a range of chloride levels could be observed. Threshold levels varied between 0.15 and 1.5 wt% of concrete. Similar results have been extensively documented by Angst et al. (2009).

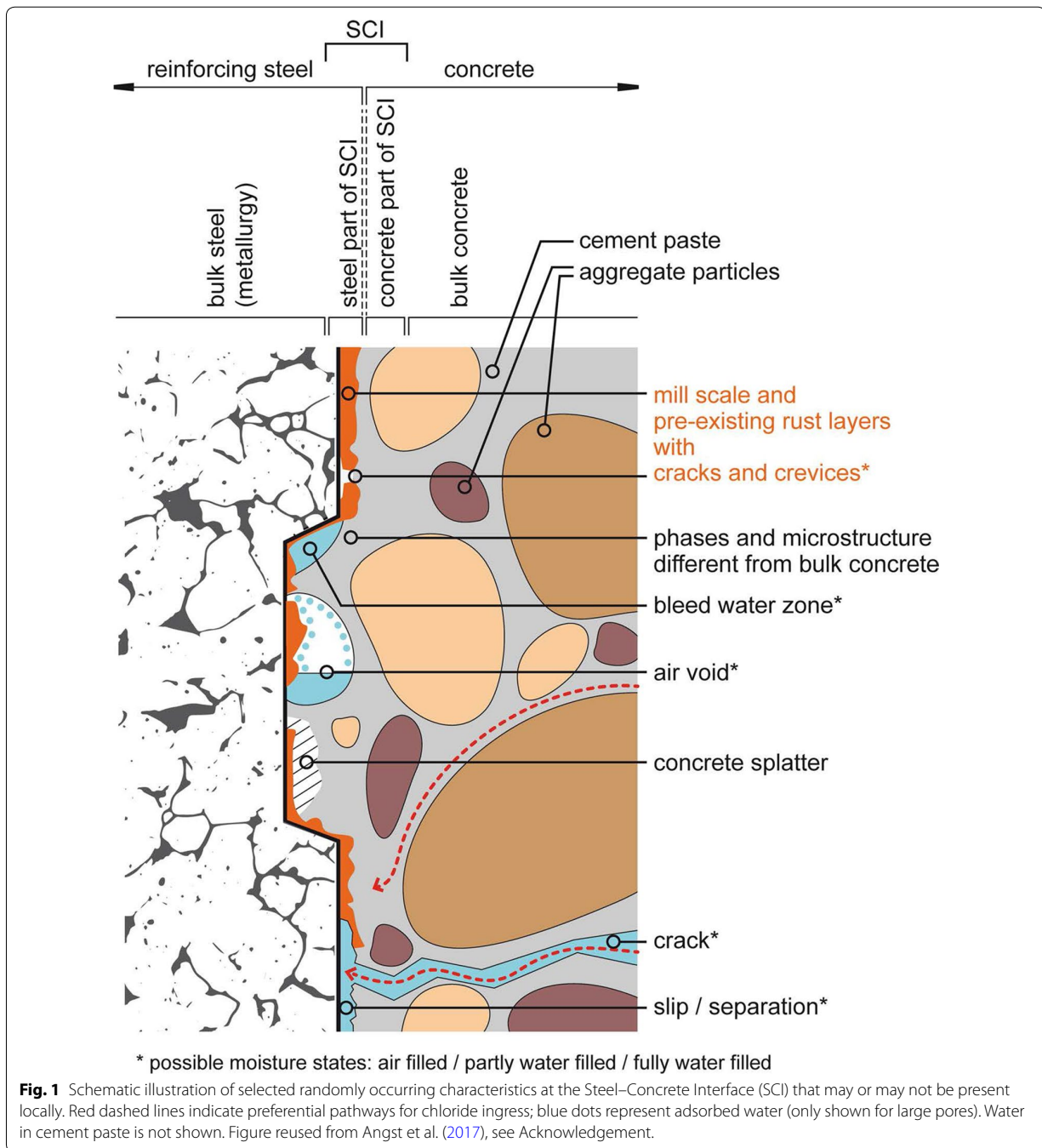
These uncertainties at SCI can be weighed against a central factor of a variable threshold or a local

threshold. As a result a probabilistic function is required to account for the spatial variation of Cl_{th} along the rebar surface. As such, anode location and size are not pre-described in this model and anodic activation can occur wherever the local Cl_{th} has been exceeded (Michel 2013) as described by $f_{CL,T}^p$. Furthermore, initiation and propagation phases are combined together in a single numerical model.

Recent experimental findings from a 20 year exposure history (Boubitsas et al. 2014) of structures exposed to marine environment in the Träslövsläge field site on the west coast of Sweden have revealed that chloride attack is far more severe in the submerged zone than in the splash zone. Therefore, more attention is required to explore the corrosion characteristics of infrastructure in the submerged zones. Similar data was recorded by extensive field studies of concrete samples submerged in seawater in different geographical locations (Lindvall 2003). Another motivation is that, historically, submerged zones have received little attention, which could be mostly attributed to difficulties in conducting experimental work. Few case studies are reported in the literature. Recent field assessment of decommissioned bridge piers in submerged zone in south Florida listed by Walsh (2015) has revealed severe localized corrosion in the submerged zones with localized active regions up to 20 cm in length. Therefore, submerged zone has been chosen as the exposure scenario for the numerical model.

In addition, numerical treatment of rust generation has been included in the model by employing solubility criteria (Yan et al. 1993; Deslouis et al. 2000; Hoche 2015). This includes modelling of surface reactions leading to rust layer growth occurring due to precipitation of corrosion products such as $Fe(OH)_2$. The presented model represents a continuum of a coupled system of field equations with accompanying non-linear boundary conditions. The finite element method has been employed (Belytschko et al. 2000, 2014) to solve the resulting system of equations. Several fundamental assumptions have been considered, balancing accuracy versus computational cost. The assumptions include:

- Adsorption and desorption hysteresis for moisture are not considered (Ozbolt et al. 2016).
- Formation of rust layer is attributed to generation of $Fe(OH)_2$ as a primary rust product. However, many other products have been identified (Vera et al. 2009).
- Mechanical damage, due to rust generation is excluded from the model. This is left for future studies.
- Theory of dilute solutions is employed.



- e. Uniform rebar surface conditions are considered. Variation of SCI parameters are included inside $f_{CL,T}$.
- f. Potential-dependent variation of chloride threshold is not included, the reader is directed to works of Sagüés et al. (2014), Walsh (2015).
- g. Chemical activity effects are not considered.

In the present paper, a 2D numerical model is presented wherein transport processes leading to corrosion initiation are coupled with electrochemical processes. Non-linear boundary conditions are used at the rebar surface to account for corrosion currents. A representation of concrete pore solution is used as electrolyte medium.

Processes leading to hydration of concrete are ignored: sufficiently aged concrete with hydration age ($T_{hy} > 180$ days) is considered. A simplified 2D geometry is employed to exhibit the FEM based coupled model in order to investigate the transport and corrosion processes. The coupling of non-mechanical processes with mechanical damage processes is under development.

2 Mathematical Formulation of Physical Processes

This study is focused on modelling transport and corrosion processes applicable to submerged zones. Governing field equations and related boundary conditions are presented. It is assumed that the concrete is in a mature condition ($T_{hy} > 180$ days): hydration processes are mostly completed and as such chloride diffusion can be assumed to be independent of the degree of hydration (Tang and Nilsson 1996). The electrolyte is defined using a concrete pore solution from Johannesson et al. (2007) and has been adopted for initial electrolyte concentration, see Table 1. All processes leading to corrosion-initiation, such as moisture transport, oxygen transport, chloride transport and other governing physical phenomena are described. The general structure of the computational model is shown in Fig. 2.

2.1 Multi Ion Laplace–Nernst Planck Model

Concrete is an intrinsically porous quasi brittle material. The theory of dilute solutions in porous media has been adopted for modelling transport of ions in water filled pore space inside bulk concrete. The movement of ions inside the pore solution is carried out using a set of extended Nernst–Planck equations for each ion. The model tries to accommodate as many ions as possible to mimic the realistic cementitious environment as it has been pointed out by Karadakis et al. (2016) that the diffusion rate of each ion inside the pore solution is governed by the electrolyte potential of the entire ionic solution as well as the concentration gradient. The flux of each specie Q_i (mol/m²/s) through the electrolyte pore system can be written as

$$Q_i = -(D_i \nabla C_i + z_i U_{i_{mob}} F C_i \nabla \phi_{el}) + C_i \mathbf{u} \quad (1)$$

and the mass balance for each specie is written as

$$\varphi_p \frac{\partial C_i}{\partial t} = -\nabla \cdot (\varphi_p Q_i) + m_{r_i} \quad (2)$$

where φ_p denotes the capillary porosity of mature concrete (m³ of voids per m³ of concrete), C_i denotes the concentration of each pore ion specie, $D_i = D_i^w \tau t_t$ is the effective diffusion coefficient of each specie, as one has to account for the effects of pore system structure (Johannesson et al. 2007; Ishida et al. 2009) such as tortuosity t_t and τ is a model parameter for each specie with charge number z_i . The ionic mobility coefficient is computed from Einstein’s relation: $U_{i_{mob}} = \frac{D_i}{(R_{gas} T)}$ with, R_{gas} as the

gas constant and T as the ambient temperature in K. ϕ_{el} is the electric potential, F is Faradays constant, m_{r_i} is the source/sink term to account for dynamic ion–ion and ion–oxide interactions and \mathbf{u} is the convection term in the electrolyte flow velocity vector, having a major effect (Hoche 2015) on corrosion under flow. Here \mathbf{u} is set to zero as mass transfer under flow does not exist inside concrete thereby, excluding the effects of convection. The approach includes the ionic species as shown in see Table 1.

For precipitates and deposition of solid species especially corrosion products, the diffusion term is set to zero in the Nernst–Planck equation. Furthermore, the model assumes electro-neutrality at each point in the electrolyte domain by assuming charge conservation at each time step in the analysis according to the relation:

$$\sum_{bulk} z_i C_i = 0 \quad (3)$$

The resulting electric current density i_{el} in the electrolyte due to transport of charge carrying ions through it, is described by Faraday’s Law:

$$i_{el} = F \sum_{bulk} z_i Q_i \quad (4)$$

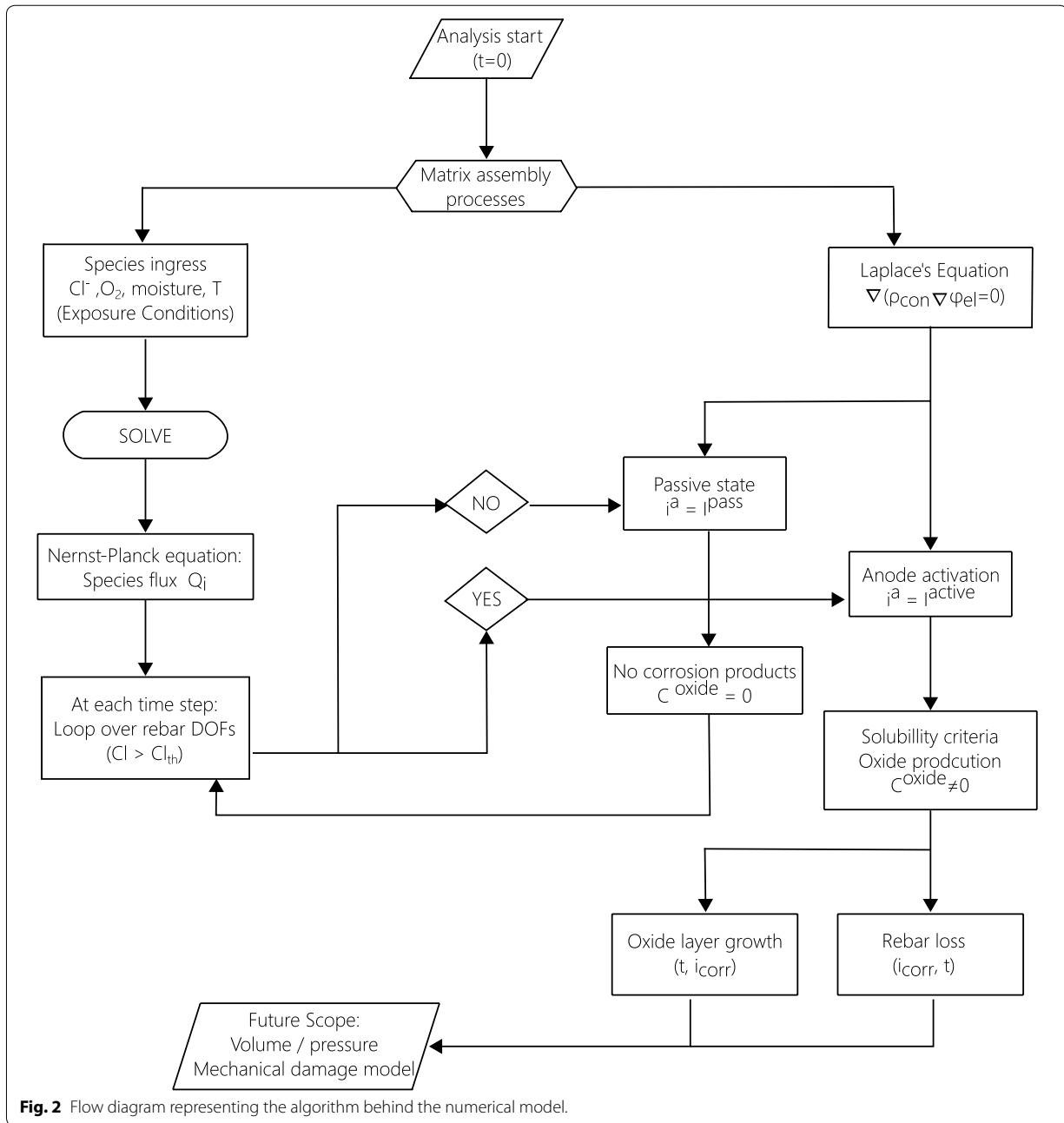
Apart from charge and mass conservation, electrical neutrality is maintained and can be written as:

$$\nabla \cdot i_{el} = 0 \quad (5)$$

The above expression can be rewritten to include the concrete resistivity ρ_{el} which is directly dependent on

Table 1 Pore solution and pore system characteristics (Johannesson et al. 2007).

Species	Cl ⁻	Na ⁺	OH ⁻	Ca ²⁺	K ⁺	SO ₄ ²⁻
$D_i^w \times 10^{-9}$ (m ² /s)	2.2	1.33	5.28	0.79	1.96	1.07
C_i (t=0) (mol/m ³)	0	85	300	10	213	9
Scaling parameter τ	0.1	0.4	1	0.2	0.4	1
Tortuosity t_t	0.015	0.015	0.015	0.015	0.015	0.015



the degree of saturation S^w of concrete as well as the capillary porosity φ_p .

$$\nabla \cdot (1/\rho_{el}(S^w, \varphi_p) \cdot \nabla \phi_{el}) = 0 \quad (6)$$

For a constant resistivity, Eq. (6) reduces to a standard Laplace equation for the domain.

$$\nabla^2 \phi_{el} = 0 \quad (7)$$

The above equation is solved for the distribution of electric potential as the field variable in order to model the movement of ions against an electrical field and to use electrochemical boundary conditions at SCI which will be discussed in the forthcoming sections. The conductivity and oxygen diffusivity in concrete in the submerged zone has been interpolated from Fig. 3.

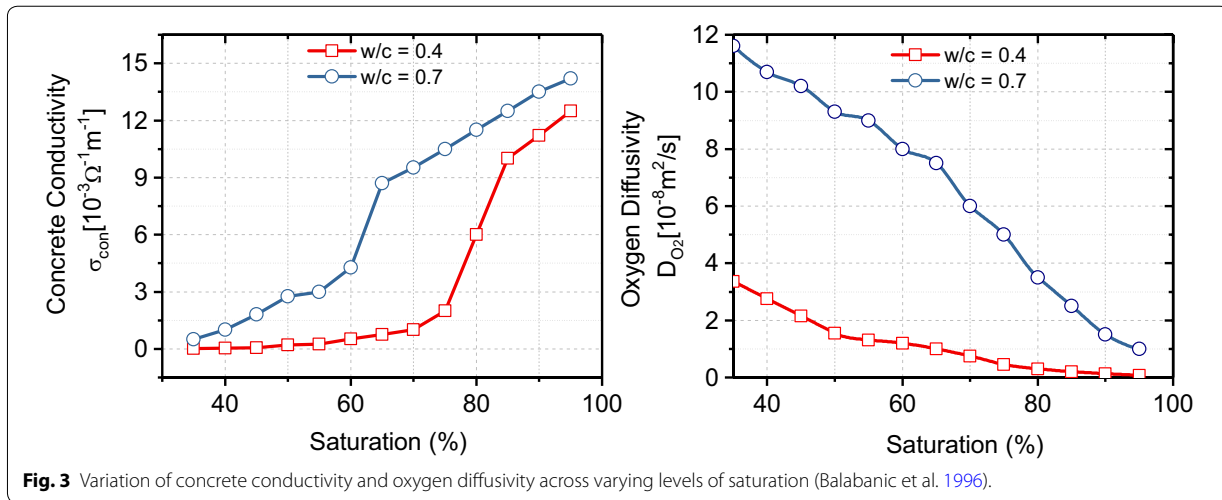


Fig. 3 Variation of concrete conductivity and oxygen diffusivity across varying levels of saturation (Balabanic et al. 1996).

2.2 Capillary Water Transport

Moisture transport is included in the model by considering diffusion-based movement of moisture through the capillary network under an external gradient. Richards’s equation is used to model moisture movement as a volume fraction of bulk concrete (Tang and Nilsson 1996; Ozbolt et al. 2010).

$$\frac{\partial \theta_h}{\partial t} = \nabla \cdot [D_h(\theta_h) \nabla \theta_h] \tag{8}$$

where, $\theta_h = S^w \varphi_p$ is the volume fraction of pore water inside concrete and $D_h(\theta_h)$ is the diffusivity coefficient of capillary water inside concrete. Previous studies (Leech et al. 2003; Ozbolt et al. 2010) have denoted capillary water as a nonlinear function of initial and saturated water contents. This nonlinear expression is denoted as

$$D_h(\theta_h) = D_{0_h} e^{n \bar{\theta}_h} \tag{9}$$

with,

$$\bar{\theta}_h = (\theta_h - \theta_{0_h}) / (\theta_{t_h} - \theta_{0_h}) \tag{10}$$

where, D_{0_h} , n , $\bar{\theta}_h$, θ_{0_h} , θ_{t_h} are the initial diffusivity coefficient, shape term, reduced water content, initial and saturated water content respectively, see Table 2. In this work, for submerged conditions, $S^w = 1$ has been considered.

2.3 Chloride Binding

It is widely accepted that the chloride binding capacity of the bulk cement is greatly responsible for extending the corrosion initiation stage. Various cement phases

Table 2 Parameters included in the computational model.

Parameter	Symbol	Value	Unit
Limiting capillary water permeability	D_{0_h}	2.2×10^{-10}	m^2/s
Shape factor	n	6.4	–
Initial fraction of water content	θ_{0_h}	0.01	m^3/m^3
Saturated water content	θ_{t_h}	0.1	m^3/m^3
Concrete porosity	φ_p	0.1	m^3/m^3
Hydration age	T_{hy}	> 180	Days
Binding rate coefficient for chloride ions	α_{rc}	1×10^{-5}	1/s
Isotherm calibration factor	β	0.7	–
Deposition constant $Fe(OH)_2$	$K_{Fe(OH)_2}^{int}$	3.7×10^{-1}	1/s
Solubility product of $Fe(OH)_2$	$K_{Fe(OH)_2}^{sp}$	8×10^{-6}	mol^3/m^9
Binder content	W_{binder}	350	kg/m^3
Density of concrete	ρ_{con}	2400	kg/m^3
Gas constant	R_{gas}	8.31×10^{-3}	$kJ/mol/K$
Thermal conductivity of concrete	λ	2.1	$W/m/K$
Specific heat capacity of concrete	c	900	$J/kg/K$
Molar mass of Cl^-	M_{Cl}	0.035	kg/mol

exhibit varying chloride binding capabilities. X-ray photoelectron spectroscopy (XPS) investigation of Johansson et al. (2007) demonstrated that AFm phases possess significantly higher binding capabilities compared to CSH phases, whereas experiments by Hirao et al. (2005) concluded otherwise. However, CSH due to its highest volume fraction certainly contributes the most to chloride binding. Total binding of chloride is a combination of physical binding of chloride with pore walls as well as chemical binding forming Friedel’s salt ($3CaO \cdot Al_2O_3 \cdot CaCl_2 \cdot 10H_2O$) at lower concentrations and Kuzel’s salt ($3CaO \cdot Al_2O_3 \cdot 0.5CaSO_4 \cdot 0.5CaCl_2 \cdot 11H_2O$) at

higher concentrations (Zibara 2001). In this work, the overall binding has been expressed with a chloride isotherm depicting a linear relationship between free chloride in the pore solution and the bound chloride.

$$\varphi_p \frac{\partial C_{Cl}}{\partial t} = -\nabla \cdot (\varphi_p Q_{Cl}) + m_{r_Cl} \quad (11)$$

$$\frac{\partial C_{clb}}{\partial t} = \alpha_{rc}(\beta C_{Cl} - C_{clb}) = -m_{r_Cl}$$

C_{Cl} is free chloride concentration of pore solution in (mol/m^3), and C_{clb} is bound chloride expressed in (kg/m^3) of concrete. α_{rc} is a binding rate constant and β is a model parameter (Saetta et al. 1993).

2.4 Oxygen Transport

The transport of oxygen from the external environment to the SCI is modelled entirely based on diffusion and as such the mass balance for oxygen can be written as

$$\varphi_p \frac{\partial C_{O_2}}{\partial t} = \nabla \cdot (\varphi_p D_{O_2} (S^w, \varphi_p) \nabla C_{O_2}) \quad (12)$$

The diffusion of oxygen is high in unsaturated concrete and considerably lower in water saturated concrete. The diffusion coefficient of oxygen has been taken from data extrapolation of Balabanic et al. (1996), see Fig. 3.

2.5 Depassivation Based on Random Distribution of Chloride Threshold

In many previous modelling approaches (Balabanic et al. 1996; Kim and Kim 2008; Michel 2013), a pre-defined anode size and location is used for numerical analysis, which is quite contrary to what is observed in the electrochemical testing of concrete. Activation events are particularly random in un-cracked members. For members experiencing pre-cracking or flexural cracking, activation events can occur directly at the crack location on the SCI (Ozbolt et al. 2010) and can be preassigned. Furthermore, in many models a single chloride threshold value is used, whereas for similar concrete mix and laboratory conditions, a clear variability is observed in depassivation as reported in the recent experiments of Angst and Elsener (2017).

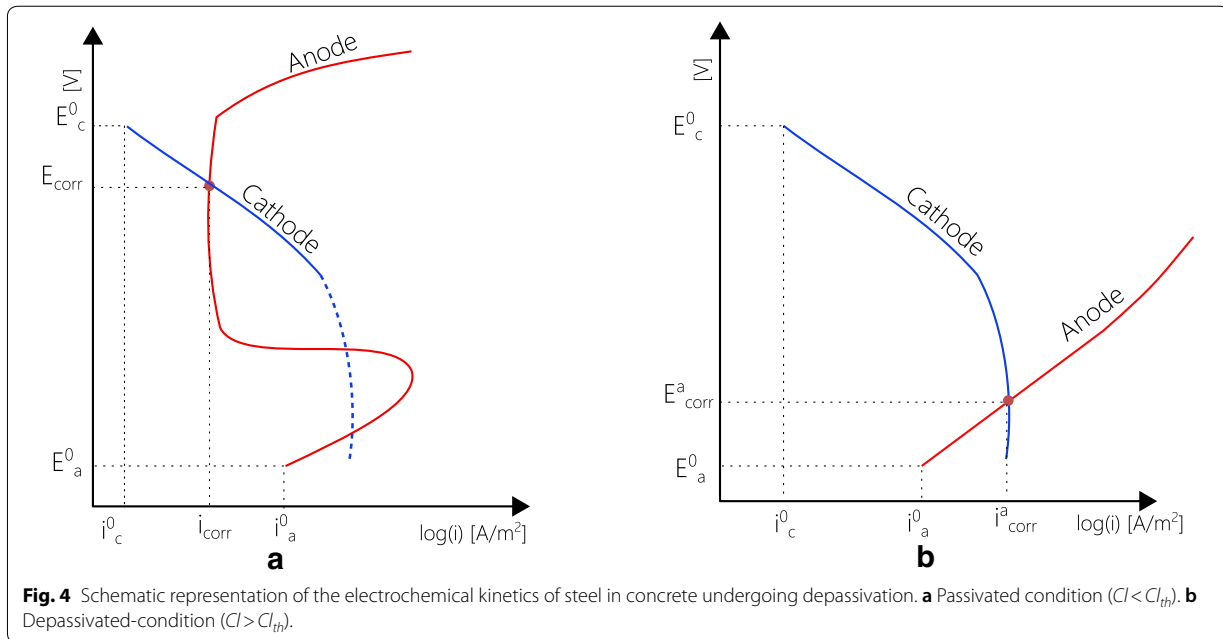
Apart from the chloride concentration at the rebar, there are other randomly varying factors which play a crucial role in depassivation. As mentioned previously, these factors include pre-cracks, air voids, water channels, bar orientation, rebar surface conditions and workmanship (Angst et al. 2017). As an example, the

presence of small air voids at the SCI can have a strong shielding effect and retard the depassivation of rebar at those locations, because a high pressure is required to fill these air voids and might take decades to completely fill in. On the contrary, water pockets usually found under horizontally placed rebars can lead to a faster attainment of depassivation. In continuum-based models, these variable factors at the SCI cannot be easily accounted for, due to their probabilistic nature and difficulties in experimental quantification. Several models would be required to investigate the effect of each factor, thereby considerably increasing the computational effort. Therefore, in this study, we have included these varying parameters into a randomly distributed mathematical function f^{CL_T} with varying chloride threshold limits along the rebar surface. The range of Cl_{th} is obtained from experiments by Alonso et al. (2000) with $0.39 < Cl_{th} < 1.16$ (free Cl^- as a percentage of binder weight) and is used as end limits for f^{CL_T} . This function includes numbers varying within the Cl_{th} range at equal intervals and fitted with a smooth cubic spline function. Anodic activation is therefore accounted in the model with spatial and temporal resolution at locations where the chloride content has exceeded its randomly assigned value at a particular location on the rebar surface. The numerical model is able to change the metal dissolution currents at these spatial locations. Other models employing a varying chloride threshold include works of Sagüés et al. (2014), Walsh (2015) and Michel (2013).

2.6 Electrochemical Boundary Conditions

The electrochemical reactions occurring at the rebar interface follow Faraday's law and can be described as oxidation of iron ($2Fe \rightarrow 2Fe^{2+} + 4e^-$) and consumption of oxygen at the cathodic sites, leading to production of hydroxyl ions ($O_2 + 4H_2O + 4e^- \rightarrow 4OH^-$). At the very beginning of the service life of RC structures, the rebars are in a passive state. Once the chloride threshold is exceeded at a particular point on the rebar surface, anodic activation is enabled at this particular location leading to metal loss and oxide generation. The model is able to dynamically make this transition by constantly looping over all mesh elements at rebar surface in each time step to check for the exceeded local Cl_{th} levels. Due to a limited number of elements on the rebar surface as compared to the bulk, this step is deemed not to be computationally expensive. The electrochemical state of rebar in passive and active stage is shown schematically in Fig. 4.

Tafel like extrapolation of the Butler–Volmer relations have been used for electrode kinetics at the interface. It



is assumed that anodic parts are subjected to activation polarization as:

$$i_a = \begin{cases} i_a^{pass}, & Cl < Cl_{th}(x) \\ i_a^0 \cdot e^{2.3(\vartheta_{el} - \vartheta_a^0)/\beta_a}, & Cl \geq Cl_{th}(x) \end{cases} \quad (13)$$

where, i_a is the anodic current density (A/m^2) and $i_a^{pass} = 10^{-4} A/m^2$ is the passive current density as reported (Hansson 1984; Poursaeed and Hansson 2007). The change from passive to active current is done using a smoothed Heaviside function to avoid computational instabilities. Here i_a^0 is the exchange current density (A/m^2), ϑ_{el} is the electric potential (V) as calculated from Laplace equations (Eq. 7) on the interface, ϑ_a^0 is the equilibrium potential and β_a is the anodic Tafel slope in (V/dec).

For the cathodic half-cell reaction, the transport of oxygen through the concrete cover and its consumption at the cathodic sites leads to a limiting oxygen diffusion current density for the attainment of a continuous flux of oxygen. The cathodic reaction is under activation and concentration polarization and is expressed based on works of Kranc and Sagues (1994) thereby including the concentration of oxygen at the SCI as:

$$i_c = -i_c^0 \cdot \left(\frac{C_{O_2}^{SCI}}{C_{O_2}^{ext}} \right) e^{2.3(\vartheta_{el} - \vartheta_c^0)/\beta_c} \quad (14)$$

where, i_c is the cathodic current density (A/m^2), i_c^0 is the exchange current density (A/m^2), ϑ_c^0 is the equilibrium potential for the cathodic and β_c is the cathodic Tafel slope in (V/dec). $C_{O_2}^{SCI}$ is the concentration of oxygen at the SCI, $C_{O_2}^{ext}$ is the external concentration of the oxygen at the concrete cover.

At the rebar interface, O_2 is consumed whereas OH^- ions are produced as a consequence of reduction reaction. Similarly, Fe^{2+} ions are produced due to oxidation of metal at the interface. For the cathodic sites, according to Faradays law, the number of oxygen molecules reduced per unit surface area per unit time at the SCI is given by the relation:

$$i_c = zFQ_{O_2}|_{SCI} \quad (15)$$

where, Q_{O_2} is the flux of oxygen in ($mol/m^2/s$) molecules reduced at the interface and $z=4$ is the number of electrons transferred in the cathodic half-cell reaction. On the other hand, the oxygen influx due to diffusion can be expressed as:

$$Q_{O_2} = -n \cdot (D_{O_2} \nabla C_{O_2})|_{SCI} \quad (16)$$

The balance between the O_2 molecules reduced at the rebar and the O_2 molecules arriving to the rebar surface with normal n from the nearby surrounding concrete. The conservation of oxygen then leads to:

$$\frac{i_c}{zF} = -n \cdot (D_{O_2} \nabla C_{O_2})|_{SCI} \quad (17)$$

Similarly the production of hydroxyl ions at the interface can be expressed as:

$$i_c = zFQ_{OH^-}|_{SCI} \tag{18}$$

where, Q_{OH^-} is the production flux in of OH^- ions and $z=4$. For the anodic half-cell reaction, the production of ferrous ions can be accounted from the anodic current density as:

$$i_a = zFQ_{Fe^{2+}}|_{SCI} \tag{19}$$

where $Q_{Fe^{2+}}$ is the flux of ferrous Fe^{2+} ions and $z=2$ is the number of electrons transferred in the anodic half-cell reaction. A schematic representation of ionic transport is depicted in Fig. 5a.

2.7 Heat Transport

The transport of heat within the bulk concrete leads to the distribution of temperature and can be expressed (Ozbolt et al. 2010) as:

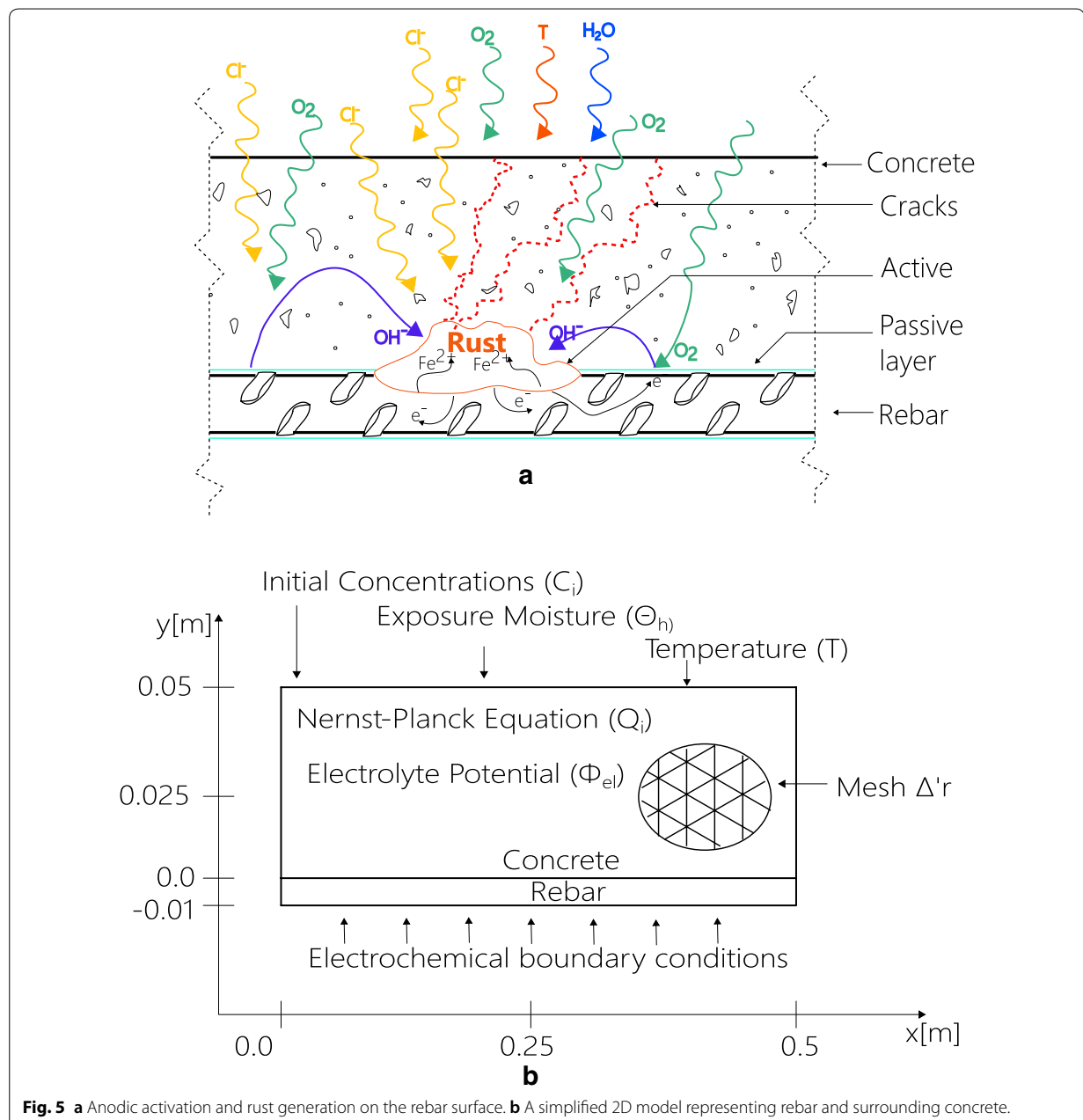


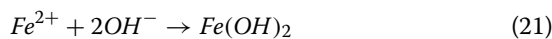
Fig. 5 a Anodic activation and rust generation on the rebar surface. b A simplified 2D model representing rebar and surrounding concrete.

$$\lambda(\Delta T) - c\rho_{con} \frac{\partial T}{\partial t} = 0 \tag{20}$$

where, T is the field variable for temperature distribution, λ is the thermal conductivity of concrete in (W/m/K), c is the thermal heat capacity of concrete (kg/m³) and ρ_{con} is the density of concrete (kg/m³).

2.8 Solubility Criteria for Self-Induced Oxide Production

Different experimental investigations have revealed a number of corrosion products formed during corrosion of steel inside concrete (Yamashita et al. 2005; Oluwadare and Agbaje 2007). Although the surface of hot rolled carbon steel is already covered with stable protective mill scale oxides, these oxides can end up dissolving once the chloride threshold is attained revealing the bare metal. As a continuation of electrochemical reactions, corrosion products are formed at the SCI and immediately start filling the concrete pores around them, forming a corrosion accommodating region (CAR). However, these corrosion products have a higher volume than that of the parent metal, leading to a build-up of pressure at SCI. This pressure increases with time, leading to formation of micro cracking zones around the SCI and in due course of time, eventually forming cracks, extending radially outwards and also longitudinally along the rebar length. The type of corrosion product depends on the exposure scenario. However, it is widely accepted that Fe(OH)₂ is the first corrosion product (Vera et al. 2009) formed immediately after depassivation. In the present model only Fe(OH)₂ has been considered for model simplicity according to the following reaction:



The above reaction describes the formation of Fe(OH)₂ in the pore solution. The corresponding reaction rate can be expressed using an interface deposition constant calculated using the solubility product as:

$$\frac{\partial C_{Fe(OH)_2}}{\partial t} = m_{r_int}^{Fe^{2+}} = K_{Fe(OH)_2}^{int} \times (C_{Fe^{2+}} C_{OH^{-}}^2 - K_{Fe(OH)_2}^{sp}) \times f^{ksp} \tag{22}$$

$$\text{where, } f^{ksp} = \begin{cases} 1 & ([Fe^{2+}][OH^{-}]^2 - K^{sp} > 0) \\ 0 & ([Fe^{2+}][OH^{-}]^2 - K^{sp} < 0) \end{cases}$$

is a step function which triggers oxide production only when the concentration of the constituent ions exceed the solubility product of the corresponding oxide. Oxide production occurs only at those points where $K_{Fe(OH)_2}^{sp}$

is exceeded. The formation rate of the oxide and the interface rate constant $K_{Fe(OH)_2}^{int}$ are based on works of Höche (2015) and Yan et al. (1993). These model constants signify a two dimensional mathematical description of the oxide film, representing hydroxide formation and its adhesion to the rebar surface. The solubility constant $K_{Fe(OH)_2}^{sp}$ is chosen to capture the initiation point of precipitation.

3 Numerical Case Study

A simplified 2D geometry has been chosen as shown in Fig. 5b to solve the above-mentioned coupled system of non-linear equations and boundary conditions. All the processes prior to cracking of concrete are described. The concrete and steel domains are discretized using finite element method. The weak forms were derived using the method of Galerkin's weighted residual (Zienkiewicz 1972; Belytschko et al. 2014) and solved via an implicit time integration scheme using COMSOL Multiphysics software. The detailed expression of the weak forms for the mentioned partial differential equations are not presented in the paper for the sake of brevity.

The domains Eqs. (2) and (7), represent a system of highly nonlinear equations which are decoupled, linearized and the resulting equation residuals are solved using a damped Newton's Raphson iterative method with a constant predictive slope (Bischoff et al. 2014). A regular mesh was constructed using Lagrange-based triangular elements. Mesh convergence studies were carried out to find an element size with balancing computational efficiency and numerical accuracy.

The average physical computational time was around 12 h, using a 44 core, 128 GB RAM workstation. An adaptive time stepping scheme was used with a minimum time step of 0.0864 h and a maximum time step of 48 h. Smaller time steps are employed during change of electrochemical boundary conditions to have better convergence. The simulated duration was 41 years.

The future development of the current model is in progress wherein the numerical coupling of the above mentioned non-mechanical system of equations with a damage based mechanical material model for concrete is in progress. The generation of cracks due to the expansion of corrosion products will be also simulated for 3D structural members in submerged conditions.

3.1 Exposure Conditions

Submerged sea water exposure has been chosen as the exposure conditions. The corresponding external chloride concentration $C_{Cl^{-}}^{ext}$ is taken equal to 450 mol/m³ (16 g/l) and the initial pore solution chloride concentration is shown in Table 1. The initial oxygen concentration is $C_{O_2} = 0.15$ mol/m³. The concentration of

external dissolved seawater oxygen concentration is set to $C_{O_2}^{ext} = 0.28 \text{ mol/m}^3$. Electric insulation is maintained by enforcing $\vec{n} \cdot \vec{i}_{el} = 0$ on the external model boundaries, where \vec{n} is the normal vector to mesh boundary. The condition $\vec{n} \cdot \vec{Q}_i = 0$ maintains symmetric boundary conditions, where the subscript i denotes all mobile chemical species inside the bulk.

4 Results and Discussion

The central goal of this study is to present the effect of a variable threshold and the associated numerical architecture to handle the change of boundary conditions from passive state to active state in time. The paper focusses on the numerical architecture and the underlying concept. The validation of this model is performed using observation of Perez and Chlorides (1999), Ozbolt et al. (2011), Michel (2013) who studied the corrosion of steel in concrete under various degrees of saturation. The exposure case studied here is the submerged zone.

4.1 Effect of a Variable Threshold Function

Randomly varying chloride function f_{CLT}^p as discussed previously is applied on the exposed rebar surface. f_{CLT}^p controls the activation at all spatial locations on the rebar as shown in the Fig. 6a, b. Prior to activation, the entire rebar surface undergoes uniform passive corrosion with a passive corrosion current density of $1 \cdot 10^{-4} \text{ A/m}^2$ as reported by experiments performed by Poursaee and Hansson (2007) and computational studies performed by Sagüés et al. (2014).

The passive stage results in a negligible rebar loss and the structural member is said to be in its initiation stage. The activation on the rebar surface depend on the accumulation of free chlorides at that location. The local chloride threshold is calculated as a function of binder weight using Eq. (23).

$$Cl_{th} = \left(\frac{C_{Cl}^{free} M_{Cl} \varphi_p \cdot 100}{W_{binder}} \right) \quad (23)$$

where, Cl_{th} is the chloride threshold as a weight percent of binder weight W_{binder} , which in turn is expressed in (kg binder per m^3 of concrete), C_{Cl}^{free} is the free concentration of chloride at the rebar surface in (mol/m^3) of pore solution, M_{Cl} is the molar mass of chloride in (kg/mol), φ_p is the capillary porosity in (m^3 pores per m^3 of concrete).

The chloride transport is modelled by using Nernst–Planck equation (Eq. 11). As the local chloride threshold as defined by f_{CLT}^p at a particular location on the rebar is exceeded, the boundary conditions on that point change from passive to active, thereby following Butler–Volmer Kinetics (Eqs. 13, 14). The effect of the variable chloride

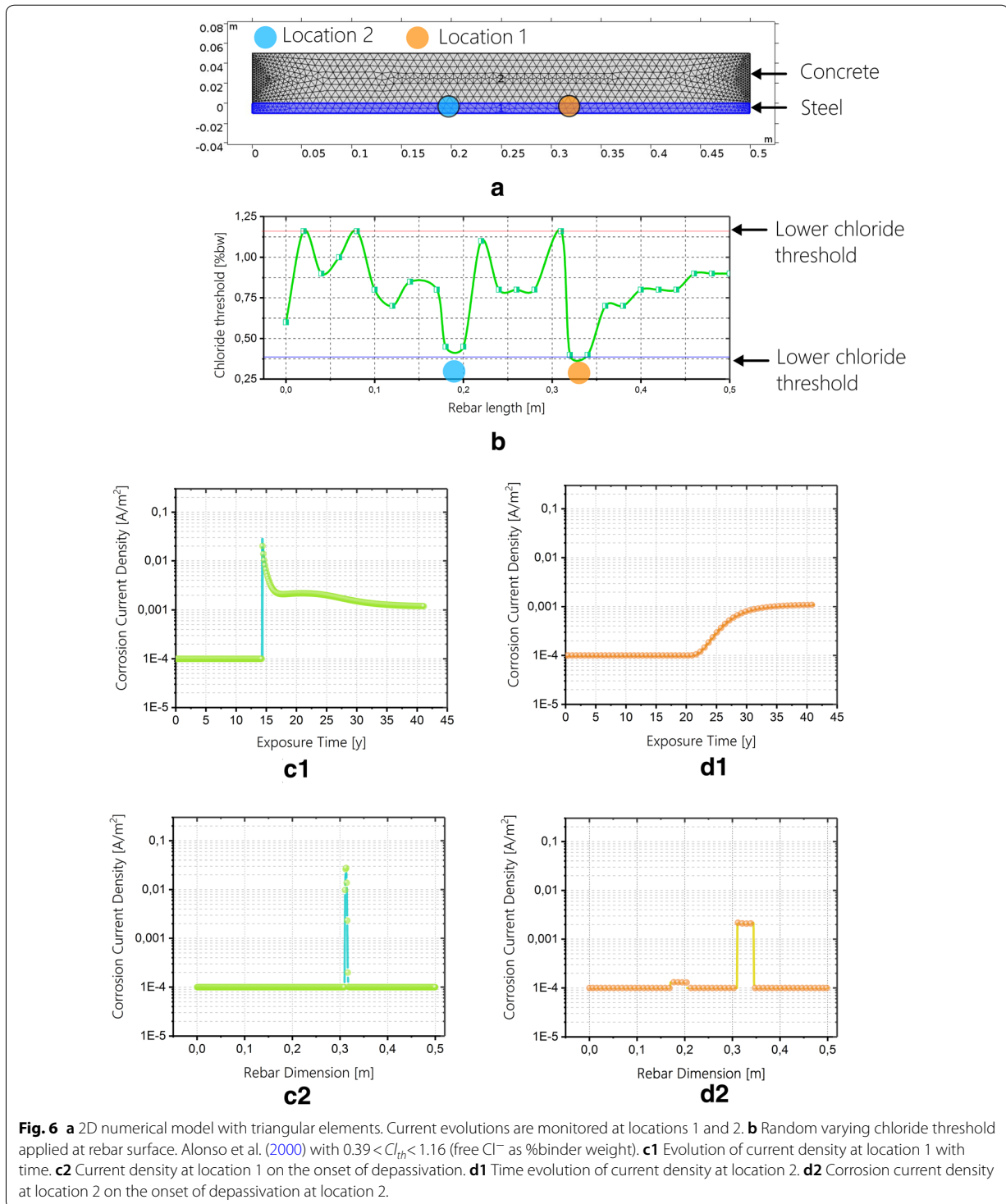
threshold and changing of boundary conditions on the rebar can be better visualized in terms of electrochemical parameters (Fig. 4).

Degradation is monitored at two locations referred as location 1 and location 2 (Fig. 6a). At location 1 (Fig. 6b), the critical chloride threshold f_{CLT}^p is equal to 0.39 ($\%W_{binder}$) and is exceeded in 14.35 years. The pre-peak curve in Fig. 6c1 represents the initiation stage. The post-peak curve designates the stage of active corrosion. The attainment of critical chloride threshold results in switching boundary conditions to activated Butler–Volmer kinetics with a peak current density of 0.0285 A/m^2 . This stage marks the end of the initiation period and the structure is said to be in degradation stage, although other regions of the rebar still maintain a passive layer. The corrosion current density profile across the rebar, on the onset of depassivation is shown in Fig. 6c2 where a sharp peak denotes the change of current from passive to active state.

At this location, the activated anodic and cathodic reactions lead to a quick consumption of the available oxygen, thus limiting the corrosion current. Once the immediately available oxygen is depleted, the corrosion process is set to be under concentration control. The magnitude of the post-peak corrosion density can be observed from Fig. 6c1 and is equal to 0.002 A/m^2 .

Chloride ingress through the bulk leads to the attainment of the critical chloride threshold equal to $f_{CLT}^p = 0.42 (\%W_{binder})$, thereby creating another activation zone, after 22.5 years. The rebar corrosion current distribution is shown in Fig. 6d2. The time evolution of corrosion current at location 2 is shown in Fig. 6d1. An initial current of $2.15 \cdot 10^{-4} \text{ A/m}^2$ is achieved which increases gradually, reaching a limiting current similar to that of the first activation spot, thereby sharing the incoming oxygen with the location 1. The effect of the increase in current at location 2 in Fig. 6d1 can be observed in the post peak current at location 1 in Fig. 6c1 after 22.5 years, where the effect of consumption of oxygen at an adjacent location is seen by a slight reduction of current. It is possible, that after a sufficiently long time and under an increasing chloride ingress, a sufficient amount of chloride is accumulated at all points on the rebar, so that the rebar would experience uniform corrosion.

Figure 7 shows the electrolyte current density along the rebar surface. At the end of the initiation stage (14.35 years) in Fig. 7a, a peak electrolyte current density is attained, which eventually reduces to a limiting current due to oxygen consumption. Correspondingly, a second peak is achieved, marking the passing of the second chloride threshold. Thus, the entire rebar dynamics have been defined as a combination of a random chloride threshold function f_{CLT}^p . Such an approach leads to new



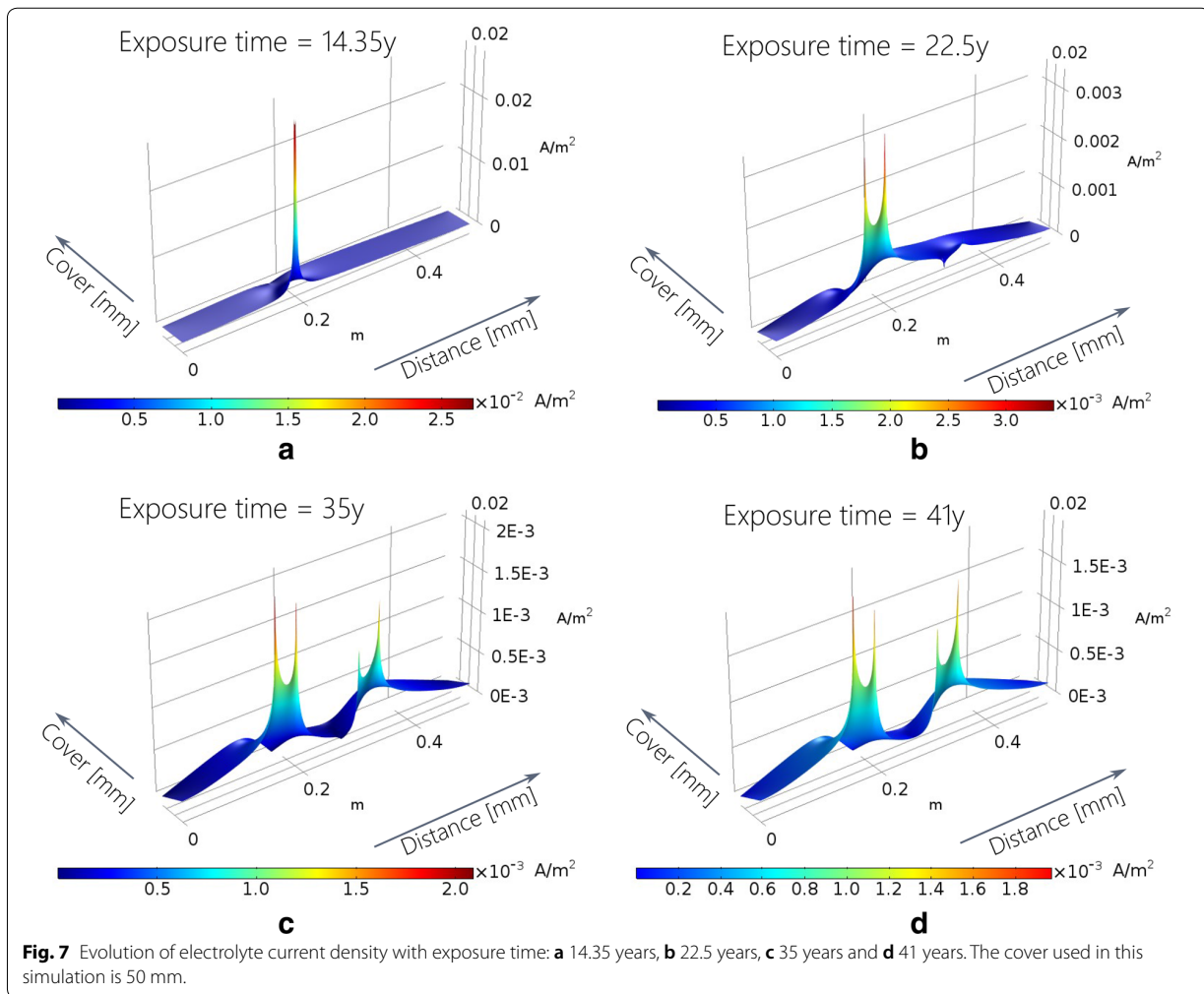


Table 3 Polarization data used in the model has been adopted from works of Kranc and Sagues (2001).

Parameter	Anodic	Cathodic	Unit
Exchange current density (i^0)	1.875×10^{-4}	6.25×10^{-6}	A/m ²
Tafel slope (β)	60	-160	V/dec
Equilibrium potential (θ^0)	-780	160	mV/SCE

possibilities in research as f_{CLT} can act as central factor against which other randomly varying factors of Steel–Concrete Interface can be weighed against.

4.2 Effect of Chloride Transport and Cover on Initiation Time

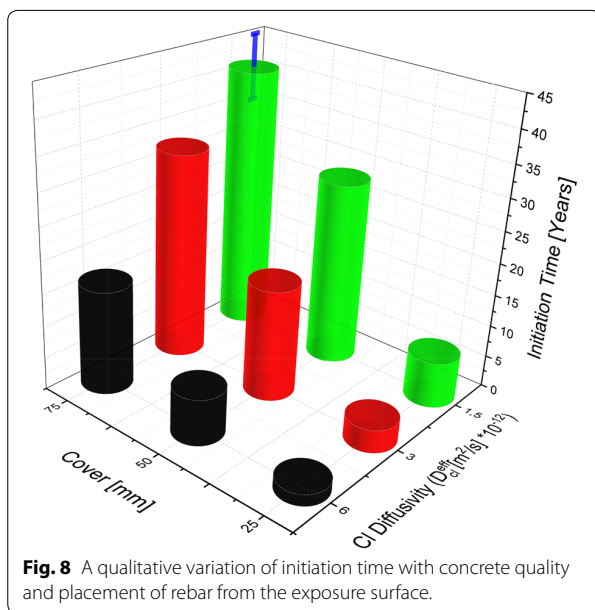
The chloride diffusion values have been taken (Johannesson et al. 2007) and corrected for tortuosity (Table 3).

However, further corrections of the diffusion coefficients may be required to account for the dependence of diffusion coefficient on concentrations gradients (Snyder et al. 2003). Other effects include the influence of temperature on the activation energy of diffusion process, as reported by the experimental investigation of Lin (1993). The present model does not consider these effects. For the sake of simplicity, and to keep the discussion around variable threshold and the underlying computational architecture, only microstructure corrections (Johannesson et al. 2007) have been accounted in the model. Recent discussions about the pore system inside concrete and associated diffusion corrections have been provided by Yang et al. (2017).

Although, it has been previously discussed that the initiation time is dependent on local Steel–Concrete Interface conditions as reflected by f_{CLT} , other factors could play a significant role. Deeply placed rebars usually suffer

less from chloride-induced corrosion. These rebars might still contribute cathodically in a macrocell configuration. Hence, cover distance as well as the quality of concrete are important factors. Parameter studies were carried out by varying diffusion coefficient of chloride against cover distance. A dense, tightly compacted concrete leads to a lower diffusion of chloride compared to a loosely packed concrete and the chosen values reflect it. It is also obvious that reducing the cover decreases the initiation time and a decrease in the chloride diffusion coefficient leads to an

elongation of the initiation time. Parameter studies were carried out with cover ranging from 25 to 75 mm and chloride diffusivity $(1.5-6) \times 10^{-12} \text{ m}^2/\text{s}$ and are presented in Fig. 8. Values with error bars represent simulations where the initiation time lasted more than final simulation time of 41 years. Apart from these, many other factors govern the length of the initiation stage and it is very difficult to study the effect of each one independently.

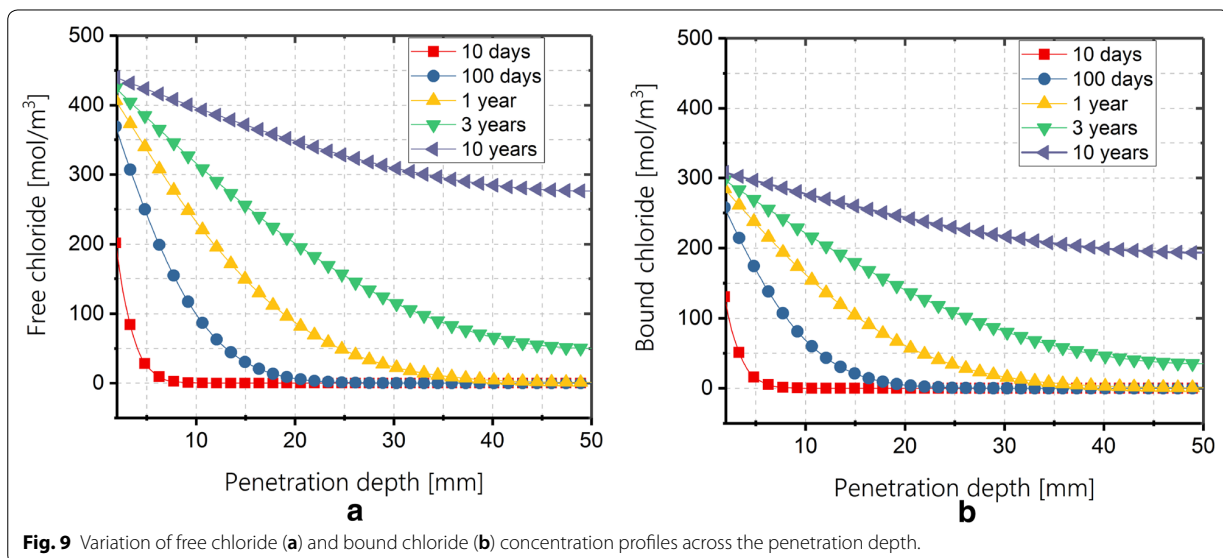


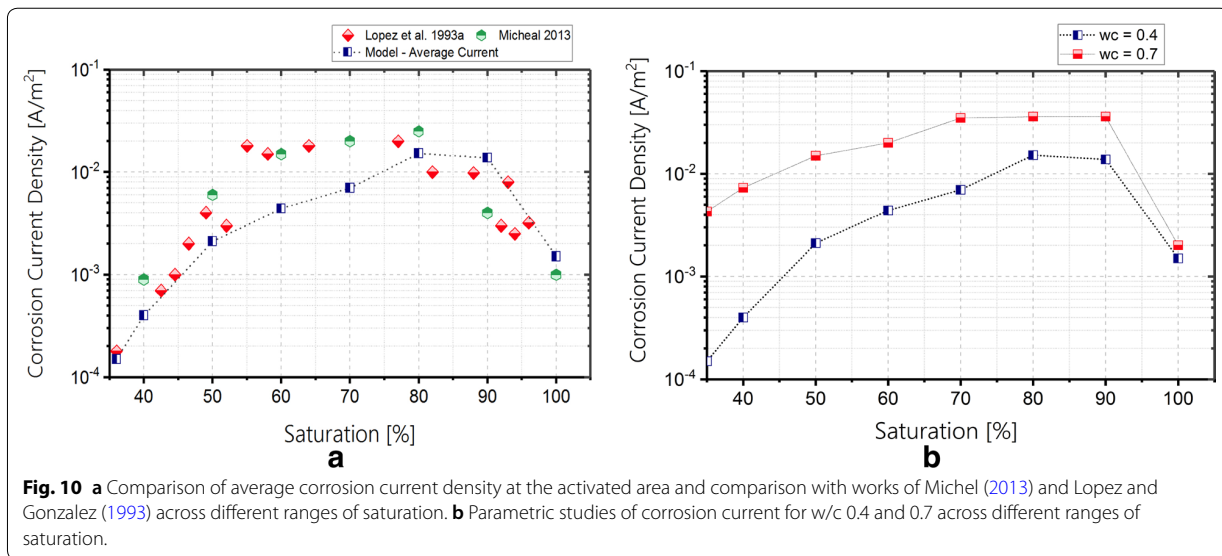
4.3 Chloride Profiles

Figure 9a, b show the evolution over time chloride profiles across penetration depth in saturated concrete. Chlorides bind to CSH structures along the influx path. The bound chlorides increases gradually with time with a similar profile as compared to free chloride concentration in solution. The characteristic chloride peak (Ozbolt et al. 2016) does not show up due to a saturated influx of macro-capillary water in submerged zone: no wetting and drying of the exposure face is considered. Furthermore, sudden crack opening events can also lead to sharp peaks in the profile.

4.4 Model Comparison

Figure 10a refers to the average corrosion current density at the anode across various degrees of saturation. The computational results are compared with the experimental works of Lopez and Gonzalez (1993) and Michel (2013) and a good agreement is observed. For the case presented in this paper, i.e. submerged zone exposure (saturated conditions), lower corrosion currents (0.015 A/m^2 for saturated case) are reported as compared to critical saturation range of 75–85%. Furthermore





saturated values less than 50% also depict a lower corrosion current due to increasing resistivity of concrete. Another important parameter governing the corrosion rate in reinforced concrete is the water-to-binder (w/c) ratio. Parameter studies are presented for w/c ratio of 0.4 and 0.7 across various degrees of saturation. Higher corrosion currents are observed for higher w/c ratio as shown in Fig. 10b.

5 Conclusion

1. The study presents a continuum based corrosion model, which is a coupled model in terms of transport of species, moisture, heat transport and coupled electrochemistry. The model is able to simulate processes before and after corrosion initiation. The broader aim of this study is to predict the service life of infrastructure in the submerged marine zone.
2. The model is able to simulate the transition between passivated to depassivated stage based on localized chloride threshold values. Development and subsequent evolution of anodic regions on the rebar is presented likewise.
3. Equations have been presented for governing non-mechanical processes leading to rebar corrosion. This includes capillary water transport, chloride transport and its binding with the matrix, transport of oxygen and other pore solution species, and as well as coupled electrochemistry. These equations are solved with finite element method.
4. A major objective of this study is to develop models to predict the behavior of new concrete recipe for

marine infrastructure. Simulations show that oxygen is able to sustain localized active areas on the rebar surface. However, the current density is dependent on the availability of oxygen and thus limited to around 0.0015 A/m^2 in the saturated cases. Comparison with previous models and experiments are reported. The macrocell coupling of the region of interest to other oxygen rich areas i.e. splash zone is not a part of the study and will be dealt in future.

6 Future Scope

- a. It is possible that with an evolution of conditions at the SCI, such as chloride content, oxygen content, pH, and temperature across the service life of the structure lead to a change in the electrochemical parameters, i.e. time evolution of corrosion parameters. In our ongoing experiments, it was observed that electrochemical parameters change dynamically inside concrete as it ages. These supporting experimental results will be reported in the future versions of the this model.
- b. The localization of corrosion onset is modelled by a random theoretical function. However random varying threshold function is based solely on a threshold range. However, other empirical and statistical relations might be developed which could describe more explicitly randomly occurring phenomena at the rebar interface.
- c. Due to the long experimentation times, chloride diffusion parameters were taken from relevant litera-

ture. An exact quantitative benefit from the current model can only be derived for our particular concrete recipe by using actual data from experimentation. However, completion of migration tests to derive effective chloride diffusivity are in progress and will be reported in future experimental studies. Correspondingly, the model will also be updated.

- d. Effect of presence of pre-cracks and crack generation due to oxide growth have not been included in the model, and will be studied in future.

Abbreviations

SCI: Steel–Concrete Interface; RC: reinforced concrete; FEM: finite element method; CSH: calcium silicate hydrate; AFm: alumina ferric oxide mono-sulfate.

Authors' contributions

ZMM, DH, CG, RS, ACB, PM devised the main conceptual idea, discussed the numerical strategy, evaluated the results and contributed in drafting the script. MGSF and MLZ supervised the work and gave critical comments to this manuscript. All authors discussed and contributed to the final manuscript. All authors read and approved the final manuscript.

Author details

¹ Institute of Materials Research, Helmholtz-Zentrum Geesthacht Centre for Materials and Coastal Research, Max-Planck Str. 1, 21502 Geesthacht, Schleswig-Holstein, Germany. ² Faculty of Mechanical Engineering, Helmut-Schmidt University, 22008 Hamburg, Germany. ³ Department of Materials and Ceramic Engineering and CICECO, University of Aveiro, 3810-193 Aveiro, Portugal. ⁴ SINTEF Materials and Chemistry, 7465 Trondheim, Norway. ⁵ Faculty of Engineering, University of Kiel, Kaiserstrasse 2, 24143 Kiel, Germany.

Acknowledgements

This research has received funding from the European Union's Horizon 2020 research and innovation program under grant agreement No: 685445 (LORCENIS—Long Lasting reinforced concrete for Energy infrastructure under Severe Operating Conditions).

The authors acknowledge the reuse of Fig. 1 which has been taken from the publication titled "The Steel-Concrete Interface", authored by Angst U.M, Geiker M. R., Micheal, A. et al. as cited in (Angst et al. 2017). The content has been used with changes in the caption solely for academic purpose under Creative Commons License 4.0 (<http://creativecommons.org/licenses/by/4.0/>).

The authors deeply acknowledge the help of Prof. Josko Ozbolt and Dr. Emiliano Sola from University of Stuttgart for discussions related to oxide layer growth. Special thanks to Mr. Muhammad Bilal from Institute of Materials Research, Helmholtz Zentrum Geesthacht (Germany). Furthermore, the constant support of colleagues from Institute of building materials (IWB) and Institute of Structural Mechanics (IBB) at university of Stuttgart (Germany) has helped in the overall completion of this study in one way or the other.

Competing interests

The authors declare that they have no competing interests.

Availability of data and materials

The numerical model developed in this study will be shared on request and after the approval of all authors is obtained.

Funding

This research has received funding from the European Union's Horizon 2020 research and innovation program under grant agreement No: 685445 (LORCENIS—Long Lasting Reinforced Concrete for Energy infrastructure under Severe Operating Conditions).

Publisher's Note

Springer Nature remains neutral with regard to jurisdictional claims in published maps and institutional affiliations.

Received: 9 May 2018 Accepted: 7 August 2018

Published online: 28 January 2019

References

- Alonso, C., Andrade, C., Castellote, M., & Castro, P. (2000). Chloride threshold values to depassivate reinforcing bars embedded in a standardized OPC mortar. *Cement and Concrete Research*, 30(7), 1047–1055.
- Andrade, C., Diez, L. M., & Alonso, C. (1997). Mathematical modeling of a concrete surface "skin effect" on diffusion in chloride contaminated media. *Advanced Cement Based Materials*, 6(2), 39–44.
- Angst, U. (2018). Challenges and opportunities in corrosion of steel in concrete. *Materials and Structures*, 51, 4.
- Angst, U., & Elsener, B. (2015). Forecasting chloride-induced reinforcement corrosion of concrete—effect of realistic reinforcement steel surface conditions. In *4th international conference on concrete, repair, rehabilitation and retrofitting (ICCCRRR)*, Leipzig, Germany.
- Angst, U. M., & Elsener, B. (2017). The size effect in corrosion greatly influences the predicted life span of concrete infrastructures. *Science Advances*, 3(8), e1700751.
- Angst, U., Elsener, B., Larsen, C. K., & Vennesland, O. (2009). Critical chloride content in reinforced concrete—A review. *Cement and Concrete Research*, 39(12), 1122–1138.
- Angst, U. M., Geiker, M. R., Michel, A., Gehlen, C., Wong, H., Isgor, O. B., et al. (2017). The steel–concrete interface. *Materials and Structures*, 50(2), 143.
- Balabanic, G., Bicanic, N., & Durekovic, A. (1996). The influence of w/c ratio, concrete cover thickness and degree of water saturation on the corrosion rate of reinforcing steel in concrete. *Cement and Concrete Research*, 26(5), 761–769.
- Bazant, Z. P. (1979). Physical model for steel corrosion in concrete sea structures—Theory. *Journal of the Structural Division-ASCE*, 105(6), 1137–1153.
- Belytschko, T., Liu, W. K., & Moran, B. (2000). *Nonlinear finite elements for continua and structures*. New York: Wiley.
- Belytschko, T., Liu, W. K., Moran, B., & Elkhodary, K. I. (2014). *Nonlinear finite elements for continua and structures* (2nd ed.). Chichester: Wiley.
- Bertolini, L., Elsener, B., Pedeferrì, P., Redaelli, E., & Polder, R. B. (2013). *Corrosion of steel in concrete: Prevention, diagnosis, repair*. New York: Wiley-VCH.
- Bischoff, M., Ramm, E., & von Scheven, M. (2014). *Advanced computational structural mechanics—Lecture Notes*. Stuttgart: Institut für Baustatik und Baudynamik, University of Stuttgart.
- Borosnyói, A., & Balázs, G. L. (2005). Models for flexural cracking in concrete: The state of the art. *Structural Concrete*, 6(2), 53–62.
- Boubitsas, D., Luping, T., & von Utgenannt, P. (2014). *Chloride ingress in concrete exposed to marine environment—Field data up to 20 years' exposure*. Stockholm: Swedish Cement and Concrete Research Institute (CBI).
- British Cement Association. (1997). *Development of a holistic approach to ensure the durability of new concrete construction*.
- Cadoni, E., Dotta, M., Forni, D., Tesio, N., & Albertini, C. (2013). Mechanical behaviour of quenched and self-tempered reinforcing steel in tension under high strain rate. *Materials and Design*, 49, 657–666.
- Castel, A., Vidal, T., Francois, R., & Arliguie, G. (2003). Influence of steel–concrete interface quality on reinforcement corrosion induced by chlorides. *Magazine of Concrete Research*, 55(2), 151–159.
- Castel, A., Vidal, T., Viriyamanont, K., & Francois, R. (2006). Effect of reinforcing bar orientation and location on bond with self-consolidating concrete. *ACI Structural Journal*, 103(4), 559–567.
- Deslouis, C., Festy, D., Gil, O., Maillot, V., Touzain, S., & Tribollet, B. (2000). Characterization of calcareous deposits in artificial sea water by impedances techniques: 2-deposit of Mg(OH)₂ without CaCO₃. *Electrochimica Acta*, 45(11), 1837–1845.
- Feng, X. G., Tang, Y. M., & Zuo, Y. (2011a). Influence of stress on passive behaviour of steel bars in concrete pore solution. *Corrosion Science*, 53(4), 1304–1311.

- Feng, X. G., Zuo, Y., Tang, Y. M., Zhao, X. H., & Lu, X. Y. (2011b). The degradation of passive film on carbon steel in concrete pore solution under compressive and tensile stresses. *Electrochimica Acta*, 58, 258–263.
- Ghods, P., Isgor, O. B., McRae, G. A., Li, J., & Gu, G. P. (2011). Microscopic investigation of mill scale and its proposed effect on the variability of chloride-induced depassivation of carbon steel rebar. *Corrosion Science*, 53(3), 946–954.
- Ghods, P., Isgor, O. B., McRae, G., & Miller, T. (2009). The effect of concrete pore solution composition on the quality of passive oxide films on black steel reinforcement. *Cement & Concrete Composites*, 31(1), 2–11.
- Gjorv, O. E. (1995). Effect of condensed silica fume on steel corrosion in concrete. *ACI Materials Journal*, 92(6), 591–598.
- Glass, G. K., & Buenfeld, N. R. (2000). The influence of chloride binding on the chloride induced corrosion risk in reinforced concrete. *Corrosion Science*, 42(2), 329–344.
- Hansson, C. M. (1984). Comments on electrochemical measurements of the rate of corrosion of steel in concrete. *Cement and Concrete Research*, 14(4), 574–584.
- Hansson, C. M., Poursaee, A., & Laurent, A. (2006). Macrocell and microcell corrosion of steel in ordinary Portland cement and high performance concretes. *Cement and Concrete Research*, 36(11), 2098–2102.
- Hirao, H., Yamada, K., Takahashi, H., & Zibara, H. (2005). Chloride binding of cement hydrates by binding isotherms of hydrates. *Journal of Advanced Concrete Technology*, 3(1), 77–84.
- Höche, D. (2015). Simulation of corrosion product deposit layer growth on bare magnesium galvanically coupled to aluminum. *Journal of the Electrochemical Society*, 162(1), C1–C11.
- Horne, A. T., Richardson, I. G., & Brydson, R. M. D. (2007). Quantitative analysis of the microstructure of interfaces in steel reinforced concrete. *Cement and Concrete Research*, 37(12), 1613–1623.
- Ishida, T., Iqbal, P. O., & Anh, H. T. L. (2009). Modeling of chloride diffusivity coupled with non-linear binding capacity in sound and cracked concrete. *Cement and Concrete Research*, 39(10), 913–923.
- Jakobsen, U. H., De Weerd, K., & Geiker, M. R. (2016). Elemental zonation in marine concrete. *Cement and Concrete Research*, 85, 12–27.
- Johannesson, B., Yamada, K., Nilsson, L. O., & Hosokawa, Y. (2007). Multi-species ionic diffusion in concrete with account to interaction between ions in the pore solution and the cement hydrates. *Materials and Structures*, 40(7), 651–665.
- Karadakis, K., Azad, V. J., Ghods, P., & Isgor, O. B. (2016). Numerical investigation of the role of mill scale crevices on the corrosion initiation of carbon steel reinforcement in concrete. *Journal of the Electrochemical Society*, 163(6), C306–C315.
- Kim, C. Y., & Kim, J. K. (2008). Numerical analysis of localized steel corrosion in concrete. *Construction and Building Materials*, 22(6), 1129–1136.
- Koch, G. H., Brongers, M. P. H., Thompson, N. G., Virmani, Y. P., & Payer, J. H. (2001). *Corrosion costs and preventive strategies in the United States*. FHWA-RD-01-156.
- Kranc, S. C., & Sagues, A. A. (1994). Computation of reinforcing steel corrosion distribution in concrete marine bridge substructures. *Corrosion*, 50(1), 50–61.
- Kranc, S. C., & Sagues, A. A. (2001). Detailed modeling of corrosion macrocells on steel reinforcing in concrete. *Corrosion Science*, 43(7), 1355–1372.
- Leech, C., Lockington, D., & Dux, P. (2003). Unsaturated diffusivity functions for concrete derived from NMR images. *Materials and Structures*, 36(260), 413–418.
- Lin, S. H. (1993). Chloride diffusion in porous concrete under conditions of variable-temperature. *Warme Und Stoffübertragung-Thermo and Fluid Dynamics*, 28(7), 411–415.
- Lindvall, A. (2003). *Environmental actions on concrete exposed in marine and road environments and its response*. Ph.D. thesis, Chalmers University of Technology.
- Lopez, W., & Gonzalez, J. A. (1993). Influence of the degree of pore saturation on the resistivity of concrete and the corrosion rate of steel reinforcement. *Cement and Concrete Research*, 23(2), 368–376.
- Marsavina, L., Audenaert, K., Schutter, G., Faur, N., & Marsavina, D. (2009). Experimental and numerical determination of the chloride penetration in cracked concrete. *Construction and Building Materials*, 23(1), 264–274.
- Martin-Perez, B. (1999). Service life modelling of R.C. highway structures exposed to chlorides. Ph.D. Thesis. University of Toronto, National Library of Canada = Bibliothèque nationale du Canada. http://www.collectionscanada.ca/obj/s4/f2/dsk1/tape8/PQDD_0007/NQ41230.pdf. <http://hdl.handle.net/1807/13268>.
- Michel, A. (2013). *Reinforcement corrosion: numerical simulation and service life prediction*. Ph.D. thesis, Technical University of Denmark (DTU).
- Mohammed, T. U., Otsuki, N., Hamada, H., & Yamaji, T. (2002). Chloride-induced corrosion of steel bars in concrete with presence of gap at steel–concrete interface. *ACI Materials Journal*, 99(2), 149–156.
- Nikolaou, J., & Papadimitriou, G. D. (2004). Microstructures and mechanical properties after heating of reinforcing 500 MPa class weldable steels produced by various processes (Tempcore, microalloyed with vanadium and work-hardened). *Construction and Building Materials*, 18(4), 243–254.
- Oluwadare, G. O., & Agbaje, O. (2007). Corrosion of steels in steel reinforced concrete in cassava juice. *Journal of Applied Sciences*, 7, 2474–2479.
- Ozbolt, J., Balabanic, G., & Kuster, M. (2011). 3D numerical modelling of steel corrosion in concrete structures. *Corrosion Science*, 53(12), 4166–4177.
- Ozbolt, J., Balabanic, G., Periskic, G., & Kuster, M. (2010). Modelling the effect of damage on transport processes in concrete. *Construction and Building Materials*, 24(9), 1638–1648.
- Ozbolt, J., Orsanic, F., & Balabanic, G. (2014). Modeling pull-out resistance of corroded reinforcement in concrete: Coupled three-dimensional finite element model. *Cement & Concrete Composites*, 46, 41–55.
- Ozbolt, J., Orsanic, F., & Balabanic, G. (2016). Modeling influence of hysteretic moisture behavior on distribution of chlorides in concrete. *Cement & Concrete Composites*, 67, 73–84.
- Ozbolt, J., Orsanic, F., Balabanic, G., & Kuster, M. (2012). Modeling damage in concrete caused by corrosion of reinforcement: Coupled 3D FE model. *International Journal of Fracture*, 178(1–2), 233–244.
- Page, C. L. (1975). Mechanism of corrosion protection in reinforced-concrete marine structures. *Nature*, 258(535), 514–515.
- Page, C. L., Short, N. R., & Eltarras, A. (1981). Diffusion of chloride-ions in hardened cement pastes. *Cement and Concrete Research*, 11(3), 395–406.
- Poursaee, A. (2016). Temperature dependence of the formation of the passivation layer on carbon steel in high alkaline environment of concrete pore solution. *Electrochemistry Communications*, 73, 24–28.
- Poursaee, A., & Hansson, C. M. (2007). Reinforcing steel passivation in mortar and pore solution. *Cement and Concrete Research*, 37(7), 1127–1133.
- Ray, A., Mukherjee, D., Sen, S. K., Bhattacharya, A., Dhua, S. K., Prasad, M. S., et al. (1997). Microstructure and properties of thermomechanically strengthened reinforcement bars: A comparative assessment of plain-carbon and low-alloy steel grades. *Journal of Materials Engineering and Performance*, 6(3), 335–343.
- Saetta, A. V., Scotta, R. V., & Vitaliani, R. V. (1993). Analysis of chloride diffusion into partially saturated concrete. *ACI Materials Journal*, 90(5), 441–451.
- Sagüés, A. A., Sanchez, A. N., Lau, K., & Kranc, S. C. (2014). Service life forecasting for reinforced concrete incorporating potential-dependent chloride threshold. *Corrosion*, 70(9), 942–957.
- Scully, J. R., & Hurley, M. F. (2007). *Investigation of the corrosion propagation characteristics of new metallic reinforcing bars—Final Contract Report VTRC 07-CR9*.
- Silva, N., Tang, L., Lindqvist, J. E., & Boubitsas, D. (2013). Chloride profiles along the concrete–steel interface. *International Journal of Structural Engineering*, 4(1–2), 100–112.
- Snyder, K. A., Feng, X. G., Keen, B. D., & Mason, T. O. (2003). Estimating the electrical conductivity of cement paste pore solutions from OH⁻, K⁺, Na⁺ concentrations. *Cement and Concrete Research*, 33, 793–798.
- Soylev, T. A., & Francois, R. (2003). Quality of steel–concrete interface and corrosion of reinforcing steel. *Cement and Concrete Research*, 33(9), 1407–1415.
- Stefanoni, M., Angst, U., & Elsener, B. (2015). Local electrochemistry of reinforcement steel—Distribution of open circuit and pitting potentials on steels with different surface condition. *Corrosion Science*, 98, 610–618.
- Tang, L., & Nilsson, L.-O. (1996). Service life prediction of concrete structures under seawater by a numerical approach. *Durability of Building Materials and Components*, 7(1), 97–106.
- Thomas, M. D. A., & Bamforth, P. B. (1999). Modelling chloride diffusion in concrete—Effect of fly ash and slag. *Cement and Concrete Research*, 29(4), 487–495.
- Tuutti, K. (1982). *Corrosion of steel in concrete*. Technical Report. Stockholm: Swedish Cement and Concrete Research Institute.
- Vera, R., Villarroel, M., Carvajal, A. M., Vera, E., & Ortiz, C. (2009). Corrosion products of reinforcement in concrete in marine and industrial environments. *Materials Chemistry and Physics*, 114(1), 467–474.

- Vollpracht, A., Lothenbach, B., Snellings, R., & Haufe, J. (2016). The pore solution of blended cements: A review. *Materials and Structures*, 49(8), 3341–3367.
- Walsh, M. T. (2015). *Corrosion of steel in submerged concrete structures*. Ph.D. thesis, University of South Florida. Retrieved from <http://scholarcommons.usf.edu/etd/6048>.
- Yamashita, M., Konishi, H., Kozakura, T., Mizuki, J., & Uchida, H. (2005). In situ observation of initial rust formation process on carbon steel under Na₂SO₄ and NaCl solution films with wet/dry cycles using synchrotron radiation X-rays. *Corrosion Science*, 47(10), 2492–2498.
- Yan, J. F., Nguyen, T. V., White, R. E., & Griffin, R. B. (1993). Mathematical-modeling of the formation of calcareous deposits on cathodically protected steel in seawater. *Journal of the Electrochemical Society*, 140(3), 733–742.
- Yang, P., Sant, G., & Neithalath, N. (2017). A refined, self-consistent Poisson–Nernst–Planck (PNP) model for electrically induced transport of multiple ionic species through concrete. *Cement & Concrete Composites*, 82, 80–94.
- Zhang, T. W., & Gjorv, O. E. (1996). Diffusion behavior of chloride ions in concrete. *Cement and Concrete Research*, 26(6), 907–917.
- Zhang, Y., & Poursaeed, A. (2015). Passivation and corrosion behavior of carbon steel in simulated concrete pore solution under tensile and compressive stresses. *Journal of Materials in Civil Engineering*, 27(8), 04014234.
- Zibara, H. (2001). *Binding of external chlorides by cement pastes*. Ph.D. thesis, University of Toronto.
- Zienkiewicz, O. C. (1972). 'Finite elements of non-linear continua, J. T. Oden, McGraw-Hill, New York, 1972. Price \$8.40. *International Journal for Numerical Methods in Engineering*, 5(1), 148. <https://doi.org/10.1002/nme.1620050117/abstract>.

Submit your manuscript to a SpringerOpen[®] journal and benefit from:

- Convenient online submission
- Rigorous peer review
- Open access: articles freely available online
- High visibility within the field
- Retaining the copyright to your article

Submit your next manuscript at ► springeropen.com

4.2. Article 3 - The Stability and Chloride Entrapping Capacity of Zn-Al-NO₂ LDH in High Alkaline/Cementitious Environment

Note: See attached article in the next pages. Reprinted without modification from [51] under CC BY 4.0 license. Published by MDPI, Basel, Switzerland.

4.2.1. A brief summary of Article 3

In this paper, experimental investigations are carried out to effectively understand the behavior of Zn-Al-NO₂ in alkaline environments similar to that of concrete. The assessment of ion exchange property of LDH is first carried out in aqueous salt solutions and cement pore solutions. A two step process is followed here. Firstly, the LDH is exposed to an environment with mostly one type of anion i.e. OH⁻ ion. Here, the OH⁻ capture and NO₂⁻ release from LDH is monitored. Secondly, LDH is exposed to a multi anionic environment containing both Cl⁻ and OH⁻ ions and the sequestration of each anion by LDH is critically assessed. Chloride binding isotherms are also determined for the entire alkaline pH range. Consequently, the stability analysis of LDH in pH range > 7 is performed to ensure the functionality of LDH in an alkaline environment.

The age effect on the Cl⁻ sequestration capacity was also investigated. This was a necessary step to understand the effect of time on the ion sequestration capacity and also to ensure that the bound Cl⁻ ions are not released back into the environment. The aim of this work is to investigate the Cl⁻ binding capacity of LDH in concrete. However, prior to studying the behavior of LDH in concrete, the compatibility of LDH with cement was studied. As a next step in this direction, mortars were cast with LDH and exposed to chloride ions. The chloride ingress was monitored in mortars with cast-in Cl⁻ ion sensitive sensors. The effect of NO₂⁻ released from LDH on the corrosion properties of steel embedded in mortar samples is also demonstrated.

4.2.2. Author contribution

In the following, the author of this dissertation is denoted by his initials ZMM. The names and initials of co-authors can be found in the appended manuscript. ZMM and CG contributed equally to this work. Conceptualization: ZMM, CG, ACB; LDH synthesis: FM and CR; Experimental execution and data treatment: ZMM and CG; writing, review and editing: ZMM and ACB; supervision: ACB, JT, DH, MGSF, and MLZ. All authors discussed and contributed to the final manuscript.



Article

The Stability and Chloride Entrapping Capacity of ZnAl-NO₂ LDH in High-Alkaline/Cementitious Environment

Zahid M. Mir ^{1,*}, Celestino Gomes ², Alexandre C. Bastos ², Rui Sampaio ², Frederico Maia ³,
Cláudia Rocha ³, João Tedim ², Daniel Höche ¹, Mario G. S. Ferreira ² and Mikhail L. Zheludkevich ^{1,4}

¹ Institute of Materials Research, Helmholtz-Zentrum Geesthacht Centre for Materials and Coastal Research, Max-Planck Str. 1, 21502 Geesthacht, Germany; daniel.hoeche@hzg.de (D.H.); Mikhail.Zheludkevich@hzg.de (M.L.Z.)

² DEMaC—Department of Materials and Ceramic Engineering, and CICECO—Aveiro Institute of Materials, Universidade de Aveiro, 3810-193 Aveiro, Portugal; jcv.gomes@ua.pt (C.G.); acbastos@ua.pt (A.C.B.); ruisampaio@ua.pt (R.S.); joao.tedim@ua.pt (J.T.); mgferreira@ua.pt (M.G.S.F.)

³ Smallmatek—Rua dos Canhas, 3810-075 Aveiro, Portugal; frederico.maia@smallmatek.pt (F.M.); claudia.rocha@smallmatek.pt (C.R.)

⁴ Faculty of Engineering, University of Kiel, Kaiserstrasse 2, 24143 Kiel, Germany

* Correspondence: zahid.mir@hzg.de

Abstract: In this work, the ZnAl-NO₂ LDH (layered double hydroxide) is investigated as a possible additive for mitigating the chloride-induced corrosion of steel in reinforced concrete. The investigation focused on the stability and chloride binding capacity of this LDH in the pH range typical of cementitious materials. Until pH = 12.5 the material was stable and effective in capturing chloride ions from the surrounding aqueous environment. For higher pH, precisely that of hydrated cement, the LDH was partially dissolved and OH⁻ preferentially entrapped instead of Cl⁻. These results suggested that ZnAl-NO₂ has excellent chloride entrapping capability at neutral pH, but this is reduced with increasing pH. However, when the LDH was incorporated into mortars, the chloride ingress was delayed, signifying that the dissolution of LDH leads to a secondary mechanism responsible for chloride capture.

Keywords: layered double hydroxide; corrosion; concrete; reinforcing steel; pH; chloride



Citation: Mir, Z.M.; Gomes, C.; Bastos, A.C.; Sampaio, R.; Maia, F.; Rocha, C.; Tedim, J.; Höche, D.; Ferreira, M.G.S.; Zheludkevich, M.L. The Stability and Chloride Entrapping Capacity of ZnAl-NO₂ LDH in High-Alkaline/Cementitious Environment. *Corros. Mater. Degrad.* **2021**, *2*, 78–99. <https://doi.org/10.3390/cmd2010005>

Received: 23 December 2020

Accepted: 18 February 2021

Published: 21 February 2021

Publisher's Note: MDPI stays neutral with regard to jurisdictional claims in published maps and institutional affiliations.



Copyright: © 2021 by the authors. Licensee MDPI, Basel, Switzerland. This article is an open access article distributed under the terms and conditions of the Creative Commons Attribution (CC BY) license (<https://creativecommons.org/licenses/by/4.0/>).

1. Introduction

The corrosion of steel in reinforced concrete affects infrastructures worldwide [1–3]. The cost of early repair and the reconstruction of these structures can lead to severe economic losses [4]. Concrete is a porous material [5], and aggressive species like chloride ions can pass through the concrete cover, until reaching the steel reinforcement, where they disrupt the steel native passive layer and initiate corrosion [6,7]. Innovative techniques are required to slow down the chloride ingress in concrete, delay the corrosion process and extend the service life of reinforced concrete infrastructures. Layered double hydroxides (LDHs) are a new class of concrete additives which can entrap aggressive anions from the environment and release selected anions (e.g., corrosion inhibitor) from their galleries. Potential applications include sequestration of chloride and carbonate ions in aggressive environments, which in turn can potentially prolong the service life of structures susceptible to corrosion. LDHs have gained attention in the recent years, due to their ion exchange properties, not only in concrete technology [8] but also in various branches of science and engineering [9], as a de-icing additive for asphalt roads [10], catalysis, [11], pharmaceutical applications [12], photochemistry [13], electrochemistry [14,15], biochemistry [16] and more.

Layered double hydroxides (LDHs), also known as “hydrotalcite-like” materials [9,17], can be synthesized by co-precipitation [18] of metal salts in alkaline medium, resulting in an ionic arrangement of positively charged brucite-like layers, together with anions

between the layers, to balance the charge. LDHs can be represented by the following generalized formula: $[M(II)_{1-x}M(III)_x(OH)_2]^{x+}(A^{n-})_{x/n}mH_2O$, with M(II) as divalent, M(III) as trivalent metallic cations and A^{n-} as the interlayer anion [17,19]. LDHs have the potential of intercalating external anions by exchanging them with the anions originally present in their galleries, as represented in Figure 1. This process is called the ion exchange process and is usually dominated by the order of ions in the selectivity series for LDH.

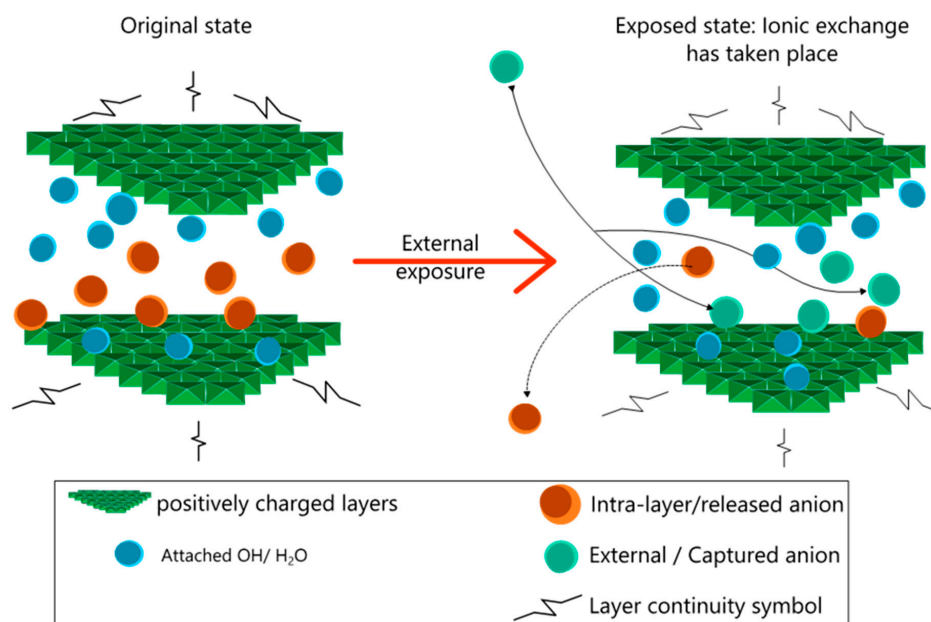


Figure 1. Schematic structure of layered double hydroxide (LDH) in original and exposed state and mechanism of ionic exchange.

Based on theoretical calculations, Costa et al. [20] concluded that Zn-Al-based LDHs have higher affinity to OH^- than Cl^- . They reported the anion selectivity order as $CO_3^{2-} > OH^- > F^- > Cl^- > Br^- > NO_3^-$. The ions towards the left of the series are preferable towards ion sequestration by LDH, as compared to the ions on the right of the selectivity series. Hibino [21] pointed out that such selectivity series for a particular LDH can change under certain conditions. Apart from the ion preference in the selectivity series, other factors, such as anion size, anion concentration and temperature, can influence the ion exchange process [8]. In cementitious materials, like cement paste, mortars or concrete, the ionic-exchange mechanism can be exploited to entrap chloride ions, thereby retarding their ingress, and simultaneously release anions with corrosion-inhibition properties, e.g., NO_2^- [8,22]. If effective, this leads to a “self-protection” capability of concrete against corrosion of steel in concrete.

Earlier works on the use of LDH in cementitious environments include the controlled release of organic admixtures [23] and the acceleration of the hardening process with CaAl-Cl LDH [24]. Zhong et al. analyzed the chloride-binding capacity of MgAl LDH intercalated with CO_3^{2-} and NO_3^- and found higher capacity for the NO_3^- LDH type [25]. The effect of MgAl LDH on the microstructure and carbonation resistance of sulfoaluminate cement concrete was studied by Duan et al. [26]. In a separate study by the present authors [27], in situ XRD analysis revealed that MgAl LDH can possibly lead to the formation of higher amounts of AFm and thereby increase the chloride-binding capacity of concrete. Chen et al. [28] investigated the use of CaAl- NO_3 LDH for the removal of

chloride ions from concrete pore solutions and from cement paste. The sequestration of Cl^- ions was explained by an ionic exchange mechanism following a Langmuir isotherm in cement matrix. Similar Langmuir-type binding isotherms were also reported by Yoon et al. for the capture of chloride ions by on calcined MgAl-based LDH in cement paste [29]. A review of LDH as smart additives of reinforced concrete for anticorrosion applications was provided by Yang et al. [30]. Most of the LDHs tested so far in concrete belong to one of the following systems: MgAl or CaAl. Only a few papers exist with ZnAl LDH studied for the chloride capture and nitrite release in saturated $\text{Ca}(\text{OH})_2$, i.e., simulated concrete pore solution [31]. Additionally, a comprehensive review on the various types and applications of LDH in cementitious materials has recently been published by the authors [8].

As mentioned previously, the use of Zn-Al LDH in cementitious systems has not been extensively studied so far. Therefore, in this work, the authors studied the behavior and stability of ZnAl- NO_2 in depth. Additionally, this paper reflects on the results obtained in European Union's LORCENIS project [32], which focused on the ZnAl- NO_2 as a potential chloride-entrapping/corrosion-inhibiting additive for concrete. Due to these reasons, ZnAl- NO_2 system has been used in this paper.

In the present work, the authors focused on characterizing the working mechanism of ZnAl- NO_2 in high-alkaline environments typical to that of concrete and cement pastes. The broader goal of this study was to quantitatively and qualitatively assess the ion exchange process related to chloride ion capture by ZnAl- NO_2 in alkaline environments. The assessment is reported for aqueous salt solutions, as well as for pore solutions. A step-wise approach was followed in this study. At first, the LDH was exposed only to an environment containing OH^- anions, in order to verify its anion-capture capability, as well as its stability in alkaline environments. This was followed by exposing LDH to a multi-anionic environment, containing both Cl^- and OH^- ions. Moreover, the sequestration of each anion was evaluated, and the results are discussed in detail. Chloride-binding isotherms as a function of pH of the environment are also presented. Then the compatibility of the LDH with cement was analyzed by observing the effect of the LDH addition to cement paste in terms of the curing time. Furthermore, the chloride transport was monitored in mortars with LDH, by employing cast-in Cl^- sensitive sensors. Finally, the corrosion properties of steel embedded in mortars containing LDH are presented, in order to highlight the role of NO_2^- release from LDH (due to ion exchange or partial dissolution of LDH).

2. Materials and Methods

2.1. Material Synthesis

The Zn-Al- NO_2 LDH studied in this work was produced by Smallmatek, Lda, Aveiro, Portugal. It was prepared in a stainless-steel reactor, by co-precipitation of hydroxides from salts of divalent and trivalent cations, in a solution with an excess of sodium nitrite, and the pH adjusted to 10.0 ± 0.5 with sodium hydroxide. More details can be found in Reference [33]. The resulting slurry was washed with deionized water, filtered and dried with an industrial spray dryer, to guarantee uniform and fine powder.

2.2. Materials Characterization

The LDH particle size was measured with a Coulter LS230 Particle Size Analyzer (Coulter Corporation, Miami, FL, USA). XRD diffractograms were obtained with a diffractometer PANalytical X'Pert MPD PRO (Almelo, The Netherlands) with Bragg-Brentano geometry, Ni-filtered $\text{CuK}\alpha$ radiation, PIXcel^{1D} detector, and step 0.026. The exposition was 2 s per step, in the angular range between 3° and 65° .

2.3. Stability of ZnAl- NO_2 in the High pH Range

The chemical stability of the LDH was analyzed at neutral pH and in the pH range from 11 to 13.5, which encompasses the pH of aged and fresh concrete. One gram of LDH was immersed in 50 mL of aqueous solutions with different pH values, prepared with distilled water and KOH. After 30 days in a closed container, the remaining powders were

washed, weighed by a lab scale and analyzed by XRD. The solution pH was measured by the potentiometric method with an Inlab Expert Pro pH combined electrode and a SevenMulti meter, both from Mettler Toledo (Columbus, OH, USA). The amount of NO_2^- in solution was measured with a UV-3100 UV-Vis-NIR spectrophotometer from Shimadzu (Kyoto, Japan), with the detection peak of interest occurring at 354 nm. Prior to the experimentation, the spectrophotometer was repeatedly calibrated by relating the intensity against various concentrations of NO_2^- in the calibration solutions.

2.4. Chloride Binding Capacity

The chloride-binding capacity of ZnAl- NO_2 was studied with NaCl solutions ranging from 0.01 to 0.5 M at neutral pH, and then with pH from 11 to 13, following the test matrix shown in Figure 2. The tests were extended to leached pore solution extracts, in order to replicate a multi-ion competition scenario. Leached pore solution 1 (PS1) was made by mixing 3.5 g of ordinary Portland cement and 1.5 g of fly ash in 1 L of water, stirring for 24 h and allowed to rest for 3 days. The resulting pH was around 12.0. Leached pore solution 2 (PS2) was prepared by adding 50 g of cement to 1 L of water, stirring for 24 h and allowing to rest for 3 days prior to testing. The resulting pH was around 12.5. For each solution, 50 mL was added to a beaker, and the chloride concentration measured with a DX235-Cl ion-selective electrode (Mettler Toledo) connected with a mercury/mercurous sulfate reference electrode to a SevenMulti meter (Mettler Toledo). After a few minutes of stable reading, 1 g of LDH was added to solution, under stirring, while the Cl^- concentration was monitored and pH measurements were carried out just before and after 5 min of LDH addition. The ion-selective electrode was calibrated against standard chloride solutions (0.001 M to 0.5 M), every time, prior to conducting measurements. The experimental setup is pictorially depicted in Figure 3. In some cases, the solid was recovered after 5 min of exposure and characterized by XRD. To verify the effect of time on the binding capacity, the Cl^- and pH measurements were repeated after 15 days of the LDH addition.

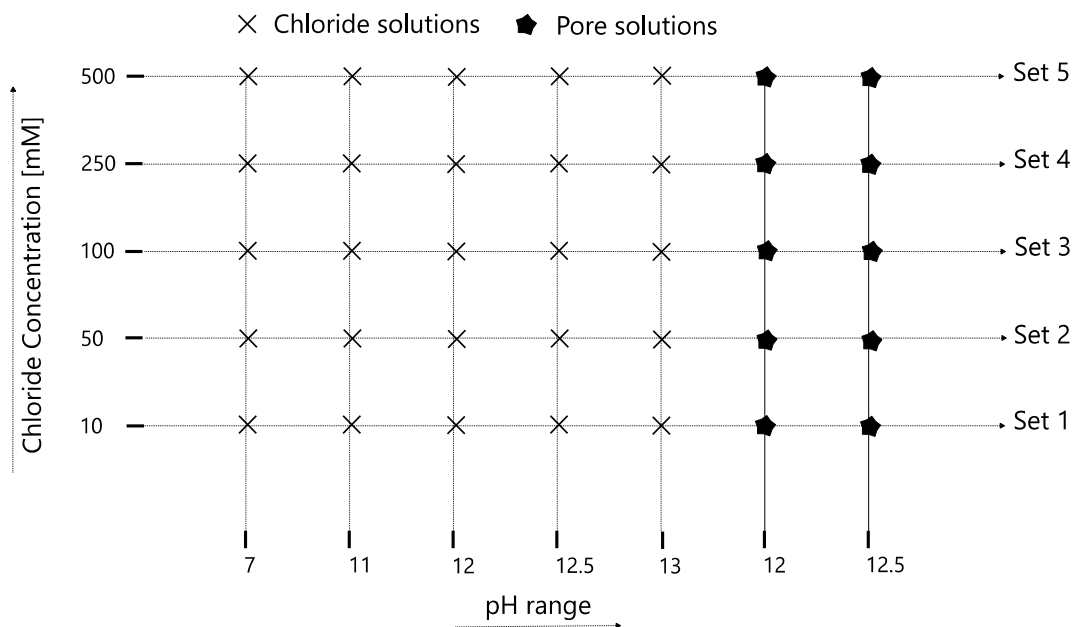


Figure 2. Test matrix for chloride-binding tests.

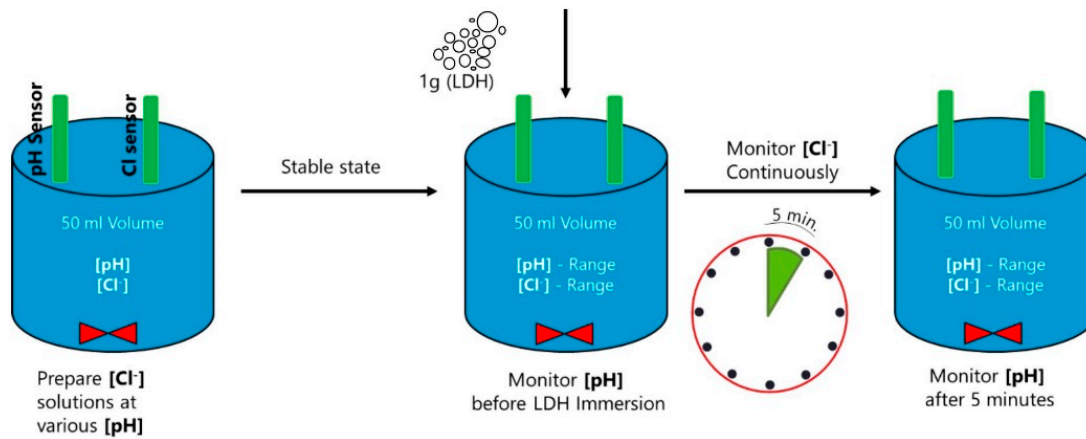


Figure 3. Experimental sequence for measuring Cl^- in the binding tests.

2.5. Compatibility of LDH with Cement Paste

Cement pastes with 0.5 water-to-cement (w/c) ratio were prepared without (reference) and with 2 wt% LDH. Specimens with $30 \times 30 \times 10 \text{ mm}^3$ were cast and cured in a humidity chamber.

2.6. Chloride Sensors Embedded in Mortars

The effect of LDH on the chloride ingress in mortars was assessed with embedded chloride sensors. The sensors consisted of 1 mm diameter silver wire, coated with silver chloride on the polished surface and encased in epoxy. The silver chloride coat was produced galvanostatically, with a constant current density of 2 mA/cm^2 , for 30 min, in 0.1 M HCl. Three of these Cl^- sensitive sensors were placed at 0.5, 1 and 1.5 mm from the surface of the mortar samples (Figure 4a). Prior to embedment in mortars, the sensors were calibrated by recording potential readings for various concentrations of Cl^- in $\text{KOH} = 0.1 \text{ M}$ ($\text{pH} \sim 13$). The response of the sensors to chloride ions in high-pH media is presented in Figure 4b. The chloride concentration in the mortars was then obtained by using the obtained calibration curve. These calibrations were repeated periodically, with sensors permanently immersed in $\text{KOH} = 0.1 \text{ M}$ ($\text{pH} \sim 13$), to certify that the response did not change with the continuous exposure to the alkaline environment of mortar.

The mortars samples were cast in $5 \times 5 \times 5 \text{ cm}^3$ samples, with a composition of 14.5 wt% CEM II/B-L 32.5 N cement, 13% water and 72.5% of 0–2 mm size siliceous sand. The water/cement ratio was equal to 0.9 and was chosen for fast permeation and, consequently, to accelerate the chloride ingress. LDH was added in an amount corresponding to 2 wt% of cement (0.3 wt% of total mass of mortar). The mortar samples were cured for 28 days, in a humidity chamber, and then the samples were immersed in 3.5% NaCl aqueous solution. The potential of the sensors was measured against a saturated calomel electrode (SCE) placed in the external solution, using a CompactStat potentiostat connected to a peripheral differential amplifier (Ivium Technologies, Eindhoven, The Netherlands), for simultaneous measurement of several channels.

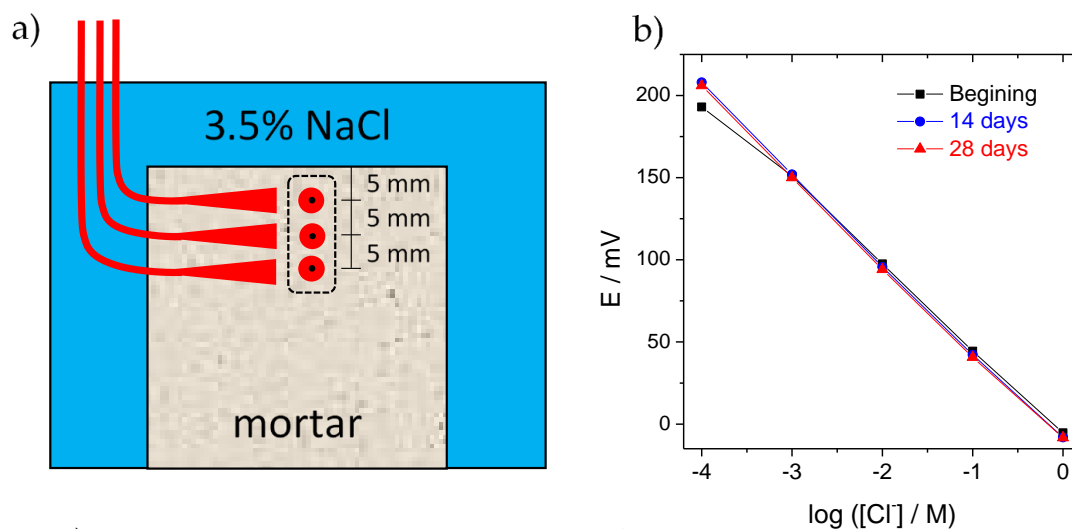


Figure 4. Studies conducted in mortars. (a) Scheme of mortar with sensors and (b) calibration curves for chloride sensors.

2.7. Corrosion Testing

Mortar samples with the composition presented in Section 2.6 and $7 \times 4 \times 4 \text{ cm}^3$ size were produced, with a non-corrugated steel bar of 8 mm diameter placed in the middle. The steel bars were cleaned with 50% vol. HCl solution and abraded down to 1200 grade SiC paper, just before the embedment in the mortars. After 24 h, the samples were demolded and were left curing for 8 days, immersed in water. The samples were finally transferred to 3.5% NaCl solution, and the open-circuit potential and polarization resistance were measured periodically with a Autolab PGSTAT 204 potentiostat with a platinum counter electrode and a SCE electrode as reference. The polarization resistance was measured from -10 to $+10$ mV, with respect to the open-circuit potential, with a scan rate of 0.1 mV s^{-1} .

3. Results and Discussion

3.1. Characterization of the ZnAl-NO₂

The particle size distribution of the LDH powder is presented in Figure 5a. It ranged between 40 nm and 150 μm , with a mean particle size of 22 μm . Almost 10% of the particles exhibited a particle size of less than 5 μm . The XRD pattern prior to exposure is depicted in Figure 5b and shows the reflections 003, 006, 110 and 113 at 11.6° , 23° , 60.2° and 61.5° . These reflections coincide with reflections reported in the literature for ZnAl-NO₂ [31] and also with other LDHs with NO₂⁻ in the interlayer space [22,34].

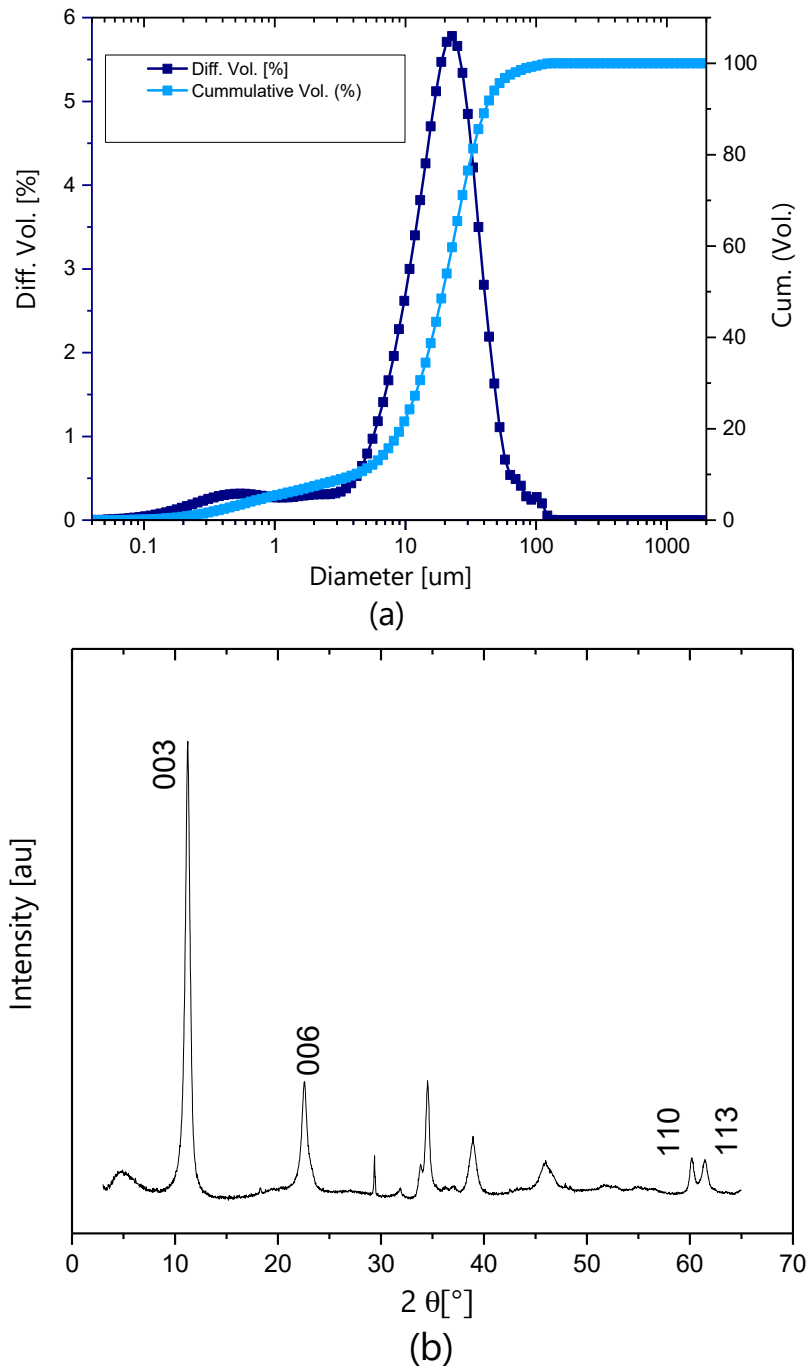


Figure 5. Characteristics of LDH particles. (a) Particle size distribution and (b) XRD pattern of ZnAl-NO₂ prior to exposure.

3.2. Stability in High-Alkaline Environment

The effect of pH in the range between 11 and 13.5 has been studied. The LDH and solution were analyzed 30 days after 1 g of powder was added to the 50 mL solution. After 30 days, the powders were extracted from the solutions and weighed. LDH powder was present in all samples. However, the amount of powder left at a high pH was less, indicating that a partial dissolution of LDH could have taken place. In a parallel experiment, it was verified that about 95% of solid remained undissolved at pH 12, decreasing to 60% at pH 13 and only 20% at pH 14. The pH of the solution just before and 30 days after the addition of LDH is presented in Figure 6(a). The pH of the solutions inside the closed containers decreased noticeably. This was attributed to the capture of OH^- in solution by the LDH powder. A drop of three units in the pH scale was observed, showing a remarkable efficiency of this LDH to capture OH^- . For a higher pH, the amount of captured OH^- decreased (almost no pH drop), because most of the LDH was dissolved. The region of partial dissolution is marked in the figure.

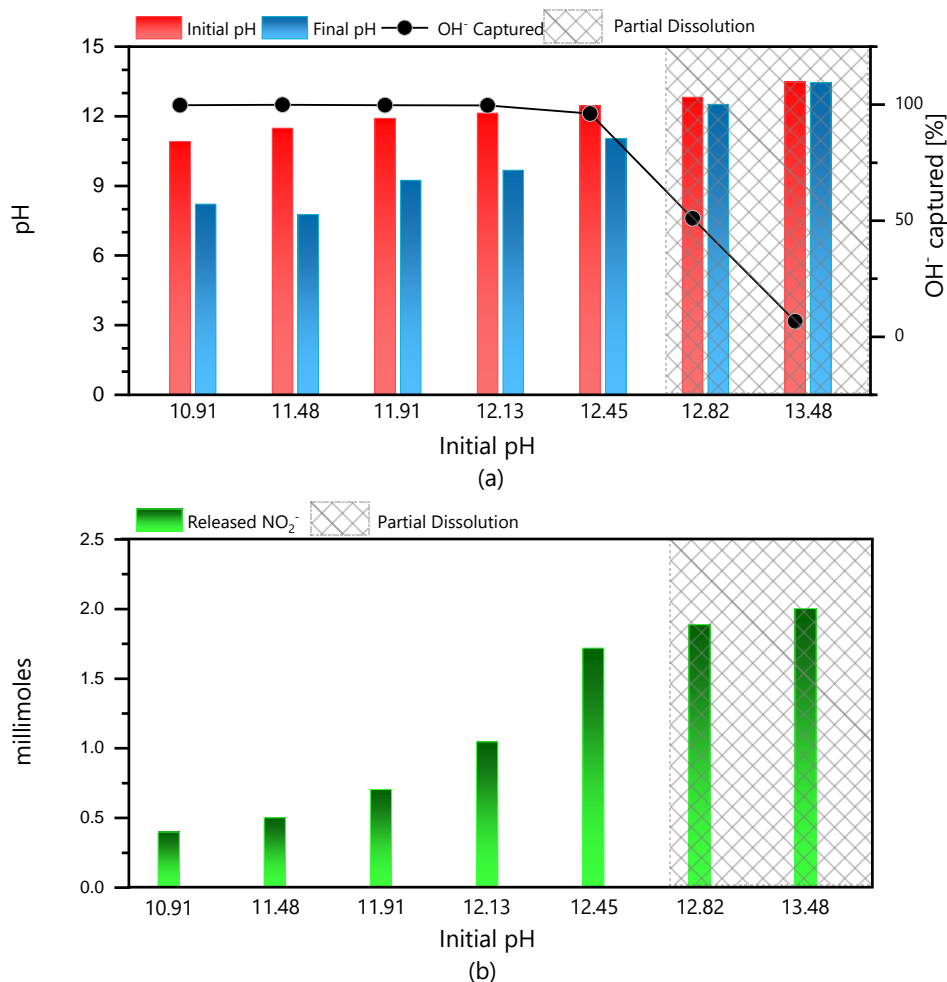


Figure 6. Stability and ion exchange property on LDH. (a) OH^- capture by LDH and in terms of pH drop and percent capture. (b) Corresponding NO_2^- release by LDH.

3.2.1. Release of NO_2^- Ions

Considering that the capture of OH^- occurs by an ionic exchange mechanism, as expected for a LDH [9,15,17,22,23,30,31,33,34], the intercalated NO_2^- ions must leave the LDH interlayer and pass to solution, to allow the entrance of the incoming OH^- ions. Indeed, after 30 days of immersion, NO_2^- was detected in all the solutions. It was observed that the concentration of NO_2^- increased with an increase of pH, as shown in Figure 6b.

3.2.2. XRD Analysis of LDH Exposed to Alkaline Solutions

After the 30-day immersion period, the remaining powders were filtered, washed and dried in a vacuum oven, at 40°C , for 24 h. Figure 7 shows the XRD patterns of the LDH before (base) and after immersion in the different solutions. The reflections 006 and 003 are related to basal planes while the peaks 110 and 113 correspond to non-basal planes. The magnification of the plot around the peak 003 (2θ between 10° and 12°) shows a shift towards a higher angle as the pH increases, signifying a contraction of the interlayer.

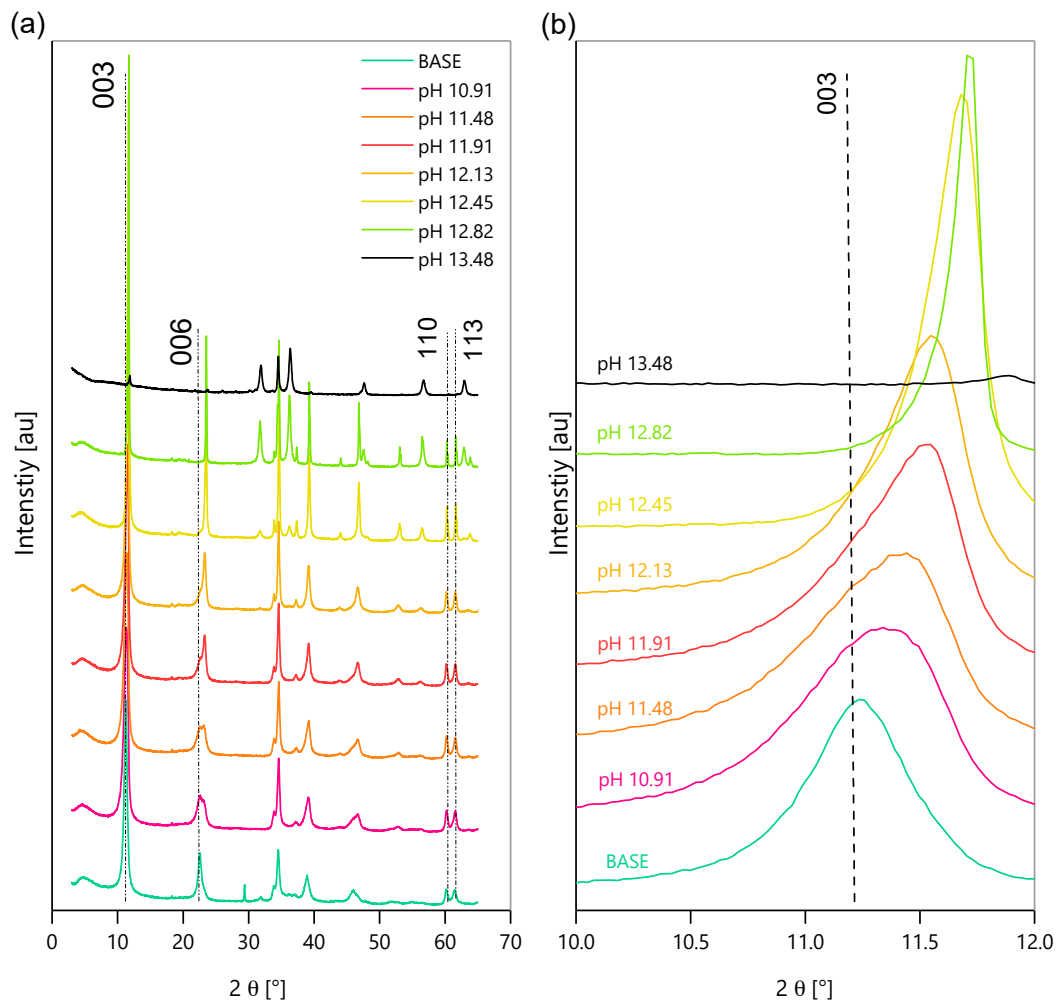


Figure 7. XRD analysis of ZnAl-NO_2 after 30 days of immersion in alkaline solutions—(a) Full XRD spectra (b) XRD spectra displaying d_{003} peaks.

Bragg's law [35] was used to calculate the interlayer spacings d_{003} and d_{110} from the 2θ peak locations, using $\lambda = 1.540598 \text{ \AA}$. The spacing d_{003} gives the thickness of a single brucite-like layer and one interlayer, while d_{110} is the distance between two-metallic cations in the brucite-like layer. A shift of d_{003} on the 2θ axis corresponds to a change in the interlayer distance, as observed in Figure 7b. In Figure 8, the calculated d_{003} and d_{110} values are plotted for each pH. A clear d_{003} shift to the right on the 2θ axis occurs as the pH increases, which is indicative of a smaller interlayer distance, signifying anion exchange with a smaller radius ion. The OH^- ion has a smaller size than the NO_2^- ion; the anionic exchange reduces the interlayer spacing, leading to higher 2θ reflections. This has also been previously reported by Tedim et al. [15]. However, the 003 peaks in mild pH could also show an overlap of LDH-NO_2^- and LDH-OH^- , due to the possible parallel placement of NO_2^- in the interlayer. The NO_2^- ion placed inclined to the cationic layers will tend to show more layer contraction upon ion exchange with OH^- (Figure 7b). The parameter for cationic spacing (d_{110}) in the brucite-like layer stays constant as the pH increases, signifying that only anionic exchange has occurred as external concentration of OH^- increased, and the cationic layer has stayed intact and unchanged.

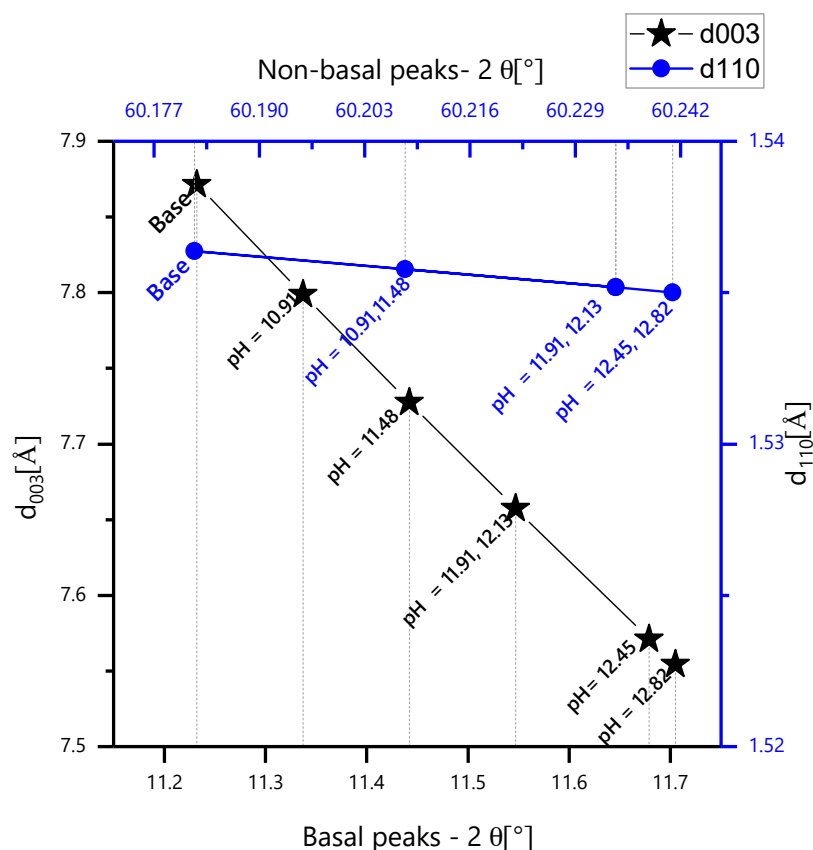


Figure 8. Shift of d_{003} and d_{110} as a function of pH.

These XRD peaks are also indicative of the structural stability in the high alkaline range. The partial dissolution of LDH starts around pH 12.5. The powders until this pH show characteristic peaks of the LDH, despite the shift in the intercalated anion, but from pH 12.5 onwards, new peaks are detected and attributed to ZnO , Zn(OH)_2 , Al_2O_3 , etc.

Finally, the XRD pattern of the small amount of solid that did not dissolve at pH 13.48 shows no peaks of the LDH (the LDH structure is lost) and is dominated by the peaks of oxides and hydroxides of Zn and Al, which were already visible in pH 12.45 and 12.82.

3.3. Chloride Entrapment and the Effect of pH

For the application of ZnAl-NO₂ as chloride-entrapping additive in cementitious environments, it is highly relevant to verify the Cl⁻ binding capacity of this LDH in the presence of a high concentration of OH⁻ ions. Therefore, the binding capacity of the LDH as a function of chloride concentration and pH was investigated. Representative results are presented in Figure 9, for starting NaCl solutions of 10, 100 and 500 mM with different pH values. The concentrations are plotted normalized, i.e., they appear divided by the starting concentration, for a better comparison of the changes in the different cases. These plots show the drop in chloride concentration after LDH was added to solution. The pH before and after the addition of LDH is also shown.

Figure 9a,b refer to the tests conducted with a starting chloride concentration of 10 mM at different pH. The highest chloride capture occurred at the lowest pH (6.94), where the concentration dropped to ~30 percent of the initial value. The process is very fast, taking less than 1 min to attain equilibrium. The Cl⁻ capture at this pH (6.94) took place with a slight increase in the pH. This pH increase could be due to the release of OH⁻ bound to the surface of the LDH or to a small dissolution of the LDH itself. In fact, the addition of 1 g of LDH to distilled water increased the pH and the conductivity of the solution, confirming that ions have passed from the LDH to solution. At pH 10.59, almost the same amount of chloride ions was captured, and it was accompanied by a decrease of pH from 10.59 to 7.5. This signifies that both Cl⁻ and OH⁻ were captured by the LDH. As the pH rises, so rises the amount of OH⁻ that is captured, while the entrapment of chloride significantly decreases. Above pH 12, the amount of Cl⁻ captured becomes very small.

A similar description applies for the other NaCl concentrations. The higher capture occurs in near-neutral solution, decreasing with the increase in pH, until it becomes almost negligible at a very high pH. However, it is noticeable that, for the same pH, the amount of OH⁻ captured is smaller as the concentration of Cl⁻ increases. The tendencies are better perceived in Figure 10. The ZnAl-NO₂ has higher selectivity to OH⁻ than Cl⁻, and for a higher pH, it is captured preferentially with almost no Cl⁻ captured. However, the capture of OH⁻ is not so effective for a higher concentration of chloride. These results show that, in spite of the higher importance of selectivity, the concentration also counts. It is also evident that LDH leads to a decrease of pH of the surrounding solution, which can bring serious risks to the stability of the passive film on the rebar surface.

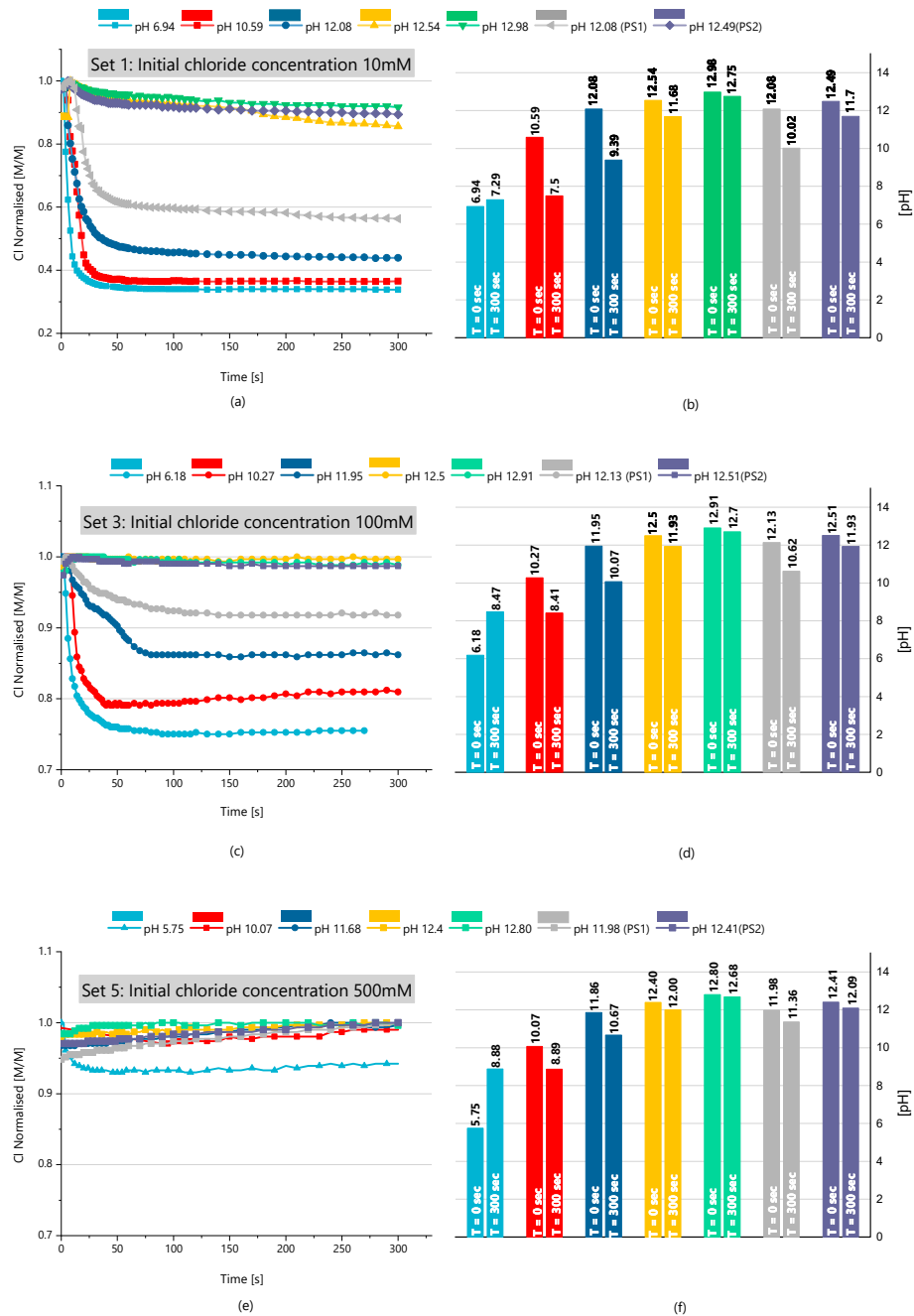


Figure 9. Results of the chloride-entrapment tests with the effect of pH. Plots on the left depict the change of chloride concentration (divided by the initial NaCl concentration) after LDH was added to solution. The graphs on the right show the solution pH before and after the addition of LDH. (a,b) Chloride ion and pH measurement in solutions at an initial chloride concentration of 10 mM, respectively. (c,d) Chloride ion and pH measurement in solutions at an initial chloride concentration of 100 mM, respectively. (e,f) Chloride ion and pH measurement in solutions, at an initial chloride concentration of 500 mM, respectively.

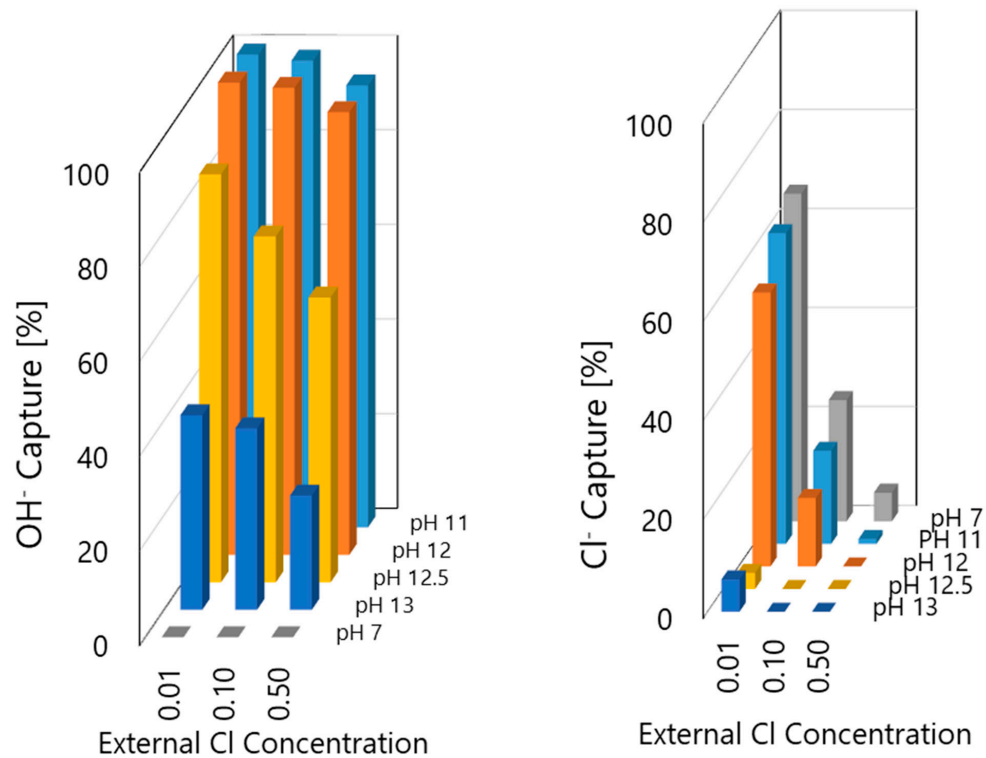


Figure 10. Comparison of the moles of Cl^- and OH^- captured, compared to the existing moles before the addition of LDH.

3.3.1. Effect of Time on the Chloride Entrapment

The entrapment tests described in the last section were conducted for just 300 s and did not continue, because the ionic exchange was quite fast after the addition of LDH, happening in less than 1 min, with the subsequent readings being stable. In any case, the samples were sealed for 15 days and then analyzed again, to look for any changes in Cl^- concentration and pH. As confirmed in Figure 11, with two representative examples, no significant changes were detected in both parameters measured after 300 s and 15 days. This confirms that the process is very fast, without further evolution.

The XRD analysis of two powders after 15-day exposure to alkaline solution, with and without NaCl, is presented in Figure 12. A clear shift of the 003 peak is seen for both the powders, as compared to the base material. The peaks of the powders exposed to just OH^- or to OH^- and Cl^- are quite close to each other and are not clearly distinguishable.

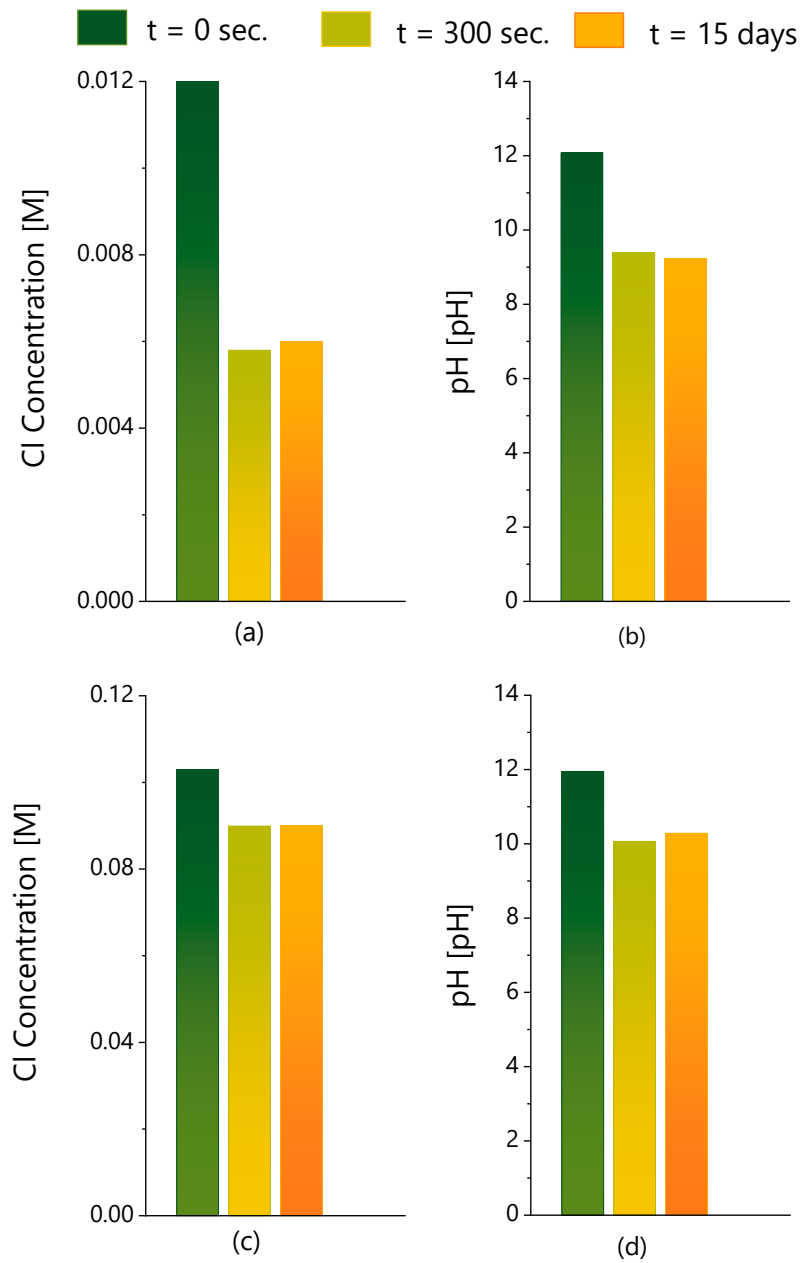


Figure 11. Long-term evaluation of chloride entrapment. (a) Cl⁻ concentration and (b) pH of a 12 mM NaCl solution with initial pH = 12.08 measured before ($t = 0$ s) and after (300 s and 15 days) the addition of LDH. (c,d) Similar measurements of a solution initially with 100 mM NaCl and pH 12.95.

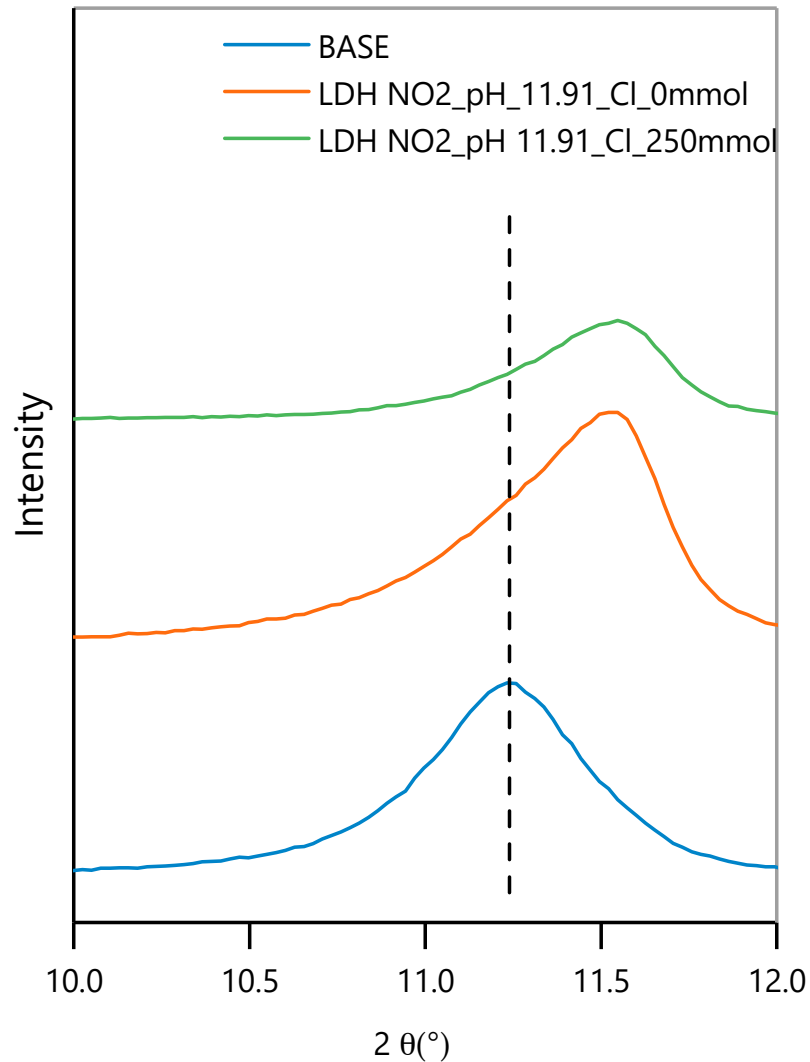


Figure 12. XRD plot detail of the 003 reflection of the LDH before tests (base) and the powder after 15 days of immersion in a solution with pH = 11.91, with and without 250 mM NaCl.

3.3.2. Chloride Binding Capacity

The chloride-binding capacity can be defined as the amount of chloride ion that is bound by a given mass of LDH. It can be expressed as the amount of Cl^- ion bound to LDH per unit mass of LDH at the onset of equilibrium. As such, the chloride-binding capacity represents a heterogeneous equilibrium between the Cl^- bound to LDH and the free Cl^- available in the solution. However, this equilibrium is sensitive to the pH of the environment and is explained later. The chloride-binding capacity can be determined by using the following formula [22,28]:

$$B_c = \frac{V_{sol} (C_0 - C_e) M_{Cl}}{m_{LDH}} \quad (1)$$

where B_c is the binding capacity (in mg/g), V_{sol} is the volume of solution (L), m_{LDH} is the mass of LDH added to the solution (g), C_0 and C_e are the initial and equilibrium chloride concentrations (mM) and M_{Cl} is the molar mass of chloride. The binding (or loading) capacity of ZnAl-NO₂ for Cl⁻ was calculated from the results of the chloride entrapment studies, using Equation (1), and is presented in Figure 13. The binding capacity increased with the Cl⁻ concentration, up to a value where it then remained constant. The highest chloride loading was ~45 mg/g (1.28 mmol/g) and occurred at near neutral pH for the initial chloride concentration of 250 mM. The binding capacity is strongly dependent of the pH. At pH 12, it was half of the value in near-neutral pH, and above pH = 12.5, no substantial chloride was captured. The data for these equilibrium isotherms were obtained at room temperature (23 ± 1 °C). It is known that the loading capacity of Zn-Al-based LDH increases with temperature [36].

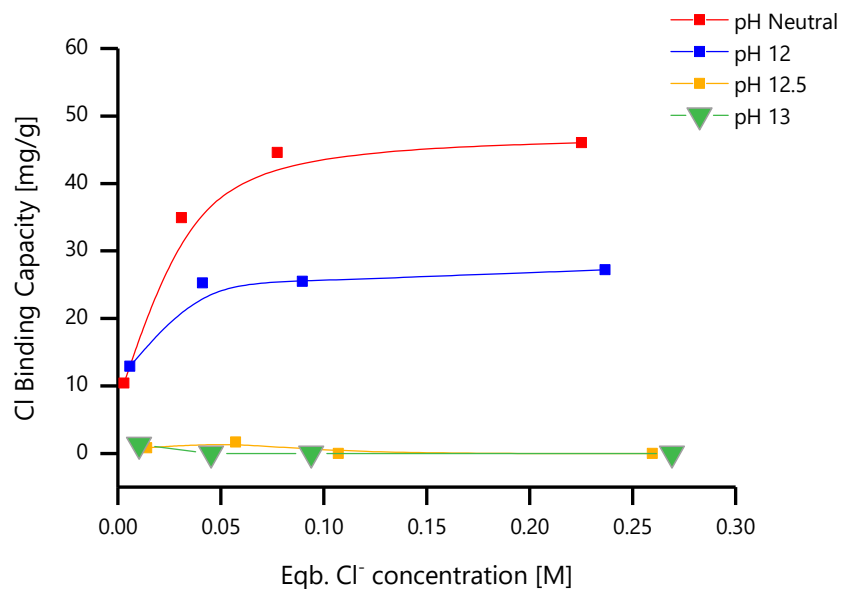


Figure 13. Chloride binding capacity of ZnAl-NO₂ in the alkaline pH range.

3.4. Compatibility with Cement

The experiments described so far were done in aqueous solution, with most of them at a high pH, to reflect the conditions inside cementitious materials. Naturally, the best approach is to test the LDH directly incorporated in these materials. It was decided to perform tests with mortars with 2% LDH with respect to cement. Before that, the compatibility of the ZnAl-NO₂ with cement was investigated (Figure 14). It was observed that addition of LDH had a retarding effect on the cement curing. The sample with LDH displayed a slow curing, as compared to the reference samples. Cement paste (w/c = 0.5) with 2 wt% LDH took a very long time to harden, that is, around 17 days, compared to one day of the reference sample (without LDH). It is well-known that zinc ions can retard the hydration process. Trezza [37] used IR, XPS and calorimetry to investigate the effect of Zn²⁺ on the hydration processes and observed the delay of the cement hydration and attributed this to the formation of a new phase, Ca(Zn(OH)₃)₂·2H₂O. Citing Asavapisit et al. [38], Trezza concluded that the formation of Ca-Zn complexes decreased the concentration of Ca²⁺ ions required to form the CSH phase. The higher the concentration of Zn²⁺, the greater the quantity of the Ca-Zn phase and the longer the hydration time. Stephan et al. [39] also

concluded that formation of the Ca-Zn phase significantly retards the hydration process by reducing the concentration of OH^- and Ca^{2+} ions.

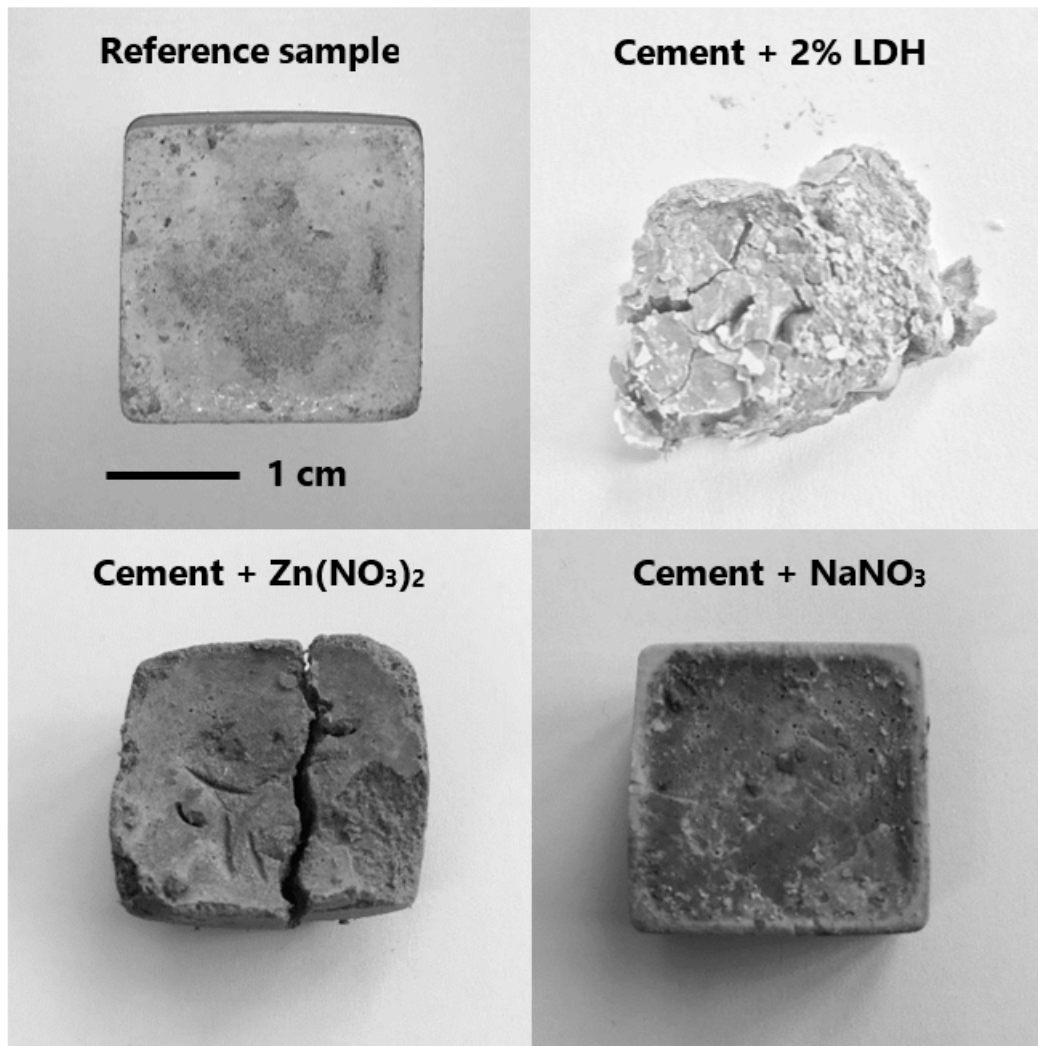


Figure 14. Compatibility of ZnAl-NO₂ with cement. Reference and cement + NaNO₃ samples harden in one day. Cement + ZnAlNO₂ or Zn(NO₃)₂ took about 20 days to harden. ($w/c = 0.5$).

To confirm that it was the Zn^{2+} from LDH dissolution that interfered with the curing, cement pastes were cast with Zn(NO₃)₂. Similar to specimens with LDH, the samples showed a clay-like behavior and took a long time to harden. To rule out the effect of NO_3^- on the hydration process, samples were cast with NaNO₃ with the same amount of NO_3^- as the samples with Zn(NO₃)₂ as shown in Figure 14. NO_3^- ions are traditionally used as setting accelerators in concrete, usually in the form of Ca(NO₃)₂ [40,41].

It is also important to note that the LDH particle size is a very important factor that should be taken into consideration. In a separate study from the authors [42], it was observed that a curing time similar to the reference samples was obtained when LDH

particles of mean size $\sim 125 \mu\text{m}$ were used, instead of the $\sim 25 \mu\text{m}$ used in the present study. Therefore, the authors acknowledge that particle size plays a crucial role as bigger LDH agglomerates can have a reduced exposed surface area, leading to a lower dissolution at high pH. The effect of the particle size of LDH on the properties on concrete, especially chloride ingress, has been documented in the studies by Qu et al. [43]. The results reported in this work are confined to only one particular particle size, i.e., $\sim 25 \mu\text{m}$. For different particle sizes, reproducibility can be affected. Further studies are being planned to better characterize the effect of LDH and its particle sizes in cement paste hydration, and such studies will be reported in the future.

3.5. Embedded Sensors and Chloride Ingress in Mortar

To directly assess the effect of LDH on the transport of Cl^- inside cementitious materials, chloride sensors were cast in mortar samples, as described in Section 2.6. The mortars were immersed in 3.5% NaCl, and the potential of the sensors was measured, over time, against a reference electrode placed in the solution. From the chloride concentrations in the different positions of the mortar and at the different times, it was possible to plot the chloride profile inside the reference mortar and inside the mortar with ZnAl-NO_2 , presented in Figure 15a,b respectively. In these plots, 0 cm corresponds to the surface of the mortar in contact with the solution, while the other values are the position of the sensors inside the mortar.

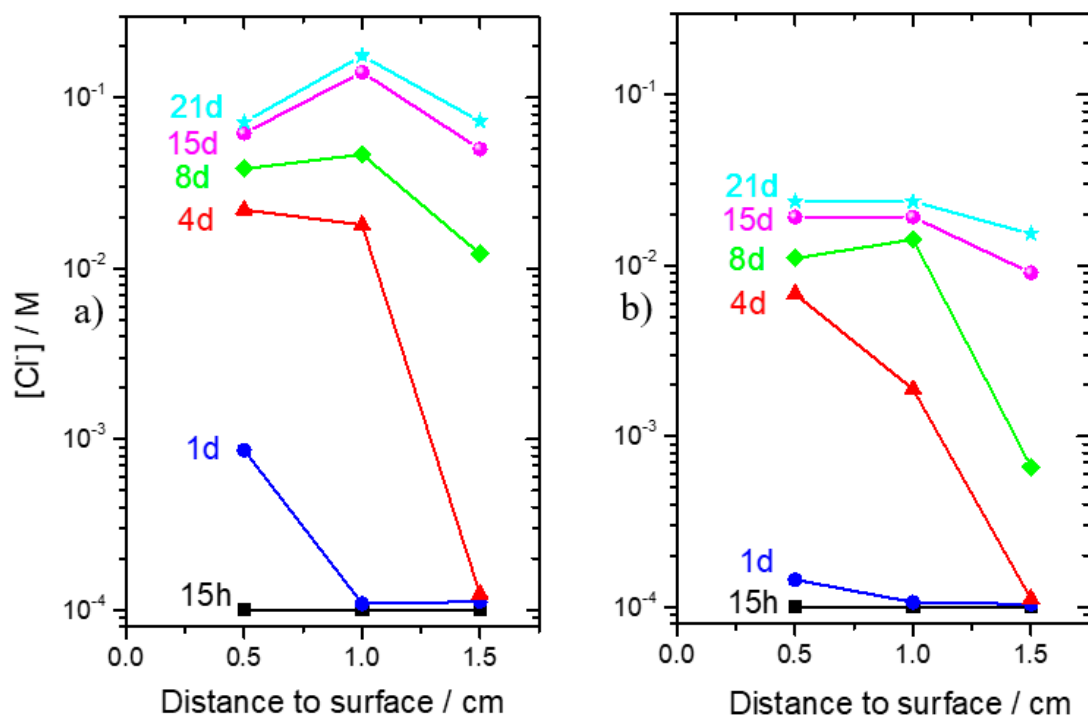


Figure 15. Studies conducted in mortars. (a) Chloride profile inside reference mortar and (b) chloride profile inside mortar with ZnAl-NO_2 .

The chloride penetration was detected first by the sensors closer to the surface. Interestingly, with time, the peak chloride concentration was found not at the surface but 1 cm inside the mortar. This is a common observation [44–46] that has been attributed to a skin

effect, i.e., to a different composition of the surface layers, compared to the bulk, due to contact with the casting mold [44,45]. Other authors attributed this effect to the gradient of moisture in the first few layers of the sample [44], as well as to surface reactions of the surface with the exposure environment [46]. The fact that the sensors were able to capture the concentration peak is an indication of their good functioning. The most important observation in Figure 15 is the slower ingress of chloride in the mortar with LDH.

3.6. Corrosion of Steel Bar in Mortar with and without ZnAl-NO₂

In a final set of tests, steel rebars were placed in mortars without and with LDH (2 wt%, with respect to cement, or 0.3 wt% with respect to the total mass of mortar). The samples were exposed to 3.5% NaCl, and the corrosion potential (E_{corr}) and polarization resistance (R_p) were monitored over time. The results are presented in Figure 16. The less negative E_{corr} and the higher R_p of the steel in mortars with LDH point to lower corrosion, compared to the reference samples. The presence of LDH in the mortar seems to play a positive role, which can be even more pronounced if a higher amount of LDH was present.

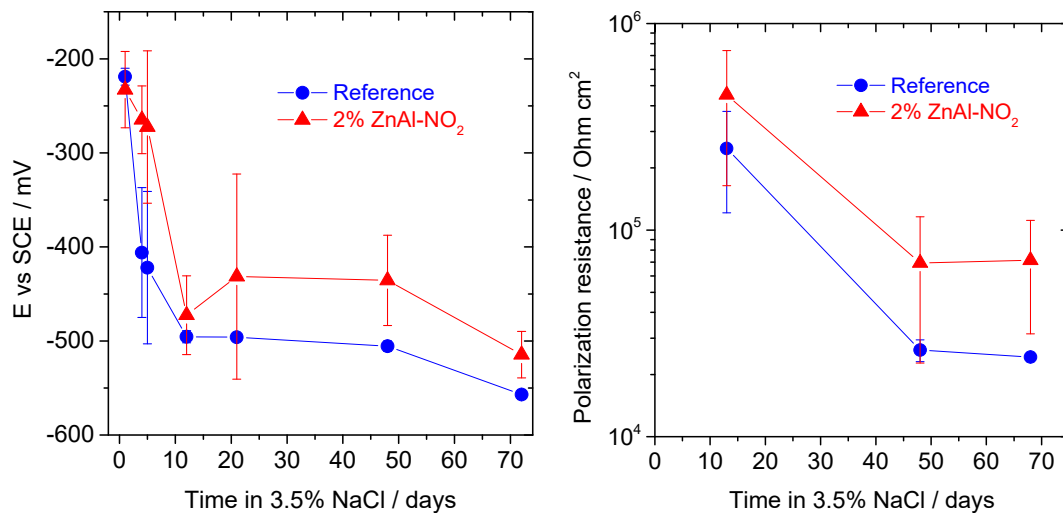


Figure 16. Corrosion potential and polarization resistance of steel rebar in mortars without and with 2 wt% (to cement fraction) ZnAl-NO₂ immersed in 3.5% NaCl.

The experiments with the LDH in mortars showed positive effects (lower ingress of chloride in mortar and higher corrosion resistance of steel), despite the low amount of LDH added (0.3 wt%) and the high porosity of the mortar. It is possible that the dissolution of LDH releases aluminum ions, which will promote the formation of more AFm phases (family of hydrated calcium aluminates) during cement hydration. This has been previously demonstrated by the authors, in a separate study, where the formation of AFm was recently confirmed by using in situ XRD on hydrating cement pastes with 2% Mg-based LDH. The reader is directed to Mir et al. [27], for detailed information on this effect. The dissolution of LDH leads to the formation of extra quantities of AFm which can chemically bind chloride ions. The extra amount of AFm phases can thus lead to additional chemical binding of chloride ions by forming Friedel's salt and Kuzel's salt and is also reported in the studies by Chen et al. [47]. Additionally, the filler effect of remaining undissolved LDH particles can play a positive role in chloride ingress by making the microstructure more tortuous, without decreasing the total porosity [43]. The higher corrosion resistance of steel in the mortar that contains LDH can be simply due to the release of NO₂⁻ to the pore solution, as a result of the LDH dissolution and ion exchange with OH⁻ on the remaining powder. This

contrast between the results with LDH in solution and in mortar needs more investigation, and additional studies are planned for the future.

These results with mortars are still preliminary because the experiments were performed with a limited number of replicate specimens (three of each type), in porous mortar (to accelerate the ion transport process), and the amount of LDH was only 0.3 wt% to the total mass of the mortar. Work is being performed with a higher number of samples, with better quality mortar, higher amounts of LDH and longer testing times in the mortar, in order to better understand the behavior of the LDH inside mortars, and will be reported in the future.

4. Conclusions

Based on the discussion presented in this work, the following conclusions can be drawn.

1. The Zn-Al LDH presents very good chloride-capture capability in near-neutral pH. Our investigations reported a peak binding capacity of about ~45 mg of Cl per gram of LDH. However, as the pH increases, the chloride-capture capability of Zn-Al LDH is reduced.
2. The LDH is stable in alkaline medium, until pH ~12.5. Partial dissolution occurs at a higher pH, with the release of the constituent anions (Zn^{2+} , Al^{3+} , NO_2^-) to the environment.
3. The ZnAl- NO_2 delays the hardening of cement paste and mortars. This has been attributed to the zinc ions released by the partial LDH dissolution which interfere with the cement hydration reaction.
4. The partial dissolution and preferential capture of OH^- at the pH values typical of cementitious material suggest the inadequacy of ZnAl- NO_2 for the chloride capture inside concrete, where a pH higher than 13 is possible.
5. Mortars with the LDH presented a slower penetration of Cl^- ions and led to higher corrosion resistance of the embedded steel rebar, even with a small amount (0.3% of total mass of mortar). Earlier studies pointed out that LDH dissolution can possibly lead to higher amounts of AFm being generated. However, additional experiments are needed to clarify this effect for ZnAl LDH. As a future scope to this work, more work will be performed to investigate the dissolution and working mechanism of LDH in concrete and will be reported in future.

Author Contributions: Conceptualization, Z.M.M., C.G. and A.C.B.; formal analysis, Z.M.M., C.G., A.C.B., R.S., F.M. and C.R.; investigation, Z.M.M., C.G. and A.C.B.; resources, F.M. and C.R.; supervision, A.C.B., F.M., C.R., J.T., D.H., M.G.S.F. and M.L.Z.; writing—original draft, Z.M.M. and A.C.B.; writing—review and editing, A.C.B. and M.L.Z. All authors have read and agreed to the published version of the manuscript.

Funding: This research was funded by the HORIZON 2020 collaborative project “LORCENIS” (Long Lasting Reinforced Concrete for Energy Infrastructure under Severe Operating Conditions, Grant agreement n° 685445), the European Union’s COST Action (SARCOS, Self-healing As preventive Repair of Concrete Structures), under grant agreement No. CA15202, and in the scope of the project CICECO—Aveiro Institute of Materials, POCI-01-0145-FEDER-007679 (FCT Reference UID/CTM/50011/2013). AB acknowledges FCT—Fundação para a Ciência e a Tecnologia, I.P., in the scope of the framework contract foreseen in the numbers 4, 5 and 6 of the article 23, of the Decree-Law 57/2016, of 29 August, changed by Law 57/2017, as of 19 July.

Data Availability Statement: The authors declare that the data presented in this work are available within the article. Extra data could be requested from the corresponding author.

Conflicts of Interest: The authors declare no conflict of interest. The funders had no role in the design of the study; in the collection, analyses or interpretation of data; in the writing of the manuscript; or in the decision to publish the results.

References

1. Page, C.L. Mechanism of Corrosion Protection in Reinforced-Concrete Marine Structures. *Nature* **1975**, *258*, 514–515. [[CrossRef](#)]
2. Tuutti, K. *Corrosion of Steel in Concrete. Technical Report*; Swedish Cement and Concrete Research Institute: Stockholm, Sweden, 1982.
3. Bertolini, L.; Elsener, B.; Pedferri, P.; Redaelli, E.; Polder, R. *Corrosion of Steel in Concrete: Prevention, Diagnosis, Repair*; Wiley: Hoboken, NJ, USA, 2013.
4. Angst, U. Challenges and Opportunities in Corrosion of Steel in Concrete. *Mater. Struct.* **2018**, *51*, 1–20. [[CrossRef](#)]
5. Lian, C.; Zhuge, Y.; Beecham, S. The Relationship between Porosity and Strength for Porous Concrete. *Constr. Build. Mater.* **2011**, *25*, 4294–4298. [[CrossRef](#)]
6. Alonso, C.; Andrade, C.; Castellote, M.; Castro, P. Chloride Threshold Values to Depassivate Reinforcing Bars Embedded in a Standardized Opc Mortar. *Cem. Concr. Res.* **2007**, *30*, 1047–1055. [[CrossRef](#)]
7. Ghods, P.; Isgor, O.B.; McRae, G.A.; Li, J.; Gu, G.P. Microscopic Investigation of Mill Scale and Its Proposed Effect on the Variability of Chloride-Induced Depassivation of Carbon Steel Rebar. *Corros. Sci.* **2011**, *53*, 946–954. [[CrossRef](#)]
8. Mir, M.Z.; Bastos, A.; Höche, D.; Zheludkevich, M.L. Recent Advances on the Application of Layered Double Hydroxides in Concrete—A Review. *Materials* **2020**, *13*, 1426. [[CrossRef](#)]
9. Li, F.; Duan, X. Applications of Layered Double Hydroxides. In *Layered Double Hydroxides*; Duan, X., David, E.G., Eds.; Springer: Berlin/Heidelberg, Germany, 2006.
10. Peng, C.; Yu, J.Y.; Zhao, Z.J.; Dai, J.; Fu, J.Y.; Zhao, M.L.; Wang, W. Synthesis and Properties of a Clean and Sustainable Deicing Additive for Asphalt Mixture. *PLoS ONE* **2015**, *10*, e0115721. [[CrossRef](#)] [[PubMed](#)]
11. Kirm, I.; Francesc, M.; Xavier, R.; Cesteros, Y.; Salagre, P.; Sueiras, J. Epoxidation of Styrene with Hydrogen Peroxide Using Hydrotalcites as Heterogeneous Catalysts. *Appl. Catalysis A General* **2004**, *272*, 175–185. [[CrossRef](#)]
12. Park, D.H.; Choi, G.; Choy, J.H. Bio-Layered Double Hydroxides Nanohybrids for Theranostics Applications. In *Photofunctional Layered Materials*; Dongpeng, Y., Min, W., Eds.; Springer International Publishing: Cham, Switzerland, 2015.
13. Ogawa, M.; Kazuyuki, K. Photofunctions of Intercalation Compounds. *Chem. Rev.* **1995**, *15*, 399–438. [[CrossRef](#)]
14. Liao, C.-S.; Wei-Bin, Y. Structure and Conductive Properties of Poly (Ethylene Oxide)/Layered Double Hydroxide Nanocomposite Polymer Electrolytes. *Electrochim. Acta* **2004**, *49*, 4993–4998. [[CrossRef](#)]
15. Tedim, J.; Kuznetsova, A.; Salak, A.N.; Montemor, F.; Snihirova, D.; Pilz, M.; Zheludkevich, M.L.; Ferreira, M.G.S. Zn-Al Layered Double Hydroxides as Chloride Nanotraps in Active Protective Coatings. *Corros. Sci.* **2012**, *55*, 1–4. [[CrossRef](#)]
16. Choy, J.H.; Kwak, S.Y.; Park, J.S.; Jeong, Y.J.; Portier, J. Intercalative Nanohybrids of Nucleoside Monophosphates and DNA in Layered Metal Hydroxide. *J. Am. Chem. Soc.* **1999**, *121*, 1399–1400. [[CrossRef](#)]
17. Martin, K.J.; Thomas, J.P. Layered Double Hydroxides as Supported Anionic Reagents. Halide-Ion Reactivity in Zinc Chromium Hexahydroxide Halide Hydrates $[Zn_2Cr(OH)_6 \cdot nH_2O]$ ($X = Cl, I$). *J. Am. Chem. Soc.* **1986**, *108*, 541–542. [[CrossRef](#)] [[PubMed](#)]
18. Crepaldi, E.L.; Paulo, C.P.; João, B.V. Comparative Study of the Coprecipitation Methods for the Preparation of Layered Double Hydroxides. *J. Braz. Chem. Soc.* **2000**, *11*, 64–70. [[CrossRef](#)]
19. He, J.; Min, W.; Bo, L.; Yu, K.; David, G.E.; Duan, X. Preparation of Layered Double Hydroxides. In *Layered Double Hydroxides*; Duan, X., David, G.E., Eds.; Springer: Berlin/Heidelberg, Germany, 2006.
20. Costa, D.G.; Rocha, A.B.; Souza, W.F.; Chiaro, S.S.X.; Leitão, A.A. Comparative Structural, Thermodynamic and Electronic Analyses of Zn-Al—Hydrotalcite-Like Compounds (an-Cl-, F-, Br-, OH-, CO₃²⁻ or NO₃⁻): An Ab Initio Study. *Appl. Clay Sci.* **2012**, *56*, 16–22. [[CrossRef](#)]
21. Hibino, T. Anion Selectivity of Layered Double Hydroxides: Effects of Crystallinity and Charge Density. *Eur. J. Inorg. Chem.* **2018**, *6*, 722–730. [[CrossRef](#)]
22. Zuo, J.D.; Wu, B.; Luo, C.Y.; Dong, B.Q.; Xing, F. Preparation of Mg-Al Layered Double Hydroxides Intercalated with Nitrite Ions and Corrosion Protection of Steel Bars in Simulated Carbonated Concrete Pore Solution. *Corros. Sci.* **2019**, *152*, 120–129. [[CrossRef](#)]
23. Raki, L.; Beaudoin, J.J.; Mitchell, L. Layered Double Hydroxide-Like Materials: Nanocomposites for Use in Concrete. *Cem. Concr. Res.* **2004**, *34*, 1717–1724. [[CrossRef](#)]
24. Xu, S.; Chen, Z.; Zhang, B.; Yu, J.; Zhang, F.; Evans, D.G. Facile Preparation of Pure Ca-Al-Layered Double Hydroxides and Their Application as a Hardening Accelerator in Concrete. *Chem. Eng. J.* **2009**, *155*, 881–885. [[CrossRef](#)]
25. Shui, Z.; Juntao, M.; Wei, C.; Xiaoxing, C. Chloride Binding Capacity of Cement Paste Containing Layered Double Hydroxide (Ldh). *J. Test. Eval.* **2012**, *40*, 796–800.
26. Duan, P.; Chen, W.; Ma, J.; Shui, Z. Influence of Layered Double Hydroxides on Microstructure and Carbonation Resistance of Sulphoaluminate Cement Concrete. *Constr. Build. Mater.* **2013**, *48*, 601–609.
27. Mir, Z.M.; Alexandre, B.; Celestino, G.; Urs, M.; Alonso, M.C.; Villar, K.; Miguel, P.; Rabade, F.M.; Cláudia, M.; Rocha, P.M.; et al. Numerical and Experimental Analysis of Self-Protection in Reinforced Concrete Due to Application of Mg–Al–No₂ Layered Double Hydroxides. *Adv. Eng. Mater.* **2020**, *22*, 2000398. [[CrossRef](#)]
28. Chen, Y.X.; Shui, Z.H.; Chen, W.; Chen, G.W. Chloride Binding of Synthetic Ca-Al-No₃ Ldhs in Hardened Cement Paste. *Constr. Build. Mater.* **2015**, *93*, 1051–1058. [[CrossRef](#)]
29. Yoon, S.; Moon, J.; Bae, S.; Duan, X.N.; Giannelis, E.P.; Monteiro, P.M. Chloride Adsorption by Calcined Layered Double Hydroxides in Hardened Portland Cement Paste. *Mater. Chem. Phys.* **2014**, *145*, 376–386. [[CrossRef](#)]

30. Yang, Z.; Fischer, H.; Polder, R. Modified Hydrotalcites as a New Emerging Class of Smart Additive of Reinforced Concrete for Anticorrosion Applications: A Literature Review. *Mater. Corros. Werkst. Korros.* **2013**, *64*, 1066–1074. [[CrossRef](#)]
31. Tian, Y.W.; Dong, C.F.; Wang, G.; Cheng, X.Q.; Li, X.G. Zn-Al-No₂ Layered Double Hydroxide as a Controlled-Release Corrosion Inhibitor for Steel Reinforcements. *Mater. Lett.* **2019**, *236*, 517–520. [[CrossRef](#)]
32. SINTEF Norway European Union's Project, Lorcenis–Long Lasting Reinforced Concrete for Energy Infrastructure under Severe Operating Conditions, European Union Horizon 2020 Programme; SINTEF: Trondheim, Norway, 2016–2020.
33. Poznyak, S.K.; Tedim, J.; Rodrigues, L.M.; Salak, A.N.; Zheludkevich, M.L.; Dick, L.F.P.; Ferreira, M.G.S. Novel Inorganic Host Layered Double Hydroxides Intercalated with Guest Organic Inhibitors for Anticorrosion Applications. *Acs Appl. Mater. Interfaces* **2009**, *1*, 2353–2362. [[CrossRef](#)]
34. Cao, Y.H.; Dong, S.G.; Zheng, D.J.; Wang, J.J.; Zhang, X.J.; Du, R.G.; Song, G.L.; Lin, C.J. Multifunctional Inhibition Based on Layered Double Hydroxides to Comprehensively Control Corrosion of Carbon Steel in Concrete. *Corros. Sci.* **2017**, *126*, 166–179. [[CrossRef](#)]
35. Ewald, P.P. William Henry Bragg and the New Crystallography. *Nature* **1962**, *195*, 320–325. [[CrossRef](#)]
36. Lv, L.; Sun, P.; Gu, Z.; Du, H.; Pang, X.; Tao, X.; Xu, R.; Xu, L. Removal of Chloride Ion from Aqueous Solution by ZnAl-No(3) Layered Double Hydroxides as Anion-Exchanger. *J. Hazard. Mater.* **2009**, *161*, 1444–1449. [[CrossRef](#)]
37. Trezza, M.A. Hydration Study of Ordinary Portland Cement in the Presence of Zinc Ions. *Mater. Res.* **2007**, *10*, 331–334. [[CrossRef](#)]
38. Asavapisit, S.; Fowler, G.; Cheeseman, C.R. Solution Chemistry During Cement Hydration in the Presence of Metal Hydroxide Wastes. *Cem. Concr. Res.* **1997**, *17*, 1249–1260. [[CrossRef](#)]
39. Stephan, D.H.; Maleki, D.K.; Eber, B.; Härdtl, R. Influence of Cr, Ni, and Zn on the Properties of Pure Clinker Phases: Part, I. C3s. *Cem. Concr. Res.* **1999**, *29*, 545–552. [[CrossRef](#)]
40. Franke, W.; Magdalena, B.-S.; Tandre, O.; Gaurav, S. The Fate of Nitrate Ions in Concrete under the Focus of Corrosion Inhibition. In Proceedings of the 2nd International Conference on Durability of Concrete Structures, ICDCS 2010, Sapporo, Japan, 24–26 November 2010.
41. Justnes, H.; Nygaard, E.C. Technical Calcium Nitrate as Set Accelerator for Cement at Low Temperatures. *Cem. Concr. Res.* **1995**, *25*, 1766–1774.
42. Gomes, G.; Mir, Z.; Sampaio, R.; Bastos, A.; Tedim, J.; Maia, F.; Rocha, C.; Ferreira, M. Use of ZnAl-Layered Double Hydroxide (Ldh) to Extend the Service Life of Reinforced Concrete. *Materials* **2020**, *13*, 1769.
43. Qu, Z.Y.; Yu, Q.L.; Brouwers, H.J.H. Relationship between the Particle Size and Dosage of Ldhs and Concrete Resistance against Chloride Ingress. *Cem. Concr. Res.* **2018**, *105*, 81–90. [[CrossRef](#)]
44. Andrade, C.; Diez, L.M.; Alonso, C. Mathematical Modeling of a Concrete Surface "Skin Effect" on Diffusion in Chloride Contaminated Media. *Adv. Cem. Based Mater.* **1997**, *6*, 39–44. [[CrossRef](#)]
45. Castro, P.; de Rincon, O.T.; Pazini, E.J. Interpretation of Chloride Profiles from Concrete Exposed to Tropical Marine Environments. *Cem. Concr. Res.* **2001**, *31*, 529–537. [[CrossRef](#)]
46. De Weerd, K.; Orsáková, D.; Müller, A.C.A.; Larsen, C.K.; Pedersen, B.; Geiker, M.R. Towards the Understanding of Chloride Profiles in Marine Exposed Concrete, Impact of Leaching and Moisture Content. *Constr. Build. Mater.* **2016**, *120*, 418–431. [[CrossRef](#)]
47. Chen, P.; Ma, B.; Tan, H.; Liu, X.; Zhang, T.; Qi, H.; Peng, Y.; Yang, Q.; Wang, J. Effects of Amorphous Aluminum Hydroxide on Chloride Immobilization in Cement-Based Materials. *Constr. Build. Mater.* **2020**, *231*, 117171.

4.3. Article 4 - Numerical and Experimental Analysis of Self-Protection Processes in Reinforced Concrete due to Application of Mg-Al-NO₂ Layered Double Hydroxides

Note: See attached article in the next pages. Reprinted without modification from [65] under CC BY 4.0 license. Published by WILEY-VCH Verlag GmbH Co. KGaA, Weinheim.

4.3.1. A brief summary of Article 4

In this paper, a numerical model is presented for modelling chloride transport in concrete under submerged conditions. The model is able to compare chloride durability of different concrete mixes in a fast and inexpensive way. The model uses experimental inputs which are easy and relatively faster to obtain as compared to conventional chloride ponding tests which take a long time to complete. These include chloride binding isotherm for bound chlorides and formation factor for microstructure quantification. The work also presents the benefits of using formation factor, which has recently gained popularity in concrete technology and is being currently standardized in European codes [66].

In this work, investigations are carried out to understand the Cl⁻ ion entrapping capacity of Mg-Al-NO₂ in concrete specimens. The numerical model is used to compare the chloride ingress between reference concrete specimens and concrete specimens with 2% LDH. As mentioned previously, investigations are carried for submerged conditions because this exposure scenario is regarded as the most severe scenario for infrastructure exposed to offshore/marine environmental conditions. This exposure scenario has been adopted as the test case scenario for all investigations carried out within the LORCENIS project [30].

4.3.2. Author contribution

In the following, the author of this dissertation is denoted by his initials ZM. The names and initials of co-authors can be found in the appended manuscript. Conceptualization: ZM, ACB, CG; LDH synthesis: FR, CR; Finite Element Model: ZM, PM; Experiments: UM, MC, KV, MP, CG, ACB; Analysis of results and data treatment: ZM, UM, ACB, CG, MC, KV, MP, PM; Manuscript writing and editing: ZM, UM, ACB; Supervision: ACB, DH, UM, MC, MGSF, MLZ.



Numerical and Experimental Analysis of Self-Protection in Reinforced Concrete due to Application of Mg–Al–NO₂ Layered Double Hydroxides

Zahid Mohammad Mir,* Alexandre Bastos, Celestino Gomes, Urs Mueller, Maria Cruz Alonso, Kristina Villar, Miguel P. Rabade, Frederico Maia, Cláudia M. Rocha, Philippe Mainçon, Daniel Höche, Mario G. S. Ferreira, and Mikhail L. Zheludkevich

Concrete possesses an intrinsic chloride binding capacity. Chloride ions from the environment bind with the hydrated cementitious phases in the form of bound chlorides. The contribution of chemically bound chlorides toward increasing the service life of concrete structures is vital as they help in slowing down the chloride diffusion in the concrete thereby delaying reinforcement depassivation. The authors attempt to increase the chloride binding capacity of concrete by adding a small amount of Mg–Al–NO₂ layered double hydroxides (LDHs) with the objective to delay reinforcement corrosion and by this to considerably extend the service life of concrete structures situated in harsh environments. This study presents numerical and experimental analysis of the action of LDH in concrete. Formation factor is used to determine the effective chloride diffusion coefficient. In addition, the chloride binding isotherms together with Poisson–Nernst–Planck equations are used to model the chloride ingress. A comparable chloride binding is observed for concrete with and without Mg–Al–NO₂, depicting only a slight chloride uptake by Mg–Al–NO₂. Further investigations are conducted to understand this behavior by studying the stability and chloride entrapping capacity Mg–Al–NO₂ in concrete.

1. Introduction

Concrete structures are prone to reinforcement corrosion induced damage due to chloride ingress.^[1,2] Chloride ingress occurs in infrastructures exposed to the marine environment (offshore or coastal structures), or due to the action of deicing salts in structures along roadways.^[3] Concrete damage due to reinforcement corrosion is the most common factor for repair and maintenance of concrete structures. This problem has global economic and social consequences with huge associated investments and strong impact on society due to closing of roads for the repair of bridges, tunnels, and bottlenecks in the water and energy production and distribution.^[4]

The alkaline environment of concrete protects the reinforcement by forming a passive layer around the rebar.^[5] As concrete is exposed to chloride ions during its service life, these ions pass through the concrete cover and in due course of time reach the

Z. M. Mir, Dr. D. Höche, Prof. M. L. Zheludkevich
Surface and Coating Technology
Institute of Materials Research
Helmholtz-Zentrum Geesthacht Centre for Materials and Coastal
Research
Max-Planck Str. 1, 21502 Geesthacht, Germany
E-mail: zahid.mir@hzg.de

Dr. A. Bastos, C. Gomes, Prof. M. G. S. Ferreira
DEMaC – Department of Materials and Ceramic Engineering
CICECO – Aveiro Institute of Materials
Universidade de Aveiro
3810-193 Aveiro, Portugal

The ORCID identification number(s) for the author(s) of this article can be found under <https://doi.org/10.1002/adem.202000398>.

© 2020 The Authors. Published by WILEY-VCH Verlag GmbH & Co. KGaA, Weinheim. This is an open access article under the terms of the Creative Commons Attribution License, which permits use, distribution and reproduction in any medium, provided the original work is properly cited.

DOI: 10.1002/adem.202000398

Dr. U. Mueller, Dr. M. P. Rabade
Infrastructure and Concrete Technology
RISE Research Institutes of Sweden
Brinellgatan 4, 504 62 Borås, Sweden

Dr. M. C. Alonso, K. Villar
CSIC
Institute of Construction Science Eduardo Torroja
Serrano Galvache, 4, 28033 Madrid, Spain

Dr. F. Maia, Dr. C. M. Rocha
SmallMaTek LDA
Rua dos Canhas, 3810-075 Aveiro, Portugal

Dr. P. Mainçon
SINTEF Materials and Chemistry
7465 Trondheim, Norway

Prof. M. L. Zheludkevich
Faculty of Engineering
University of Kiel
Kaiserstrasse 2, 24143 Kiel, Germany

Q-00

rebar surface.^[6] Chloride concentrations above a certain threshold can damage the passive layer and initiate corrosion on the rebar surface.^[7] Continuation of this process leads to accumulation of corrosion products at the steel–concrete interface (SCI).^[8] Corrosion products are less denser than parent steel and therefore exhibit a higher volume.^[2,9] Due to the limitation of space at the SCI, the accumulation of corrosion products leads to an increase in the interface pressure resulting in microcracking of the concrete around the rebar.^[10,11] As the process continues, these microcracks coalesce to form macrocracks^[12,13] which can potentially lead to spalling of the concrete cover and eventually turn the structure nonoperational or in need of repair.

Chloride ions enter the concrete via the pore system filled with pore solution in the saturated state.^[14] Most of the pore system consists of interstices formed by the nano- and micro-sized crystals and lamellas of the hydrate phases (C–S–H, AFm, Aft, CH, and so on^[15]). Only a smaller amount of porosity consists of air voids or larger capillary pores. Chloride ions therefore transport themselves in the pore solution (free chlorides) and interact with the cementitious microstructure surrounding the pore system. This interaction can lead to chemical and physical binding of chloride ions with hydration products (bound chlorides).^[16,17] The total chloride content in concrete is therefore a combination of free and bound chlorides. The binding of chlorides slows the ingress of free chlorides along the pore network. Therefore, an accurate determination of chloride binding is necessary to create precise service life estimation models.

There are many ways by which the concrete’s ability to bind chlorides can be increased. The addition of supplementary cementitious materials such as fly ash, ground granulated blast furnace slag, and metakaolin has been reported to increase the binding capacity in concrete.^[18] In the LORCENIS project,^[19] novel chloride entrapping nanocontainers were developed with an aim to impart additional chloride binding capabilities to concrete. In this study, one of the recently developed nanocontainers of Mg–Al–NO₂ layered double hydroxides (LDHs) are used as chloride binding additives inside concrete.

LDHs are finely powdered materials which can be easily added to concrete during the mixing process. LDH can be prepared by the coprecipitation method^[20] of two different metallic hydroxides, in our case Mg and Al. As a result of coprecipitation,

bimetallic hydroxides are formed with a layered structure, hence the name LDHs. These hydroxide layers are composed of positively charged cations with anions in between the layers (galleries) to balance the charge (Figure 1). LDH possesses a unique ability, in the sense that they can intercalate an external anion from the environment, e.g., a Cl[−] ion, by exchanging it with an originally intercalated anion, e.g., a corrosion inhibiting ion.^[21] This property is termed as the ionic exchange property of LDH.^[22] With this application in mind, LDH is a potential candidate to release anions from its interlayers which can be a corrosion inhibiting ion/species and can also provide additional chloride capture in concrete. Concrete mixed with LDH could show improved chloride binding capability and controlled corrosion inhibitor release. This property has been termed as “self-protection” of reinforced concrete in the LORCENIS project. This work only focuses on the chloride capture capability and not on the inhibitor release from LDH.

In the recent years, many studies have focused on the use of LDH in concrete. Cao et al.^[23] used Mg-based LDH in chloride solutions and observed a decrease in the chloride ion concentration with time. Zuo et al.^[24] conducted studies related to the chloride ion capture capacity by Mg-based LDH and reported considerable chloride loading in aqueous solutions following a Langmuir-type isotherm. Yang et al.^[25] used Mg–Al LDH into cement pastes and mortars and found that an appropriate addition increased the time to corrosion. X-ray diffraction (XRD) analysis and thermogravimetric analysis (TGA) studies by Yang et al.^[26] focused on chloride uptake by Ca–Al-based LDH in chloride solutions. They demonstrated a considerable chloride uptake by Ca-based LDH. The effect of addition of LDH in cement paste on the setting, hydration, as well as microstructure development was investigated by Wu et al.^[27]

In this study, we investigated the use of LDH for additional chloride capture in concrete. Two concrete recipes, one control (without LDH) and another one with 2% LDH (with respect to cement content and 0.3% of overall concrete), were compared and results were gained experimentally as well as by modeling. To accurately model the chloride ingress, mostly two major input parameters are required, i.e., microstructural information and chloride binding capacity isotherms. An accurate estimation of

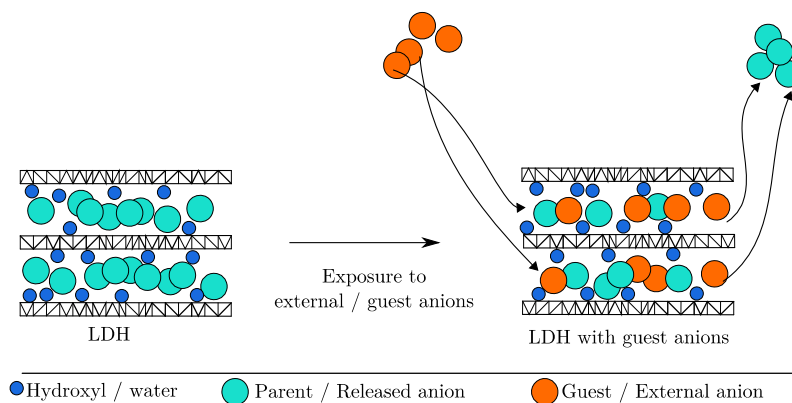


Figure 1. A schematic representation of the ionic exchange property of LDHs.

microstructure in terms of diffusion coefficient can aid in the modeling of transport of free chlorides.

The formation factor (\mathcal{F}_c) was used to quantify the effect of microstructure on the ionic transport.^[28,29] \mathcal{F}_c has been regarded as a fundamental measure toward microstructural characterization of porous media. Due to the ease with which \mathcal{F}_c can be obtained, it is possible to quickly obtain transport properties of various concrete recipes in a rapid and reliable way. Together with \mathcal{F}_c , the second vital parameter for service life modeling is the chloride binding capacity. Freundlich-type isotherm was used due to its good fit with our experiments.^[30] These inputs were derived for both types of concretes, i.e., control (REF) and with 2% LDH (+2% LDH).

Chloride transport was modeled in water-saturated concrete using the Nernst–Planck equation and combines information from \mathcal{F}_c and chloride binding isotherms.^[31] The transport of charged ions through the pore network gives rise to a potential field which is accounted via the Poisson's equation.^[32] The resulting coupled system of equations was solved using the finite element method^[33] for a 1D domain. The numerical model was used to compare the chloride transport in the concrete with and without LDH. Experimental verification of simulation results is also presented. In addition, the article highlights the stability of LDH in cementitious environments to explain the reduced chloride uptake by Mg–Al–NO₂ in the cementitious matrix.

2. Materials

2.1. Synthesis of LDH

The LDH used in this study was provided by Smallmatek, Lda (Portugal) and prepared according to their own production procedures. Briefly, the Mg/Al–NO₂ LDH was prepared by coprecipitation of Mg and Al salts in a solution with excess of sodium nitrite, where the pH range was adjusted with sodium hydroxide (Poznyak et al.^[34]). The production process was conducted in a custom-made pilot-scale reactor equipped with a proportional–integral–derivative (PID) controller, which allows the control and correction of important process parameters (i.e., pH and temperature), and peristaltic pumps for precise addition of chemicals. Finally, the obtained slurry was washed with deionized water and filtered under reduced pressure, then dried using an industrial spray dryer to guarantee uniform fine powders.

2.2. Concrete Mix Description

Two series of concrete specimens were prepared: the reference concrete (REF) without and with 2% LDH (+2% LDH). The respective mix details are shown in **Table 1**. The cement was supplied by Dyckerhoff (Germany) and the specimens were cast at Research Institutes of Sweden (RISE, Sweden). Tests were conducted jointly at RISE, Spanish National Research Council (CSIC, Spain), University of Aveiro (Portugal), and Helmholtz-Zentrum Geesthacht (HZG, Germany). In addition, cement paste specimen were cast with the CEM I 42.5 LA SR consisting of low calcium aluminate content having 0.5 water cement ratio (w/c) and 2%-4% LDH content for investigating the stability of LDH in cement pastes, as explained later in Section 4.

Table 1. Concrete composition for REF and +2% LDH mixes. Chemical and mineralogical composition of binder is also included.

Property [unit]	REF	+2% LDH
Cement CEM I/52.5 R [kg m ⁻³]	350	350
LDH [mass% binder] [mass% total mass]	0	2 (0.3)
Aggregate 0–4 mm [kg m ⁻³]	1151	1151
Aggregate 4–8 mm [kg m ⁻³]	265	265
Aggregate 8–16 mm [kg m ⁻³]	355	355
Super plasticizer [mass% binder]	0.8	0.8
Water/cement ratio [1]	0.6	0.6
Chemical composition (binder)		
SiO ₂ [%]	–	21.39
Al ₂ O ₃ [%]	–	3.69
Fe ₂ O ₃ [%]	–	1.29
CaO [%]	–	64.66
MgO [%]	–	0.72
SO ₃ [%]	–	3.43
K ₂ O [%]	–	0.57
Na ₂ O [%]	–	0.21
Mineralogical composition (binder)		
C ₃ S [%]	–	70.3
C ₂ S [%]	–	6.5
C ₃ A [%]	–	8.9
C ₄ AF [%]	–	2.4
Calcite [%]	–	4.7
Gypsum [%]	–	3.7
Others [%]	–	3.6

3. Numerical Model

3.1. Application of Formation Factor for Microstructure Characterization

The exact determination of diffusion coefficients of chloride ions in the concrete pore solution D_{cl}^p is a difficult parameter to obtain, due to ionic interactions, heterogeneity of concrete, and variability of samples, and can lead to deviations. In contrast, the diffusion coefficient of chloride ions at infinite dilution in a volume of liquid D_{cl}^∞ is well established ($D_{cl}^\infty = 2.030 \times 10^{-9} \text{ m}^2 \text{ s}^{-1}$). The diffusion of chloride ion in a single linear pore without any other interactions can be obtained using the D_{cl}^p . When up-scaling the transport parameter from a single pore to a representative volume element (RVE) of concrete, the porous microstructure in the RVE can be accounted using an effective diffusion coefficient D_{cl}^{eff} .^[35] It also does not include any ion–ion or ion–solid interactions and accounts only for the hindrance offered by the porous microstructure of the RVE. D_{cl}^{eff} is sometimes also referred to by other authors as the microstructural diffusion coefficient.^[29]

The ion–ion and ion–solid interactions may then well be considered using the apparent diffusion coefficient or bulk diffusion coefficient D_{cl}^{app} . D_{cl}^{app} is commonly used in many service-life

models but it does not distinguish microstructural corrections and chloride binding effects. It is of vital importance to separate the effects of microstructure and ionic interactions to deeply understand the chloride transport in a concrete mix and in our case the effect of LDH. As complex as it may sound, these two properties can be separated by a material property known as the formation factor (\mathcal{FF}_c).

\mathcal{FF}_c simply uses the electrical properties of a medium to quantify the microstructure, independently of the chemistry of the conducting fluid. The concept was originally used by Archie in geological research.^[36] The formation factor can be defined as the ratio of pore solution conductivity to the bulk conductivity of a saturated porous material. It can be expressed as

$$\mathcal{FF}_c = \frac{\sigma_p}{\sigma_b} \quad (1)$$

where σ_p is the pore solution conductivity (S m^{-1}) and σ_b is the bulk solution conductivity (S m^{-1}), which includes the effect of porosity.

The overall conductivity of an electrolyte is directly proportional to the mobility of each ion in the solution. According to the Einstein's mobility equation, the mobility of an ion is directly proportional to the diffusion coefficient of the ion.^[29,37] Therefore

$$\sigma \propto U_i^m \propto D_i \quad (2)$$

where U_i^m is the ionic mobility and D_i is the diffusivity of the ion.

Using Equation (2), \mathcal{FF}_c can be further expressed as

$$\mathcal{FF}_c = \frac{D_{cl}^\infty}{D_{cl}^{\text{eff}}} \quad (3)$$

As such, \mathcal{FF}_c is a fundamental material parameter which sets up a direct relation between the D_{cl}^∞ and the effective diffusion coefficient D_{cl}^{eff} of a porous nonconducting material filled with a conducting liquid. For a detailed underlying mathematical and physical understanding, the reader is directed to the works of Weiss et al.^[28] and Snyder.^[29] Chloride diffusion tests usually take months or years to complete and \mathcal{FF}_c can be obtained very fast by setting up simple conductivity experiments in the lab and applying Equation (1).

Once \mathcal{FF}_c is known, D_{cl}^{eff} can be expressed as function of \mathcal{FF}_c and D_{cl}^∞

$$D_{cl}^{\text{eff}} = \frac{D_{cl}^\infty}{\mathcal{FF}_c} \quad (4)$$

\mathcal{FF}_c is a nondimensional parameter and independent of ionic interactions, and it does not consider chloride binding. There are four major benefits of this approach: 1) Once \mathcal{FF}_c is evaluated, the effective diffusivity of any ion in a porous medium can be easily obtained. 2) The biggest advantage of using \mathcal{FF}_c lies in service life models where effective diffusion coefficients are required for chloride ion transport and as such service life models can be set up easily and accurately. This is discussed later in more detail. 3) Microstructure and transport properties of many different concrete mix/recipes can be quickly compared in terms of durability requirements.

4) As \mathcal{FF}_c is independent of the ion-ion and ion-solid interactions, one can separately account for the chloride binding effects. The biggest benefit comes from the fact that using \mathcal{FF}_c it is possible to not only quantify the microstructure but also separate ion binding effect of the ion from the transport phase. Therefore, the chloride binding can be evaluated separately using suitable data of isotherms^[17,38] and can be easily added to the transport equations.

The significance of using \mathcal{FF}_c in this study is that a direct influence of the addition of 2% LDH on the porous network can be acquired, to obtain the effective diffusion coefficients and also account for separately the chloride binding of hydrate phases as well as LDH in the transport model. This is explained in the later sections.

3.2. 1D Transport Model

The transport of an ion in a single saturated confined pore may be expressed using Nernst-Planck transport equation as^[32]

$$\frac{\partial}{\partial t} (C_i^f) + \nabla \cdot \left(-D_i^p \left(\nabla C_i^f + C_i^f \frac{z_i \mathcal{F}}{\mathcal{R}T} \nabla \psi_e + C_i^f \nabla (\ln \Upsilon_i) \right) \right) = 0 \quad (5)$$

where C_i^f is the free ion concentration (in mol m^{-3}) in the pore solution, D_i^p is the diffusion coefficient of the ion in pore solution (in $\text{m}^2 \text{s}^{-1}$), z_i is the charge number, \mathcal{F} is the Faraday's constant (96485 C mol^{-1}), \mathcal{R} is the ideal gas constant ($8.314 \text{ J mol}^{-1} \text{ K}^{-1}$), T is temperature (293 K), ψ_e is the electric potential (V) in the electrolyte, and Υ_i is the chemical activity coefficient.

To account for the porous network, Equation (5) can be alternatively written for a RVE of concrete using the formation factor as described in Qiao et al.^[31]

$$\theta_p \frac{\partial}{\partial t} (C_i^f) + \nabla \cdot \left(-\frac{D_i^p}{\mathcal{FF}_c} \left(\nabla C_i^f + C_i^f \frac{z_i \mathcal{F}}{\mathcal{R}T} \nabla \psi_e + C_i^f \nabla (\ln \Upsilon_i) \right) \right) = 0 \quad (6)$$

where θ_p is the porosity of the RVE.

Equation (6) expresses the transport of ionic species considering the effect of the concrete microstructure in a completely saturated state. To include the amount of chlorides that may bind to the cementitious microstructure, a source/sink term can be introduced in Equation (6). The resulting equation can be expressed as

$$\theta_p \frac{\partial}{\partial t} (C_i^f) + \frac{\partial}{\partial t} (C_i^b) + \nabla \cdot \left(-\frac{D_i^p}{\mathcal{FF}_c} \left(\nabla C_i^f + C_i^f \frac{z_i \mathcal{F}}{\mathcal{R}T} \nabla \psi_e + C_i^f \nabla (\ln \Upsilon_i) \right) \right) = 0 \quad (7)$$

$$\text{with } C_i^b = 0 \quad \forall i \neq \text{Cl}^- \quad (8)$$

where C_i^b is the amount of bound ions (mol m^{-3} of concrete).

Equation (7) includes diffusive flux, migration flux, and ion interactions taking place in ionic solution due to chemical activity effects. As we are mostly interested in chloride binding, the binding term for other species is equated to zero as described in

Equation (8). The bound chlorides can be specifically expressed as a function of free chlorides, determined usually by fitting an Freundlich-type isotherm to the experimental data points as

$$C_{CCl}^e = f(C_{CCl}^f) = a(C_{CCl}^f)^b \quad (9)$$

where a and b are Freundlich isotherm parameters.^[38]

The experimental procedure for obtaining the chloride binding isotherm is explained later. The total chloride in concrete may then be expressed as

$$C_{CCl}^e = \theta_p C_{CCl}^f + C_{CCl}^b \quad (10)$$

where C_{CCl}^e is expressed as mol m^{-3} of concrete.

The concrete pore solution is composed of different ions and the velocity with which ions move in the solution is different. In this study, six commonly present^[32] ionic species are taken into account namely Cl^- , K^+ , OH^- , Na^+ , Ca^{2+} , and SO_4^{2-} . In addition, one solid phase in the form of bound chloride is also accounted. This phase is assumed to be electrically neutral. Al^{3+} and NO_2^- were also detected in the pore solution but were not included to keep the model computationally inexpensive. However, the role of these species is explained later in the stability studies.

In a diluted state, different ionic species move at different velocity and as such some charged species move faster than others. This creates an electric field between the species which slows down fast moving ions and subsequently accelerates slow moving ions to maintain an electrically neutral environment. As such, a gradient of potential is created which is responsible for the migration flux in the diluted medium.

This electric field ψ_e , can be expressed as function of concentration of species and their respective charge via Poisson's equation as^[39,40]

$$\nabla^2 \psi_e = -\frac{\mathcal{F}}{\mathcal{E}_0 \mathcal{E}_r} \left(\sum_{i=1}^{i^t} C_i z_i \right) \quad (11)$$

where \mathcal{E}_0 is the permittivity of the vacuum and \mathcal{E}_r is the relative permittivity of water.^[40] The index i^t includes all ionic species and i^t is the total number of species.

The electrostatic interactions between opposite and like charged species also affect the movement of ions. At low solute concentrations, chemical activity effects are almost negligible. However, at higher concentrations, these effects can considerably affect the transport of ions. These interactions can be accounted using the modified Davies equations as reported by Samson et al.^[32,41]

$$\ln \gamma_i = A_i z_i^2 I_m \left(\frac{-I_m^{-0.5}}{1 + a_i B I_m^{0.5}} + \frac{(0.2 - 4.17 \times 10^{-5} I_m)}{\sqrt{1000}} \right) \quad (12)$$

where A and B are temperature-dependent parameters, I_m is the ionic strength and a_i being the respective diameters of each ion. The detailed expressions and given values of some species are mentioned in ref.[41] and **Table 2**.

Chloride transport can be modeled as a 1D problem for concrete samples exposed to chlorides only along one planer surface. A simplified 1D domain, 100 mm in length, was set up and meshed with linear elements. A finer mesh (0.25–0.5 mm element size) was used for the first 5 mm of the domain to handle steep concentration gradients and the rest was meshed with a relatively coarse mesh (1 mm element size) as shown in **Figure 2**. The aforementioned system of equations was solved using finite element method^[33] in COMSOL Multiphysics software package. Only strong forms of the equations are presented for the sake of brevity and conciseness. Quadratic Lagrange shape functions were used and the resulting system of equations was solved using an implicit time integration scheme, as implicit time marching is unconditionally stable.

To compare the two mixes, i.e., REF and +2% LDH, the model simulates a standard ponding test for both the mixes. As such one end of the geometry at $x = 0$ (mm) is exposed to a NaCl concentration of 165 g L^{-1} (2823 mol m^{-3}).^[31,42] The details of

Table 2. Diffusion coefficient at infinite dilution and ionic radii as per refs. [39,54].

Species	D_i^∞ [$\text{m}^2 \text{s}^{-1}$]	a_i [\AA]
Cl^-	2.030×10^{-9}	3
K^+	1.960×10^{-9}	3
OH^-	5.270×10^{-9}	3.5
Na^+	1.330×10^{-9}	4
Ca^{2+}	0.793×10^{-9}	6
SO_4^{2-}	1.070×10^{-9}	6

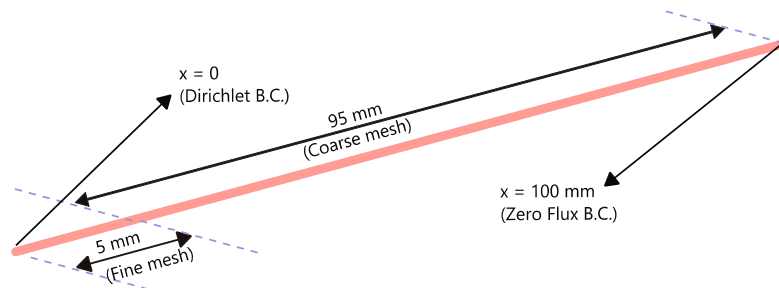


Figure 2. 1D modeling domain. Exposure end at ($x = 0$ mm; B.C. stands for boundary conditions).

the ponding test as well as the initial conditions for both the mixes are described in Section 4.

4. Experimental Section

4.1. Experimental Determination of Formation Factor

The formation factor was calculated by measuring the resistivity of lime saturated concrete samples at 28 days of age and from resistivity of pore solutions obtained from cement pastes at 7 days of age. The respective mix details are shown in Table 1.

During the curing period, the electrical resistance evolution was measured weekly. The samples were saturated under vacuum, by applying vacuum for 3 h and then adding saturated lime. When the samples were completely covered, the vacuum pump was left running for additional 1 h. The electrical resistivity was determined through the impedance measured with an FRA module applying an AC current of a frequency of 1000 Hz based on standard for determination of electrical resistivity.^[43] The samples were in contact with two stainless steel meshes used as electrodes connected to the equipment. Two sponges were moistened using limewater to improve the contact of the sample with the electrodes. The electrical resistance of the sponges was also measured to remove its value from the calculation. The measured values of conductivity are shown in Table 3.

The electrical resistivity of the pore solution was measured in cement paste samples after 7 days of curing. To determine this, the pore fluid of the cement paste was extracted by the pore pressing method. The procedure from Alonso et al. was followed.^[44] Approximately 125 g of the sample was placed into the cavity of the pore pressing apparatus. Pressure is then applied to a piston according to a maximum pressure of 400–500 MPa up to 650 MPa. Pressure is increased gradually with a mean rate of 50 MPa min⁻¹. The pore fluid is collected in a syringe, which was connected to the hole of the bottom plate via a short flexible plastic tube. After collection, the pore fluid was immediately

Table 3. Experimentally measured input parameters for REF and +2% LDH. Conductivity values are presented instead of resistivity. ρ_{con} refers to the density of concrete.

Parameter	REF	+2% LDH
σ_p [S m ⁻¹]	7.238	7.36
σ_b [S m ⁻¹]	0.0242	0.02
$\mathcal{F}\mathcal{F}_c$	298.9	368
θ_p [%]	11.6	12.1
ρ_{con} [kg m ⁻³]	2340	2340

Table 4. Initial concentration measured experimentally from pore solution. These concentrations are used as initial conditions in the FEM model excluding Al³⁺ and NO₂⁻. All concentration are expressed in mol m⁻³.

Mix	Species included in the model						Species not included	
	Cl ⁻	K ⁺	OH ⁻ /(pH)	Na ⁺	Ca ²⁺	SO ₄ ²⁻	Al ³⁺	NO ₂ ⁻
REF	1.86	275.27	285.10/(13.45)	140.57	0.41	1.276	0.042	–
+2% LDH	2.805	282.73	239.88/(13.38)	179.54	0.188	1.61	0.0415	37.25

filtered through a 0.45 μm filter and stored in a sealed plastic container protected from atmospheric CO₂ until further analysis. Two pore pressing tests were made for each cement paste type, i.e., with and without LDH. Immediately after collecting the pore solution, the electrical conductivity and pH of this aqueous solution was measured and is shown in Table 3. Further analyses were conducted to measure the ionic content of the pore fluids using inductively coupled plasma optical emission spectrometry (ICP-OES) and ionic chromatography (IC) (Table 4).

4.2. Chloride Binding Capacity

The chloride binding was evaluated by exposing ground cement pastes to various chloride solutions as in previous works.^[17,38,45] Two cement pastes with 2% LDH and without LDH were prepared with deionized water with w/c of 0.5 instead of 0.6^[46] to avoid cement bleeding. The pastes were cast in cylindrical airtight containers and rotated at slow speed within the first 24 h to prevent any segregation. After 28 days of curing, the samples were ground to a fine powder and dried at room temperature in a sealed lab desiccator with silica gel. 10 g of each powder was then exposed to 50 mL solutions of seven different chloride concentrations: 0.1, 0.3, 0.5, 0.7, 1.0, 2.0, and 3.0 M, respectively, for 7 days in sealed containers. The samples were stirred using a magnetic stirrer each day for 1 h. All samples were kept airtight during the experimental process to reduce the risk of carbonation. After 7 days, the free chloride concentration in the samples was measured by performing potentiometric measurement using a Mettler Toledo S7 Excellence together with a chloride sensitive electrode (Mettler Toledo Dx-235 Cl sensitive sensor). As a result of physical and chemical chloride binding, the concentration of chloride ion in the solution decreases. The total bound chlorides can be calculated by measuring the decrease in chloride concentration in the test solution. After 7 days, it is assumed that an equilibrium is established between the bound and free chlorides and the solution characteristics match the pore solution characteristics.

A plot between the final equilibrium chloride concentration (C_{Cl}^{Eq}) and the amount of bound chlorides (C_{Cl}^b) results fitted to a Freundlich isotherm, as shown in Equation (9) and is the so-called chloride binding isotherm. Table 5 shows the fitted parameters for a Freundlich isotherm for each mix.

4.3. Porosity, Density, and Ponding Test

The water-accessible porosity and saturated density tests were conducted according to UNE 83980^[47] after 28 days of age of

Table 5. Freundlich isotherm parameters for REF and +2% LDH mixes.

Property	REF	+2% LDH
a	5.7037	5.4898
b	0.4617	0.4749
Fitted R^2	0.89	0.85

the concrete samples in the curing chamber (98% RH and 20 °C). The samples were conditioned at 105 °C for a minimum of 24 h until weight variation was less than 0.5% in measures spaced 1 h and dry weight was measured at 20 °C. Then, the samples were immersed in water and weight was measured after 48 h and cycles of 24 h up to weight difference was less than 0.5% in consecutive measurements, eliminating the surface water of the samples. After the immersion, the samples were saturated under vacuum, applying vacuum for 2 h and then adding demineralized water slowly. When the samples were completely covered, the vacuum was removed and samples were kept in water for 24 h. The weight was measured eliminating the water in the surface. Finally, apparent weight was measured using a hydrostatic scale. The calculated porosity and saturated density are shown in Table 3.

The ponding test for the two concrete mixes was conducted according to EN 12390-11^[48] but with a salt (NaCl) concentration of 165 g L⁻¹ of solution as defined in NT Build 443.^[42] The chloride profiles were obtained after 46 days of exposure.

4.4. Isothermal Calorimetry and In Situ XRD Analysis

To investigate the compatibility of the LDH in a high alkaline cement paste system, additional analyses were performed. They consisted of isothermal calorimetry and XRD studies on cement pastes containing two amounts of LDH. For this, cement paste samples (CEM I 42.5 LA SR) were prepared (w/c = 0.5) without, with 2 and 4 mass% LDH (calculated on the dry cement mass). This cement was chosen to better ascertain the interaction of LDH with cement. The XRD measurements (Rigaku MiniFlex 600, Cu X-ray tube at 2° min⁻¹, detected with a high-speed silicon strip detector) were performed on the hydrating cement pastes in situ over a 56 d period. The samples were casted into the XRD sample holder, covered by a Kapton film, and then periodically measured by XRD. When not measured, samples covered by the Kapton film were stored in a desiccator. Isothermal calorimetry (TamAir isothermal calorimeter) was done with in situ paste samples from 1 min to over 7 days of hydration. The samples were externally mixed in the sample vial and placed in the calorimeter.

5. Results and Discussion

5.1. Model Validation Using Accelerated Ponding Tests

The aforementioned finite element-based numerical model was used to predict the 46 day chloride profiles for both REF and +2% LDH mixes. The initial concentrations for each

mix were taken from Table 4 and diffusion coefficients at infinite dilution for each species were taken from Table 2. The used Freundlich isotherm parameters are shown in Table 5. Likewise formation factor and other parameters were included from Table 3. The simulation results were compared with experimentally measured chloride profile at 46 days obtained from ponding tests.

Figure 3a shows the experimentally determined Freundlich-type chloride binding isotherm from cement paste for the REF mix. A comparison of model-predicted chloride profiles after 46 days with experimentally determined chloride profiles is shown in **Figure 3b**. Out of the three experimentally measured chloride profiles for REF mix, only two profiles (S1-REF and S2-REF) are considered here because one chloride profile (S3-REF, not shown here) had missing points and unusually high scatter. As shown in **Figure 3b**, the model does not seem to capture the first few millimeters of the chloride profile, especially the occurrence of sharp peak (skin effect) in the first few millimeters. Other physical phenomena apart from diffusion could be predominant in this region. A comparatively better prediction is observed toward deeper depths of the penetration profile with lower concentrations of Cl in the concrete. **Figure 3c** shows a comparison of the averaged experimental profile and modeled profile and also confirms the same conclusion.

To computationally measure the effect of Mg–Al–NO₂ in concrete, a similar simulation was carried for +2% LDH mix. **Figure 4a** shows the experimentally determined Freundlich-type chloride binding isotherm from cement paste for the +2% LDH mix. **Figure 4b** shows a comparison of 46 day model predicted chloride profile with experimentally determined chloride profile for each sample. A better agreement is observed between the modeled and experimental chloride profiles in concrete with LDH. The accuracy of the model in comparison with experiments is shown in **Figure 4b**. The modeled chloride front passes through the experimental scatter in the first few centimeters along the penetration path and merges very well with the experimental points along higher penetration depth of chloride front. Furthermore, S1-2% LDH and S2-2% LDH show a predominant peak in the first few millimeters, whereas the peak is less predominant in S3-2% LDH sample. As was the case with REF mix, the model does not capture the peaks in the chloride profiles but fits well beyond the first few millimeters. In general, a better fit is observed which can be appreciated from the comparison of averaged experimental profiles and modeled chloride profile as shown in **Figure 4c**.

In all the computations presented so far, the model is able to predict the chloride profile for a particular concrete mix with reasonable accuracy. This is primarily due to the benefit of using the formation factor, which accurately characterizes the microstructure, thereby yielding a good estimate of effective diffusion coefficient for chloride ions. Deviations in predictions especially in the first few millimeters along the penetration path can be attributed to many factors: first, the occurrence of skin effect^[49–51] causes a sharp chloride peak in the first few millimeters; second, the model is sensitive to the variability in the chloride binding isotherm and also the fact that formation factor was measured at 28 d age, whereas the chloride profiles were measured after 46 days of exposure time.

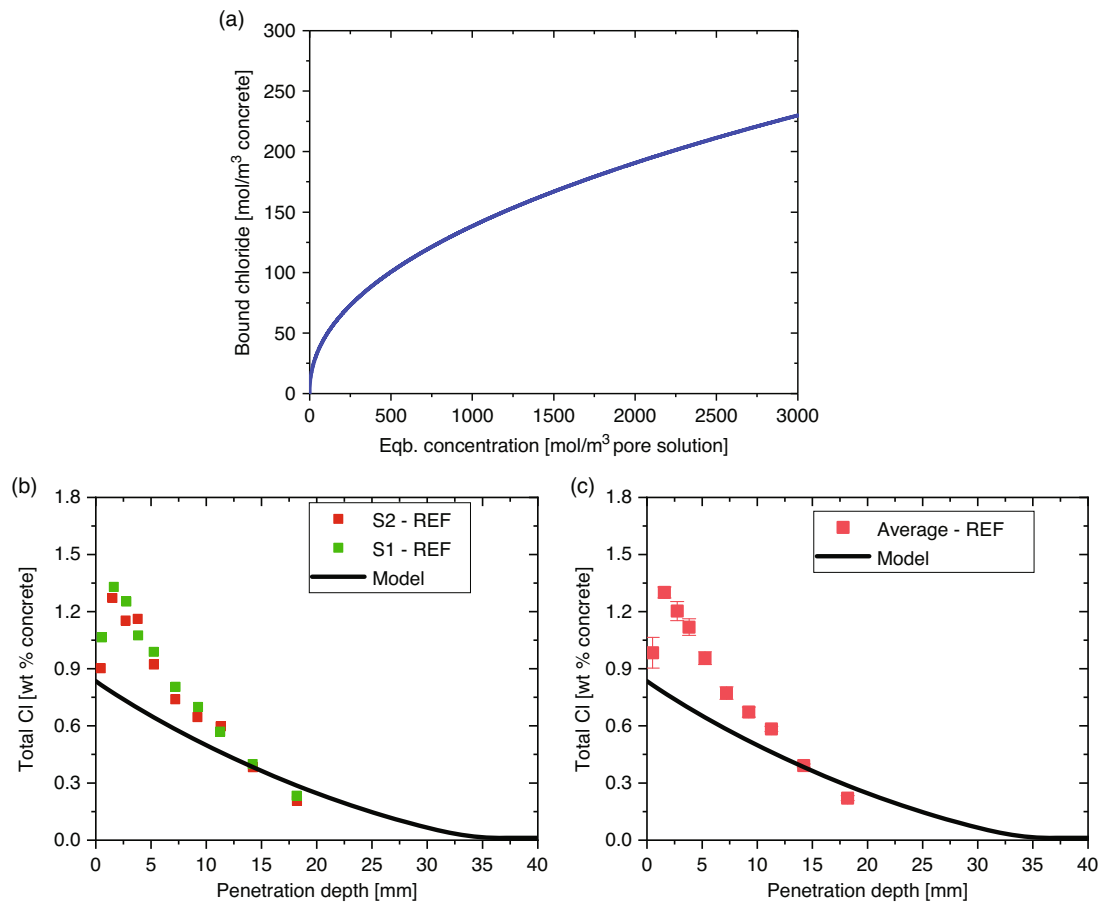


Figure 3. a) Chloride binding isotherm for cement paste from REF mix. b) A comparison of predicted 46 day chloride profiles with experiments from concrete with REF mix. Prefixes S1, S2, and S3 represent the chloride profile for each sample from the ponding test. c) A comparison of predicted profile and averaged experimental profiles.

The authors recommended that both chloride profile and formation factor should be measured at the same age to have a better numerical prediction of chloride profiles. The error of prediction for both the sets is shown in **Figure 5**. The strong influence of skin effect in the first few millimeters is represented by the high error of prediction in this region. It is also observed that the error of prediction decreases along the penetration path.

5.2. Mg–Al–NO₂ Efficiency toward Additional Chloride Binding

One of the most important properties of LDHs in corrosion control is its ability to capture negatively charged ions, e.g., Cl⁻ from the environment together with the possibility to deliver a corrosion inhibitor such as NO₂⁻ via the ion exchange process. Our previous investigations have revealed that LDH can significantly decrease chloride concentrations in the surrounding environments. However, the capacity to capture chloride ions can be influenced by the amount of LDH itself as well as pH

of the surrounding environment.^[52] The chloride capture is very fast and a thermodynamic heterogeneous equilibrium is established almost instantly.

The modeled profile for +2% LDH mix is slightly below the REF mix as shown in **Figure 6a**, suggesting only a moderate chloride capture in +2% LDH compared with REF mix. Similarly in **Figure 6b**, a comparison of experimental obtained averaged chloride profile shows only a moderate difference, with the +2% LDH profile slightly under the REF mix. The chloride binding isotherms as well show only slight differences between the two mixes as shown in **Figure 6c**.

This suggests that a major gain in chloride binding capacity of LDH could not be achieved. Many factors can contribute to this effect. First, a major contributing factor could be that LDH conducts a preferential exchange of NO₂⁻ with OH⁻ instead of Cl⁻. This can also be observed from the pore solution analysis where high concentrations of NO₂⁻ was observed despite no exposure to chloride (**Table 4**). This implies that either LDH conducted exchange with OH⁻/other ions in the pore solution or lost its

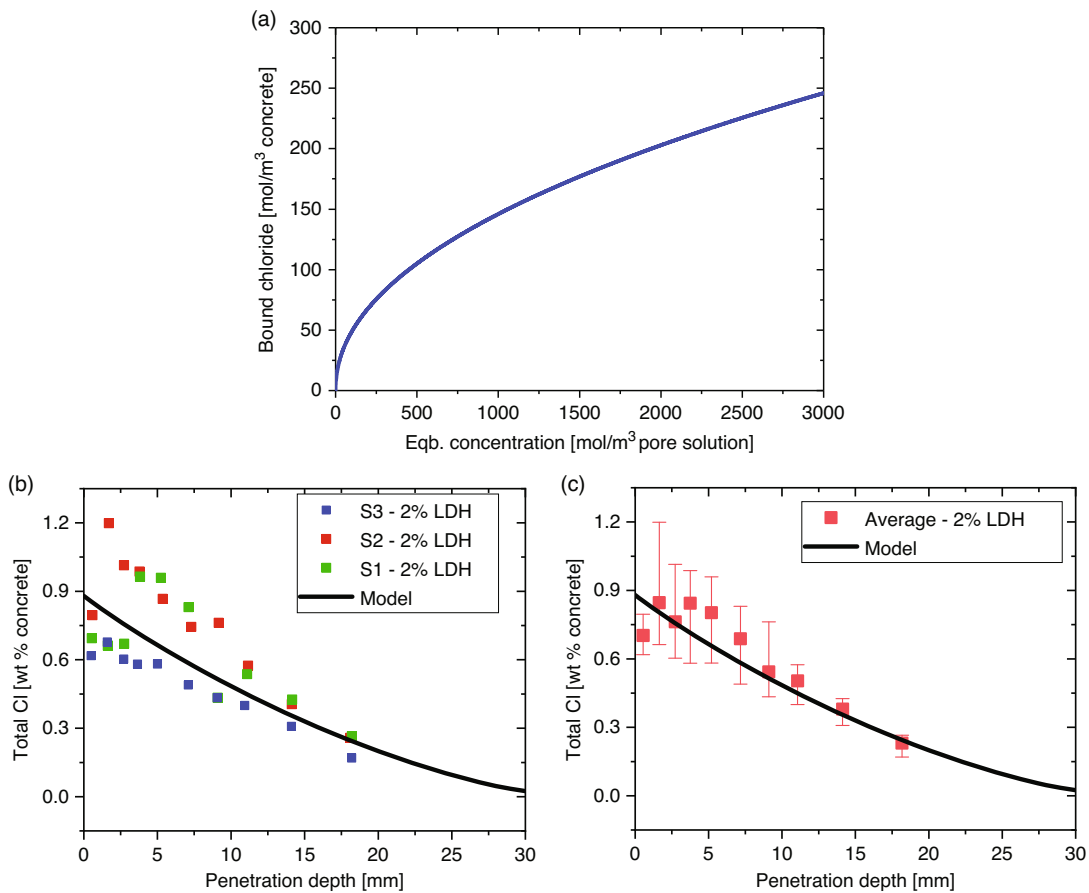


Figure 4. a) Chloride binding isotherm for +2% LDH mix. b) A comparison of predicted 46 day chloride front compared with experiments. Prefixes S1, S2, and S3 represent the chloride profile for each sample from the ponding tests. c) A comparison of predicted profile and averaged experimental profiles.

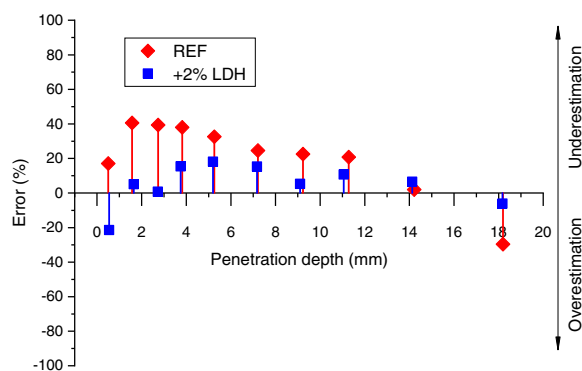


Figure 5. Error between simulation-assisted and experimentally obtained profiles for REF and +2% LDH mix.

structural stability at high alkaline pH. To confirm the release of NO_2^- in pore solution, additional pore solutions from cement paste with varying w/c ratios were analyzed (Appendix). In all

the samples with LDH, the presence of NO_2^- was found in the pore solution. Second, the overall percentage of the LDH in concrete is only 2% of the binder, which is overall a very small percentage. Third, LDH could also undergo a slight dissolution at high alkaline pH ranges as mentioned previously. All these factors can potentially act together but in different proportions. To better understand the stability of LDH in cementitious environments, additional stability tests were conducted and are explained in the next section.

5.3. Stability Analysis of Mg–Al–NO₂ in Cementitious Systems

The heat flow and total heat release curves from isothermal calorimetry are shown in **Figure 7**. Heat flow curves for pastes with LDH-NO₂ showed a strong acceleration of the hydration reaction. More LDH-NO₂ seems to increase the acceleration. The earlier onset of the induction and acceleration period shifted the peak heat release from 11.4 to 10.2 h and 9.1 h, respectively. The sulfate depletion shoulder of CEM I at ≈ 18 h appeared earlier and moved back into the main peak

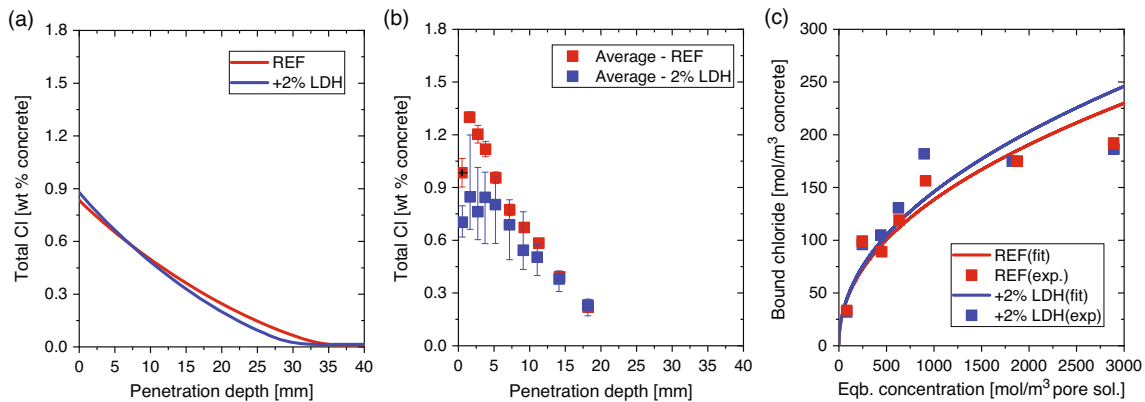


Figure 6. a) Model-predicted chloride profiles for REF and 2% Mix. b) Experimentally obtained chloride profiles including scatter for measurements. c) Experimentally obtained chloride binding isotherms and fitted Freundlich isotherms.

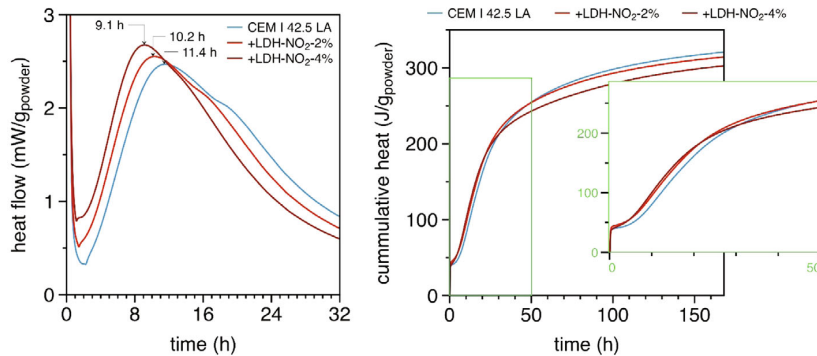


Figure 7. Heat flow curves of cement paste without and with two concentrations of LDH.

with increasing LDH content. Other authors attribute this shoulder with the formation of AFm.^[53] Cumulative heat curves of LDH-NO₂ pastes had higher heat production between 30 (4%) and 45 h (2%) of hydration. The total heat release in this range was higher with the increase in LDH in the pastes compared with the paste with CEM I only. Afterward, the curves converged to similar values but slightly below the curve of the pure CEM I paste.

The results from XRD measurements are shown in **Figure 8**. The CEM I paste showed in all ages a moderate amount of ettringite. From 7 days appeared an ettringite double peak at 8.5° 2-theta. Some artifact peaks between 13° and 15° 2-theta appear in the 4, 7, 14, 28, 40 days measurements, probably caused due to interference with the sample holder. Even after 56 days of hydration, only minor amounts of AFm phases in the form of hemi- and monocarbonate were visible. This was due to a very low C₃A content of the CEM I, which was a sulfate-resistant cement.

In pastes containing CEM I + LDH-NO₂ moderate amounts of ettringite were visible. In pastes with 4% LDH-NO₂ hemi- and monocarbonate was formed after 2 d of hydration; in pastes with 2% LDH, both AFm phases appeared later.

A monosulfate peak (9.9° 2-theta) was faintly visible in some of the hydration ages. A peak between hemi- and monocarbonate was either identified as a hydrotalcite-type phase or rests of LDH-NO₂ (main base peak 11.36° 2-theta).

There is strong evidence from the heat flow/total heat curves and from phase developments that the LDH reacts to a certain degree within the first hours of hydration. No LDH peaks can be found even at 4% in early hydration ages. The formation of AFm phases and possibly a hydrotalcite-like phase hints at a dissolution of the Mg–Al–NO₂ LDH. Acceleration of the hydration in isothermal calorimetry indicates substantial reaction of LDH. A filler effect is less probable because the induction/acceleration periods and sulfate depletion/AFm formation shoulder are shifted significantly toward earlier times, which indicates a chemical reaction of the LDH and a change in nucleation kinetics of C–S–H, initiated by LDH.

The results do not clearly indicate how much of the LDH reacted and the underlying mechanism, but due to the results of the calorimetry and the amounts of formed AFm phases, it is assumed that a substantial amount of the finer particles might have reacted. Any effects of LDH in cement pastes

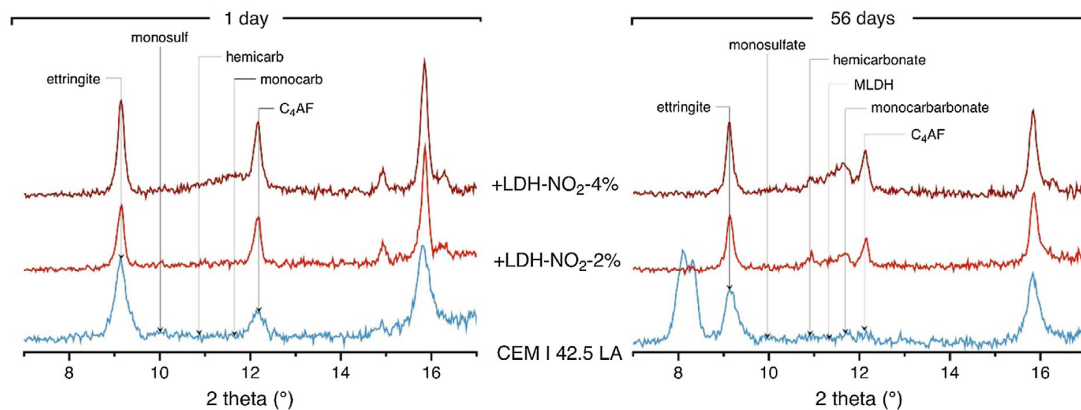


Figure 8. XRD pattern of CEM I pastes without and with LDH after 1 and 56 days of hydration.

toward chloride solutions might therefore also be due to chemical binding of chloride by AFm phases rather than with LDH.

6. Conclusions

The formation factor is a material property of porous media and can be easily determined by electrical measurements.^[28,36,43] Formation factor is accurately able to measure the hindrance offered by the porous microstructure on the ionic transport without taking chloride binding into account.^[29] Effective diffusion coefficients obtained as such tend to be very accurate. Thus, the experimental determination of formation factor by electrical conductivity measurements is an efficient way to establish effective diffusion coefficients needed in chloride transport models.

Based on chloride binding and formation factor, different concrete mixes can be easily compared in terms of their durability toward chloride ingress. These inputs are cheaper and relatively fast to obtain. Determination of formation factor can be a suitable alternative for expensive and time-consuming standard laboratory diffusion tests.

Based on the 1D transport model described in the article, two concrete recipes i.e., with and without Mg–Al–NO₂ were compared. A comparison of model-predicted chloride and experimentally obtained chloride profiles from accelerated natural ponding tests was presented. The model is able to predict the chloride ingress profile with a reasonable accuracy. In REF mix, the model is not able to capture the chloride peak but converges well with experimental observed chloride profiles at deeper depth with lower Cl content. For +2% LDH mix, the chloride peak is not so predominant in the experiments and the model shows a better match with experimentally obtained profiles.

Based on the evaluation of model predicted and experimentally derived chloride profiles, only a moderate difference is observable between the two recipes with the +2% LDH mix showing slightly lower ingress compared with REF mix. This can be attributed to reduced functionality of LDH particles in hydrating cementitious matrix. Similar information is obtained from binding isotherms which do not show any significant

difference, indicating that both mixes show almost similar chloride uptake values.

Calorimetry measurements indicated that the addition of LDH caused a slight acceleration of the hydration process as well as formation of AFm phases and possibly a hydrotalcite-like phase hints at a dissolution of the Mg–Al–NO₂ LDH. The AFm phases generated could in turn bind chloride ions from the pore solutions.

Based on in situ XRD analysis, LDH particles in cement pastes were not observed even at 4% dosage. The authors believe that this could be in part due to LDH undergoing partial dissolution followed by subsequent reactions leading to AFm formation and in part to the small quantity of LDH, which if not dissolved is too less in quantity to be detected during XRD analysis. In addition, if LDH stays undissolved, preferential exchange with OH⁻ instead of Cl⁻ together with moderate dissolution of LDH at high alkaline pH can also be contributing factors toward reduced chloride capture. The authors recommended that in future additional studies must be conducted to specifically determine the exact LDH dissolution/reaction mechanism in cement paste.

Appendix

Pore solution analysis of cement paste without (REF) and with 2% Mg–Al–NO₂ (+2% LDH) with varying w/c ratios: Concentrations of ions are in ppm (Table A1).

Calculation of bound chloride:

The bound chloride is calculated for each sample as

$$C_{Cl^-}^b = \left(\frac{(C_{Cl^-}^o - C_{Cl^-}^{Eq.}) \cdot V_{sol.}}{M_s} \right) \quad (13)$$

where $C_{Cl^-}^o$ is the initial chloride concentration, $C_{Cl^-}^{Eq.}$ is the final equilibrium chloride concentration after 7 days of exposure, $V_{sol.}$ is volume of the solution (50 mL), and M_s and is the mass of ground cement paste powder (10 g).

Table A1. Pore solution analysis of cement pastes with different w/c.

Series-ID-(w/c)	Al ³⁺	Ca ²⁺	Mg ²⁺	K ⁺	Na ⁺	Cl ⁻	NO ₂ ⁻	NO ₃ ⁻	SO ₄ ²⁻	pH
REF-1-(0.5)	0.46	20.10	–	1709.13	938.41	74.86	–	–	53.07	13.24
REF-2-(0.5)	0.48	20.06	–	2350.86	1073.72	104.67	–	–	56.33	13.28
REF-1-(0.55)	1.35	21.75	–	14846.2	5248.74	73.92	–	–	136.12	13.40
REF-2-(0.55)	1.05	35.41	–	10841.6	3264.13	313.91	–	–	269.60	13.42
REF-1-(0.6)	1.10	11.94	–	11374.5	3469.85	64.06	–	–	131.31	13.47
REF-2-(0.6)	1.17	21.63	–	10113.6	2991.01	–	–	–	–	13.44
+2% LDH-1-(0.5)	0.43	45.50	–	2230.53	1193.68	42.46	887.28	72.31	49.94	13.27
+2% LDH-2-(0.5)	0.49	44.34	–	2166.44	1184.05	49.03	963.97	76.37	47.61	13.25
+2% LDH-1-(0.55)	1.42	32.64	–	11360.2	4511.28	58.93	1994.54	105.78	144.71	13.38
+2% LDH-2-(0.55)	1.25	41.38	–	11682.1	4482.01	80.19	1923.89	110.97	123.93	13.40
+2% LDH-1-(0.6)	1.30	7.30	–	12125.6	4613.18	161.60	2018.66	104.89	199.98	13.38
+2% LDH-2-(0.6)	0.94	7.83	–	9944.91	3638.54	37.36	1409.18	46.82	109.40	13.38

Acknowledgements

This research was funded by the European Union's Horizon 2020 research and innovation program under grant agreement number 685445 (LORCENIS—Long Lasting Reinforced Concrete for Energy infrastructure under Severe Operating Conditions).

Conflict of Interest

The authors declare no conflict of interest.

Author Contributions

Conceptualization: Z.M., A.C.B., C.G., and L.D.H. Synthesis: F.R. and C.R. Finite element model: Z.M. and P.M. Experiments: U.M., M.C., K.V., M.P., C.G., and A.C.B. Analysis of results and data treatment: Z.M., U.M., A.C.B., C.G., M.C., K.V., M.P., and P.M. Manuscript writing and editing: Z.M., U.M., and A.C.B. Supervision: A.C.B., D.H., U.M., M.C., M.G.S.F., and M.L.Z.

Keywords

concrete, corrosion, finite element analysis, layered double hydroxides

Received: April 2, 2020

Revised: May 8, 2020

Published online:

- [1] K. Tuutti, *Corrosion of Steel in Concrete: Technical Report*, Swedish Cement and Concrete Research Institute, Stockholm **1982**.
- [2] B. E. L. Bertolini, P. Pedferri, E. Redaelli, R. Polder, *Corrosion of Steel in Concrete: Prevention, Diagnosis, Repair*, Wiley-VCH, Weinheim **2013**.
- [3] Z. P. Bazant, *J. Struct. Div. ASCE* **1979**, *105*, 1137.
- [4] U. Angst, *Mater. Struct.* **2018**, *51*, 1.
- [5] A. Poursaee, C. M. Hansson, *Cement Concrete Res.* **2007**, *37*, 1127.
- [6] D. Boubitsas, T. Luping, P. Utgenannt, *Chloride Ingress in Concrete Exposed to Marine Environment – Field Data up to 20 Years' Exposure*, Swedish Cement and Concrete Research Institute (CBI), Sweden **2014**.

- [7] P. Ghods, O. B. Isgor, G. J. C. Carpenter, J. Li, G. A. McRae, G. P. Gu, *Cement Concrete Res.* **2013**, *47*, 55.
- [8] U. M. Angst, M. R. Geiker, A. Michel, C. Gehlen, H. Wong, O. B. Isgor, B. Elsener, C. M. Hansson, R. Francois, K. Hornbostel, R. Polder, M. C. Alonso, M. Sanchez, M. J. Correia, M. Criado, A. Sagues, N. Buenfeld, *Mater. Struct.* **2017**, *50*, 1.
- [9] R. Vera, M. Villarroel, A. M. Carvajal, E. Vera, C. Ortiz, *Mater. Chem. Phys.* **2009**, *114*, 467.
- [10] F. J. Molina, C. Alonso, C. Andrade, *Mater. Struct.* **1993**, *26*, 532.
- [11] C. Andrade, C. Alonso, F. J. Molina, *Mater. Struct.* **1993**, *26*, 453.
- [12] E. Sola, Ph.D. Thesis, Institute of Construction Materials, University of Stuttgart **2017**.
- [13] E. Sola, J. Ozbolt, G. Balabanic, Z. M. Mir, *Cement Concrete Res.* **2019**, *120*, 119.
- [14] Q. Yuan, C. J. Shi, G. De Schutter, K. Audenaert, D. H. Deng, *Constr. Build. Mater.* **2009**, *23*, 1.
- [15] I. G. Richardson, *Cement Concrete Comp.* **2000**, *22*, 97.
- [16] H. Justnes, *Nordic Concrete Res.*, **1998**, *21*, 48.
- [17] B. Martin-Perez, H. Zibara, R. D. Hooton, M. D. A. Thomas, *Cement Concrete Res.* **2000**, *30*, 1215.
- [18] H. Zibara, *Binding of External Chlorides by Cement Pastes*, University of Toronto, Toronto, Canada **2001**.
- [19] European Union's Project, *Lorcenis – Long Lasting Reinforced Concrete for Energy Infrastructure Under Severe Operating Conditions*, SINTEF, Norway **2016–2020**.
- [20] E. L. Crepaldi, P. C. Pavan, J. B. Valim, *J. Brazil. Chem. Soc.* **2000**, *11*, 64.
- [21] J. Tedim, A. Kuznetsova, A. N. Salak, F. Montemor, D. Snihirova, M. Pilz, M. L. Zheludkevich, M. G. S. Ferreira, *Corros. Sci.* **2012**, *55*, 1.
- [22] M. Meyn, K. Beneke, G. Lagaly, *Inorg. Chem.* **1990**, *29*, 5201.
- [23] Y. H. Cao, D. J. Zheng, S. G. Dong, F. Zhang, J. Y. Lin, C. Wang, C. J. Lin, *J. Electrochem. Soc.* **2019**, *166*, C3106.
- [24] J. D. Zuo, B. Wu, C. Y. Luo, B. Q. Dong, F. Xing, *Corros. Sci.* **2019**, *152*, 120.
- [25] Z. Yang, R. Polder, J. Mol, C. Andrade, *Cement Concrete Res.* **2017**, *100*, 186.
- [26] Z. X. Yang, H. Fischer, R. Polder, *Cement Concrete Comp.* **2014**, *47*, 87.
- [27] Y. Y. Wu, P. Duan, C. J. Yan, *Appl. Clay Sci.* **2018**, *158*, 123.
- [28] W. J. Weiss, T. J. Barrett, C. Qiao, H. Todak, *Adv. Civ. Eng. Mater.* **2016**, *5*, 179.
- [29] K. A. Snyder, *Concr. Sci. Eng.* **2001**, *3*, 216.
- [30] L. P. Tang, L. O. Nilsson, *Cement Concrete Res.* **1993**, *23*, 247.

- [31] C. Y. Qiao, A. T. Coyle, O. B. Isgor, W. J. Weiss, *Adv. Civ. Eng. Mater.* **2018**, 7, 206.
- [32] K. Karadakis, V. J. Azad, P. Ghods, O. B. Isgor, *J. Electrochem. Soc.* **2016**, 163, C306.
- [33] T. Belytschko, W. K. Liu, B. Moran, K. I. Elkhodary, *Nonlinear Finite Elements for Continua and Structures*, Wiley, Chichester, West Sussex **2014**.
- [34] S. K. Poznyak, J. Tedim, L. M. Rodrigues, A. N. Salak, M. L. Zheludkevich, L. F. P. Dick, M. G. S. Ferreira, *ACS Appl. Mater. Inter.* **2009**, 1, 2353.
- [35] P. Spiesz, H. J. H. Brouwers, *Cement Concrete Res.* **2013**, 48, 116.
- [36] G. E. Archie, *Trans. AIME* **1942**, 146, 54.
- [37] D. Hoche, *J. Electrochem. Soc.* **2015**, 162, C1.
- [38] T. Luping, L.-O. Nilsson, *Cement Concrete Res.* **1993**, 23, 247.
- [39] E. Samson, J. Marchand, *J. Colloid Interface Sci.* **1999**, 215, 1.
- [40] Q. F. Liu, D. Easterbrook, J. Yang, L. Y. Li, *Eng. Struct.* **2015**, 86, 122.
- [41] E. Samson, J. Marchand, *Cement Concrete Res.* **2007**, 37, 455.
- [42] NT BUILD 443, *Concrete, Hardened: Accelerated Chloride Penetration, Nord Test Method*, Nordtest, Finland **1995**.
- [43] Pwi pren 12390-xz Determination of Electrical Resistivity-updated 2020-Feb Draft Version, European Standard – Technical Committee CEN/TC 104 – Secretariat: DIN.
- [44] M. C. Alonso, J. L. García Calvo, S. Pettersson, I. Puigdomenech, M. A. Cuñado, M. Vuorio, H. Weber, H. Ueda, M. Naito, C. Walker, Y. Takeshi, C. Cau-Dit-Coumes, in *Cement-Based Materials for Nuclear Waste Storage*, Springer, New York, NY **2012** pp. 251–259.
- [45] A. Delagrave, J. Marchand, J. P. Ollivier, S. Julien, K. Hazrati, *Adv. Cement Base. Mater.* **1997**, 6, 28.
- [46] C. Y. Qiao, W. Ni, Q. H. Wang, J. Weiss, *J. Mater. Civil Eng.* **2018**, 30.
- [47] UNE 83980 : 2014 – Concrete Durability. Test Methods. Determination of the Water Absorption, Density and Accessible Porosity for Water in Concrete. Spanish Association for Standardization and Certification, **2014**, <https://www.une.org/encuentra-tu-norma/busca-tu-norma/norma/?c=N0054056>.
- [48] BSI, EN 12390-11:2015 – Testing Hardened Concrete. Determination of the Chloride Resistance of Concrete, Unidirectional Diffusion, **2015**, <https://shop.bsigroup.com/ProductDetail?pid=00000000030351885>.
- [49] C. Andrade, L. M. Diez, C. Alonso, *Adv. Cement Base. Mater.* **1997**, 6, 39.
- [50] P. Castro, O. T. De Rincon, E. Pazini, *Cement Concrete Res.* **2001**, 31, 529.
- [51] K. De Weerd, D. Orsáková, A. C. Müller, C. K. Larsen, B. Pedersen, M. R. Geiker, *Constr. Build. Mater.* **2016**, 120, 418.
- [52] C. Gomes, Z. Mir, R. Sampaio, A. Bastos, J. Tedim, F. Maia, C. Rocha, M.G.S. Ferreira, *Materials* **2020**, 13, 1769.
- [53] A. Fernandez, M. C. Alonso, J. L. Garcia-Calvo, B. Lothenbach, *Mater. Construct.* **2016**, 66, 1.
- [54] K. Karadakis, *Numerical Investigation of the Chemistry of the Pore Solution in the Mill Scale Crevices of Carbon Steel Rebar*, Vol. Master of Applied Science, Department of Civil and Environmental Engineering, Carleton University, Ottawa, ON, Canada **2010**.

5. Discussion of published results

Layered double hydroxide has been extensively studied in the last few decades across a multitude of scientific disciplines. With a potential to capture Cl^- ions inside concrete exposed to chloride ingress, LDH has recently gained popularity as a new class of cement additive. The ion exchange property is quite unique to LDH and it is the focal point of this work, albeit so far it hasn't been fully understood in the field of concrete technology. In addition to that, a critical review of the application of LDH in cementitious systems revealed that most of the studies conducted so far were carried out in aqueous alkaline solutions, mortars or in cement pastes and very few studies report on the application of LDH in concrete itself [39]. As a consequence, an in-depth understanding of LDH in high alkaline/cementitious systems has not been reported so far. Furthermore, despite considerable advances in the application of LDH in concrete, many key concepts regarding its functionality and stability in concrete stay unsettled.

This work showcases a predictive modelling methodology to evaluate efficiency of any chloride binding additive, although in this work the application is restricted only to LDH. Another numerical model discussing the electrochemical processes on the rebar surface in reinforced concrete is also presented. As mentioned previously, this work intends to provide a basic understanding of LDH in cementitious medium, therefore this work also critically reflects upon the basic functionality of LDH in cementitious environments from an experimental point of view as well. This chapter showcases an understanding of the above mentioned fundamental factors and presents the main findings of the work with an in-depth discussion.

5.1. Chloride sequestration efficiency of LDH in alkaline environment

The chloride ion entrapping efficiency of various types of LDH at near-neutral pH is well known [67, 68]. Although excellent chloride binding capacity has been reported in this pH range [69], these findings cannot be directly extrapolated to concrete systems in the high

alkaline range. Other researchers have studied chloride entrapping capacity of LDH in pore solutions and cement pastes [39], but the exact quantitative influence of OH^- ion on chloride binding capacity has not been reported so far in detail. Additionally, none of the studies so far have focused on the stability of LDH in the alkaline regime. In this work Zn-Al- NO_2 was used as a starting material with an aim of using it as a Cl^- entrapping additive in alkaline environment. The use of Zn-Al- NO_2 in concrete is a novel application as this type of LDH has not been studied previously in concrete systems. The motivation to use Zn-Al- NO_2 is further reinforced by the fact that Zn-Al- NO_2 can deliver a corrosion inhibiting ion (NO_2^-) during the ion exchange process, which can potentially mitigate steel corrosion in concrete.

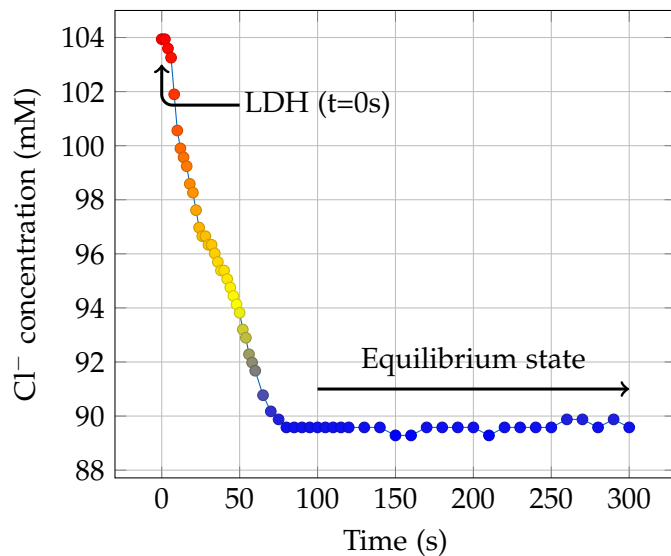


Figure 5.1.: Chloride sequestration by LDH in an aqueous salt solution at a starting pH of 11.95 under continuous stirring.

As a first step, the chloride binding capacity of Zn-Al- NO_2 across the entire alkaline pH spectrum is presented. The investigations highlight the influence of OH^- ion on Cl^- uptake, and also present the stability of Zn-Al- NO_2 in the pH similar to that of concrete. Figure 5.1 presents the kinetics of Cl^- capture in an alkaline solution with an initial Cl^- concentration of 103.9 mM and an initial pH = 11.95. The LDH in its powdered state was carefully dropped into the solution at time ($t = 0$ s) under continuous stirring using a magnetic stirrer. The Cl^- ion sequestration was instant and converged to an equilibrium state in about a minute. The equilibrium state refers to a heterogeneous equilibrium that is formed between the free Cl^- ions in the solution and the Cl^- ions captured by LDH. A decrease in Cl^- concentration clearly validates the functionality of the starting material.

As mentioned previously, the Cl^- sequestration is pH sensitive. Apart from that, the ion

sequestration capacity of LDH is strongly influenced by other factors, such as temperature, concentration of an anion (or competing anions), anion size etc. as discussed previously in chapter 2. In an exposure state with more than one type of anion, LDH can exhibit a multi-anion uptake. In such a situation, the uptake is governed by the affinity of the ion for that LDH. In a case where both OH^- and Cl^- are present, a combined uptake of both ions can take place, but in different proportions. In the experimental case described in Figure 5.1, the pH of the solution decreased from pH = 11.95 to pH = 10.07 signifying that OH^- was also captured by LDH. In a multi-ion exposure scenario, LDH forms a separate heterogeneous equilibrium with each anion. It is important to mention that these heterogeneous states can significantly differ from each other.

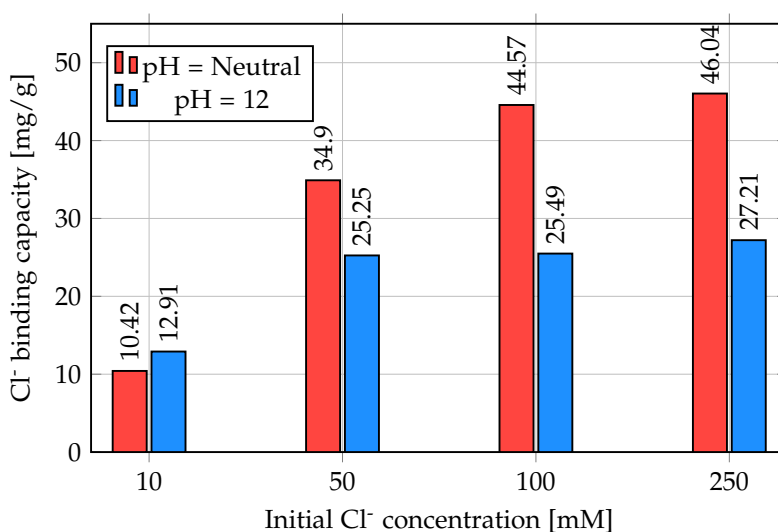


Figure 5.2.: Variation of chloride binding capacity of LDH at various pH levels.

Additionally, the concentration of the ion present in the exposure environment is also a key factor regarding its uptake by LDH. Generally, the higher the concentration of the anion, the higher is its uptake. In Figure 5.2, as the Cl^- ion concentration increases, its sequestration also increases and the equilibrium state is shifted. A peak chloride binding capacity of $\simeq 45$ milligrams of Cl^- per gram of LDH is observed at an initial Cl^- concentration of 250 mM at neutral pH after 300 seconds of exposure. However, in the presence of competing ions such as OH^- , the Cl^- sequestration is reduced as multi-anion sequestration takes place. As can be observed in Figure 5.2, the chloride sequestration is considerably reduced in a OH^- containing exposure environment. The Cl^- binding capacity at an initial concentration of 100 mM and pH = 12 is ~ 25 mg/g which is almost half of the value at neutral pH. The selective preference in ion exchange is governed by the selectivity series for the LDH in consideration. Based on the results presented in section 4.2 and also as per another recent publication by the

author [70] and as generally stated by Miyata [71], the affinity series regarding monovalent anions for Zn-Al-NO₂ can be written as OH⁻>Cl⁻>NO₂⁻>NO₃⁻. The anions on the left of the selectivity series will be preferred over anions to the right. Therefore, it is concluded that a pH drop in alkaline state is expected in addition to a decrease in Cl⁻ concentration in a multi anion capture scenario (see Figure 9 in section 4.2). This also infers that the ability of LDH to capture Cl⁻ ions decreases as pH increases in the exposure environment.

In the experimental results presented in this work (section 4.2), it was also observed that if the concentration of the lagging anion (e.g. Cl⁻), in the selectivity series is sufficiently high as compared to the preceding anion (say OH⁻), the lagging anion can force its uptake owing to its high concentration in the environment. This was also observed by Iyi et al. [72] as they were able to substantially reduce the carbonate content in LDH by exposing the LDH to high concentrations of Cl⁻ and Br⁻ ions.

5.2. Stability analysis of LDH in alkaline environment

Stability analysis of LDH in alkaline environments forms one of the basic building blocks towards understanding its behavior in cementitious systems. Previous works [73, 36, 39] suggest that LDH can accelerate formation of hydration products and also enhance formation of hydration phases like AFt and AFm. This interference in hydration kinetics suggests that apart from a possible filler effect, LDH is reactive in nature and could undergo dissolution during cement hydration because of the high pH in the surrounding environment. To clarify this, this work presents the stability analysis of Zn-Al-NO₂ not only in the desired alkaline range but also across the entire pH spectrum. It is to be noted that prior to this work, the stability of Zn-Al-NO₂ has not been studied in cementitious systems.

It is to be emphasized here that understanding the stability of LDH in alkaline pHs has a high practical importance for this work, considering the fact that the final aim of using LDH is to be able to use it inside cementitious environments. The pH of fresh concrete as well as mature concrete is very alkaline and can vary from pH ~12.7 to pH >>13. Therefore, the stability of LDH was investigated in a range of pH from 11 to 13.5, by immersing 1 gram of LDH for 30 days in alkaline solutions. It was observed that at pH beyond ~>12.5, LDH can suffer significant dissolution. As a consequence, the capacity to conduct ion sequestration is reduced due to a decrease in the amount of available LDH (see Figure 6 in section 4.2). Due to the partial dissolution, constituent ions of Zn-Al-NO₂ pass into the solution where the cations (Al³⁺ and Zn²⁺) can form metallic complexes with OH⁻ ions present in the solution and with additional amount of OH⁻ released from the dissolution of LDH.

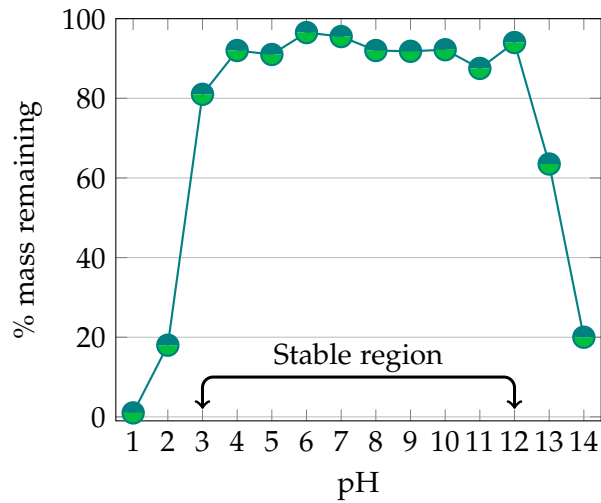


Figure 5.3.: Stability of Zn-Al-NO₂ across the entire pH spectrum. Reprinted with modifications from [70] under CC BY 4.0 license.

In another collaborative work by the author [70], the effect of pH on LDH stability across the entire pH range was further investigated. A measured quantity of Zn-Al-NO₂ was exposed to solutions with pH ranging from 1 to 14 for 30 days. After 30 days the remaining powders were recovered, weighed and plotted as percentage of mass remaining at each pH as shown in Figure 5.3. It was observed that LDH suffers heavy dissolution in acidic range up to pH ~3 and beyond pH ~12. The authors also suggested that between pH = 4 and 12, it is also possible that LDH undergoes moderate/insignificant dissolution. At pH = 1, the LDH endured complete dissolution whereas at pH ~>13, only ~ 60% of LDH was recovered.

5.3. Effect of LDH dissolution on hydration kinetics

The dissolution of LDH into its constituent cations and anions can effect the cement hydration kinetics. For different types of LDH, a variable effect has been reported [39]. However in the special case of Zn-Al-NO₂, a possible release of Zn²⁺ ions can significantly retard cement hydration as Zn²⁺ ion is a well known retardant [74, 75, 76]. In this work, it was observed that cement pastes cast with 2% LDH having a particle size of ~25 μm (section 4.2) depicted a clay like behavior and took an unusually longer time to harden as shown in Figure 5.4. This strong influence on cement hydration again confirms the dissolution of LDH leading to the release of Zn²⁺ ions. The underlying mechanism is attributed to the formation of Ca-Zn complexes during the hydration process which reduces the concentration of Ca²⁺ in the nearby pore solution and delays the precipitation of cement hydration phases [75].

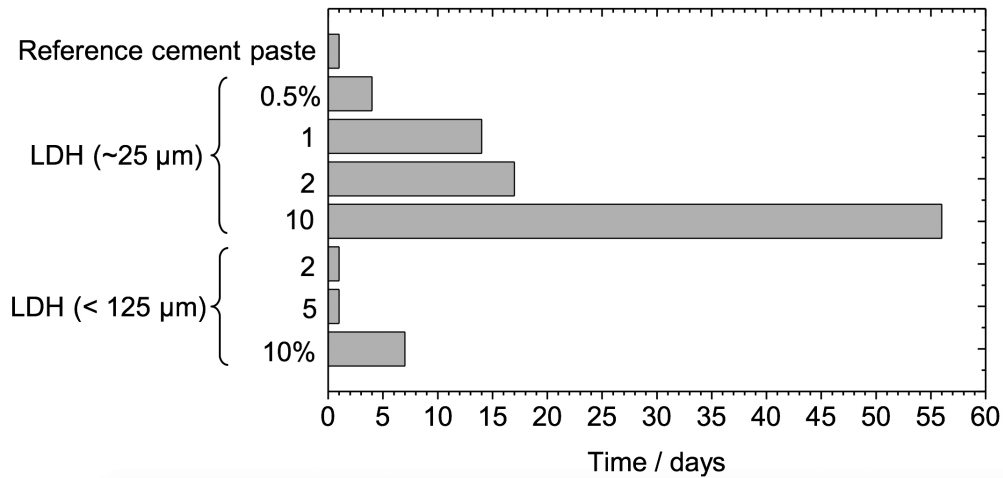


Figure 5.4.: Effect of the LDH particle size and dosage on cement hydration. Reprinted from [70] under CC BY 4.0 license.

In order to further investigate the compatibility of LDH with cement, the effect of particle size on LDH was investigated. Two different Zn-Al-NO₂ type with mean particle size of ~25 μm and <125 μm were used in cement pastes (w/c = 0.5) with dosage ranging from 0.5% to 10%. It was observed that as dosage of LDH increased, higher was the absolute degree of dissolution and more significant was the effect on the curing time. However, for bigger LDH particles, the curing time was significantly less as compared to finer particles. It is observed that finer the particles, higher is the reactivity due to the large surface area. This demonstrates the relation between the LDH particle size and relative degree of dissolution. These studies inspired the development of a second generation of LDH i.e. Mg-Al-NO₂. This new LDH was incorporated in to concrete and further investigations were carried out both numerically and experimentally as explained in section 5.5.

5.4. Stability analysis of Mg-Al-NO₂ in cementitious environment

In order to investigate the behavior and stability of Mg-Al-NO₂ in concrete, a set of stability studies were performed. These included in-situ XRD and isothermal calorimetry measurements on hydrating cement pastes. A detailed evaluation of in-situ tests is presented in section 4.3. For these tests, cement pastes were prepared with CEM I 42.5 LA SR type cement, 2-4% Mg-Al-NO₂ and a water to cement (w/c) ratio of 0.5.

Calorimetry studies revealed that Mg-Al-NO₂ participated in the hydration process with an accelerating effect on hydration kinetics. This suggested an early reaction of Mg-Al-NO₂

during the hydration process. In-situ XRD analysis suggested that a partial dissolution of Mg-Al-NO₂ led to the formation of AFm and other hydrotalcite like phases. Due to the qualitative nature of these tests, the exact amount of dissolved/un-reacted Mg-Al-NO₂ is difficult to ascertain. However, the presence of higher amounts of AFm in samples with Mg-Al-NO₂ was clearly observed. Due to the fact that AFm possesses chloride binding capability, the moderate gain in chloride resistance in concrete mix with +2% LDH can be attributed to the formation of AFm. It is due to the unique chemistry of LDH that despite suffering dissolution, it is still indirectly beneficial with regard to chloride durability.

5.5. A predictive modelling approach towards evaluation of chloride sequestration capacity of LDH in concrete

In general, numerical methods help towards development of a better understanding of the physical processes. At present, numerous models exist for LDH at an electronic scale [77, 78] but not many modelling studies are reported at a continuum level. A recent FEM based Fickian transport model was developed by Yoon et al. [67] to study the interaction of a single LDH grain with cement paste. In this work, a numerical methodology to evaluate the effect of chloride binding additives in concrete is presented. This numerical methodology can be used to understand two vital properties: (i) the effect of additive on concrete microstructure, (ii) functionality and efficiency of the additive in concrete. Here the aforementioned numerical methodology is presented for Mg-Al-NO₂ but can be also used to study any other LDH or Cl⁻ entrapping additive. In order to numerically evaluate the role of Mg-Al-NO₂ towards chloride entrapping in concrete, two sets of concrete and cement paste samples were cast i.e. "REF" set with no LDH and "+2% LDH" set with 2% Mg-Al-NO₂ in the mix. The details of concrete mix are shown in Table 3.2. The aim was to clearly demonstrate the effect of Mg-Al-NO₂ in concrete exposed to chloride ingress. To achieve this, the chloride binding capacity and the formation factor of the two mixes was measured as per procedures detailed out in chapter 3. Based on these inputs, a FEM based numerical model was set up as explained in section 4.3.

Formation factor FF_c was used not only to determine the effective diffusion coefficient but also to quantify the change in effective diffusion coefficient due to addition of LDH (section 4.3). It effectively measures the hindrance offered by the microstructure to the transport of ionic species [58]. The biggest advantage in using formation factor is that it is independent of chloride binding which can be then incorporated separately in the numerical model using a suitable chloride binding isotherm. Therefore, by using formation factor it is easier to make a distinction in the microstructure due to the addition of LDH. Additionally, formation factor provides effective diffusive coefficient for any ion present in the pore solution, and not just

for Cl^- ion.

According to the multi-ion transport model described in section 4.3, the transport of chloride ions in concrete can be mathematically expressed as

$$\theta_p \frac{\partial}{\partial t} (C_{\text{Cl}^-}^f) + \frac{\partial}{\partial t} (C_{\text{Cl}^-}^b) + \nabla \cdot \left(- \frac{D_{\text{Cl}^-}^\infty}{FF_c} \left(\nabla C_{\text{Cl}^-}^f + C_{\text{Cl}^-}^f \frac{z_{\text{Cl}^-} F}{RT} \nabla \psi_e + C_{\text{Cl}^-}^f \nabla (\ln \gamma_{\text{Cl}^-}) \right) \right) = 0, \quad (5.1)$$

where bound chlorides $C_{\text{Cl}^-}^b$ can be expressed as function of free chlorides $C_{\text{Cl}^-}^f$ as

$$C_{\text{Cl}^-}^b = \alpha (C_{\text{Cl}^-}^f)^\beta \rightarrow \text{Freundlich isotherm}, \quad (5.2)$$

here:

- α, β = Freundlich isotherm parameters
- θ_p = porosity of concrete
- z_{Cl^-} = charge number of Cl^- ion
- F = Faraday's constant [96485 C/mol]
- R = ideal gas constant [8.314 J/(mol·K)]
- T = temperature [293 K]
- ψ_e = electric potential [V]
- γ_{Cl^-} = chemical activity coefficient

The eq.(5.1) and eq.(5.2) are known as the Nernst-Planck transport equation and Freundlich isotherm respectively. The expression for electric potential ψ_e and chemical activity coefficient γ_{Cl^-} are mentioned in section 4.3. In order to predict the chloride profiles in ponding tests (section 3.3.6), the problem is idealised with a 1D domain as shown in Figure 5.5(a). On end of the domain is subjected to a salt concentration of 165 g/l using Dirichlet boundary conditions.

Using the generic form of eq.(5.1) for Na^+ , Cl^- and other ions present in the pore solution, the transport of these species can be modelled in the 1D domain. For the REF mix, Figure 5.5(b) depicts the pore concentration evolution of Na^+ and Cl^- ions at 10 mm, 20 mm and 30 mm from the exposed end, for a total exposure time of 46 days. The details on initial conditions, and other properties such as porosity and density for the REF mix are mentioned in section 4.3. For curves at $x = 10$ mm location, the pore/free concentration starts to increase after the 8th day. Due to the fact that there are initially 140.5 mol/m³ of Na^+ ions in the pore solution, the curves for Na^+ ions are initially above the curves of Cl^- ions but tend to

converge as time progresses. Despite chloride binding, the free Cl^- ions move faster than Na^+ ions because the diffusion coefficient of Cl^- is almost 1.5 times higher than that of Na^+ ion. For points situated far away from the exposure end, the increase of concentration is not so rapid. As time proceeds, the chloride ions move further ahead along the penetration path of the domain. This is also observed from the simulation results shown in Figure 5.5(c). Here, the total chlorides (free + bound) are presented as a weight percentage of concrete. It is observed that the chloride front proceeds ahead along the penetration path with time.

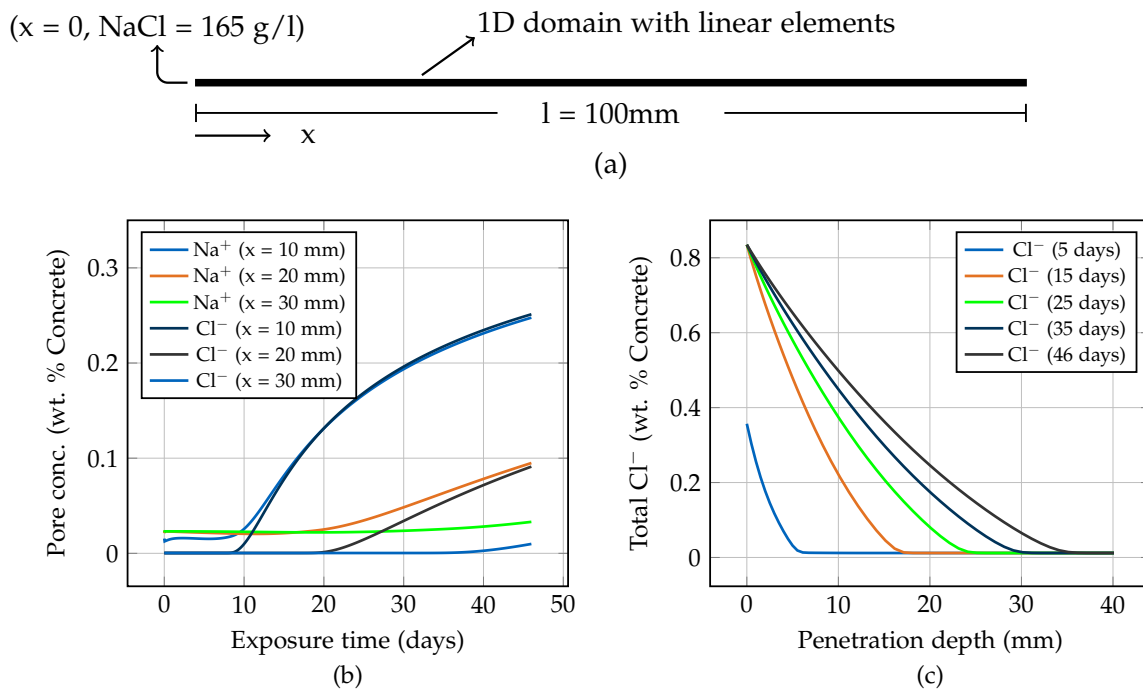


Figure 5.5.: (a) One-dimensional modelling domain. (b) Evolution of pore solution concentration for Na^+ and Cl^- ion at 10 mm, 20 mm and 30 mm from the exposed end. (c) Total chloride profiles for the REF mix plotted against penetration direction.

The model validation has been presented in detail in section 4.3. The accuracy of predicted total chloride profile in comparison to experimental chloride profile for the REF and +2% LDH mix is shown in Figure 5.6. The vertical axis represents the ratio of experimental and predicted chloride concentration plotted against the penetration depth. If the ratio is >1 , it infers that the model underestimates the actual concentration obtained from the tests. On the other hand, if the ratio is <1 , it reflects that the model overestimates the actual concentration. In general, it can be observed that the ratio decreases considerably for both the concrete types as penetration depth increases. In the first few millimeters the model underestimates the

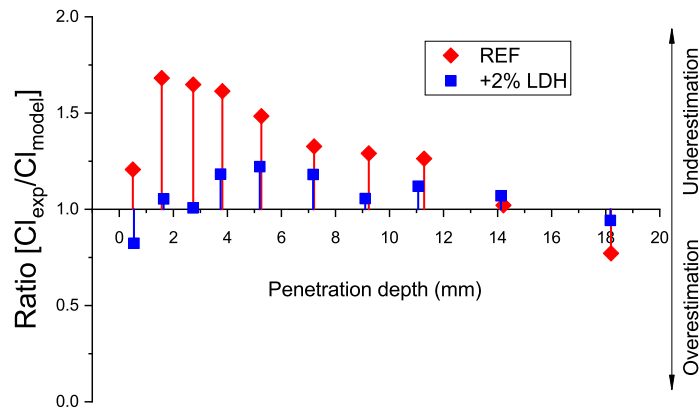


Figure 5.6.: Ratio of experimentally obtained and numerically predicted chloride profiles.

chloride concentration. This can be attributed to the skin effect [79, 80, 81] which corresponds to the presence of a sharp peak in the concentration profile, occurring in the first few layers of the exposed specimen. Additionally, the model is very sensitive to the variations in the chloride binding isotherm. It is further recommended that in order to have a better accuracy of prediction, the formation factor should be measured regularly for the same duration of time as in the ponding test. In doing so, any change in the diffusion coefficient due to the hydration reactions will be incorporated and that would in turn result in a better accuracy of prediction. For the experiments conducted in this work, the formation factor was measured at an age of 28 days, whereas the chloride profiles were measured at 46 days of exposure time.

From a comparison of numerically predicted chloride profiles for concrete without and with 2% Mg-Al-NO₂ as detailed out in section 4.3, it is observed that the incorporation of Mg-Al-NO₂ has a slight enhancing effect on the chloride binding capacity of concrete. Likewise, a comparison of the formation factor (section 4.3) reveals that addition of Mg-Al-NO₂ has also a slight refinement effect on the microstructure signifying an early reaction of the Mg-Al-NO₂.

5.6. Numerical modelling of corrosion initiation processes at the steel-concrete interface

This work also presents an insight into the electrochemical processes at the steel-concrete interface. In the corrosion model presented in section 4.1, transport and electrochemical processes occurring in the concrete bulk and on the steel surface are modelled for a concrete member exposed to chloride ingress in submerged marine conditions. A randomly varying chloride threshold function is used to make a transition from passive stage to actively

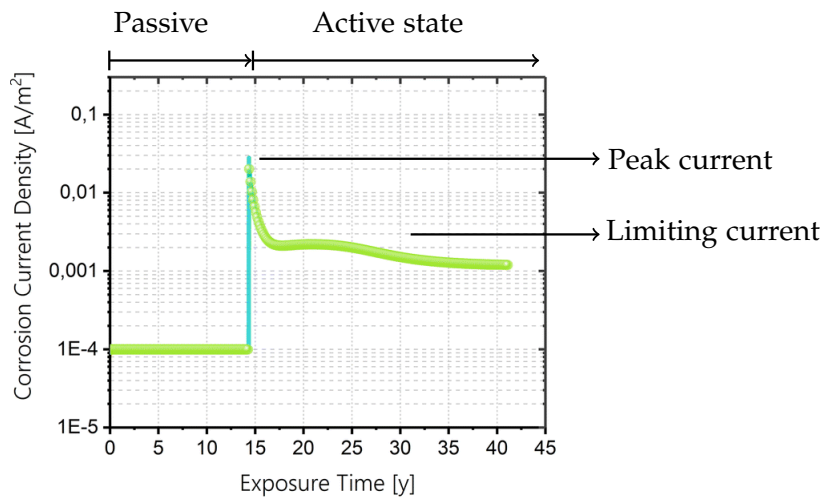


Figure 5.7.: Current density in passive and active states for a total exposure time of 41 years. Reprinted with modifications from [64] under CC BY 4.0 license.

corroding stage. The submerged conditions are chosen as the exposure scenario because it has been observed that the most severe chloride ingress occurs in this zone [8, 82]. For this reason, this exposure scenario is chosen in this work and also in the LORCENIS project [30].

In order to predict the service life of concrete members, it is intended to combine both the corrosion initiation stage and the propagation stage in a single model. For the test case presented in section 4.1, the chloride threshold is surpassed on the rebar surface after 14.35 years and the first activation event takes place as shown in Figure 5.7. This is observed by the peak in corrosion current density. Prior to this event, the rebar is in its passive state. As the corrosion process is in concentration control, the current density starts to decrease as oxygen is consumed and attains a limit state in which only the amount of oxygen that enters through the concrete cover is consumed at the rebar. Model validation and other parameteric studies are presented in section 4.1. The mechanical effect of rust is not included in this model and is part of another model developed within LORCENIS project [30] and will be published as a separate work.

6. Conclusions and Future Work

This work presents LDH as a potential chloride entrapping additive in concrete. The numerical and experimental investigations included in this work place emphasis on the role of LDH with respect to chloride transport and corrosion inhibiting processes in concrete. It is observed that LDH is able to provide a moderate enhancement of the chloride durability of concrete. Although LDH is very efficient at Cl^- sequestration in neutral pH environments, its efficiency is reduced in the alkaline region. Therefore, this work reflects a deeper understanding of the behavior of LDH in high alkaline/cementitious environments. Based on the results presented in this work, the following conclusion can be drawn:

- This work presents a numerical model in order to computationally evaluate the role of LDH in concrete. The model is able to highlight the effect of LDH on the chloride transport in concrete specimens. The underlying methodology is generic and can be used for any other chloride binding additive as well.
- Based on the comparison of numerically predicted chloride profiles for concrete with and without Mg-Al- NO_2 , it is observed that the addition of Mg-Al- NO_2 to concrete is only moderately beneficial towards chloride resistance. This observation is also confirmed by comparing the chloride binding isotherms and experimentally obtained chloride profiles.
- The transport model presented in this work incorporates formation factor as an indirect measure of effective diffusion coefficient. It is independent of chloride binding and easy to incorporate in chloride transport models. The effective diffusion coefficients obtained from formation factor tend to be very accurate than those obtained from conventional chloride ponding tests. By comparing formation factor for concrete with and without Mg-Al- NO_2 , it is also observed that the addition of Mg-Al- NO_2 results in a slightly refined microstructure as compared to reference mix.
- The corrosion model showcased in this work is able to predict corrosion currents in un-cracked concrete samples exposed to chloride ingress. The model combines corrosion initiation and propagation stage.
- The Zn-Al- NO_2 used in this work exhibits a maximum chloride loading of ~ 45 mg of

Cl⁻ per gram of LDH at neutral pH. The ion sequestration process is almost instant and takes only a few seconds to achieve equilibrium. It is also stable at this pH. However, the uptake of Cl⁻ ions by Zn-Al-NO₂ is pH sensitive i.e. as pH increases, the Cl⁻ uptake decreases. There is no significant chloride sequestration above pH 12.5.

- For Zn-Al-NO₂ the selectivity series can be written as NO₃⁻ < NO₂⁻ < Cl⁻ < OH⁻. The ion sequestration is also sensitive to the concentration of anion. A higher concentration of an anion can dominate the sequestration over another anion that is preferable according to the selectivity series.
- LDH can undergo partial dissolution at pH ~ > 12.5. Dissolution influences the ion entrapping capacity of LDH. Moreover, the dissolution process in concrete can release Zn²⁺ ions in the surrounding pore solution. This considerably delays the hydration processes in cementitious matrix.
- Furthermore, based on the investigation in this work and the reviewed literature, a 2% dosage of LDH is used in this work and recommended for use in concrete. However, incorporation of Mg-Al-NO₂ particles resulted in a slight acceleration in the hydration processes. This suggests an early reaction of Mg-Al-NO₂ during the hydration phase.
- The moderate gain in chloride ingress is attributed to the formation of additional AFm in concrete. The partial dissolution of Mg-Al-NO₂ can contribute to the formation of AFm in concrete. The degree of dissolution is not known but it is concluded that dissolution of Mg-Al-NO₂ in concrete can certainly be one of the factors towards its inefficiency in concrete. The part of Mg-Al-NO₂ that stays intact (without dissolution) might be preferable towards OH⁻ instead of Cl⁻ ions. A combination of these factors contributes towards the reduced efficiency of Mg-Al-NO₂ in concrete.

It must be stated that the particle size of LDH is a very important parameter and can influence many properties of concrete. The relationship of particle size with degree of dissolution in pH range > 12 certainly demands more investigation. Although it is well understood that aluminium ions from LDH contribute towards AFm formation, more studies are necessary to fully understand this process. In the present work, the presence of AFm is qualitatively known but the amount AFm itself is not known. Subsequently, the relation of dosage of LDH with the amount of AFm that is additionally generated should also be investigated. Saturation limit of LDH should be investigated as well in a multi-ion exposure scenario. A potential release of captured Cl⁻ in the event of carbonation is a very crucial point and also needs more research. Cost consideration of LDH is a vital factor as construction sector is very cost competitive. All these investigations, although highly important and interesting, could not be initiated in the course of this work due to the time limitations.

7. Outlook on multiscale modelling

7.1. Article 5 - Interoperability architecture for bridging computational tools: application to steel corrosion in concrete

Note: See attached article in the next pages. Reprinted without modification from [83] under CC BY 3.0 license. Published by IOP Publishing Ltd, UK.

7.1.1. A brief summary of Article 5



The field of computational science has quickly and keenly adopted the use of multiscale modelling approaches in order to understand applications and problems of interest at different resolutions. The entire process aims at obtaining a deeper level of understanding regarding the governing laws and effects, as well as material behaviour and associated phenomena at various scales, usually ranging from electronic level to macro scale level [84]. Each modelling scale uses different types of computational tools, which in turn rely on various formats ranging from custom closed formats to easily adaptable open standard formats [83]. Quantities of interest are usually up-scaled and transferred across scales. The arrangement could be simply linked or fully coupled depending on the nature of the problem at hand and the architecture of the multiscale modelling approach.

In recent times, there has been a rapid increase in computational power which has resulted in very fast and efficient solvers that are capable of performing large computations on big data sets. However, least attention has been paid in facilitating data exchange between different solvers at different modelling scales. This paper presents an approach of ontology based data classification and data transfer. The paper also highlights the use and application of an intermittent software tool SOFT (SINTEF open framework and tools) which can assist in establishing data handling architecture across heterogeneous software and modelling scales. The tool employs use of meta data structures.

7.1.2. Author contribution

In the following, the author of this dissertation is denoted by his initials ZMM. The names and initials of co-authors can be found in the appended manuscript. ZMM, JF, and DH proposed the main concept behind this work. ZMM and JF worked on the software application, debugging and associated data transfer. ZMM, JF, TFH, IHS, IGR, NK, and DH co-wrote the manuscript. JF, MLZ and DH supervised the work and gave critical comments. All authors read and reviewed the manuscript.

Interoperability architecture for bridging computational tools: application to steel corrosion in concrete

Zahid M Mir^{1,5} , Jesper Friis², Thomas F Hagelien³,
Ingeborg-Helene Svenum², Inga G Ringdalen² ,
Natalia Konchakova¹, Mikhail L Zheludkevich¹ and
Daniel Höche^{1,4}

¹ Institute of Materials Research, Helmholtz-Zentrum Geesthacht, Max-Planck Str. 1, D-21502 Geesthacht, Germany

² SINTEF Industry, NO-7465 Trondheim, Norway

³ SINTEF Ocean, NO-7465 Trondheim, Norway

⁴ Computational Material Design, Helmut-Schmidt-University, D-22043 Hamburg, Germany

E-mail: zahid.mir@hzg.de, jesper.friis@sintef.no, thomas.f.hagelien@sintef.no, ingeborg-helene.svenum@sintef.no, inga.ringdalen@sintef.no, natalia.konchakova@hzg.de, mikhail.zheludkevich@hzg.de, daniel.hoeche@hzg.de and hoeched@hsu-hh.de

Received 12 June 2019, revised 21 November 2019

Accepted for publication 16 December 2019

Published 15 January 2020



CrossMark

Abstract

A multiscale modelling framework, especially for corrosion modelling, requires not only robust computational tools but also an efficient datacentric architecture for handling information exchange at different modelling scales. Different computational solvers require and produce data in different programming languages and specific formats signifying a strong non-uniformity for an easy nexus with other solvers. This non-uniformity has created a need to focus on intermittent state-of-the-art datacentric software tools which aim to bridge data exchange heterogeneity across diverse set of solvers. Data organization in the form of metadata structures are presented as a standard for a coherent information representation regardless of the diverse nature of data formats specific to a scientific discipline. This fundamental work presents the

⁵ Author to whom any correspondence should be addressed.



Original content from this work may be used under the terms of the [Creative Commons Attribution 3.0 licence](https://creativecommons.org/licenses/by/3.0/). Any further distribution of this work must maintain attribution to the author(s) and the title of the work, journal citation and DOI.

concept, underlying terminology and working mechanism of a datacentric architecture tool SOFT5 for exchanging and interfacing data-flow between solvers and its present application to a concrete technology multiscale simulation network as a potential application.

Keywords: multiscale framework, data science, datacentric platform, data inter-exchange, metadata structures, semantic interoperability, JSON

(Some figures may appear in colour only in the online journal)

1. Introduction

The recent decades in the modelling science have been marked with an unprecedented growth in the computational power. This fact has been further complemented with a sharp shift towards multiscale approaches regarding a particular domain problem. As such, multiscale scientific programs have gained pace in the recent years across all branches of science. A multiscale approach involves understanding of a particular problem usually stretching across multiple modelling scales ranging from electronic-atomic level to macro-structure level. Such simulation strategies involve use of multiple software and solvers with the general aim of approaching the same problem at different levels of understanding (nanoscale to macroscale).

Each modelling scale in time and space is usually associated with at least one computational solver often forming an overall pipeline structure across all scales. At each scale, data is extracted and exchanged. Thus, these solvers are associated with handling and processing of enormous amounts of data from different sources and in varying formats. As an example, the process simulator in a chemical manufacturing plant would typically involve exchange of data ranging across varying time and spatial domains. An extension of such a flow simulator structure by incorporating additional sub-modules and facilitating coherent data exchange in the modified structure via a generic datacentric platform would be a very efficient approach. However, least attention is usually paid in terms of data science, which is essential in bridging computational tools employed at different levels of modelling.

Classifying data is a basic strategy for data exchange. Usually data originates from various different sources such as open or propriety based software and in various formats from closed-custom formats to commonly used open standard formats. Moreover, data is usually incomplete in its understanding such as it lacks supporting data ‘metadata’ such as units, data type, description of data and source, making it difficult for other computational models to interpret the data. Therefore, classification of data on a semantic level forms the starting point of data interoperability.

The conceptual use of metadata has been traced back to around 280 BC at the Great Library of Alexandria wherein library contents were tagged to provide information about the author, title and the subject to which the literature belonged [1]. This served in sorting and cataloguing the library contents and helped in directing the users to the books they wanted to read instead of opening and going through all the books. The benefits of using metadata later helped in creating more detailed system of cataloguing in the libraries, such as the dewy decimal system, which has been recently replaced by modern digital database cataloguing systems. Thus, metadata has been used in many different fields i.e. from organizing libraries to listing contents on a compact disc. The purpose of such representation is to provide information about a system, without itself being a part of it, but complementing it to complete its meaning or function. As an example, Standard Book Numbering was created in 1966,

which was a 9-digit entity to identify a book [2]. It would give information about a book without itself being a part of the book content. This was later changed to 13-digit entity and is referred to as International Standard Book Number (ISBN). ISBN is a metadata attached to book and contains all the necessary information about the book such as registration country, publisher details as well as the title.

In the last few decades, the continuous evolution of numerical technology has resulted in a huge number of versatile stand-alone computational tools. As such, bridging these numerical tools has become cumbersome and therefore more attention is required to connect these systems using machine interpretable syntactic tools. Data sharing between computational solvers should resort to some agreeable formats and standard content sharing definitions. In this regard, well-established standards such as ISO/IEC 11179 covers all aspects of data sharing in information technology. The standard focuses on entire spectrum of data science such as data classification, relationships, formulations, nomenclature and identification principles and many other aspects of metadata based data science.

Although the field of information technology has since long time resorted to standardization mostly in terms of programming language aspects, it has experienced a significant shift towards use of metadata standards. This had made it quite easier to associate correct description and uniform treatment of data during interoperability operations.

Non-standardization usage of metadata can lead to severe failures as there is a big chance of incorrect or misinterpretation of data associated to metadata. One of the most famous examples is the failure of NASA Mars Climate Orbiter in the year 1999 [3]. It occurred due to misinterpretation of data between two technical teams, one of which assumed data values in SI units and the other in metric units. The result was a disastrous accident and a complete loss of the orbiter. It is important to emphasize that, although the exact and correct value was transferred across the two teams, the interpretation of the quantity itself was different i.e. metadata was not part of the data transfer. Manual interpretation of data should be avoided as far as possible and machine-readable metadata should always accompany data for smooth and secure interoperable operations.

This paper presents an approach towards development of a data handling framework for multiscale simulation programs using SOFT5 tool and develop a strategy of coupling heterogeneous syntactic model data using concept of metadata structures. The entire framework is based on data abstraction at multiple levels as illustrated in figure 1. At the concrete level we have the actual data that is formalized into a representation which can be completely described by the metadata. The metadata itself is described by the metadata schema, which in turn is described by the *basic metadata schema*. The basic metadata schema is capable to describe itself, breaking the sequence of higher and higher levels of abstraction. Additional levels of abstraction are possible, but seldom needed in practice. This hierarchy of abstractions opens possibilities for cross-domain interoperability both between domains using different metadata systems and between different physical domains using SOFT5 for metadata representation. Figure 1 shows the latter case. An example of this is the entity representation of diffusivity at the atomic scale that maps to a different entity describing diffusivity at the microscale level. The basic metadata schema can describe the metadata schemata for each domain that describe the domain-specific metadata. To achieve interoperability between two domains, one still has to implement concrete mappings, but the mappings can be implemented at different levels of abstraction. That both domains has a common root, the basic metadata schema, ensures that it is possible to do the mappings.

This makes it easy and convenient to accomplish data handling and data transfer without losing its meaningful value. Relationships between data can then be formed and a structured multiscale workflow can be established where different modelling software and solvers can be

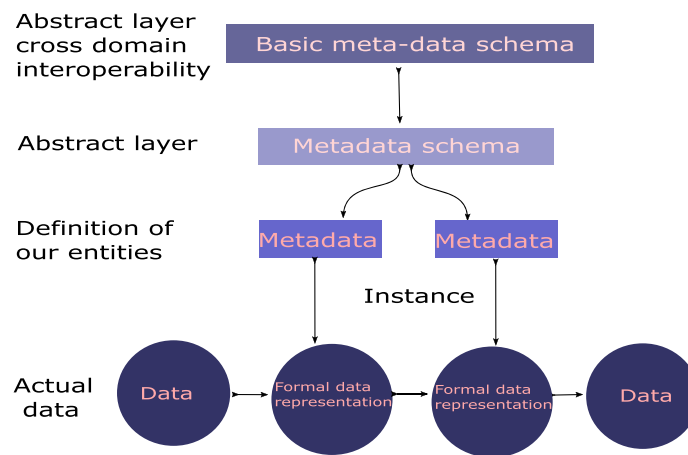


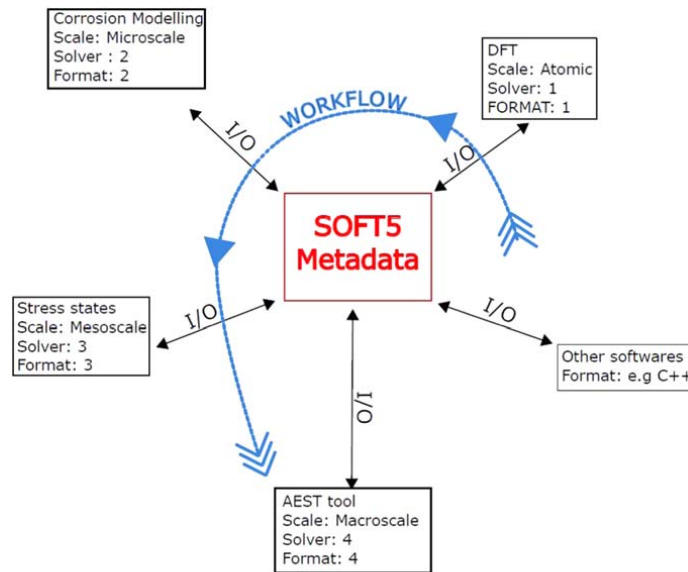
Figure 1. Cross-domain interoperability by metadata, metadata schemata and the basic metadata schema.

connected. Such a framework helps in an easy recognition of domain specific simulation data as well as helps in maintaining trace-ability and version control over it. This results in easier categorization of different domain specific data and facilitates fast development of the entire simulation framework.

This paper refers to the modelling framework and methodology adopted in the LORCENIS project [4]. The LORCENIS project focuses on developing specialized concrete recipes with the aim of extending life and imparting additional functionality benefits to energy infrastructure exposed to severe operating conditions. The scales of investigation vary from electronic level and up to macro level. SOFT5 tools has been partially applied for bridging the heterogeneity of different modelling software to facilitate a robust and easy to setup data-centric architecture to handle data flow across the scales. Figure 2 shows the state-of-the-art multiscale materials modelling (M3) framework, that is under development in the LORCENIS project [4], for accurate prediction of service life of structures exposed to corrosive marine environment. This paper presents the direct application of metadata structure and interoperability technology used in the M3 LORCENIS framework.

The modelling architecture is divided into four distinct modelling scales (one discrete and three continuum) ranging from electronic/atomistic level, microscale, mesoscale and eventually to a macroscale level with engineering purpose at the top of modelling chain. A distinct modelling task is assigned to each modelling scale. Furthermore, as illustrated in figure 2, each modelling scale is employing a different computational solver to achieve its modelling goals.

To achieve this task, an efficient data-handling scheme is required to handle the coupling arrangement of these different solvers (open source and propriety based) in order to achieve a smooth compatibility between them. This broad multiscale simulation strategy paves a necessity for a robust state-of-the-art modelling infrastructure. As such, SOFT5 tool has been adopted inside this modelling framework to serve as an interface for data handling between scales. Data sharing aspects are highlighted in this paper, as well as scale based metadata structures, and the working principle are presented. The paper highlights the actual working sequence of SOFT5 inside the various modelling scales along with corresponding programmable metadata structures. The coupling features presented in this study involve data



A graphical explanation of Incorporation and working action of SOFT5 into LORCENIS.

Figure 2. Overall structure of the M3 LORCENIS framework. Picture credits [4].

linking aspects of electronic (discrete) model with microscale (continuum) model as part of framework testing and presenting a proof of concept.

Additionally, a significant point of multiscale modelling concepts is the interoperability between the software used for the computation at difference scales. Usually, different scientific or industrial communities participate in the development of software in order to solve complex materials modelling problems. Thereby they have established different terminologies. The developed modelling codes focus typically on specific application domains and on particular types of models. A general issue is evolving, wherein the different software codes owning specific terminologies of software owners, academic model developers and end-users (SMEs or big companies) for the definition of the same computational problems, but using a different vocabulary. Hence, there is a strong need for standardization. One effort in this direction has been taken by the European Materials Modelling Council (EMMC), who has published CEN Workshop Agreement on modelling terminology, classification and metadata for materials modelling [5]. The document is publicly available as a reference document from the National Members of CEN.

A standardized description of multiscale scientific problems using a uniform vocabulary referred to as materials modelling data table (MODA) [6] is used as key approach to develop and establish successful software interoperability. MODA is an effective instrument for documentation of simulations and understanding of modelling approaches, general project structure as well as the model interaction within workflows. It has established now as a growing industrial and academic standard for computational problems. It is a required tool for the preparation of European research and innovation projects, joint research activity for different modelling scales and application areas.

The use of ontology based organization of scientific data has emerged to be quickly adaptable by many scientific branches such as biomedicine [7] molecular material design and selection [8]. Ontology based data assures interoperability to be easily accessible by users as such mappings and extensions are easily to create on existing data sets. As an example,

existing ontology based frameworks include CAPE-OPEN standard [9] which sets standards for computer aided process engineering applications to interoperate. Similarly, Gene Ontology Consortium [10] maintains a comprehensive organization of huge amount of molecular biology experiments.

Ashino [11] has provided a very basic detail of ontology based representation of data. Similarly other works focusing on standardization of data and associated ontology include this [12]. Furthermore a comprehensive take on scientific breakthrough via studying massive data-sets has been provided by Hey *et al* [13]. A basic understanding of technical data is provided by Peter Murray Rust [14]. Cheung [15], Hunt *et al* [16] have identified data science field to be an important asset for the scientific community.

2. Interoperability, metadata and workflow technology

2.1. Interoperability

Interoperability, coupling and linking are latest terminologies in the computational materials modelling community. It is a consequence of the rapid development of numerical software during the last decade with a majority arising from the academic community. The rapidly growing community and the capabilities of computational approaches have thus lead to a wide spectra of models and methods. Software belonging to different domains has been developed independent of each other. Making them communicate is very challenging, since they are based on different concepts and uses different vocabularies. Thus, dedicated tools are required which are feasible to handle different data and data formats. Information exchange which allows software to share data during any kind of simulation step in a efficient way, also requires mature semantic interoperability frameworks and tools [17]. The paradigm change relates to the fact that not information on file formats or protocols are exchanged, but the software systems itself shares relevant information by using a standard semantic framework as a mediator. This framework belongs to an overarching ontology capable to handle all relevant data schemes and metadata respectively. This field of data science is relatively new and often undiscovered respectively and its impact underestimated. Currently, no shared standards for such frameworks exist, but research and funding schemes addressing this issue have been initiated.

2.2. Metadata definitions and concepts

According to the latest guidelines RoMM 6 [6] and [5] from the EMMC⁶, metadata is defined as ‘metadata are data that describe and give information about other data’. In other words it is a vocabulary tool for expressing data in a generic way and attaching more information to it for its easier handling [18, 19]. For a particular multiscale modelling scenario, data that is to be exchanged needs to be described completely. This forms the basis of interoperability and data exchange. Metadata structures help in formal description of exchangeable data in a generic sense.

To cite a good example, the field of image-based analysis relies heavily on metadata exchange when images are transferred from one software to another. Here, the EXIF-info attached to the digital images contains information about the image such as name, pixel size, GPS coordinates, image resolution, creation time, date and source. This additional information about the image is nothing but metadata information about the image. Without this

⁶ See <https://emmc.info/>.

metadata, another user who is not the default user of the image would not be able to perform image based analysis as there will be no information on the pixel size and resolution of the image. Hence, quantification of features on the image will be practically impossible to achieve and as such interoperability would be lost. Another example of commonly used metadata is the Digital Object Identifier which acts as a digital identity tag for any digital entity.

With these enhanced data conditioning properties, metadata structures find their broad application across all field of science.

2.3. MODA format for computational problem description

MODA refers to a standardized and concise representation of a simulation problem and the underlying process. With MODA as a standardized terminology, an easier and efficient exchange of a computational methodology could be achieved among users of material modelling codes such as academicians, industrial end-users and experimentalists. MODA therefore facilitates understanding of models by any interested user. MODA tables report on the structure of a simulation and on the relationship between the different model in a workflow.

MODA has the following structure:

- Heading, including name of the user case, project, owner.
- Overview of the simulation, including the chain of models used.
- Workflow, i.e. a graphical representation of the simulation.
- Description of each part of the simulation pertaining to each model used in the chain.

Each MODA should report on these mentioned aspects. A graphical representation of the workflow is also accompanied with MODA and helps in a faster understanding of the workflow path. For a deeper understanding of MODA, the reader is referred to [6]. An user-case example employing MODA is presented later.

2.4. SOFT

SOFT is an acronym for SINTEF Open Framework and Tools. SOFT5 is a set of open source libraries and tools to support scientific software development. The development of SOFT5 was motivated by many years of experience with developing scientific software, where it was observed that a lot of effort went into developing parts that had little to do with the domain. A significant part of the development process was spent on different software engineering tasks, such as code design, the handling of I/O, correct memory handling of the program state and writing import and export filters in order to use data from different sources. In addition, comes the code maintenance with support of legacy formats and the introduction of new features and changes to internal data state in the scientific software. With SOFT5, it is possible to utilize reusable software components that handle all this, or develop new reusable software components that can be used by others in the same framework.

The main components of SOFT5 is shown in figure 3. The key modules are the tools, storage support and plugin framework. The key tools are the scripting utility and the code generator.

SOFT5 contains a core library with plugin support. The library also comes with an application programming interface to create extensions and custom plugins. The core library is used to connect a software application with the framework.

The main approach to developing software with SOFT5 is to incrementally describe the domain of the software using entities (see below). The entities can represent different

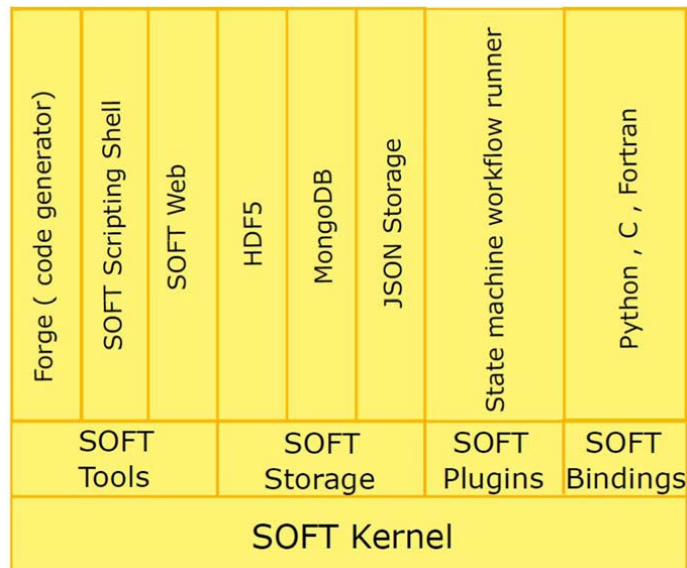


Figure 3. The main components in the SOFT5 platform.

independent elements of the software, and be used in handling I/O as well as in code generation and documentation. Entities can also be used for annotating data and data sets. This might be useful in cases where for instance the origin of the data, license and ownership are of importance.

Since any complex software will have many entities and often multiple instances of the same entity, SOFT5 allows for creating collections of instances with defined relationships between them. These entity collections are called ‘collections’ (see below).

An approach of SOFT5 is that software may be written in such a way that business logic is handled by the codebase, while I/O, file-formats, version handling, data import/export and interoperability can be handled by reusable components in the SOFT5-framework, thus reducing risk and development time.

2.4.1. Entities. An entity can be a single thing or object that represents something physical or nonphysical, concretely or abstract. The entity contains information about the data that constitutes the state of thing it describes. The entity does not contain the actual data, but describes what the different data fields are, in terms of name, data types, units, dimensionality etc. It can be described as formalised metadata that enables for the correct interpretation of a set of data. Hence the entities should be made available together with the software or application in which they are used.

An example of an entity is ‘atom’, which can be defined as something that has a position, an atomic number (which characterizes the chemical element), mass, charge, etc. Another example of a completely different kind of entity can be a data reference-entity with properties such as name, description, license, access-url, media-type, format, etc. The first entity is suitable as an object in a simulation code, while the latter is more suitable for a data catalogue distribution description (see *dcats:Distribution*)⁷. Entities allow now to describe dedicated

⁷ DCAT: Data Catalogue Vocabulary.

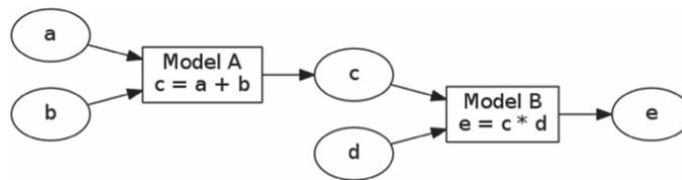


Figure 4. A very simple workflow that connects the output of model A to the input of model B.

aspects of the domain. While each entity describes a single unit of information, a collection of entities can describe the complete domain (check collections below).

Each published entity needs to be uniquely identified in order to avoid confusion. The entity identifier has therefore three separate elements: a name, a namespace and a version number. An entity named ‘particle’ is unlikely to have the same meaning and the set of parameters across all domains. In particle physics, the entity ‘particle’ would constitute matter and charge, while in other fields the term ‘particle’ can be a general term to describe something small. For this reason the SOFT5 entities have namespaces, similar to how vocabularies are defined in OWL⁸. The version number is a pragmatic solution to handle how properties of an entity might evolve during the development process. In order to handle different versions of a software, the entity version number can be used to identify the necessary transformation between two data sets.

2.4.2. Collections. A collection is a container whose instances holds references to a set of entity (or collection) instances and relations between them. Relations are triplets of the form (subject, predicate, object), where subject and object both labels an instance and predicate describes a relation between the subject and object, like ‘child-of’, ‘connected-to’, ‘reactant-of’, etc. This is much more general than hierarchical structures and allow to represent the knowledge of the domain where the data exists. Hence, a collection could also have been called a *context*. It also opens possibilities like deductive databases.

Collections are useful to represent the knowledge of the domain, to find data that relates to other data or to uniquely identify a complete data set with a single identifier.

2.4.3. Storage. A *storage* is a module that can transfer a given state to an external medium (file or database). It is an important abstraction in SOFT5 which allows to transparently handle input to or output from modelling software. This is realised via a plugin-system of drivers (or backends) that translate to and from the external formats. A storage backend may either be generic or specific. A specific storage backend is tied to a given entity and could e.g. read experimental data from a specific instrument into an instance of the entity or write an instance of the entity to file using a specific format expected by a third party software. SOFT has three generic built-in storages, HDF5, JSON and the MongoDB database, that can read or write instances of any entity [20–22]. Furthermore SOFT5 allows the user to write dedicated plugins for a given entity, typically for reading or writing data from or to a specific file format.

2.5. Workflow technology

We will use the very simple example of a workflow shown in figure 4 to illustrate the basic concepts. We have two models A and B, where the output of A is used as input to B. Circles

⁸ OWL—Web Ontology Language.

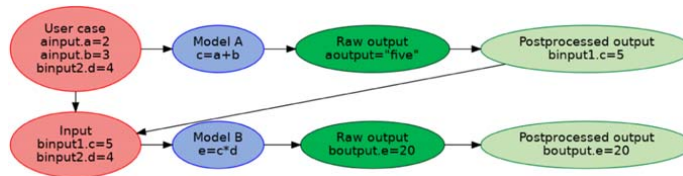


Figure 5. The same workflow as in figure 4 using the MODA template. The translation of the output of model A to the representation expected by model B is performed in postprocessing of the raw output from model A.

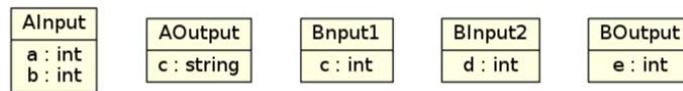


Figure 6. Entities used in this workflow.

represent *physical system state* and boxes *transitions* between different snapshots of the physical system state.

A typical challenge in setting up workflows in real life, is that the output from model A is not represented in the way expected by model B. But, if the output of model A is semantically equivalent to the input needed by model B, it is possible to translate (postprocess) the output of A to the form expected by B and hence establish a robust workflow. Such a case is shown in figure 5, where Model A returns its results as a string ‘five’ while model B expects a number.

2.5.1. Workflow implementation using SOFT5. To implement this workflow as depicted above, we proceed towards defining the entities as shown in figure 6. The initial state is described by instances of *AInput* and *BInput2* and the final result will be given as an instance of *BOutput*.

A typical and easier way to handle data flow in SOFT, is to let all data flow between models and the system flow via a central storage. A centralized storage not only helps in maintaining an overview of the different tasks, but also allow for easy data backup and version control. To keep track of the instances created for each invocation of the workflow, we create a collection specific to each invocation, in which we store references to all instances belonging to this invocation. The workflow can then be broken down into a set of tasks exposing the same interface. Each task is simply provided a reference to the storage and the collection for the current invocation of the workflow.

Running the workflow involves the following steps:

1. *Initialization:* Create the collection, populate it with new instances for the initial state defined by the user case and store everything in the storage.

2. *Run Model A:* This model is implemented as an external program taking the name of a file containing the two integers to be added as the only argument. The result is written to standard output. In order to integrate model A in our workflow we create a wrapper function that performs the following steps:

1. *Pre-process:* Fetch *AInput* and serialize it to a temporary file in the format expected by model A.
2. *Compute:* Execute Model A with the name of the temporary file provided on the command line.

3. *Post-process*: Creates an instance of entity AOutput, populate it with the result of Model A and push it to the common storage. Latter also removes the temporary file.

3. *Run Model B*: This model is implemented as an external program that uses SOFT. As arguments, it takes references to the storage and the Collection. When called it asks for BInput2 and AOutput, the latter as represented as an instance of BInput1. SOFT will then check if it can find an Translator that can translate an instance of AOutput to an instance of BInput1. When this Translator is found, it is applied. This will create BInput1 from AOutput. The new instance is then handed to model B. Model B then creates an instance of BOutput populated with the product and stores it in the storage.

3. Applying workflow on advanced concrete technology. Bridging density functional theory (DFT) to a continuum corrosion model (CCM) via SOFT5

The above mentioned methodology is applied to the DFT output transfer to a microscale CCM embedded in a multi-scale model consisting of 4 different modelling scales. The aim of this modelling chain is to predict accurately the service life limitation due to chloride ingress of reinforced concrete structures exposed to submerged marine environment. The task consists of bridging four different scales as shown in figure 2. Each scale communicates data with each other. The paper here focuses on data transfer between the first two scales i.e. atomistic/electronic scale to CCM at microscale via SOFT5.

3.1. M3 framework on service life prediction of concrete structures

The proposed workflow involves calculating and up-scaling entities of interest at the atomic/electronic level and their transfer via SOFT5 to the continuum based micro-scale model (CCM). A brief description of the concept and the underlying models is presented.

The atomistic model in this case deals with the flow of corrosion inducing species i.e. chloride ions through a representative cement matrix composed of tobermorite.

The flow of chloride ions through the calcium silicate hydrate (CSH) matrix is considered to be the rate determining step for chloride ingress in cement. The flow through the pore network is CSH will occur as a significantly faster rate than through CSH itself given a non-continuous pore network. Further, the swelling of CSH is also an up-scaling input parameter required by the CCM. The binding of chloride to the cement paste is a well known phenomena and its greatly attributed for extending the time to corrosion initiation as it slows down the transport of chloride ions. The hydration of cement leads to the formation of CSH as a major volumetric phase among many others. CSH is responsible for the majority of chloride binding in concrete [23].

The structure and volume correlations of CSH depending on water content in addition to the interaction of Cl in CSH are investigated from first principles, and is presented in Svenum *et al* [24]. The calculations are performed using the DFT calculations at the PBE-GGA level [25] using the Vienna *ab-initio* simulation package (VASP) [26, 27]. The model takes as input an approximate atomic structure found by manipulating the theoretical model of tobermorite to a correct Ca/Si ratio with the desired water content. The structure and volume of the model is then minimized, and the minimum energy, volume and atomic positions are the output from the simulations. To investigate the chloride diffusion, transition state theory calculations using nudge elastic band is performed [28]. The input for these calculations are the minimized start and end atomic structures. The energy barrier to go from the start structure to the end structure is calculated, in addition to the reaction coordinate. The diffusivity

coefficient can be calculated from the energy barriers to move an atom through the periodic cell by

$$D = D_0 \exp\left(-\frac{E_a}{k_B T}\right), \quad (1)$$

where D_0 is the pre-exponential factor, E_a is the activation barrier for diffusion, k_B is the Boltzmann constant and T is the temperature. The pre-exponential factor D_0 can be obtained either by transition state theory [29], or found experimentally [30]. The diffusion should be equal in all directions within the interlayer, while it can be assumed to be zero between the interlayers. This results in a diffusion of D in two directions and 0 in one. Since the microstructure is not considered explicitly in this framework, a simple averaging is performed and the diffusion tensor is estimated to be $D_{ii} = 2/3D$.

On the other hand, the CCM model is a FEM based model implemented in COMSOL multiphysics software which models flow of free chlorides in the pore network and also accounts for bound chlorides in the mass balance. Corrosion processes occurring due to chloride induced breakdown of passive film (native oxide layer) [31, 32] are also considered.

Nernst–Planck equation is used to model transport of chloride ions inside concrete (equation (2)) which is exposed to 3% NaCl. Here Cl represents the concentration of free chloride ions inside the pore network, ϕ_p represents the average concrete porosity, D_{eff} represents the effective diffusion coefficient for flow of Cl in pore network, z_i is the valency number, F represents Faraday constant, R is the ideal gas constant, T is the absolute temperature and φ_{el} is the electric potential. $\frac{\partial \text{Cl}_b}{\partial t}$ represents the rate of bound chlorides Cl_b acting as a sink term in the mass balance (equation (2)). A distribution of electric potential is obtained from Laplace equation (equation (3)) and consequently corrosion currents can be derived, as presented in [33, 34].

$$\phi_p \frac{\partial \text{Cl}}{\partial t} = -\nabla \cdot \left[-D_{\text{eff}} \left(\nabla \text{Cl} + \text{Cl} \frac{z_i F}{RT} \nabla \varphi_{\text{el}} \right) \right] - \frac{\partial \text{Cl}_b}{\partial t} \quad (2)$$

$$\nabla^2 \varphi_{\text{el}} = 0. \quad (3)$$

The rate of chloride binding $\frac{\partial \text{Cl}_b}{\partial t}$ can be related to the diffusivity of Cl ion in the CSH derived from electronic scale model which tends to be a very slow process, wherein CSH entraps Cl ion [24]. Data verification, validation as well as physical relevance of up-scaling of data between scales is an on-going process at this stage. To get a more accurate estimate of the diffusion coefficient in the future, it will be necessary to add a scale which take the microstructure of CSH into account. The framework is well suited to adding this extension.

3.2. Data storage and transfer

The presented workflow is shown in figure 7 and focuses on the data handing between Electronic scale model and the CCM. The Electronic scale model starts with an appropriate atomistic structure of Tobermorite with different calcium to silica ratios as well as different water to Silica ratio. This forms the basic inputs of the Electronic scale model. This model used DFT for performing calculations related to favourable positions of chloride binding and associated diffusion energy of the chloride ion inside the tobermorite matrix.

The computed outputs details on the swelling of the matrix as well as density change of the cementitious matrix. Furthermore atom fraction of water, diffusion corrections for chloride-ion transport and corresponding activation energies are also computed. These listed inputs are directly used as inputs in other models along the modelling chain.

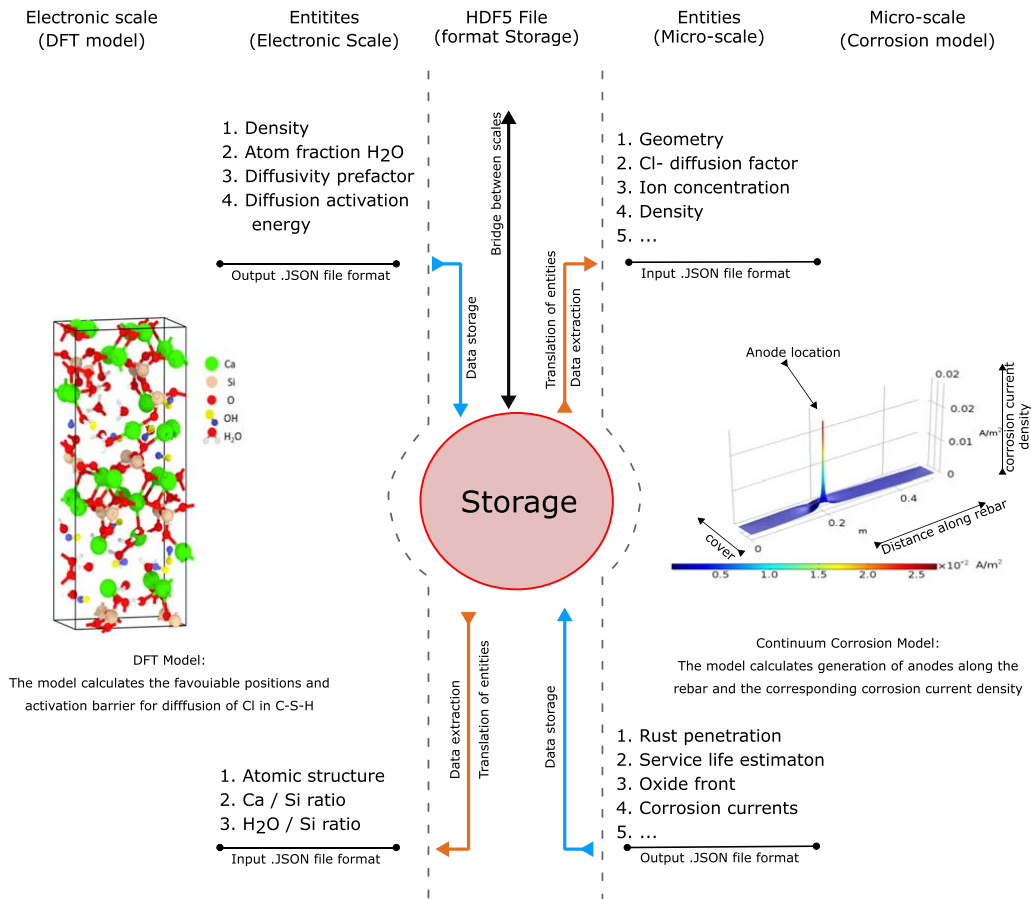


Figure 7. Workflow and data transfer entities between DFT model and continuum corrosion model. The output from .JSON (such as rust penetration, corrosion currents etc in CCM) can be derived from material relations on data in each model.

The CCM can therefore rely on information related to chloride-ion diffusivity and chloride ion binding from the Electronic model in the proposed framework. Together with the geometry of the structural member and other related input factors, the CCM calculates the rust penetration on the rebar surface. The oxide front is calculated likewise as a consequence of corrosion currents and an estimation can be drawn on the service life of the concrete structure.

The input/output of data and entities for each respective model is handled using .json files representing the entities and associated metadata. The listing below shows the entity describing the input to the micro-scale corrosion model.

```
{
  "name": "Ion",
  "version": "0.1",
  "namespace": "https://powerfolder.hzg.de/Lorcenis/meta",
  "description": "Input to micro-scale corrosion model."
  "dimensions": [
    {
      "name": "ncoords",
      "description": "Number of spatial coordinates"
    }
  ]
}
```

```

    }
  ],
  "properties": [
    {
      "name": "ion_diffusion",
      "type": "double",
      "dims": ["ncoords", "ncoords"],
      "unit": "m2/s",
      "description": "Diffusion tensor for ions."
    },
    {
      "name": "concentration",
      "type": "double",
      "unit": "mol/m3",
      "description": "Ion concentration in bulk."
    },
    {
      "name": "density",
      "type": "double",
      "unit": "kg/m3",
      "description": "Bulk density."
    },
    {
      "name": "geometry",
      "type": "double",
      "dims": ["nnodes", "ncoords"],
      "unit": "cm",
      "description": "Coordinate"
    }
  ]
}

```

The name, version and namespace identifies the entity uniquely. The descriptions are meant to be read by humans. One dimension is defined, the number of spatial coordinates in the diffusion tensor (which is always 3). The properties that follows, describes the data records that we want to transfer. Separate instances of four entities are shown in figure 7.

3.3. Application

The above mentioned simulation framework employing SOFT5 shows the workflow of the simulation action and data exchange within the multiscale corrosion modelling framework between the DFT model and the CCM as depicted in figure 7. The atomic supercell represents a typical cement paste CSH structure containing defined arrangement of relevant ions close to the concrete reinforcement. The model allows to calculate relevant entities based on dedicated model input (from the literature) is introduced as well. All data is stored (thereby belonging to a semantic ontology) and accessible for the microscale model. DFT related data is applied as (translated to) model input. In the next step entities like rust penetration changes can be computed within a set of nonlinear PDE's by finite elements and stored back.

4. Discussion

4.1. Data science

The aim of this work is to demonstrate how interoperability between two software, VASP and a user-defined model in COMSOL Multiphysics, that belongs to two completely different domains can be achieved. For this purpose the SOFT framework was used, which is a framework for describing data in a concise and interoperable way. SOFT is not a semantic framework in the sense that it is tied to an ontology for a specific domain. Instead SOFT allows to represent the knowledge and data of any ontology (via collections). In this sense SOFT can be compared to tools like web ontology language (OWL), but is much closer linked to actual software code. The metadata model in SOFT is by design as simple and minimal as possible, while still being complete enough to allow unambiguous data representation and communication as well as code generation.

The shown MODA template itself was developed by the materials modelling community based on gained experience, and works in that way as well, thereby considering pure modelling data but also transformation information. The red, green and light green nodes represent computational data directly related to the physical state of the system, while the blue nodes represent a transformation. In that way the template might be mature enough for extend unambiguous model description.

4.2. Technical limitations and modelling constraints

Modelling and simulation of corrosion process along the entire length and time scale, especially in concrete environment, is a highly demanding computational problem. Feature extraction from each simulation step thereby keeping accuracy and computational efforts at tolerant level is a huge challenge. Limitations are mainly related to modelling gaps. Data generated at lower scales cannot be used directly at higher scale, which belongs to scale-bridging issues of described physio-chemical entities. Due to the multispecies nature of the concrete environment and due to the fact that mixing rules cannot be applied straightforward. Calculations of e.g. density properties or diffusion activation energies are still limited to the single phases and predefined species concentration scenarios. Since even the next modelling scale requires tremendous homogenization action, lower scale information cannot be exchanged. A modelling approach for this is lacking or in other words data representing the scenario adequately at electronic level cannot be or better can be very limited transferred and reduced to data applicable in the microscale corrosion model (translation of entities in figure 7).

Another issue relates to the change of the DFT scenario if the system changes according to the microscale corrosion model. The duration of the time step within the transient corrosion model is limited by the fact that the system change due to microscale entities do not induce atomistic structural changes leading to the need of adaptive action within the DFT model. Within the shown example, such feedback is excluded. However, in terms of accuracy a feedback is strongly recommended. Realization is very demanding and not feasible considering computational costs.

Furthermore, regarding data transfer from a fine-scale model to a coarse-scale model, significant work using adaptive sampling approach in a multiscale framework has been carried out by Rouet-Leduc *et al* and Knap *et al* [35, 36]. In both of these works, data is communicated between fine scale and coarse scale models. Here as well, the transferred data may be described using SOFT5 entities as it can offer some advantage with respect to

usability and code maintenance. Specifically, for the fine scale results in Knap *et al* [36], SOFT5 entities may be useful to enable reuse of fine-scale results in other applications.

4.3. Future developments

The multiphysical nature of many of the engineering tasks demands interaction of multiple software and respective data structures covering a wide range of scales and related data. In order to achieve engineering relevance, or in other words reproducible prediction capabilities, the quality respectively complexity of modelling approaches should increase. Contrarily data reduction is requested and computational costs shall be minimized. Complimentary, uncertainty aspects should be considered. The occurring conflict requires balancing of all mentioned aspects which can be achieved by improved:

1. Model.
2. Coarse-graining.
3. Chloride bonding.
4. Uncertainty quantification and propagation.

While interoperability based on a common shared ontology has not been the scope of this paper, it is definitely something that we will see more of in the future (EMMC is for instance working on an ontology for materials science). However, the ideas and concepts discussed in this paper will most likely be very relevant in the future to, as a way to go from an ontological description of an domain to actual classes and data structures in a software model. One could e.g. imagine future tools that, given a user case formulated in the frame of an ontology, generates the involved SOFT entities. One can then use the code generator in SOFT to generate corresponding code (e.g. C++), such that the model developer only need to implement the transformations between these classes while leaving the rest to the framework.

5. Conclusions

Computational data entities which are expressed in a standard form using relevant application specific metadata structures has inter-operable characteristics. This data can be stored in a structured manner in a centralized storage. As such results, this leads to an easier development and management of complex simulation workflows.

Multiscale modelling approaches for concrete technology and related service life prediction demand huge methodical capabilities of software interaction. Thereby multiphysical tasks, data aspects, but also feature extraction define hard constraints for a modelling and simulation environment. For the shown example of a submodel interaction within a service-life prediction related framework for damage initiation due to chloride ingress, SOFT5 platform has shown to be a useful data science tool. Data Interaction at different scales for different computational methods (discrete versus continuum) was realized.

Interoperability between two models was achieved via a meta-data scheme implemented within the SOFT environment. DFT data output structure was reorganized in a way to enable interaction with the continuum simulation. Surprisingly, despite moderate efforts, the inhibition threshold to use the SOFT concept was not the limiting aspect. There was an issue to make people getting started to use the tool. It seems that the level of abstractions is hindering fast adaption of software like this.

Access to proper databases without any bandwidth limitations was found to be crucial for the concept realization since it is needed for concurrent read/write to the storage. This

limiting problem was solved in SOFT by the mongodb backend. Thus, wise definition of entities towards reduction of the amount of concurrent data transferred is highly recommended.

For future applications within highly complex coupled multiscale simulation frameworks interacting on different scales in time and space, a robust and mature metadata structure allowing the interaction of a variety of data formats is required. SOFT and its metadata abstraction enable this computational progress in materials modelling. Based on modelling data (MODA) schemes the transfer of modelling and simulation chains into a working data interaction environment is simplified. However lacking model and data input availability will still limit respective modelling frameworks. Experiments, accuracy studies and related post-processing will still remain an essential part of the working effort.

Acknowledgments

The authors wish to thank European Union's LORCENIS project, European Materials Modelling Council (EMMC) and SIGMA2 for computational resources. The authors acknowledge that part or parts of figure 7 have been taken from the publication 'Enhanced Predictive Modelling of Steel Corrosion in Concrete in Submerged Zone Based on a Dynamic Activation Approach' authored by Mir *et al* (2019) and published in International Journal of Concrete Structures and Materials. The content has been used with modifications solely for academic purpose under Creative Commons License 4.0 (<http://creativecommons.org/licenses/by/4.0/>).

Competing interests

The authors declare that they have no competing interests.

Authors' contributions

ZMM, JF, and DH proposed the main concept behind this work. This research is a part ZMM's Doctoral studies and parts of this work will be included in his PhD thesis. JF and TFH did the software implementation. ZMM and JF worked on the software application, debugging and associated data transfer. ZMM, JF, TFH, IHS, IGR, NK, and DH co-wrote the manuscript. JF, MLZ and DH supervised the work and gave critical comments. All authors read and reviewed the manuscript

Funding

This research has received funding from the European Union's Horizon 2020 research and innovation program under grant agreement No. 685445 (LORCENIS—Long Lasting Reinforced Concrete for Energy infrastructure under Severe Operating Conditions).

Author information

Authors qualifications, current positions, institution address and contact details are included on page 1.

Data availability

Some of the raw/processed data required to reproduce these findings cannot be shared at this time as the data also forms part of an ongoing study.

ORCID iDs

Zahid M Mir  <https://orcid.org/0000-0001-6488-1167>

Inga G Ringdalen  <https://orcid.org/0000-0001-9844-4352>

References

- [1] TIME Magazine USA 2019 The Genius Innovation That Made the Great Library of Alexandria Work <https://time.com/4730810/first-card-catalog/>
- [2] Foster G 1966 Technical report International Standard Book Numbering (ISBN)<https://web.archive.org/web/20110430024722/http://www.informaticsdevelopmentinstitute.net/isbn.html>
- [3] NASA 1999 Mars Climate Orbiter Failure Board Releases Report, Numerous Nasa Actions Underway in Response <https://mars.jpl.nasa.gov/msp98/news/mco991110.html>
- [4] LORCENIS 2019 Long Lasting Reinforced Concrete for Energy Infrastructure under Severe Operating Conditions <https://www.sintef.no/lorcenis>
- [5] CEN Workshop Agreement 2018 *Materials modelling - Terminology, classification and metadata* (CWA) 17284
- [6] de Bass A F 2017 *What makes a material function?*
- [7] Rubin D L *et al* 2006 National center for biomedical ontology: advancing biomedicine through structured organization of scientific knowledge *OMICS: J. Integr. Biol.* **12** 185–98
- [8] Ashino T and Fujita M 2006 Definition of web ontology for design-oriented material selection *Data Sci. J.* **5** 52–63
- [9] CAPE OPEN LABORATORIES NETWORK 2019 Computer-Aided Process Engineering <http://www.colan.org/>
- [10] Gene Ontology Consortium 2019 The Gene Ontology Project <http://geneontology.org/>
- [11] Ashino T 2010 Materials ontology: an infrastructure for exchanging materials information and knowledge *Data Sci. J.* **9** 54–61
- [12] Chalk S J 2016 SciData: a data model and ontology for semantic representation of scientific data *J. Cheminf.* **8** 54
- [13] Hey T, Tansley S and Tolle K 2009 *The Fourth Paradigm: Data-intensive Scientific Discovery* (Redmond, WA: Microsoft Research)
- [14] Rust P M 2010 PPI 0.1—What is Scientific Data? <https://blogs.ch.cam.ac.uk/pmr/2010/07/25/pp01-what-is-scientific-data/>
- [15] Cheung K, Drennan J and Hunter J 2008 Towards an ontology for data-driven discovery of new materials *AAAI Spring Symp.: Semantic Scientific Knowledge Integration* 9–14
- [16] Hunt W H Jr. 2006 Materials informatics: growing from the bio world *JOM* **58** 88
- [17] Ojo A, Janowski T and Estevez E 2009 Semantic interoperability architecture for electronic government *Proc. 10th Annual Int. Conf. on Digital Government Research: Social Networks: Making Connections between Citizens, Data and Government* (Digital Government Society of North America) pp 63–72
- [18] Schmitz G J, Böttger B, Apel M, Eiken J, Laschet G, Altenfeld R, Berger R, Boussinot G and Viardin A 2016 Towards a metadata scheme for the description of materials—the description of microstructures *Sci. Technol. Adv. Mater.* **17** 410–30
- [19] Hagelien T F, Chesnokov A and Johansen S T 2017 A framework for semantic interoperability of scientific software *12th Int. Conf. on CFD in Oil and Gas, Metallurgical and Process Industries (Trondheim, NORWAY)* (SINTEF) pp 317–30
- [20] 2017 Standard ECMA-404 The JSON Data Interchange Syntax <http://www.ecma-international.org/publications/files/ECMA-ST/ECMA-404.pdf>

- [21] The HDF Group 2000–2010 Hierarchical Data Format Version 5 <http://www.hdfgroup.org/HDF5>
- [22] Chodorow K 2013 *MongoDB: The Definitive Guide* (Sebastopol, CA: O'Reilly Media, Inc.)
- [23] Saetta A V, Scotta R V and Vitaliani R V 1993 Analysis of chloride diffusion into partially saturated concrete *Am. Concr. Inst.—Mater. J.* **90** 441–51
- [24] Svenum I-H et al 2020 Structure, hydration, and chloride ingress in C-S-H: Insight from DFT calculations *Cem. Concr. Res.* **129** 105965
- [25] Perdew J P, Burke K and Ernzerhof M 1996 Generalized gradient approximation made simple *Phys. Rev. Lett.* **77** 3865–8
- [26] Kresse G and Furthmüller J 1996 Efficient iterative schemes for *ab initio* total-energy calculations using a plane-wave basis set *Phys. Rev. B* **54** 11169–86
- [27] VASP 2018 The Vienna Ab initio Simulation Package (VASP) <https://www.vasp.at/about/>
- [28] Henkelman G, Uberuaga B P and Jónsson H 2000 A climbing image nudged elastic band method for finding saddle points and minimum energy paths *J. Chem. Phys.* **113** 9901–4
- [29] Løvrvik O M, Sagvolden E and Li Y J 2013 Prediction of solute diffusivity in al assisted by first-principles molecular dynamics *J. Phys.: Condens. Matter* **26** 025403
- [30] Lin S H 1993 Chloride diffusion in porous concrete under conditions of variable temperature *Wärme-und Stoffübertragung* **28** 411–5
- [31] Saremi M and Mahallati E 2002 A study on chloride-induced depassivation of mild steel in simulated concrete pore solution *Cem. Concr. Res.* **32** 1915–21
- [32] Ghods P, Isgor O B, McRae G A, Li J and Gu G P 2011 Microscopic investigation of mill scale and its proposed effect on the variability of chloride-induced depassivation of carbon steel rebar *Corros. Sci.* **53** 946–54
- [33] Ožbolt J, Balabanić G and Kušter M 2011 3d numerical modelling of steel corrosion in concrete structures *Corros. Sci.* **53** 4166–77
- [34] Höche D 2015 Simulation of corrosion product deposit layer growth on bare magnesium galvanically coupled to aluminum *J. Electrochem. Soc.* **162** C1–11
- [35] Rouet-Leduc B et al 2014 Spatial adaptive sampling in multiscale simulation *Comput. Phys. Commun.* **185** 1857–64
- [36] Knap J, Barton N R, Hornung R D, Arsenlis A, Becker R and Jefferson D R 2008 Adaptive sampling in hierarchical simulation *Int. J. Numer. Methods Eng.* **76** 572–600

A. Appendix

A.1. Chloride diffusion in concrete - a test example

In order to present a brief overview of the FEM and its application in modelling the transport of chloride ions in concrete, we now introduce a test example to demonstrate the use of finite element method. This test example is supported by a simple code written in the open source language Julia [38], which the reader, if interested can run on a computer.

For our problem, we consider a part of a substructure of a bridge pier which is completely submerged under sea water. The chloride concentration in the exposure environment is assumed to be 550 [mol/m³]. An exposure time of 5 years is considered. Although chloride diffusion coefficient changes with time, for the sake of this example we assume a constant apparent diffusion coefficient of concrete ($D^a = 1 * 10^{-12}$ [m²/s]).

Idealized problem in 1D

The problem can be modelled in a 1D domain as shown in Figure A.1. Considering concrete to be a homogenized continuum in $0 \leq x \leq l$ and with no chloride sink/source terms, Fick's second law can be used as the governing equation for chloride transport. As defined previously in section 3.2, let $C_x(x, t)$ represent the value of chloride concentration in space and time, therefore the governing equation can be expressed as

$$C^c(x, t)_{,t} - (D^a C^c(x, t)_{,x})_{,x} = 0. \quad (\text{A.1})$$

In order to have a well posed problem, the following boundary and initials conditions are set

$$\begin{cases} C^c(x, t)(x = 0, t) = 550 & \text{Dirichlet condition ,} & (\text{A.2}) \\ J^c(x, t)(x = l, t) = 0 & \text{Neumann condition ,} & (\text{A.3}) \\ C^c(x, t)(x, t = 0) = 0 & \text{Initial condition .} & (\text{A.4}) \end{cases}$$

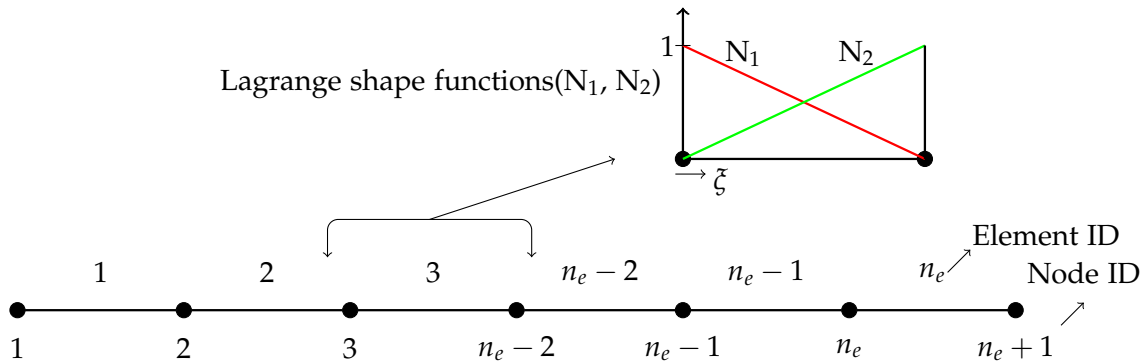


Figure A.1.: 1D domain discretized with linear elements in space. " ζ " represents the isoparametric coordinate.

Numerical solution using an implicit scheme

The 1D domain is discretized into n_e finite elements as shown in Figure A.1. The elements are constructed with linear Lagrange shape functions and exact integration is followed wherever necessary. Exact integration facilitates computation of integrals by evaluating the integrand at specific points called Gauss points and multiplying by respective weights. The number and location of Gauss points depends on the order of the integrand. Using the implicit time integration scheme as defined in eq.(3.15), the numerical solution can be easily computed. Additionally, a comparison of the numerically computed solution with the analytical solution is presented. The details of the code and expression for analytical solution are presented later.

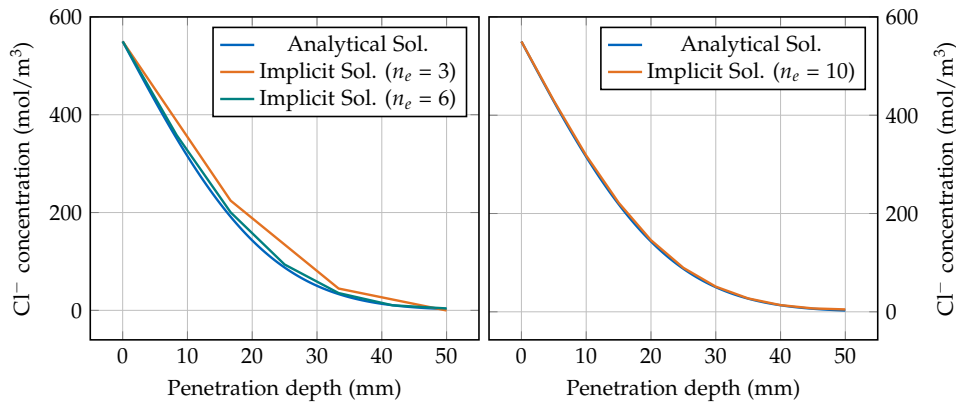


Figure A.2.: A comparison of implicit numerical solution with analytical solution after 5 years of exposure. Here " n_e " refers to the number of elements in the 1D domain.

Figure A.2 presents a comparison of solution computed with implicit scheme with the analytical solution of Fick's second law. It can be observed that the method approaches the analytical solution when the number of elements is increased, so called "mesh convergence".

The solution is interpolated linearly between the elements due to the nature of linear Lagrange shape functions.

Numerical solution using explicit scheme

An explicit time integration scheme for eq.(3.13) is presented. Again, the time derivative is approximated explicitly where at time "t" the solution is known and the solution at time "t + Δt" can be explicitly calculated as

$$\overline{\overline{\mathbf{M}}} \left(\frac{\mathbf{C}^c_{t+\Delta t} - \mathbf{C}^c_t}{\Delta t} \right) + \overline{\overline{\mathbf{K}}} \mathbf{C}^c_t = \overline{\overline{\mathbf{F}}}_t, \quad (\text{A.5})$$

$$\left(\Delta t^{-1} \overline{\overline{\mathbf{M}}} \right) \mathbf{C}^c_{t+\Delta t} = \mathbf{C}^c_t \left(\Delta t^{-1} \overline{\overline{\mathbf{M}}} - \overline{\overline{\mathbf{K}}} \right) + \overline{\overline{\mathbf{F}}}_t. \quad (\text{A.6})$$

Diagonalization of the consistent capacity matrix can make the system very efficient as no linear system of equations needs to be solved. The resulting mass matrix is called a lumped matrix $\overline{\overline{\mathbf{M}}}_{i,i}$. One of the ways of diagonalizing a consistent capacity matrix is to sum up the entries of an entire row and assign it to the diagonal entry in that row [44, 85]. As a consequence, eq.(A.6) is decoupled and can be easily solved for the concentration at each node at each time step as

$$\mathbf{C}^c_{i,(t+\Delta t)} = \mathbf{C}^c_{i,(t)} + \frac{\Delta t}{\overline{\overline{\mathbf{M}}}_{i,i}} \left(\overline{\overline{\mathbf{F}}}_{i,(t)} - \overline{\overline{\mathbf{K}}}_{i,j} \mathbf{C}^c_{i,(t)} \right). \quad (\text{A.7})$$

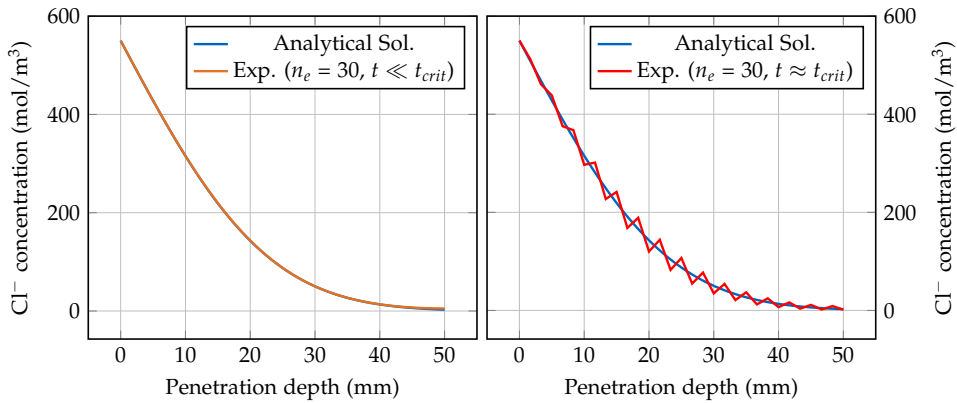


Figure A.3.: A comparison of explicit numerical solution with analytical solution after 5 years of exposure. Here n_e refers to the number of elements in the 1D domain.

Figure A.3 presents a comparison of solution computed with explicit scheme with the

analytical solution of Fick's second law. Here, restrictions are laid on the time step. When the time step is below the critical time step, the solution converges well with the analytical solution. However, for time steps approaching the critical time step, the solution can oscillate with a progressive growth of error. The code for explicit simulation is also presented later.

Analytical solution

The analytical solution of Fick's second law assuming a semi-infinite domain by Crank [86] is presented below. A constant surface concentration and apparent diffusion coefficient is assumed. Here, the same initial conditions are applied as defined previously. Here, a surface concentration $C_s = 550$ [mol/m³] is assumed together with a chloride concentration at the infinite end of the domain equal to zero [87]. The solution is expressed as

$$C^c(x, t) = C_s \left(1 - \operatorname{erf} \left(\frac{x}{2\sqrt{D^a t}} \right) \right), \quad (\text{A.8})$$

with $\operatorname{erf}(\cdot)$ as the error function, defined as

$$\operatorname{erf}(\kappa) = \frac{2}{\pi} \int_0^{\kappa} e^{-t^2} dt. \quad (\text{A.9})$$

Test code

The below presented code uses exact integration wherever necessary by employing suitable number of Gauss points. Standard linear Lagrange shape function are used. The domain length "l" is set to 50 mm and "n_e" refers to the number of elements in the domain. The time step can be changed by modifying the "Del_t" parameter. To run the code, Julia programming language (open-source) installed on Atom interface (open-source) is recommended.

```

1 #.....Importing packages.....
2 clearconsole()
3 using Pkg
4 using Plots
5 using LinearAlgebra
6 using SymEngine
7 using QuadGK
8 using SpecialFunctions

```


A. Appendix

```

9 #.....Parameters and variables.....
10 l = 0.050 #-----Length of bar in m
11 n_e = 5 #-----No. of elements
12 f0 = 0 #-----Flux value
13 T_t = 24*3600*365*5 #-----Total time 5 years
14 Del_t = 24*3600*5 #-----Time step - CHANGE HERE
15 N_t = Int(round(T_t/Del_t)) #--No. of time steps
16 CO = 550 #-----External concentration in mol/m^3
17 D_CI = 1*10^-12 #-----Apparent diffusion coefficient

18 #.....ID Matrix for n_e elements....
19 ID_mat = zeros(Int,n_e,2) #includes nodes

20 #.....Assembly of ID matrix for 2 noded elements....
21 for a = 1:n_e
22     for b = 1:2
23         ID_mat[a,b] = b+(a-1)
24     end
25 end

26 #.....Elemental consistent capacity matrix....
27 eta=symbols(:eta)
28 N1= (1/2*(1-eta)) #-----Shape functions
29 N2= (1/2*(1+eta)) #-----Shape functions
30 N = [N1 N2]
31 M = (transpose(N)*N)*1
32 M_e = zeros(2,2)

33 #.....Jacobian.....
34 coors = zeros(n_e+1) #Assigning coordinates
35 for i = 1:n_e
36     l_e = l/n_e
37     coors[i+1] = coors[i]+l_e
38 end
39 x = coors[1]*N1+coors[2]*N2
40 J = diff(x,eta) #Calculating Jacobian for the first element

41 #.....Element diffusion operator matrix....
42 N1_x = diff(N1,eta)*(1/J)
43 N2_x = diff(N2,eta)*(1/J)
44 H_x = [N1_x N2_x]
45 K = transpose(H_x)*H_x*D_CI
46 K_e = zeros(2,2)

47 #.....Fetching Gauss points.....
48 Val_e,wt = gauss(2)

49 #.....Exact element capacity matrix....
50 for c = 1:2
51     for d = 1:2
52         M_e[c,d] = subs(M[c,d]*(wt[1]*J),eta=>Val_e[1])+
53             subs(M[c,d]*(wt[2]*J),eta=>Val_e[2])
54     end
55 end

56 #.....Global capacity matrix....
57 M_S = zeros(1+n_e,1+n_e)
58 for e = 1:n_e
59     for i = 1:2
60         for j = 1:2
61             M_S[ID_mat[e,i],ID_mat[e,j]] = M_S[ID_mat[e,i],ID_mat[e,j]] + M_e[i,j]
62         end
63     end
64 end

```

A. Appendix

```
65 M_red = M_S[2:n_e+1,2:n_e+1] #Reduced capacity matrix

66 #.....Exact diffusion operator matrix.....
67 for e= 1:2
68     for f = 1:2
69         K_e[e,f] = subs(K[e,f]*(wt[1]*J),eta=>Val_e[1])+
70                 subs(K[e,f]*(wt[2]*J),eta=>Val_e[2])
71     end
72 end

73 #.....Global diffusion operator matrix.....
74 K_S = zeros(1+n_e,1+n_e)
75 for e = 1:n_e
76     for i = 1:2
77         for j = 1:2
78             K_S[ID_mat[e,i],ID_mat[e,j]] = K_S[ID_mat[e,i],ID_mat[e,j]] + K_e[i,j]
79         end
80     end
81 end
82 K_red = K_S[2:n_e+1,2:n_e+1] #Reduced K_S matrix

83 #.....Calculation of force vector.....
84 F = zeros(n_e+1)
85 F[n_e+1] = f0
86 F[2] = -K_S[2,1]*CO
87 F_red = F[2:n_e+1]

88 #.....Calculating solution using Implicit method.....
89 #Comment out this section if Explicit method is used (see below).
90 U = zeros(n_e+1,N_t) #each column of this matrix stores solution at each time step
91 U[1,:] = map(x -> CO, U[1,:]) # Boundary condition at LHS (DBC)
92 sol_time = @elapsed for t = 2:N_t
93     U[2:n_e+1,t] = inv(M_red/Del_t+K_red)*(F_red+1/Del_t*M_red*U[2:n_e+1,t-1])
94 end

95 #.....Calculating solution using Explicit method.....
96 #Comment out this section if Implicit method is used.

97 #.....Diagonalization.....
98 M_Con = zeros(1+n_e,1+n_e)
99 for i = 1:length(M_S[:,1])
100     M_Con[i,i]=sum(M_S[i,:])
101 end

102 M_red = M_Con[2:n_e+1,2:n_e+1] #With Diagonalization

103 #.....Calculating solution using FD.....
104 U = zeros(n_e+1,N_t) #each column of this matrix stores solution at each time step
105 U[1,:] = map(x -> CO, U[1,:]) # Boundary condition at LHS (DBC)
106 sol_time = @elapsed for t = 2:N_t
107     for u = 2:n_e+1
108         pivot_1 = 0
109         for v = 2:n_e+1
110             pivot_1 = pivot_1 + K_red[u-1,v-1]*U[v,t-1]
111         end

112         U[u,t] = U[u,t-1] +Del_t*(F_red[u-1]-pivot_1)/M_red[u-1,u-1]
113     end
114 end

115 #.....Outputting arrays(optional).....
116 outfile = "Data.txt"
```

A. Appendix

```
117 counter = 1
118 open(outfile, "w") do f
119   println(f,"X\tY")
120   for i in U[:N_t]
121     println(f,coors[counter],"\t",i,)
122     global counter +=1
123   end
124 end

125 #.....Plot results at last time step.....
126 T = zeros(N_t)
127 T[1] = 0
128 for i = 2:N_t
129   T[i] = T[i-1]+Del_t
130 end
131 plot(coors[:, U[:N_t]])
132 print("\nsolution time is ",sol_time )
133 print("\nNt is ", N_t)

134 #.....Analytical solution.....
135 t = T_t
136 limit = 1/(2*sqrt(D_Cl*t))
137 #Err(x) = quadgk((2/sqrt(pi))*exp(x^2),0,x/2)
138 int(x) = 2/sqrt(pi)*(1)*exp(-x^2)
139 Eff(x) = quadgk(int,0,(x*limit)) #Exact integration
140 C(j) = CO- Eff(j)[1]
141 Ct(j) = CO*(1-Eff(j)[1]) #2nd argument of quadgk is the error in exact integration
142 plot!(Ct,0:l/100:l)
```

Bibliography

- [1] C. R. Gagg. "Cement and concrete as an engineering material: an historic appraisal and case study analysis". In: *Engineering Failure Analysis* 40 (2014), pp. 114–140.
- [2] U. DESA. *United Nations, Department of Economic and Social Affairs, Population Division. World Population Prospects 2019: Highlights*. 2019.
- [3] Á. Fernández, M. Alonso, J. Garcia-Calvo, and B. Lothenbach. "Influence of the synergy between mineral additions and Portland cement in the physical-mechanical properties of ternary binders". In: *Materiales de construcción* 66.324 (2016), p. 097.
- [4] S. A. Miller, A. Horvath, and P. J. Monteiro. "Impacts of booming concrete production on water resources worldwide". In: *Nature Sustainability* 1.1 (2018), pp. 69–76.
- [5] D. N. Huntzinger and T. D. Eatmon. "A life-cycle assessment of Portland cement manufacturing: comparing the traditional process with alternative technologies". In: *Journal of Cleaner Production* 17.7 (2009), pp. 668–675.
- [6] S. Mahadevan, V. Agarwal, K. Neal, D. Kosson, and D. Adams. "Interim Report on Concrete Degradation Mechanisms and Online Monitoring Techniques". In: (Sept. 2014). doi: 10.2172/1168628.
- [7] L. Bertolini, B. Elsener, P. Pedferri, E. Redaelli, and R. Polder. *Corrosion of steel in concrete: prevention, diagnosis, repair*. 2013. Vol. 392. Wiley Online Library, 2013.
- [8] D. Boubitsas, L. Tang, and P. Utgenannt. "Chloride Ingress in Concrete Exposed to Marine Environment-Field data up to 20 years exposure". In: *CBI Report to SBUF Project 12684* (2014).
- [9] R. B. Polder and W. H. Peelen. "Characterisation of chloride transport and reinforcement corrosion in concrete under cyclic wetting and drying by electrical resistivity". In: *Cement and Concrete Composites* 24.5 (2002), pp. 427–435.
- [10] U. M. Angst. "Challenges and opportunities in corrosion of steel in concrete". In: *Materials and Structures* 51.1 (2018), p. 4.
- [11] U. Angst, B. Elsener, C. K. Larsen, and Ø. Vennesland. "Critical chloride content in reinforced concrete—a review". In: *Cement and concrete research* 39.12 (2009), pp. 1122–1138.

- [12] K. Tuutti. *Corrosion of steel in concrete - (Technical report)*. Cement-och betonginst CBI Sweden., 1982.
- [13] P. Ghods, O. Isgor, G. Carpenter, J. Li, G. McRae, and G. Gu. "Nano-scale study of passive films and chloride-induced depassivation of carbon steel rebar in simulated concrete pore solutions using FIB/TEM". In: *Cement and Concrete Research* 47 (2013), pp. 55–68.
- [14] P. Ghods, O. Isgor, G. McRae, J. Li, and G. Gu. "Microscopic investigation of mill scale and its proposed effect on the variability of chloride-induced depassivation of carbon steel rebar". In: *Corrosion Science* 53.3 (2011), pp. 946–954.
- [15] A. Poursaee and C. Hansson. "Reinforcing steel passivation in mortar and pore solution". In: *Cement and Concrete Research* 37.7 (2007), pp. 1127–1133.
- [16] U. M. Angst, M. R. Geiker, A. Michel, C. Gehlen, H. Wong, O. B. Isgor, B. Elsener, C. M. Hansson, R. François, K. Hornbostel, et al. "The steel–concrete interface". In: *Materials and Structures* 50.2 (2017), p. 143.
- [17] C. Alonso, C. Andrade, M. Castellote, and P. Castro. "Chloride threshold values to depassivate reinforcing bars embedded in a standardized OPC mortar". In: *Cement and Concrete research* 30.7 (2000), pp. 1047–1055.
- [18] K. Suda, S. Misra, and K. Motohashi. "Corrosion products of reinforcing bars embedded in concrete". In: *Corrosion science* 35.5-8 (1993), pp. 1543–1549.
- [19] F. Molina, C. Alonso, and C. Andrade. "Cover cracking as a function of rebar corrosion: Part 2—Numerical model". In: *Materials and structures* 26.9 (1993), pp. 532–548.
- [20] E. Sola. "Experimental and numerical study of chloride induced corrosion in reinforced concrete". PhD Thesis. 2017. URL: <http://elib.uni-stuttgart.de/handle/11682/9772>.
- [21] M. L. Allan. "Probability of corrosion induced cracking in reinforced concrete". In: *Cement and Concrete Research* 25.6 (1995), pp. 1179–1190.
- [22] H. Justnes. "A review of chloride binding in cementitious systems". In: *Nordic Concrete Research Publications* 21 (1998), pp. 48–63.
- [23] I. Richardson. "The nature of the hydration products in hardened cement pastes". In: *Cement and Concrete Composites* 22.2 (2000), pp. 97–113.
- [24] G. Glass and N. Buenfeld. "The influence of chloride binding on the chloride induced corrosion risk in reinforced concrete". In: *Corrosion Science* 42.2 (2000), pp. 329–344.

- [25] B. Martín-Pérez, H. Zibara, R. Hooton, and M. Thomas. "A study of the effect of chloride binding on service life predictions". In: *Cement and Concrete Research* 30.8 (2000), pp. 1215–1223.
- [26] O. Kayali, M. Ahmed, and M. Khan. "Friedel's salt and hydrotalcite-layered double hydroxides and the protection against chloride induced corrosion". In: *Civil Envir. Res* 5 (2013), pp. 111–117.
- [27] R. Dhir, M. El-Mohr, and T. Dyer. "Chloride binding in GGBS concrete". In: *Cement and Concrete Research* 26.12 (1996), pp. 1767–1773.
- [28] F. Luna, Á. Fernández, and M. Alonso. "The influence of curing and aging on chloride transport through ternary blended cement concrete". In: *Materiales de Construcción* 68.332 (2018), p. 171.
- [29] X. Duan and D. G. Evans. *Layered double hydroxides*. Vol. 119. Springer-Verlag, Berlin, Heidelberg, 2006.
- [30] European Union's Horizon 2020 research and innovation programme. *Long Lasting Reinforced Concrete for Energy Infrastructure under Severe Operating Conditions - Grant agreement: 685445*. <https://www.sintef.no/lorcenis>. Accessed : 13-02-2020.
- [31] S. K. Poznyak, J. Tedim, L. M. Rodrigues, A. N. Salak, M. L. Zheludkevich, L. F. P. Dick, and M. G. S. Ferreira. "Novel Inorganic Host Layered Double Hydroxides Intercalated with Guest Organic Inhibitors for Anticorrosion Applications". In: *Acs Applied Materials and Interfaces* 1.10 (2009), pp. 2353–2362. ISSN: 1944-8244. DOI: 10.1021/am900495r.
- [32] D. G. Evans and R. C. T. Slade. "Structural Aspects of Layered Double Hydroxides". In: *Layered Double Hydroxides*. Ed. by X. Duan and D. G. Evans. Berlin, Heidelberg: Springer Berlin Heidelberg, 2006, pp. 1–87. ISBN: 978-3-540-32495-9. DOI: 10.1007/430_005.
- [33] J. Tedim, A. Kuznetsova, A. N. Salak, F. Montemor, D. Snihirova, M. Pilz, M. L. Zheludkevich, and M. G. S. Ferreira. "Zn-Al layered double hydroxides as chloride nanotraps in active protective coatings". In: *Corrosion Science* 55 (2012), pp. 1–4. ISSN: 0010-938x. DOI: 10.1016/j.corsci.2011.10.003.
- [34] M. Meyn, K. Beneke, and G. Lagaly. "Anion-exchange reactions of layered double hydroxides". In: *Inorganic Chemistry* 29.26 (1990), pp. 5201–5207.
- [35] Z. Qu, Q. Yu, and H. Brouwers. "Relationship between the particle size and dosage of LDHs and concrete resistance against chloride ingress". In: *Cement and Concrete Research* 105 (2018), pp. 81–90.
- [36] Y. Wu, P. Duan, and C. Yan. "Role of layered double hydroxides in setting, hydration degree, microstructure and compressive strength of cement paste". In: *Applied Clay Science* 158 (2018), pp. 123–131.

- [37] T. Belytschko, W. K. Liu, B. Moran, and K. Elkhodary. *Nonlinear finite elements for continua and structures*. John Wiley & Sons, 2013.
- [38] J. Bezanson, A. Edelman, S. Karpinski, and V. B. Shah. “Julia: A fresh approach to numerical computing”. In: *SIAM review* 59.1 (2017), pp. 65–98. DOI: 10.1137/141000671.
- [39] Z. M. Mir, A. Bastos, D. Höche, and M. L. Zheludkevich. “Recent Advances on the Application of Layered Double Hydroxides in Concrete—A Review”. In: *Materials* 13.6 (2020), p. 1426. DOI: 10.3390/ma13061426.
- [40] L. Tang and H. Sørensen. “Precision of the Nordic test methods for measuring the chloride diffusion/migration coefficients of concrete”. In: *Materials and Structures* 34.8 (2001), p. 479.
- [41] T. J. Hughes. *The finite element method: linear static and dynamic finite element analysis*. Courier Corporation, 2012.
- [42] O. C. Zienkiewicz, R. L. Taylor, and J. Z. Zhu. *The finite element method: its basis and fundamentals*. Elsevier, 2005.
- [43] R. D. Cook et al. *Concepts and applications of finite element analysis*. John Wiley & Sons, 2007.
- [44] K. Willner and A. Schmidt. *Lecture notes on Discretization Methods- An Introduction, Institut für Mechanik - Universität Stuttgart*. Oct. 2006.
- [45] F. Li and X. Duan. “Applications of Layered Double Hydroxides”. In: *Layered Double Hydroxides*. Ed. by X. Duan and D. G. Evans. Berlin, Heidelberg: Springer Berlin Heidelberg, 2006, pp. 193–223. ISBN: 978 – 3 – 540 – 32495 – 9.
- [46] K. J. Martin and T. J. Pinnavaia. “Layered double hydroxides as supported anionic reagents. Halide-ion reactivity in zinc chromium hexahydroxide halide hydrates $[Zn_2Cr(OH)_6]X \cdot nH_2O$ (X= Cl, I)”. In: *Journal of the American Chemical Society* 108.3 (1986), pp. 541–542. ISSN: 0002-7863.
- [47] Z. Yang, H. Fischer, and R. Polder. “Modified hydrotalcites as a new emerging class of smart additive of reinforced concrete for anticorrosion applications: A literature review”. In: *Materials and Corrosion-Werkstoffe Und Korrosion* 64.12 (2013), pp. 1066–1074. ISSN: 0947-5117.
- [48] Y. W. Tian, C. F. Dong, G. Wang, X. Q. Cheng, and X. G. Li. “Zn-Al-NO₂ layered double hydroxide as a controlled-release corrosion inhibitor for steel reinforcements”. In: *Materials Letters* 236 (2019), pp. 517–520. ISSN: 0167-577x.

- [49] Y. H. Cao, S. G. Dong, D. J. Zheng, J. J. Wang, X. J. Zhang, R. G. Du, G. L. Song, and C. J. Lin. "Multifunctional inhibition based on layered double hydroxides to comprehensively control corrosion of carbon steel in concrete". In: *Corrosion Science* 126 (2017), pp. 166–179. ISSN: 0010-938x.
- [50] J. D. Zuo, B. Wu, C. Y. Luo, B. Q. Dong, and F. Xing. "Preparation of MgAl layered double hydroxides intercalated with nitrite ions and corrosion protection of steel bars in simulated carbonated concrete pore solution". In: *Corrosion Science* 152 (2019), pp. 120–129. ISSN: 0010-938x. DOI: 10.1016/j.corsci.2019.03.007.
- [51] Z. M. Mir, C. Gomes, A. C. Bastos, R. Sampaio, F. Maia, C. Rocha, J. Tedim, D. Höche, M. G. S. Ferreira, and M. L. Zheludkevich. "The Stability and Chloride Entrapping Capacity of ZnAl-NO₂ LDH in High-Alkaline/Cementitious Environment". In: *Corrosion and Materials Degradation* 2.1 (2021), pp. 78–99. ISSN: 2624-5558. DOI: 10.3390/cmd2010005. URL: <https://www.mdpi.com/2624-5558/2/1/5>.
- [52] T. Luping and L.-O. Nilsson. "Chloride binding capacity and binding isotherms of OPC pastes and mortars". In: *Cement and concrete research* 23.2 (1993), pp. 247–253. ISSN: 0008-8846.
- [53] A. Delagrave, J. Marchand, J. P. Ollivier, S. Julien, and K. Hazrati. "Chloride binding capacity of various hydrated cement paste systems". In: *Advanced Cement Based Materials* 6.1 (1997), pp. 28–35. ISSN: 1065-7355.
- [54] G. E. Archie. "The electrical resistivity log as an aid in determining some reservoir characteristics". In: *Transactions of the AIME* 146.01 (1942), pp. 54–62. ISSN: 0081-1696.
- [55] W. J. Weiss, T. J. Barrett, C. Qiao, and H. Todak. "Toward a Specification for Transport Properties of Concrete Based on the Formation Factor of a Sealed Specimen". In: *Advances in Civil Engineering Materials* 5.1 (2016), pp. 179–194. ISSN: 2165-3984. DOI: 10.1520/Acem20160004.
- [56] C. Y. Qiao, A. T. Coyle, O. B. Isgor, and W. J. Weiss. "Prediction of Chloride Ingress in Saturated Concrete Using Formation Factor and Chloride Binding Isotherm". In: *Advances in Civil Engineering Materials* 7.1 (2018), pp. 206–220. ISSN: 2165-3984. DOI: 10.1520/Acem20170141.
- [57] V. Jafari Azad, A. R. Erbehtas, C. Qiao, O. B. Isgor, and W. J. Weiss. "Relating the Formation Factor and Chloride Binding Parameters to the Apparent Chloride Diffusion Coefficient of Concrete". In: *Journal of Materials in Civil Engineering* 31.2 (2018), p. 04018392.

- [58] K. Snyder. "The relationship between the formation factor and the diffusion coefficient of porous materials saturated with concentrated electrolytes: theoretical and experimental considerations". In: *Concrete Science and Engineering* 3.December (2001), pp. 216–224.
- [59] M. Alonso, J. G. Calvo, S. Pettersson, I. Puigdomenech, M. Cunado, M. Vuorio, H. Weber, H. Ueda, M. Naito, C. Walker, et al. "Round Robin Test for Defining an Accurate Protocol to Measure the Pore Fluid pH of Low-pH Cementitious Materials". In: *Cement-Based Materials for Nuclear Waste Storage* (2012), p. 251.
- [60] *UNE 83988-1 Concrete durability. Test methods. Determination of the electrical resistivity. Part 1: Direct test (reference method)*. Standard (In Spanish). Madrid, ES: Asociación Española de Normalización, UNE, 2008.
- [61] *SS-EN 12390: Part 11 Determination of the chloride resistance of concrete, unidirectional diffusion*. Standard. Swedish Standards Institute, Stockholm, Sweden., 2015.
- [62] *NT Build 443 - Concrete, Hardened: Accelerated Chloride Penetration*. Tech. rep. Nordtest Espoo, Finland, 1995.
- [63] *UNE 83890 Concrete durability. Test methods. Determination of the water absorption, density and accessible porosity for water in concrete (2014)*. Standard (In Spanish). Madrid, ES: Asociación Española de Normalización, UNE, 2014.
- [64] Z. M. Mir, D. Höche, C. Gomes, R. Sampaio, A. C. Bastos, P. Mainçon, M. Ferreira, and M. L. Zheludkevich. "Enhanced Predictive Modelling of Steel Corrosion in Concrete in Submerged Zone Based on a Dynamic Activation Approach". In: *International Journal of Concrete Structures and Materials* 13.1 (2019), p. 11. DOI: 10.1186/s40069-018-0321-0.
- [65] Z. M. Mir, A. Bastos, C. Gomes, U. Mueller, M. C. Alonso, K. Villar, M. P. Rabade, F. Maia, C. M. Rocha, P. Mainçon, D. Höche, M. G. S. Ferreira, and M. L. Zheludkevich. "Numerical and Experimental Analysis of Self-Protection in Reinforced Concrete due to Application of Mg-Al-NO₂ Layered Double Hydroxides". In: *Advanced Engineering Materials* n/a.n/a (2020), p. 20000398. DOI: 10.1002/adem.202000398.
- [66] *PWI prEN 12390-xz Determination of electrical resistivity -updated 2020-Feb - Working draft-2020-02-06*. Standard. Technical Committee CEN/TC 104, 2020.
- [67] S. Yoon, J. Moon, S. Bae, X. Duan, E. P. Giannelis, and P. M. Monteiro. "Chloride adsorption by calcined layered double hydroxides in hardened Portland cement paste". In: *Materials Chemistry and Physics* 145.3 (2014), pp. 376–386.
- [68] S. Zhonghe, M. Juntao, C. Wei, and C. Xiaoxing. "Chloride binding capacity of cement paste containing layered double hydroxide (LDH)". In: *Journal of Testing and Evaluation* 40.5 (2012), pp. 796–800.

- [69] Y. Zhao, W. Hu, J. Chen, and L. Lv. "Factors influencing the chloride removal of aqueous solution by calcined layered double hydroxides". In: *Desalination and Water Treatment* 36.1-3 (2011), pp. 50–56.
- [70] C. Gomes, Z. Mir, R. Sampaio, A. Bastos, J. Tedim, F. Maia, C. Rocha, and M. Ferreira. "Use of ZnAl-Layered Double Hydroxide (LDH) to Extend the Service Life of Reinforced Concrete". In: *Materials* 13.7 (2020), p. 1769.
- [71] S. Miyata. "Anion-exchange properties of hydrotalcite-like compounds". In: *Clays and Clay minerals* 31.4 (1983), pp. 305–311.
- [72] N. Iyi, K. Okamoto, Y. Kaneko, and T. Matsumoto. "Effects of anion species on deintercalation of carbonate ions from hydrotalcite-like compounds". In: *Chemistry letters* 34.7 (2005), pp. 932–933.
- [73] S. Xu, Z. Chen, B. Zhang, J. Yu, F. Zhang, and D. G. Evans. "Facile preparation of pure CaAl-layered double hydroxides and their application as a hardening accelerator in concrete". In: *Chemical Engineering Journal* 155.3 (2009), pp. 881–885.
- [74] P. Šiler, I. Kolářová, J. Másilko, R. Novotn, and T. Opravil. "The Effect of Zinc on the Portland Cement Hydration". In: *Key Engineering Materials*. Vol. 761. Trans Tech Publ. 2018, pp. 131–134.
- [75] M. A. Trezza. "Hydration study of ordinary portland cement in the presence of zinc ions". In: *Materials research* 10.4 (2007), pp. 331–334. ISSN: 1516-1439.
- [76] S. Asavapisit, G. Fowler, and C. Cheeseman. "Solution chemistry during cement hydration in the presence of metal hydroxide wastes". In: *Cement and Concrete Research* 27.8 (1997), pp. 1249–1260.
- [77] J. L. Suter, R. L. Anderson, H. C. Greenwell, and P. V. Coveney. "Recent advances in large-scale atomistic and coarse-grained molecular dynamics simulation of clay minerals". In: *Journal of Materials Chemistry* 19.17 (2009), pp. 2482–2493.
- [78] D. G. Costa, A. B. Rocha, W. F. Souza, S. S. X. Chiaro, and A. A. Leitão. "Comparative Structural, thermodynamic and electronic analyses of Zn-Al- A^{n-} hydrotalcite-like compounds ($A^{n-} = Cl^{-}, F^{-}, Br^{-}, OH^{-}, CO_3^{2-}$ or NO_3^{-}): An ab initio study". In: *Applied clay science* 56 (2012), pp. 16–22.
- [79] C. Andrade, J. M. Diez, and C. Alonso. "Mathematical modeling of a concrete surface "skin effect" on diffusion in chloride contaminated media". In: *Advanced Cement Based Materials* 6.2 (1997), pp. 39–44.
- [80] P. Castro, O. T. De Rincon, and E. Pazini. "Interpretation of chloride profiles from concrete exposed to tropical marine environments". In: *Cement and Concrete Research* 31.4 (2001), pp. 529–537.

- [81] K. De Weerd, D. Orsáková, A. C. Müller, C. K. Larsen, B. Pedersen, and M. R. Geiker. “Towards the understanding of chloride profiles in marine exposed concrete, impact of leaching and moisture content”. In: *Construction and Building Materials* 120 (2016), pp. 418–431.
- [82] M. T. Walsh. “Corrosion of steel in submerged concrete structures”. PhD Thesis. 2015. URL: <https://scholarcommons.usf.edu/etd/6048>.
- [83] Z. M. Mir, J. Friis, T. F. Hagelien, I.-H. Svenum, I. G. Ringdalen, N. Konchakova, M. L. Zheludkevich, and D. Höche. “Interoperability architecture for bridging computational tools: application to steel corrosion in concrete”. In: *Modelling and Simulation in Materials Science and Engineering* 28.2 (2020), p. 025003. DOI: 10.1088/1361-651X/ab6209.
- [84] A. De Baas and R. Lula. *What makes a material function? Let me compute the ways*. 2015.
- [85] A.-K. Schäuble. “Variationally consistent inertia templates for speed-up and customization in explicit dynamics”. PhD Thesis. 2019.
- [86] J. Crank. *The Mathematics of Diffusion*. Oxford University Press, Oxford, UK, 2004.
- [87] M. U. Khan, S. Ahmad, and H. J. Al-Gahtani. “Chloride-induced corrosion of steel in concrete: an overview on chloride diffusion and prediction of corrosion initiation time”. In: *International Journal of Corrosion* 2017 (2017).